

## N O T I C E

THIS DOCUMENT HAS BEEN REPRODUCED FROM  
MICROFICHE. ALTHOUGH IT IS RECOGNIZED THAT  
CERTAIN PORTIONS ARE ILLEGIBLE, IT IS BEING RELEASED  
IN THE INTEREST OF MAKING AVAILABLE AS MUCH  
INFORMATION AS POSSIBLE

MDC 22052

NASA CR-  
160392

(NASA-CR-160392) OPTICAL DIGITAL TECHNIQUES  
Final Report (McDonnell-Douglas Astronautics  
Co.) 226 p HC A11/MP A01 CSCL 20F

N80-13922

Unclas  
G3/74 46250

# OPTICAL DIGITAL TECHNIQUES

## FINAL REPORT

**MCDONNELL DOUGLAS ASTRONAUTICS COMPANY-ST. LOUIS DIVISION**

**MCDONNELL DOUGLAS**

**CORPORATION**



COPY NO. 11

---

# OPTICAL DIGITAL TECHNIQUES

---

FEBRUARY 1979

MDC E2052

## FINAL REPORT CONTRACT NO. NAS9-15051

*Prepared for: NASA Lyndon B. Johnson Space Center  
Avionics Systems Integration Branch, Houston, Texas 77058*

**MCDONNELL DOUGLAS ASTRONAUTICS COMPANY-ST. LOUIS DIVISION**

Box 516, Saint Louis, Missouri 63166 (314) 232-0232

**MCDONNELL DOUGLAS**



TABLE OF CONTENTS

<u>SECTION</u>	<u>PAGE</u>
Table of Contents. . . . .	ii
List of Figures. . . . .	iv
List of Tables . . . . .	ix
List of Pages. . . . .	ix
1.0 INTRODUCTION . . . . .	1
2.0 OPTICAL FIBER SYSTEM COMPONENTS. . . . .	3
2.1 Optical Fiber Waveguides and Fiber Cable . . . . .	3
2.1.1 Light Propagation in Cylindrical Waveguides. . . . .	3
2.1.2 Step-Index Multimode Fibers. . . . .	3
2.1.3 Graded Index Fibers. . . . .	7
2.1.4 Single Mode Fiber. . . . .	8
2.1.5 Optical Loss Mechanisms in Fibers. . . . .	9
2.1.6 Strength Properties of Fibers. . . . .	11
2.1.7 Temporal Dispersions in Fiber Optics . . . . .	14
2.1.8 Radiation Properties of Fibers . . . . .	16
2.1.9 Summary and Vendor Tables. . . . .	20
2.2 Sources. . . . .	21
2.2.1 Light Emitting Diodes and Injection Laser Diodes . . . . .	21
2.2.2 Lifetime of Devices. . . . .	31
2.2.3 Table of Sources and Contract Summary. . . . .	31
2.3 Photodetectors for Fiber Systems . . . . .	33
2.3.1 General Characteristics of Photodetectors. . . . .	33
2.3.2 Application Considerations . . . . .	36
2.3.3 Contract Summary, Vendor Information . . . . .	42
2.4 Optical Losses in Fiber Systems. . . . .	50
2.4.1 Source-to-Fiber Connectors . . . . .	58
2.4.2 Fiber-Bundle to Fiber-Bundle Connectors. . . . .	67
2.4.3 Fiber-to-Receiver Losses . . . . .	67
2.4.4 Vendor Optical Connectors. . . . .	68
2.5 Star and Tee Coupler . . . . .	70
2.6 Single-Fiber vs. Bundle-Fiber Systems. . . . .	73
2.7 System Considerations. . . . .	75
2.7.1 Sources. . . . .	75
2.7.2 Fibers . . . . .	78
2.7.3 Detectors. . . . .	79
2.7.4 Link Length. . . . .	80
2.7.5 Nuclear Hardness . . . . .	81
2.7.6 Different System Architectures . . . . .	83
2.7.7 Vendor Fiber Optic System Tables . . . . .	85
3.0 DATA BUS SYSTEM. . . . .	88
3.1 Space Shuttle Data Bus System. . . . .	88
3.2 Fiber System Size, Weight, and Power . . . . .	88
3.3 Fiber Optic System Interface with Space Shuttle. . . . .	88
3.4 Security Capability. . . . .	90
3.5 EMI Susceptibility . . . . .	92
3.6 Two Shuttle Fiber Optic Busses . . . . .	92



TABLE OF CONTENTS (Cont'd)

<u>SECTION</u>	<u>PAGE</u>
4.0 FIBER OPTIC HARDWARE. . . . .	101
4.1 Baseline System Hardware. . . . .	101
4.2 Fiber Optic Data Bus System Tests . . . . .	103
4.2.1 Connector-to-Connector Losses . . . . .	105
4.2.2 Connector Indexing Losses . . . . .	107
4.2.3 Star Coupler Throughput Losses. . . . .	107
4.2.4 Bit Error Rate Measurement. . . . .	111
4.3 EMI Tests . . . . .	118
4.3.1 Radiation Environment . . . . .	118
4.3.2 Waveguide Below Cutoff. . . . .	123
4.3.3 EMI Susceptibility Measurement Criterion. . . . .	129
4.3.4 Low Radio Frequency Electromagnetic Interference Test . . . .	130
4.3.5 High Radio Frequency Electromagnetic Interference Test. . . .	134
4.4 Lightning Test. . . . .	146
5.0 REFERENCES. . . . .	149
Appendix A - Requirements Definition Document . . . . .	A-1
Appendix B - Bus Losses . . . . .	B-1

List of Figures

<u>Fig. No.</u>		<u>Page</u>
2-1	PROPAGATION OF LIGHT IN A FIBER . . . . .	4
2-2	VARIOUS TYPES OF FIBER AND THEIR INDEX PROFILES . . . .	6
2-3	IMPURITY ABSORPTION EFFECTS . . . . .	10
2-4	ORIGIN OF LOSS IN OPTICAL GLASS FIBERS . . . . .	10
2-5	TIME TO FAILURE VS. STRESS . . . . .	13
2-6	RADIATION INDUCED LOSS VS. TIME . . . . .	18
2-7	RADIATION INDUCED LOSS VS. DOSE . . . . .	18
2-8	FIBER RESPONSE TO RADIATION . . . . .	19
2-9	LED EMITTER CONFIGURATION . . . . .	25
2-10	LED OUTPUT POWER . . . . .	26
2-11	LASER DIODE OUTPUT POWER . . . . .	26
2-12	LED EMISSION PATTERN . . . . .	29
2-13	LASER DIODE EMISSION PATTERNS . . . . .	30
2-14	PHOTODETECTOR EQUIVALENT CIRCUIT . . . . .	41
2-15	BUNDLE/DETECTOR INTERFACE . . . . .	41
2-16	PIN PHOTODIODE RESPONSE . . . . .	43
2-17	CONSERVATION OF RADIANCE . . . . .	57
2-18	FIBER LOSS VS. CLADDING THICKNESS . . . . .	60
2-19	19 FIBER BUNDLE . . . . .	61
2-20	PACKING FRACTION LOSS . . . . .	62
2-21	NUMERICAL APERTURE LOSS . . . . .	65
2-22	UNINTERCEPTED ILLUMINATION LOSS . . . . .	66
2-23	FIBER OPTIC DATA DISTRIBUTION NETWORKS . . . . .	71
2-24	COMPARISON OF WORST CASE LOSSES FOR T, START & HYBRID SYSTEMS . . . . .	74
2-25	SINGLE FIBER REDUNDANCY APPROACH . . . . .	76
2-26	FIBER OPTIC SYSTEMS . . . . .	77
2-27	REPEATER SPACING FOR MULTIMODE/SINGLE MODE FIBER LINK (IDEAL TRANSMITTER AND RECEIVER) . . . . .	82
2-28	FIBER RESPONSE TO RADIATION . . . . .	82
2-29	BIT ERROR RATE VS. AVERAGE OPTICAL POWER INTO SINGLE MODE FIBER OF MMIFOT (FOR 20 Mb/s NRZ) . . . . .	84

List of Figures (Cont.)

<u>Fig. No.</u>		<u>Page</u>
3-1	SINGLE DATA BUS-OPTICAL SYSTEM . . . . .	89
3-2	OPTICAL DATA BUS COUPLER . . . . .	89
3-3	SINGLE CABLE BUS . . . . .	91
3-4	BIFURCATED CABLE BUS . . . . .	91
3-5	ELECTRICAL DATA BUS FLIGHT CRITICAL . . . . .	93
3-6	LINEAR OPTICAL DATA BUS FLIGHT CRITICAL 2 . . . . .	93
3-7	LINEAR OPTICAL DATA BUS FLIGHT CRITICAL 2 (REPEATER IN- STALLED) . . . . .	93
3-8	RADIAL OPTICAL DATA BUS FLIGHT CRITICAL 2 . . . . .	97
3-9	ELECTRICAL DATA BUS INSTRUMENTATION 1 . . . . .	99
3-10	LINEAR OPTICAL DATA BUS INSTRUMENTATION . . . . .	99
3-11	RADIAL OPTICAL DATA BUS INSTRUMENTATION 1 . . . . .	100
4-1	FIBER OPTIC STAR DATA BUS SYSTEM COMPONENTS. . . . .	102
4-2	FOUR FUSED FIBERS . . . . .	104
4-3	CONFIGURATION FOR LOSS MEASUREMENT . . . . .	106
4-4	FIBER #2 SIDE A . . . . .	109
4-5	FIBER #2 SIDE B . . . . .	109
4-6	FIBER #5 SIDE A . . . . .	110
4-7	FIBER #5 SIDE B . . . . .	110
4-8	INTERVAL LENGTH VS. NO. OF SAMPLES FOR 99.99% CONFIDENCE LEVEL . . . . .	115
4-9	BIT ERROR RATE MEASUREMENT SYSTEM . . . . .	116
4-10	ERROR PROBABILITY VERSUS AVERAGE LIGHT POWER AT OUTPUT END OF PCS FIBER . . . . .	117
4-11	INTERFERENCE IN 7400 NAND GATE . . . . .	119
4-12	INTERFERENCE IN AMPLIFIER CIRCUIT CONTAINING OPERATIONAL AMPLIFIER. RF ENTERS INVERTING INPUT TERMINAL AT 3.0 GHz . . . . .	119
4-13	TYPICAL INTERFERENCE EFFECTS DUE TO MODULATION OF THE INTERFERING RF SIGNAL . . . . .	121
4-14	BASIC SITUATION OF INTEREST. ELECTROMAGNETIC RADIATION CAN CAUSE INTERFERENCE IN ELECTRONIC SYSTEMS . . . . .	121
4-15	POSSIBLE TE AND TM MODES IN A HOLLOW CYLINDRICAL WAVE- GUIDE AS A FUNCTION OF FREQUENCY . . . . .	125

List of Figures (Cont.)

<u>Figure No.</u>		<u>Page</u>
4-16	DB LOSS VS. FREQUENCY FOR CYLINDRICAL WAVEGUIDES . . . . .	127
4-17	DB LOSS VS. FREQUENCY FOR CYLINDRICAL WAVEGUIDES (BELOW, ABOVE CUTOFF) . . . . .	128
4-18	NASA FIBER OPTIC EMI PRETEST (NO RADIATION) . . . . .	131
4-19	LOW RF EMI TEST SET-UP . . . . .	132
4-20	LOW RF EMI TEST (PERPENDICULAR CASE) . . . . .	135
4-21	LOW RF EMI TEST (PARALLEL CASE) . . . . .	135
4-22	HIGH RADIO FREQUENCY ELECTROMAGNETIC INTERFERENCE TEST SET . . . . .	137
4-23	NASA/JSC FIBER OPTIC EMI TEST 31 . . . . .	138
4-24	UNRADIATED TEST DENSITY AND DISTRIBUTION . . . . .	140
4-25	NASA FIBER OPTIC EMI STUDY . . . . .	142
4-26	NASA FIBER OPTIC EMI STUDY . . . . .	143
4-27	NASA FIBER OPTIC EMI STUDY . . . . .	143
4-28	NASA/JSC FIBER OPTIC EMI TEST 39 . . . . .	144
4-29	NASA/JSC FIBER OPTIC EMI TEST 40 . . . . .	145
4-30	NASA/JSC FIBER OPTIC EMI TEST 41 . . . . .	147
A-1	SHUTTLE DATA BUS . . . . .	A12
A-2	MANCHESTER II CODE . . . . .	A13
A-3	WORD SYNC . . . . .	A14
A-4A	LINEAR OPTICAL DATA BUS CONFIGURATION . . . . .	A15
A-4B	RADIAL OPTICAL DATA BUS CONFIGURATION . . . . .	A16
A-5	"T" COUPLER OUTLINE . . . . .	A17
A-6	ILLUSTRATION OF POWER SPLITTING FACTOR . . . . .	A18
A-7	RADIAL DATA BUS COUPLER . . . . .	A19
A-8	GPC/BTU COUPLER . . . . .	A20
A-9	OPTICAL REPEATER CONFIGURATION . . . . .	A21
A-10	(TO BE SPECIFIED.) TRANSMITTER OUTLINE . . . . .	A22
A-10A	TRANSMITTER INPUT WAVEFORM . . . . .	A23
A-11	(TO BE SPECIFIED.) RECEIVER OUTLINE . . . . .	A24
A-12	CONDUCTED NARROWBAND EMISSION LIMIT . . . . .	A25

List of Figures (Cont.)

<u>Figure No.</u>		<u>Page</u>
A-13	CONDUCTED NARROWBAND EMISSION LIMIT . . . . .	A26
A-14	CONDUCTED SUSCEPTIBILITY LIMIT . . . . .	A27
A-15	CONDUCTED SUSCEPTIBILITY LIMIT . . . . .	A28
A-16	TRANSIENT SUSCEPTIBILITY WAVEFORM . . . . .	A29
A-17	RADIATED NARROWBAND EMISSION LIMIT . . . . .	A30
A-18	RADIATED BROADBAND EMISSION LIMIT . . . . .	A31
A-19	RADIATED SUSCEPTIBILITY LIMIT . . . . .	A32
B-1	BUS 1C-1 . . . . .	B2
B-2	BUS 1C1 . . . . .	B3
B-3	BUS 1C-2 . . . . .	B4
B-4	BUS 1C2 . . . . .	B5
B-5	BUS 1C-3 . . . . .	B6
B-6	BUS 1C3 . . . . .	B7
B-7	BUS 1C-4 . . . . .	B8
B-8	BUS 1C4 . . . . .	B9
B-9	BUS 1C-5 . . . . .	B10
B-10	BUS 1C5 . . . . .	B11
B-11	BUS FC-1 . . . . .	B12
B-12	BUS FC1 . . . . .	B13
B-13	BUS FC-2 . . . . .	B14
B-14	BUS FC2 . . . . .	B15
B-15	BUS FC-3 . . . . .	B16
B-16	BUS FC3 . . . . .	B17
B-17	BUS FC-4 . . . . .	B18
B-18	BUS FC4 . . . . .	B19
B-19	BUS FC-5 . . . . .	B20
B-20	BUS FC5 . . . . .	B21
B-21	BUS FC-6 . . . . .	B22
B-22	BUS FC6 . . . . .	B23
B-23	BUS FC-7 . . . . .	B24
B-24	BUS FC7 . . . . .	B25

List of Figures (Cont.)

<u>Figure No.</u>		<u>Page</u>
B-25	BUS FC-8 . . . . .	B25
B-26	BUS FC8 . . . . .	B26
B-27	BUS DK-1 . . . . .	B27
B-28	BUS DK1 . . . . .	B28
B-29	BUS DK-2 . . . . .	B29
B-30	BUS DK2 . . . . .	B30
B-31	BUS DK-3 . . . . .	B31
B-32	BUS DK3 . . . . .	B32
B-33	BUS DK-4 . . . . .	B33
B-34	BUS DK4 . . . . .	B34

List of Tables

<u>Table No.</u>		<u>Page</u>
2-1	OPTICAL FIBER COMPARISON . . . . .	22
2-2	COMPARISON OF VARIOUS FIBER OPTIC CABLES . . . . .	23
2-3	OPERATIONAL PARAMETERS . . . . .	27
2-4	SOURCE CHARACTERISTICS . . . . .	32
2-5	HEWLETT PACKARD PIN PHOTODIODES . . . . .	38
2-6	EG&G SILICON PHOTODIODES . . . . .	44
2-7	EG&G SILICON DIFFUSED PIN PHOTODIODES . . . . .	45
2-8	RCA (SINGLE ELEMENT SILICON p-i-n) p-TYPE . . . . .	46
2-9	RCA (SINGLE ELEMENT SILICON p-i-n) n-TYPE . . . . .	47
2-10	RCA (SINGLE ELEMENT SILICON p-i-n) n-TYPE . . . . .	48
2-11	RCA SILICON AVALANCHE PHOTODIODES . . . . .	49
2-12	UNITED DETECTOR TECHNOLOGY INC. PINs AND UDT PHOTO ps . .	51
2-13	HAMAMUTSA SILICON PHOTOCELL . . . . .	52
2-14	QUANTRAD CORP. PIN AND PV SERIES SILICON PHOTODIODES . . .	53
2-15	HARSHAW, SILICON IR DETECTORS . . . . .	54
2-16	MATH ASSOCIATES PIN PHOTODIODES . . . . .	55
2-17	AVAILABLE MULTI-PIN CONNECTORS . . . . .	69
2-18	FIBER OPTIC DEVICE . . . . .	86
2-19	OPTO-ELECTRONIC DEVICE COMPARISON . . . . .	87
4-1	CONNECTOR LOSSES . . . . .	108
4-2	CONNECTOR LOSSES . . . . .	108
4-3	AVERAGE STAR THROUGH-PU LOSS (dB) . . . . .	112
4-4	VARIANCE OF STAR LOSSES . . . . .	112
4-5	SKEWNESS IS STAR THROUGH-PUT LOSS . . . . .	112
4-6	LOSS PORT (I,J) - LOSS PORT (J,I) . . . . .	113
4-7	LOSS PER PORT-AVERAGE LOSS OF STAR . . . . .	113

## LIST OF PAGES

Title

ii through ix

1 through 150

A1 through A32

B1 through B34

ix

## 1.0 INTRODUCTION

The concept of using light to transmit information in a communication system took a significant step forward with the invention of the laser. However, it wasn't until the advent of low-loss optical fibers that a new dimension was added to the optical communication link. At the present time it is not a question of whether or not fiber optic links will be used on future spacecraft avionics systems, but how soon this will happen. How soon depends on the individual component development of the fiber optic system. The goal of this study was to determine the feasibility of implementing a fiber optics system for potential Space Shuttle Orbiter application. The overall requirement was to provide an intercommunications channel that could survive the Space Shuttle Orbiter manufacturing and flight environment while satisfying the need for a low-loss, multipoint widely distributed system.

Presently, heavy shielded twisted pairs (wire) are used for the intercommunication interface between spacecraft avionics. While this system is satisfactory, vehicle manufacturing is difficult and vehicle capabilities are limited due to EMI susceptibility and limited intercommunications rate. With the use of a fiber optic digital data bus system, most of the above problems are significantly reduced. The objective of the contract was to identify the current supplies of fiber optics components, those components that are presently developed or are being developed, address system applications and system designs, and finally identify any problem areas and make recommendations.

A detailed study of the fiber optics market was made along with a system evaluation of a 9-port star fiber optic data bus system for Bit Error Rate (BER) measurements, Electromagnetic Interference (EMI), lightning effects and system losses. The state-of-the-art of fiber optics components was examined in detail. These components included step-index fibers, graded index fibers, and single mode fibers. The optical loss mechanisms, strength properties, temporal dispersion, and radiation properties of fibers were examined. Light sources (such as ILD and LED) and detectors (such as PIN and APD) were studied for lifetime, radiation hardness, and radiation patterns of the devices. Tables listing vendors are given for the sources and detectors.



A detailed study was made of optical interface losses between transmitter-to-fiber interface, connector-to-connector interface, and fiber-to-receiver interface. System effects such as pulse dispersion, risetimes of the sources and detectors, type of fibers used, output power of the sources, and detector sensitivity were considered. Data bus systems such as TEE, Star, and Hybrid were analyzed. A brief study of single fiber versus bundle technologies for future avionics systems was conducted. The existing data bus system on Space Shuttle was examined and an optical analog was derived for a fiber bundle system, along with the associated power margin.

Finally, system tests were performed on a feasibility model of a 9-port Star data bus system including BER, star losses, connector losses, etc. The same system was subjected to EMI between the range of 200 Hz to 10 GHz at 20V/m levels. A lightning test was also performed which simulated the conditions similar to those on Space Shuttle. The data bus system was found to be EMI and lightning hard.

It was concluded that an optical data bus system is feasible for Shuttle Orbiter type vehicles. Space qualification would be required for some components. Such a system should consider utilization of single fibers and Star coupler technology. The basic design has inherently large growth potential to satisfy higher data rates and optical mux-demux capability requirements.

## 2.0 OPTICAL FIBER SYSTEM COMPONENTS

### 2.1 OPTICAL FIBER WAVEGUIDES AND FIBER CABLE

#### 2.1.1 Light Propagation in Cylindrical Waveguides

There are primarily three different kinds of fibers available in the commercial market, step index, graded index (both of which are multimode fibers), and single mode. Light is contained in the fiber by the index of refraction difference between the core and the cladding. This difference causes the fiber to act as waveguide to the light. A typical fiber is shown in Figure 2-1 with core index  $n_1$ , cladding index  $n_2$ , and a protective coating which has an index of refraction  $n_3$ . The core is usually made of some form of silica which has a higher index than that of the cladding where dopants have been added to increase its index of refraction. The protective coating may or may not be a higher index of refraction than  $n_2$  depending on the material of which it is made.

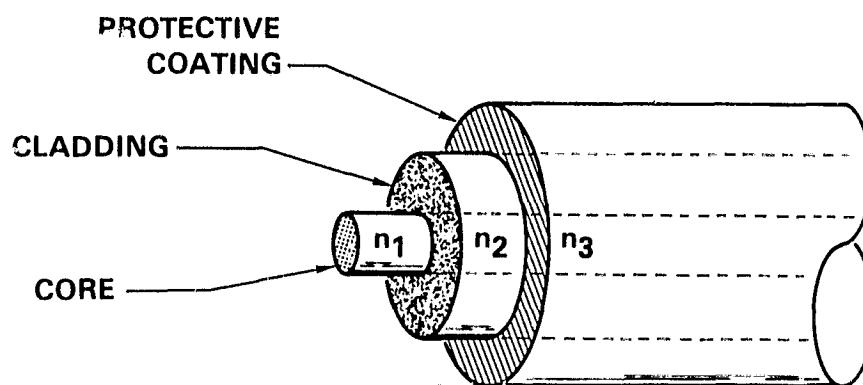
The manner in which light propagates in the fiber depends on the index of refraction,  $n$ , profile of the core, the index difference between the core/cladding, and to some extent the diameter of the fiber. If the core diameter of the fiber is many wavelengths of light, then the propagation of light may be described by geometric or ray optics. By assuming some incident angle  $\theta$  defined as in Figure 2-1, it is possible to determine the maximum angle that light incident on the face of the fiber can enter without exceeding the critical angle. This critical angle is called the numerical aperture (N.A.) of the fiber. For rays incident with angles greater than N.A., the fiber will not waveguide the light ray. The N.A. may be determined by applying Snell's Law at the face of the fiber and once again at the core-cladding interface; it may be shown to be  $\sin \theta = \text{N.A.} = [n_1^2 - n_2^2]^{1/2}$ . Hence, light rays will propagate in the fiber, as shown in Figure 2-1, in a zig-zag path if they are incident on the surface with an angle less than or equal to  $\theta$ . The fiber optic waveguide described above is known as a step-index multimode type guide.

#### 2.1.2 Step-Index Multi-Mode Fibers

The Step-index fibers are usually of three types: glass cladding-glass core, plastic cladding-glass core, or plastic cladding-plastic core. In order to describe light propagation and mode structure in a fiber, it is necessary to

PROPAGATION OF LIGHT IN A FIBER  
Typical Fiber Waveguide

10-1990



## HOW LIGHT PROPAGATES

$$\theta = \sin^{-1} [n_1^2 - n_2^2]^{1/2}$$

$$NA = [n_1^2 - n_2^2]^{1/2}$$

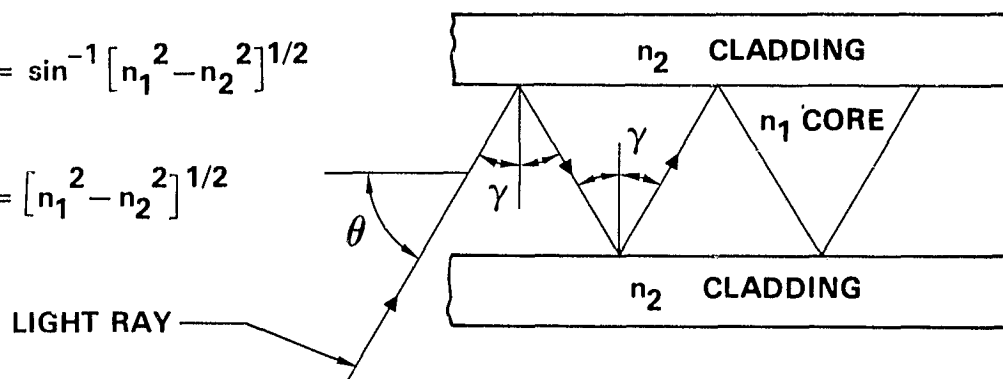


FIGURE 2-1

solve Maxwell's equations for a cylindrical dielectric waveguide. This is a complicated process that involves solving a transcendental equation. One of the parameters resulting from this analysis is a quantity called the normalized frequency,  $v$ , defined as:<sup>(1)</sup>

$$v = \frac{2\pi a}{\lambda} (n_1^2 - n_2^2)^{1/2} \quad (2.1)$$
$$= \frac{\pi d}{\lambda} \text{N.A.}$$

where

$a$  is the core radius of the fiber,

$\lambda$  is the wavelength of the light, and

N.A. is the numerical aperture of the fiber.

Using the normalized frequency, it is possible to estimate the number of modes propagating in the fiber by  $N = v^2/2$ .<sup>(1)</sup> If the value  $v$  is 2.4 or less, the fiber will only support one mode and hence is called a single mode fiber. For most glass-glass step index fibers with a  $\sim 35 \mu\text{m}$  and N.A.  $\sim 0.25$ ,  $N$  will be  $\sim 200$ ; hence, most step index fibers are multi-mode. The number of modes that a fiber supports is directly related to the amount of temporal dispersion in the fiber (see Section 2.1.7).

From Equation 2.1, increasing  $d$  increases  $v$  and hence the amount of temporal dispersion present in a fiber; however, increasing the core diameter also makes alignment in optical connectors easier and less lossy (see Section 2.5). The amount that  $d$  can increase in a glass-glass fiber is limited due to the size of the preform that the fiber is pulled from. To improve this situation, a new kind of fiber was developed called plastic clad silica fiber.

Most of the initial funding for the development of the plastic clad silica fiber was provided by the U.S. Army Electronics Command, Fort Monmouth, New Jersey.<sup>(2)</sup> The objectives of the program were to develop a lightweight, flexible, rugged cable which was capable of operating between 600 and 1060 nanometers for both analog and digital transmission data rates of up to 20 Mbps. The profile of this fiber is shown in Figure 2-2b. The core of plastic-clad step index fiber is about twice that of the glass-glass step index fiber. Typical values of core diameters for plastic clad fiber are between 100 and 200  $\mu\text{m}$ . In

10-1979

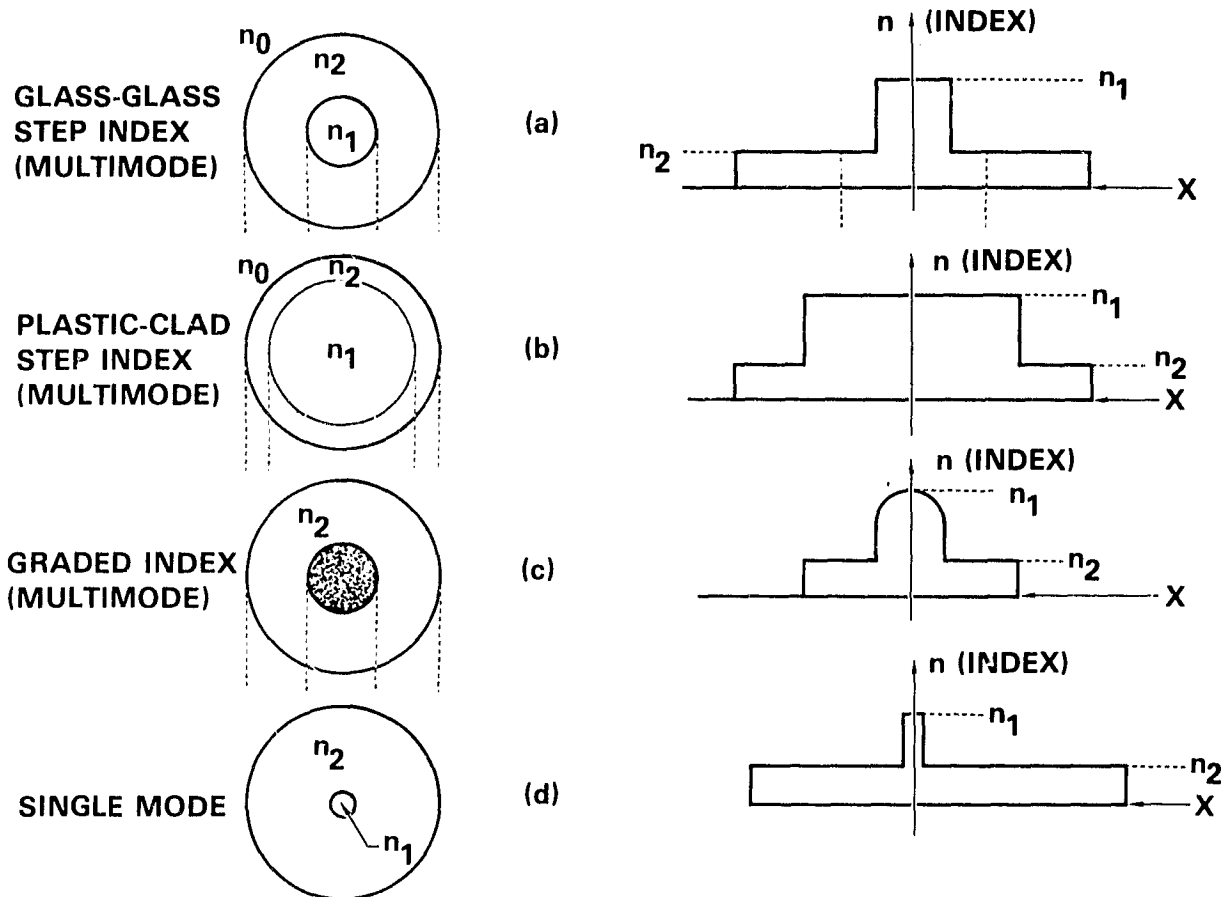
**VARIOUS TYPES OF FIBER AND THEIR INDEX PROFILES**

FIGURE 2-2

general, the plastic clad fiber tends to have a larger numerical aperture than the glass-glass step index fibers, being on the order of 0.3 and higher. The numerical aperture is an important parameter as far as coupling between the source and the fiber is concerned (see Section 2.5.1). Care must be taken when using this fiber as the N.A. drops with temperature.<sup>(2)</sup>

There is also a third kind of stepped-index fiber which has a plastic cladding-plastic core and a very high N.A. ( $\sim 0.6$ ); however, this fiber is very lossy, being about 1 dB/m at 820 nm, and is not very practical except for short run applications. With the plastic-plastic configuration, it is possible to have core diameters on the order of 400 to 600  $\mu\text{m}$ .

In general, the step index fibers are good for lower data rate, short run systems. As the data rate increases, a graded index fiber is more suited to handle the increase in information rate.

### 2.1.3 Graded Index Fibers

The graded index fiber profile is shown in Figure 2-2c. In this type of fiber, the index of refraction of the core is quadratically varied from a maximum value at the center of the core to a minimum value at the fiber cladding. The physical basis for the graded index fiber depends upon the speed of light in a dielectric, which is given by:

$$V = c/n \quad (2.2)$$

where  $c$  is the speed of light in free space ( $3 \times 10^8$  m/s). In a stepped index fiber of length  $\ell$ , light incident on the face of the fiber at an angle  $\theta$  must travel  $\ell/\cos\theta$ . A similar situation exists in the graded index case; however, the rays entering at an angle  $\theta$  see a lower index of refraction; hence, propagate faster than those that enter with small angles of  $\theta$  which propagate for most of the time in the higher index (lower speed) center of the core. In this manner, most of the light rays, independent of entrance angle, arrive at the output end of the fiber at the same time, eliminating most of the waveguide delay dispersion.<sup>(3)</sup>

One of the main disadvantages of the graded index fiber is that the coupling efficiency between the source and the fiber is considerably poorer than that of the step index type. This loss is typically 10 dB for a glass-glass fiber and may be as high as 4 dB for a graded index fiber (see Section 2.5.1).

The main advantage of the graded index fiber is its increased bandwidth, however, as the data rate increases or the length of the link increases, even the graded index may not be suitable. If this occurs, single mode fiber may have to be employed.

#### 2.1.4 Single Mode Fiber

As the core diameter of a stepped index multimode fiber is made smaller (Equation (2.1)), the value of  $v$  becomes smaller. As  $v$  becomes smaller, the number of modes that the fiber can support becomes less. When  $v$  becomes less than or equal to 2.402, the fiber will only support the lowest order hybrid mode  $HE_{11}$ , this mode has no cutoff value of  $v$ . However, as  $v$  decreases below 2.4, more and more of the radiation is forced to propagate in the cladding. This ratio of total power to power in the cladding is given approximately by<sup>(4)</sup>

$$\frac{P_{\text{clad}}}{P_T} = \frac{u_m^{\infty} a}{v}^4 \left(1 - \frac{2}{v}\right) \quad (2.3)$$

where  $u_m^{\infty}$  is the  $m$ th root of the equation  $J_v(u_m^{\infty} a) = 0$   
 $v$  is defined in Equation (2.1)  
 $a$  is core radius of the fiber.

As  $v$  decreases, the amount of light forced into the cladding increases; in the cladding this light is attenuated exponentially. This implies that the value of  $v$  should be as close to 2.402 as possible.

The value of  $v$  is a function of the parameters  $a$  and N.A. Both of these parameters can be varied independently in fiber fabrication so that close tolerances can be held on  $v$ . One practical consideration in reaching this value of  $v = 2.4$  is that if it is increased to reduce source to fiber alignment problems, then the N.A. is decreased. A decrease in the N.A. of the fiber increases the coupling loss between the source and fiber. On the other hand, increasing N.A. to reduce fiber to source coupling loss increases the amount of material dispersion (see Section 2.1.7) and also reduces  $a$ ; hence, increasing the alignment problem. Typical values for single mode fiber are  $a = 2.5 \mu\text{m}$ , N.A. = 0.1 for  $\lambda = 820 \text{ nm}$ .

### 2.1.5 Optical Loss Mechanisms in Fibers

The amount of optical loss in a fiber is related to the amount of material absorption, material scattering, waveguide scattering, and cladding losses present.

The amount of material absorption is directly related to amounts of impurities in the fiber. These impurities such as  $\text{Fe}^{+2}$ ,  $\text{Cu}^{+2}$ ,  $\text{C}^{+3}$ , and  $\text{OH}^-$  have energy bands corresponding to wavelengths in the 0.6 to 1.1  $\mu\text{m}$  range. The light in the fiber interacts with these ions and undergoes photoabsorption. This photoabsorption process causes loss in the fiber. An optical loss curve for the various ions are shown in Figure 2-3<sup>(5)</sup> with their respective concentrations in parts per billion (ppb). Figure 2-4 shows a typical fiber loss curve and the intrinsic scattering limit.<sup>(5)</sup> At the shorter wavelength most of the optical attenuation in the fiber is caused by the drawing process itself. During this process, local color sites are formed (dark spots in the glass) where photoabsorption occurs. These sites are caused by the  $\text{SiO}_2$  bonds breaking. The drawing induced loss effects are usually limited to the region below 750 nm; and can be reduced by either increasing the water content of the glass during drawing or heat treatment (annealing) afterwards. Between the wavelengths of 0.75  $\mu\text{m}$  to 0.90  $\mu\text{m}$  most of the optical attenuation in the fiber is caused by metallic ions, while at the higher wavelength the most significant loss occurs because of the OH-radical.

There are primarily four different types of material scattering mechanisms in the fiber Rayleigh, Mie, Stimulated Raman, and Stimulated Brillouin.<sup>(6)</sup> Rayleigh scattering is always present and is independent of amplitude of the field in the fiber. This loss in a well-made fiber is on the order of 1 dB/km ( $1\lambda^4$ ). Rayleigh scattering is caused by particles which are small compared to the wavelength of light while Mie scattering is caused by inhomogeneities comparable in size to the wavelength of light. Rayleigh is predominately scattering in the backward direction; Mie predominately in the forward direction.

Unlike Rayleigh and Mie scattering, Raman and Brillouin, which are nonlinear scattering effects are field amplitude dependent and can be used to determine the upper limit on the optical input power to the fiber. Below a certain threshold these scattering effects are negligible. For Raman scattering the maximum allowed power is:<sup>(7)</sup>



## IMPURITY ABSORPTION EFFECTS

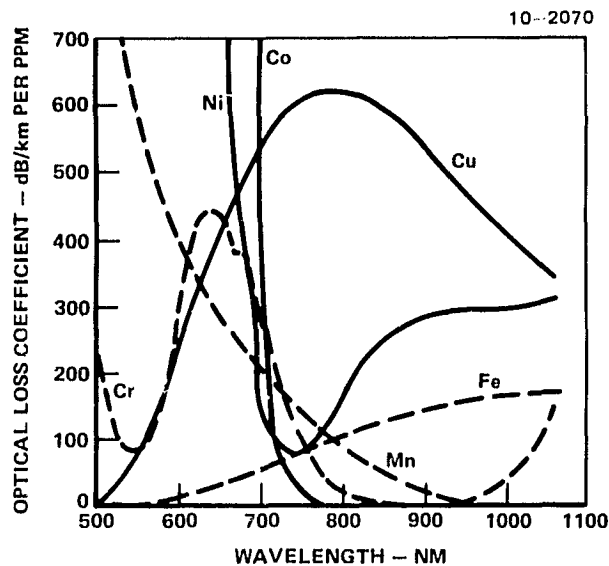
(TEAGER<sup>(5)</sup>)

FIGURE 2-3

## ORIGIN OF LOSS IN OPTICAL GLASS FIBERS

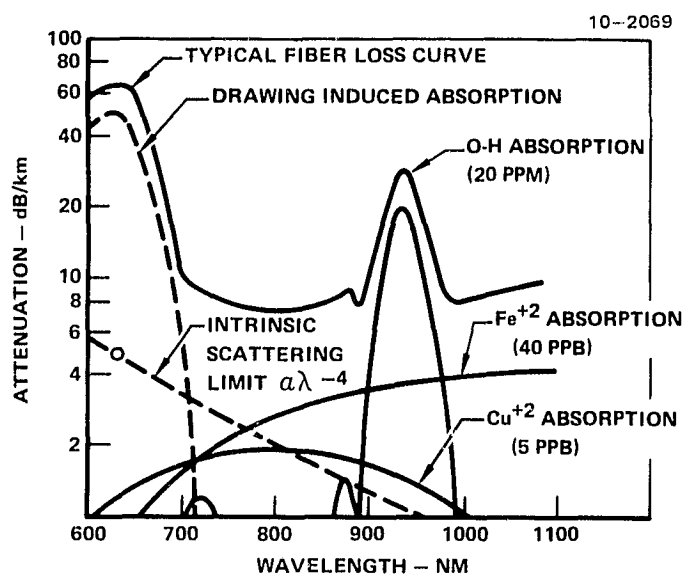
(TEAGER<sup>(5)</sup>)

FIGURE 2-4

$$P_{\max} = 4 \times 10^{-2} \alpha w^2 \text{ watts} \quad (2.4)$$

while for Brillouin it is:<sup>(8)</sup>

$$P_{\max} = 8 \times 10^{-5} \alpha w^2 \Delta\lambda \text{ watts} \quad (2.5)$$

where in Equations 2.4 and 2.5  $\alpha$  is dB loss meter,  $w$  (in microns) is fullwidth at half-maximum power density for the light; and  $\Delta\lambda$  is wavelength spread at the source. Also, Equation 2.4 is for vitreous silica at  $\lambda = 1 \mu\text{m}$ .

In the case of waveguide scattering, the main cause is core size variations in the fiber. At points in the fiber where the core changes size the number of modes that the fiber can support changes, causing modal conversion to take place. In the ideal case, propagation constants for the different modes are coupled in a unique way to insure complete power transfer between modes. In reality, this conversion is never complete, hence, loss occurs and light is radiated into the cladding.

Cladding loss occurs because there is an evanescent wave in the cladding. Unlike the core, which is usually very pure, the cladding has more impurities and because of this, intrinsic attenuation in the cladding and the core are different. Total attenuation in the fiber is given by:<sup>(1)</sup>

$$a_{\text{fiber}} = a_{\text{core}} + \frac{a_{\text{clad}} - a_{\text{core}}}{2 \alpha k (\text{NA})} \quad (2.6)$$

where the  $a$ 's are in dB/km.

#### 2.1.6 Strength Properties of Fibers

One of the more important physical fiber properties is how well it holds up under stress. Generally, the fiber's tensile strength is related to the number of flaws or microcracks present on the surface of the fiber. When the fiber is placed under tensile load, the stress concentration at the microcracks increases many times over the externally applied values. This increase is caused by the crack geometry. If the external stress is not relieved, the flaw starts to propagate (thus becoming a larger microcrack)

with the propagation speed being directly proportional to flaw size. The flaw eventually reaches a critical value (fatigue limit) where the fiber breaks. The environment in which the fiber is placed generally has an effect on fiber tensile strength. These effects are summarized below and are the results of work done at ITT Electro-Optical Products Division.

1. Water is a determining factor affecting the aging characteristics of silica fibers.
2. In plastic coated silica fibers, there is a drastic increase in fatigue resistance below pH=0. Solutions with pH>0 have an effect on fatigue resistance similar to that of water.
3. n, the parameter relating time to failure and applied stress, is dependent on both water concentration and on temperature; and
4. The activation energy of the water reaction with silica is a function of the stress applied to the fiber.

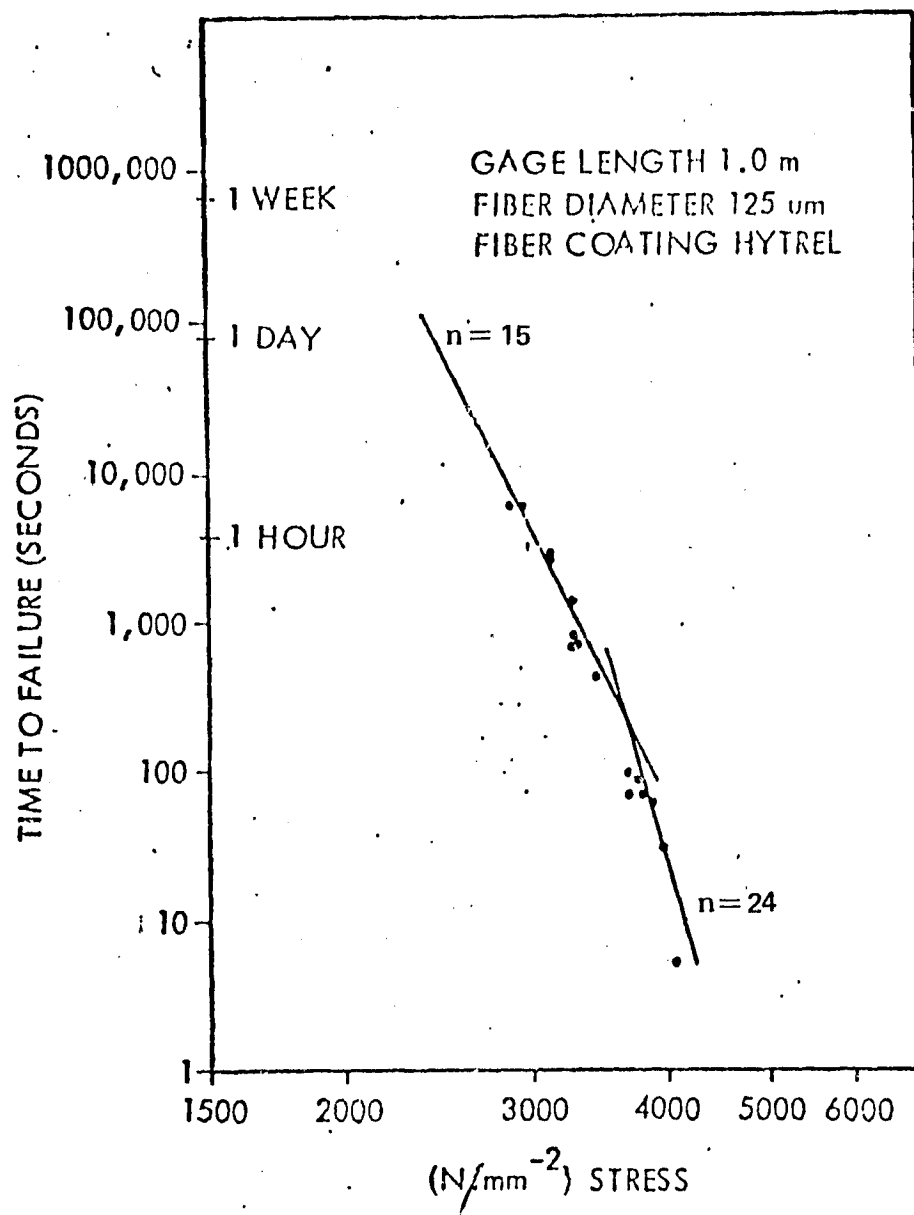
Determining tensile strength on long sections of fiber is an impractical process. Instead, the strength of shorter sections is determined and by extrapolation, the larger lengths. This is accomplished by assuming that fiber strength along its length obeys a Weibal distribution.<sup>(9)</sup>

$$F = 1 - \exp \left( \left( \frac{\sigma}{\sigma_0} \right)^m \left( L/L_0 \right) \left( T/T_0 \right)^b \right) \quad (2.7)$$

Where  $\sigma$  is the critical fast fracture stress,  $\sigma_0$ ,  $L_0$ ,  $T_0$ , m, and  $b=m/n - 2$  are experimentally determined constants. Equation 2.7 can be used to determine the tensile stress of longer length fibers provided enough short samples are used. In general, high strength fibers can be made if high quality starting materials, cleanliness in drawing, proper preform handling, and on-line non-damaging processes to coat the silica fibers with a UV-cured epoxy-acrylate are used.

An interesting aspect of the tensile strength problem is shown in Figure 2-5. This figure indicates that the fiber optic can withstand large stress forces for short periods of time but won't hold up under small forces for long periods. This leads to problems in permanent installation of fiber systems; any tension on the fiber will eventually lead to its failure.

## TIME TO FAILURE VS STRESS



(ITT)

FIGURE 2-5

### 2.1.7 Temporal Dispersion in Fiber Optics

The amount that an optical pulse spreads (in time) as it travels down a fiber is related to the amount of material dispersion, waveguide delay, and multi-mode group-delay present in the fiber. If the amount of dispersion is large, it may set the upper limit of the information rate for the fiber system. A rough order of magnitude estimate of the overall fiber system risetime may be made by using:<sup>(10)</sup>

$$t_r = 1.1 (\sum_i t_i^2)^{1/2} \text{ sec} \quad (2.8)$$

where  $t_i$  are the individual risetimes of the electrical elements and the fiber. The fiber risetime may be computed from vendor's specs by multiplying the dispersion given in ns/km by the length of the fiber.

The magnitude of dispersion is related to the kind of fiber, with single mode fibers having the least followed by graded index and finally step index fibers. The cause of material dispersion is the index of refraction of the core is not, in general, a constant but varies with the wavelength of light. Hence, an LED which contains many different wavelengths of light has much more material dispersion (typically 3.5 ns/km) than ILD. The cause of waveguide delay distortion is that for a given mode of radiation, the wave arrives at the end of the fiber at different times depending on the wavelength, while multimode group-delay spread is caused by the variation in group delay among the propagating modes at a single frequency.

If the material dispersion characteristics of the core and the cladding for a stepped index fiber are similar, the total fiber delay (dispersion) may be expressed approximately by:<sup>(4)</sup>

$$\tau = \frac{1}{c} \{N_1 + (N_1 - N_2) \frac{m}{M}\} \text{ m/s} \quad (2.9)$$

where

$$N_1 = \frac{d(kn_1)}{dk}$$

$$N_2 = \frac{d(kn_2)}{dk}$$

$$k = \frac{2\pi}{\lambda}$$

$$c = 3 \times 10^8 \text{ m/s}$$

$$m = \text{mode designation number}$$

$$M = \text{is maximum that } m \text{ can assume}$$

If the fiber is single mode and the source has a finite bandwidth the approximate expression for the total fiber dispersion is given by<sup>(4)</sup>

$$S \approx \frac{\Delta\lambda}{\lambda} \cdot \frac{1}{c} (A + B) \quad \text{s/m} \quad (2.10)$$

where  $\Delta\lambda$  is bandwidth of source (nm)  
 $\lambda$  is center wavelength of the source (nm)  
 $A$  material dispersion term  
 $B$  waveguide effect term

For a good single mode fiber the value of  $A$  is 0.05 while  $B$  is on the order of 0.0030 hence most of the dispersion is caused by material effects.

If the source is a laser diode centered at 850 nm with a .2nm spectral bandwidth then from equation (2.9)

$$S \approx \frac{.2}{850} \cdot \frac{1}{3 \times 10^8} \cdot [0.05] = 4 \times 10^{-5} \text{ ns/km.} \quad (2.11)$$

A value of  $4 \times 10^{-5}$  ns/km dispersion indicates that tens of kilometers length data link are possible at GHz rates without repeaters.

The approximate amount of dispersion present for a multimode stepped index fiber as a function of source bandwidth is given by<sup>(4)</sup>

$$S \approx \frac{\Delta\lambda}{\lambda_0} \cdot \frac{1}{c} \left\{ \frac{k}{dk} \frac{dN_1}{dk} - 2(N_1 - N_2) \frac{m}{M} \right\} \quad (2.12)$$

The second term in Equation (2.12), which is the multimode dispersion term, usually dominates for step index fibers glass-glass fibers. Typically, the glass-glass fibers have Temporal dispersion which is on the order of a few tens of ns/km. Although this figure is quite good when compared to conventional wire systems there are 5 orders of magnitude difference between the dispersion present in the stepped index fibers as compared to that of the single mode fibers. The penalty paid in using a single mode fiber in a communication system is severe, increased loss at source fiber interface, mechanical alignment problems, etc. With the development of the graded-index profile fiber, most of the waveguide and multimode dispersion effects have been eliminated. The amount of dispersion present on a well-made graded fiber is  $\sim 2.5$  ns/km.

#### 2.1.8 Radiation Properties of Fibers

The effect that radiation has on fibers depends on the type of fiber used and the amount and kind of radiation present. The most damaging radiation to fibers being gamma radiation. The main cause of space radiation is the Van Allen Radiation Belt. This radiation is trapped, being centered about the geomagnetic equator of the earth. The belt is usually broken into two regions: the inner region, located between 100 to 5,000 miles above the earth and extending approximately  $40^\circ$  on each side of the earth's equator and the outer region, located 3,000 to 20,000 miles above the earth and extending  $60^\circ$  on each side of the equator. The inner region's radiation consists mainly of protons and low-energy electrons while the outer region's radiation is primarily electron.

There is also the possibility that space fiber systems will be exposed to neutron and gamma rays from nuclear reactions in the spacecraft. This radiation consists of fast neutrons and high-energy gamma rays. Fast neutrons are those with high kinetic energies, while high-energy gamma rays are electromagnetic radiation (photons) which travel at the speed of light. The gamma ray is physically identical to an x-ray except for origin.

The quantity used to characterize the amount of radiation is called a RAD. (Roentgen-Absorbed-Dose) which is defined by:

$$1 \text{ RAD} = \text{absorption dose of } 100 \text{ erg/g (material)}$$

Since the RAD is a measure of energy absorption for a given material, the material must be specified each time a dose is given. The following conversion may be used to obtain the relationship between the various damaging particles.

$$1 \text{ rad(Si)} = 3.0 \times 10^7 \text{ electrons/cm}^2 \text{ at 1 MeV (electrons)}$$

$$1 \text{ rad(Si)} = 1.0 \times 10^6 \text{ protons/cm}^2 \text{ at 1 MeV (protons)}$$

$$1 \text{ rad(Si)} = 3.0 \times 10^{10} \text{ neutrons/cm}^2 \text{ at 1 MeV (neutrons)}$$

$$1 \text{ rad(Si)} = 2.2 \times 10^9 \text{ photons/cm}^2 \text{ at 1 MeV (photons)}$$

It has been shown by Walkins and Barsis<sup>(11)</sup> that the effect that a dose of neutrons or electrons has on a fiber is the same as an equivalent dose of gamma radiation using the above conversion factors. Figure 2-6 shows the excess loss of fiber's irradiated with <sup>60</sup>Co radiation as a function of total dose. The results are valid for only low dose rates and do not apply for high rates where transient effects introduce severe losses. Generally, space avionics systems are not expected to operate in environments where a large pulse of short duration radiation is present; however, it has been shown by Skoog<sup>(12)</sup> that the fiber gamma radiation may be treated as a linear system. Thus, if the response of the fiber is known to an impulse of radiation then the results of any other shaped radiation pulse may be determined by convoluting the impulse response with the pulse whose radiation response is under question. The impulse response for a number of fibers to a 3700 rad dose (Si) delivered in 3 nsec is shown in Figure 2-7. Generally, when the fibers are exposed to a pulse of radiation they superfluoresce for a short time. If they are glass-glass fibers, they become very lossy and then gradually (sometimes) return to their intrinsic value. If they are PCS fibers, the initial loss is not quite as high as the glass fibers.

There also is a strong dependence on wavelength with radiation induced optical attenuation. This is shown in Figure 2-8 for glass-glass fiber. The longer the wavelength (up to about 1.2μ) then the better the radiation response of the fibers.



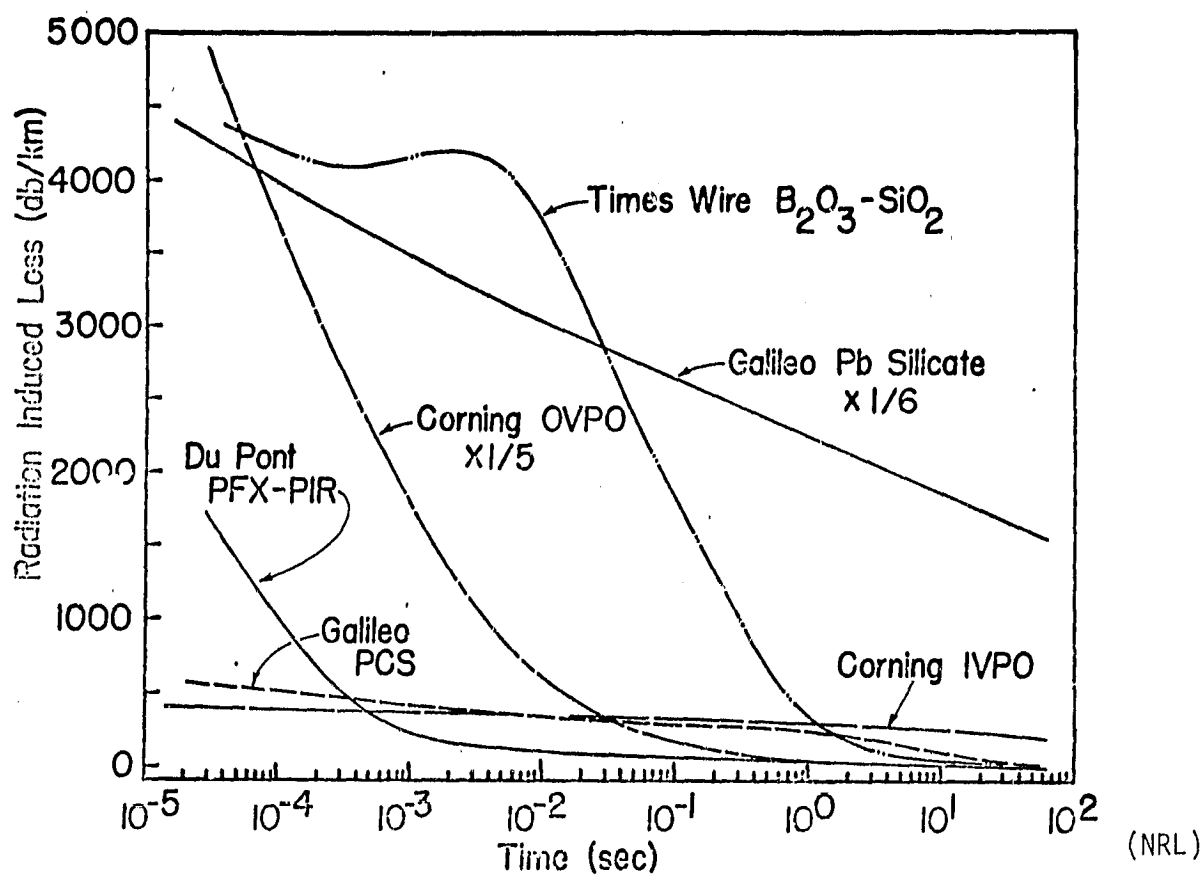


FIGURE 2-6

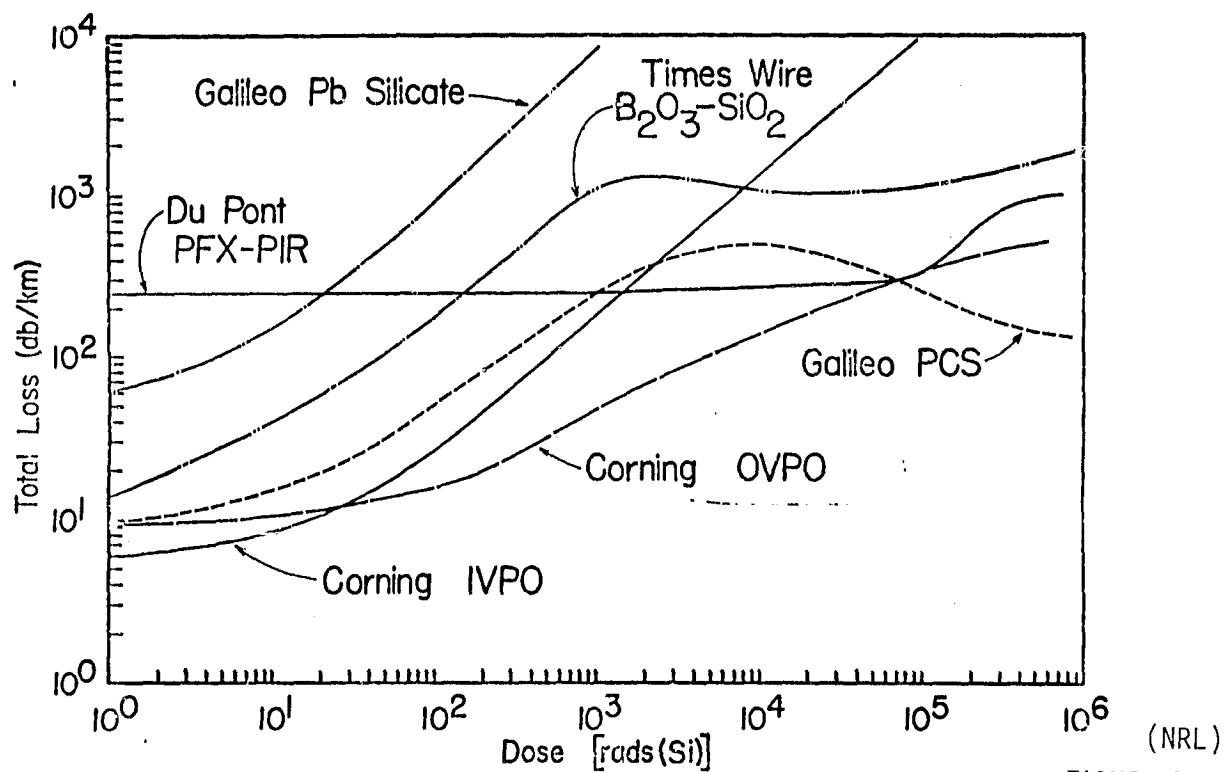
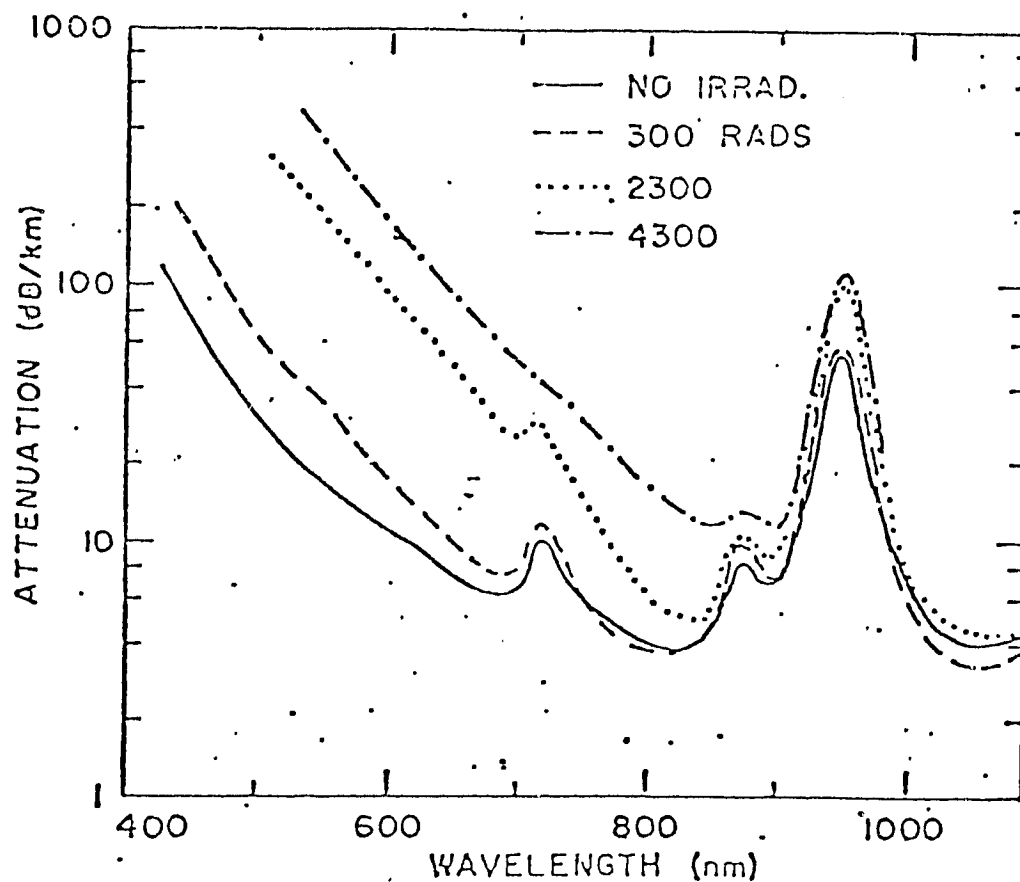


FIGURE 2-7

## FIBER RESPONSE TO RADIATION



(SANDIA LABORATORIES)

FIGURE 2-8

### 2.1.9 Summary and Vendor Tables

The selection of an optical fiber depends on the transmission distance, bandwidth or data rate, and fiber-source compatibility. The attenuation per kilometer (dB/km) will limit the transmission distance. High attenuation fibers such as Dupont's all plastic fibers can be used only on short runs (>100m), while low attenuation fibers such as the ones made by Corning and IT&T which are in the range of 10 dB/km or less can be used up to 1 km with bandwidths of 500 MHz. The bandwidth can be used to calculate the maximum transmission of data, although bit error rates will have to be calculated in order to give a more precise limit to the number of bits/sec. In general, step index fibers can handle data rates up to 50 MB/s with lower dispersion, graded index fibers up to 500 mb/s. Pulse spreading, which limits bandwidth, depends on the spectral width of the source as well as the material dispersion in the fiber.

Fiber source compatibility can be considered to include wavelength similarity, risetime, and numerical aperture. Normally, the wavelength accompanying an optical fiber will be the wavelength in which the attenuation is the lowest and should, but not necessarily, match the LED wavelength. The risetimes of the fiber and LED should be approximately equal. Finally, the numerical aperture (N.A.) should be as large as possible for the best coupling. High loss cables typically have a high N.A. of 0.5 or more, medium and low loss fibers have lower numerical aperture (typically 0.5 to 0.1), but the information carrying capacity as higher. With both step index and graded index fibers, dispersion increases with higher values of N.A. putting a practical limit on the use of high numerical apertures to increase coupling efficiency.

Various manufacturers produce an assortment of optical fibers made up of a variety of materials and dopants. All plastic fibers (Dupont) which are low in cost and high attenuation have both a plastic core and plastic cladding. Plastic clad fibers made by IT&T, Voltec, and Galileo have an outer plastic coating to increase the stability and mechanical strength of the fibers, a plastic cladding and a fixed silica core; both all-plastic and plastic clad silica fibers are step index. Nearly all manufacturers make a glass core with a glass cladding which may be either step or graded index. Recently, prices have become similar for all varieties of optical fibers. One should

be aware that various dopants (boron, phosphorus, and germanium) are used and these affect the degree to which a fiber is considered radiation hardened, while a thorough discussion is beyond the scope of this report, a designer confronted with the problem should make himself familiar with the various published papers on the subject.

The selection of the optical cables depends, in large part, on the environmental conditions of the application, such as whether a cable will be laid out in the field or used inside a structure such as an aircraft. IT&T cables are extremely rugged and have been selected for field applications where vehicles will run over the cable. Nearly all cables can be used for the second application, and in extreme cases aluminum conduit can be used to cover the cable (Valtec). Also some companies (Dupont) limit cable sizes to one or two fibers, while others (Corning) restrict cables to even numbers of fibers. However, most companies will design a cable to fit the designer's need, often the extra fiber can become very useful when unsuccessful terminations occur. Note also that flexible, high tensile strength, metal or plastic strength members are usually included inside the cable. The designer has other considerations such as bending losses when the optical fibers are flexed beyond a certain point, temperature effects, tensile strength, and crush resistance, all of which need to be considered but are not often given on the spec sheet. Tables 2-1 and 2-2 give a list of the major manufacturers, and a list of the optical fibers and their parameters.

## 2.2 SOURCES

Two semiconductor devices offer the most promise as optical sources for aerospace optical data bus systems. These sources are light emitting diodes (LED's) and double heterojunction stripe geometry laser diodes (ILD). LED's have been available for several years while the stripe geometry laser diodes are a relatively new device.

### 2.2.1 Light Emitting Diodes and Injection Laser Diodes

Light emitting diodes, suitable for application to data bus systems, are noncoherent light sources operating in the near infrared range of 800-950 nm wavelength. The semiconductor chip configuration for high radiance LED's are

TABLE 2-1  
OPTICAL FIBER COMPARISON

COMPANY	PART #	FIBER TYPE	dB/Km	RADIATION HARDENING	CORE DIAM. $\mu$ m	FIBER DIAM. $\mu$ m	N.A.	AVAILABLE	FIBER COST /M	INDEX PROFILE	CABLING COMMENTS
GALILEO	3000	GLASS	60	?	56	68	.66	YES	.85	STEP	o PRELIMINARY SINGLE FIBER SUPPLIER, CAN SUPPLY 7,19 FIBER BUNDLES.
GALILEO	4000	PCS	20	FAIR	20.3	22.9	.48	YES	1.00	STEP	
GALILEO	5000	GLASS	10	GOOD	60	125	.20	YES	1.00	STEP	
GALILEO	6000	GLASS	10	GOOD	60	125	.20	YES	1.00	GRADED	
VALTEC	MG05	GLASS	10	FAIR	65	125	.23	YES	1.00	GRADED	o AVAILABLE IN 1,7,19 FIBER CABLES o CUSTOM-DESIGN BUNDLES AVAILAB
VALTEC	PC-05	PCS	40	FAIR	125	200	.3	YES	1.00	STEP	
VALTEC	PC-10	PCS	15	FAIR	250	430	.3	YES	1.00	STEP	
DUPONT	PFX-S	PCS	50	FAIR	200	600	.4	YES	9.00/M	STEP	SINGLE FIBER
CORNING	10020	GLASS	10	GOOD (1)	63	125	.21	YES	.65/M	GRADED	o AVAILABLE IN 1,2,4,6,8,10 FIBER CABLES
CORNING	4080 4040	GLASS	4	GOOD	63	125	.21	YES	2 1.75	GRADED	
CORNING	5040	GLASS	5	GOOD	63	125	.21	YES	1.5	GRADED	o PRIMARILY GLASS-GLASS FIBER TECHNOLOG
CORNING	6080 6060 6040	GLASS	6	GOOD	63	125	.21	YES	1.6 1.5 1.3	GRADED	
CORNING	8080 8040	GLASS	8	GOOD	63	125	.21	YES	1.6 1.04	GRADED	
CORNING	8020	GLASS	8	GOOD	63	125	.21	YES	.75	GRADED	
IT&T	T-102	GLASS	8	GOOD	55	125	.25	YES	.65/M	STEP	o STANDARD 1,7,19 FIBER CABLES SUPPLIED o EXPERIENCED IN CUSTOM CABLE CONFIGURATIONS
IT&T	T-202	GLASS	8	GOOD	55	125	.25	YES	.75/M	GRADED	
IT&T	T-212	GLASS	8	GOOD	55	125	.25	YES	.75/M	GRADED	
IT&T	T-303	PCS	10	FAIR-GOOD	125	500	.3	YES	.55/M	STEP	

TABLE 2-2  
COMPARISON OF VARIOUS FIBER OPTIC CABLES

Company	Fiber Part Number	Tensile Strength	dB Loss	Can be Radiation Hardened	Connector Parts Number	Availability of Cable	Cost	Number of Fibers	Crush Resistance
11leo	5000	110 lbs	10-20dB/Km	Yes	Developmental	Developmental	\$1/m \$2.08	1 7	5 ft-1b
11leo	4000	110 lb	50-100dB/Km	Yes	Developmental	off-the-shelf	\$1.05/m \$1.57/m	1 7	5 ft-1b
11leo	3000	110 lb	50-100dB/Km	No	Amphenol 905-119-5009	off-the-shelf	\$ .92/m \$1.43/m	1 7	5 ft-1b
1tec	PC-05	150 lb	30dB/Km	Yes	Amphenol 905-119-5011	off-the-shelf	\$5.50/m	7	Not Available
1tec	PC-10	150 lb	15dB/Km	Yes	Not Available	off-the-shelf	\$2.00/m	1	Not Available
Pont	PFX-P240R	180 lb	1000dB/Km	Yes	Not Available	off-the-shelf	\$3.30/m	2	Not Available
Pont	PFX-P140R	80 lb	1000dB/Km	Yes	Not Available	off-the-shelf	\$2.30/m	1	Not Available
Pont	PFX-S120R	110 lb	30dB/Km	Yes	Amphenol 905-119-5022	off-the-shelf	\$4.00/m	1	Not Available
orning	Strengthened Siecor	80-200 lb	10dB/Km	Yes	Corning Metal Connector	off-the-shelf	\$2.9/m	1	1 ft-1b
Company	Fiber Part Number	Tensile Strength	dB Loss	Can be Radiation Hardened	Connector Parts Number	Availability of Cable	Cost	Number of Fibers	Crush Resistance
orning	Strengthened Siecor	80-200 lb	10dB/Km	Yes	Corning Metal Connector	off-the-shelf	\$5.60/m	2	1 ft-1b
orning	Strengthened Siecor	80-200 lb	10dB/Km	Yes	Corning Metal Connector	off-the-shelf	\$13.50/m	6	1 ft-1b
orning	Strengthened Siecor	80-200 lb	10dB/Km	Yes	Corning Metal Connector	off-the-shelf	\$17/m	8	1 ft-1b
orning	1300 1302	110 lb	10-20dB/Km	Yes	Amphenol 905-119-5018	Short supply	\$10/m \$13.5/m	7	1 ft-1b
T&Tannon	Strengthened	400 lb	10dB	Yes	Developmental	off-the-shelf	\$10/m	7	3-5 ft-1b

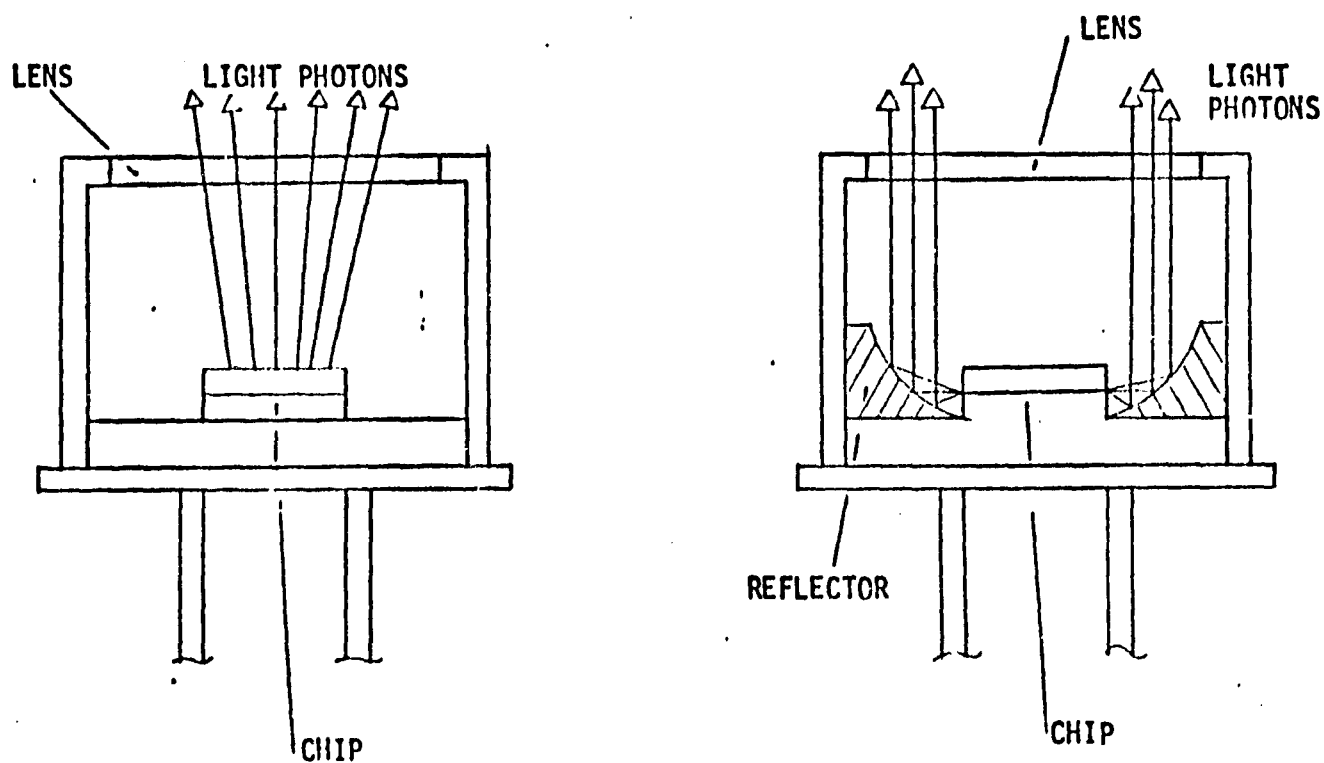
of two types: the surface emitter (Burros type) and the edge emitter. Examples of the surface and edge emitters are shown in Figure 2-9. The surface emitter can generate more optical power than the edge emitter but, because of the wider beam angle, it is difficult to couple the light from the surface emitter into optical cables having low numerical apertures. By utilizing a lens on the LED or the cable, or by employing high numerical aperture fibers, the coupling efficiency from surface emitters may be increased.

Both surface emitting and edge emitting LED's provide several milliwatts of output power at drive currents of 50-200 milliamperes. Figure 2-10 shows the output power as a function of drive current for the RCS SG 1009A.

Double heterojunction stripe geometry laser diodes emit coherent light in the 800-900 nm wavelength range. The laser diode emission is in a narrow beam which permits efficient coupling to low numerical aperture fiber cables. Optical power outputs in excess of 10 milliwatts for drive currents of a few hundred milliamperes are possible. Figure 2-11 shows the output power as a function of drive current for the RCA C30130 AlGaAs laser diode. The dashed line in Figure 2-11 denotes the threshold current. For drive currents below the threshold level the optical output is noncoherent light and above the threshold level the output is coherent light.

Table 2-3 presents a comparison of typical LED's and laser diodes for several operational parameters. The output power for laser diodes is greater than that of LED's; however, the laser diodes require higher drive current. In laser diodes, the drive current must be above the threshold level (usually 100 mA or higher) before the light emission becomes a coherent signal. For drive currents less than the threshold level, the output is noncoherent and the efficiency of the laser diode is quite low. The quantum efficiency of laser diodes is about twice that of LED's provided the laser diode is operating above the threshold current. The most efficient laser diode operation is at drive currents of twice the threshold level.

LED EMITTER CONFIGURATIONS



(a) SURFACE EMITTER

(b) EDGE EMITTER

FIGURE 2-9



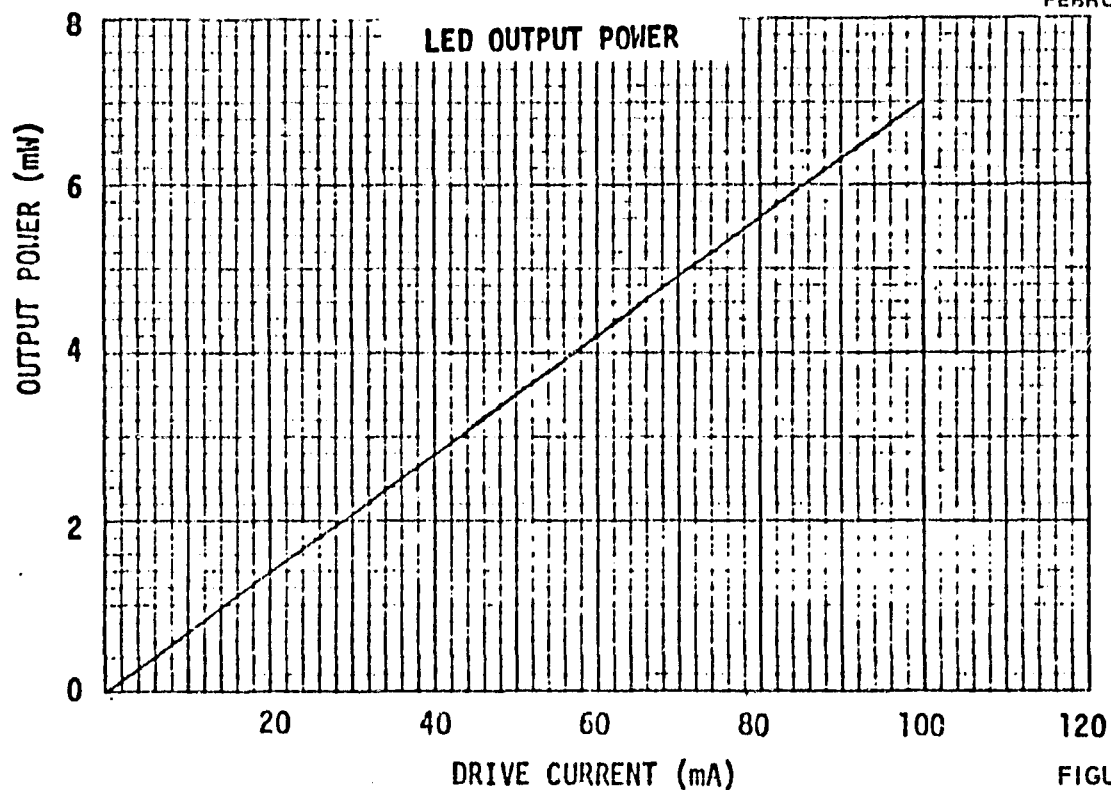


FIGURE 2-10

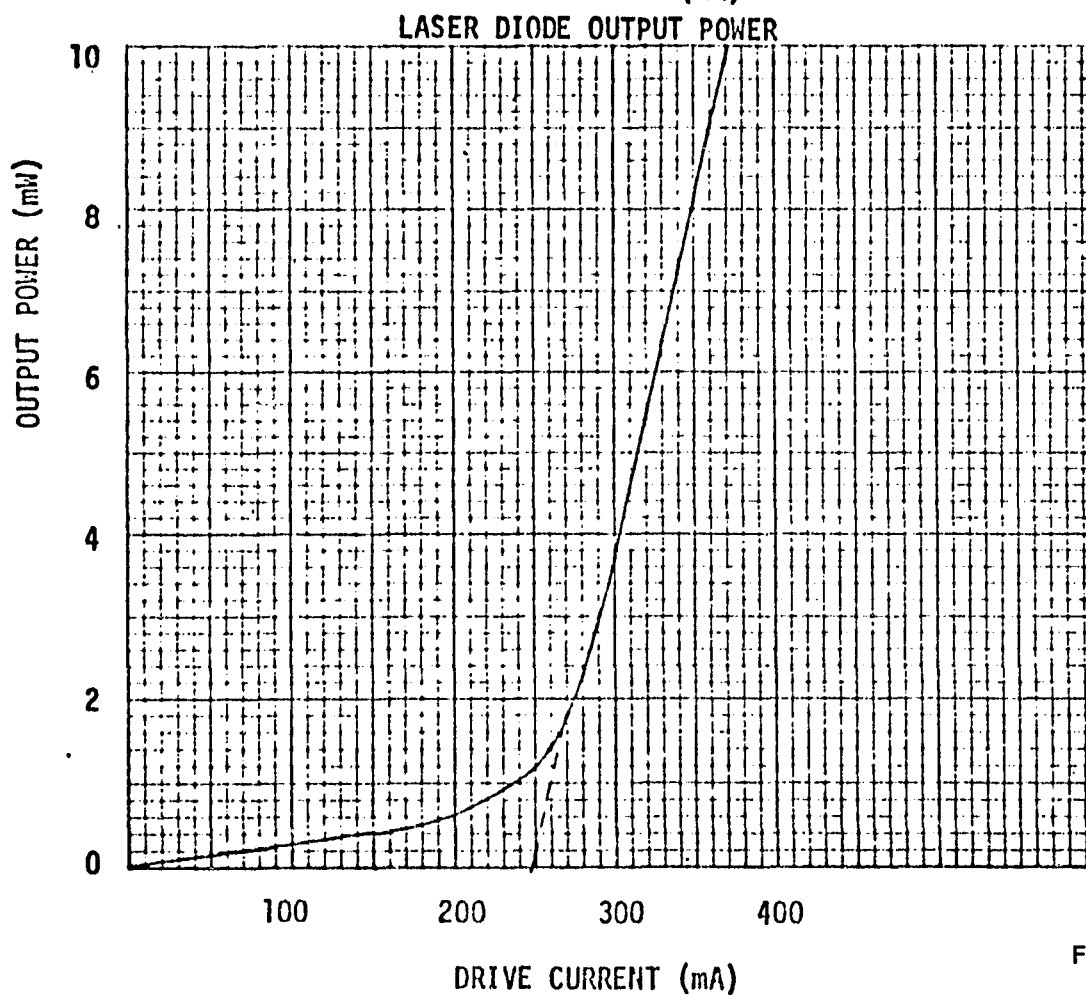


FIGURE 2-11

TABLE 2-3  
OPERATIONAL PARAMETERS

PARAMETER	LED	LASER DIODE
OUTPUT POWER	1 - 7 mW	5 - 15 mW
DRIVE CURRENT	50 - 200 mA	100 - 500 mA
QUANTUM EFFICIENCY	3%	8%
OUTPUT WAVELENGTH	800 - 950 nm	800 - 900 nm.
SPECTRAL WIDTH	20 - 40 nm	1 - 3 nm
EMISSION ANGLE	10° - 65°	1 - 5°
LIFE (HI TEMP)	10,000 HOURS	1000 HOURS
FREQUENCY RESPONSE	<200 MHz	>1 GHz
TEMPERATURE EFFECTS	.6%/°C	1.2%/°C

Both LED's and laser diodes generate signals in the 800-950 nm wavelength. The spectral width of the laser diode signal is an order of magnitude narrower than that of the LED. Narrow spectral width is important at very high data rates and for long transmission distances in order to prevent bit dispersion effects from becoming a significant problem.

For surface emitting LED's the intensity of the emission is nearly Lambertian. The intensity of the emission at any point depends upon the cosine of the angle between that point and the axis perpendicular to the surface of the emitter. By using lenses or edge emitting configurations, the emission pattern of LED's can be compressed. Figure 2-12 shows the Lambertian distribution (dashed line) and the actual distribution of an edge emitting LED. For the example shown in Figure 2-12, the half-power emission angle is  $30^\circ$  and the angle that includes 90% of the emitted power is  $60^\circ$ ; for efficient coupling, the fiber used with this LED should have an acceptable half-angle of at least  $30^\circ$  and preferably  $60^\circ$ .

The emission pattern for stripe geometry laser diodes is elliptical. The beam spread in the plane perpendicular to the junction plane is generally between  $10^\circ$  and  $30^\circ$  and the beam spread in the plane parallel to the junction plane is between  $3^\circ$  and  $10^\circ$ . The narrow beam permits efficient coupling of the laser diode output to low numerical aperture fibers. An illustration of the emission pattern of a laser diode is shown in Figure 2-13.

While the frequency response of laser diodes is an order of magnitude faster than that of LED's, both laser diodes and LED's are capable of accommodating the data rates found on aerospace vehicles. Both LED's and laser diodes can be directly current modulated.

The deleterious effects of temperature changes upon laser diodes is twice that of LED. With both laser diodes and LED's, the wavelength and output power change with temperature; however, with laser diodes the change is greater. In addition, the threshold current of laser diodes increases with high temperature. If the junction temperature of the laser diode increases without a corresponding increase in drive current, the light output of the diode will cease to be coherent.

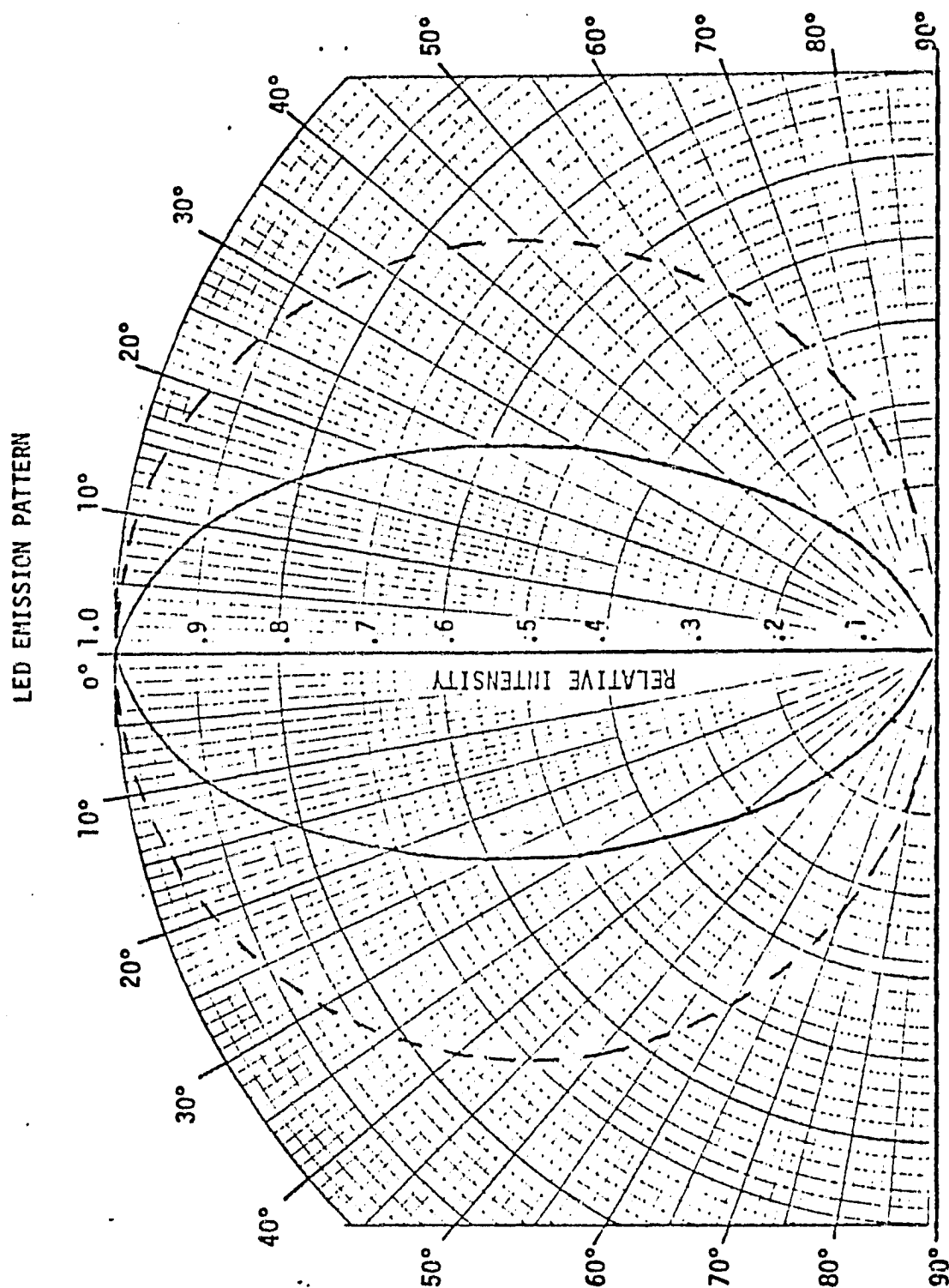


FIGURE 2-12

LASER DIODE EMISSION PATTERNS

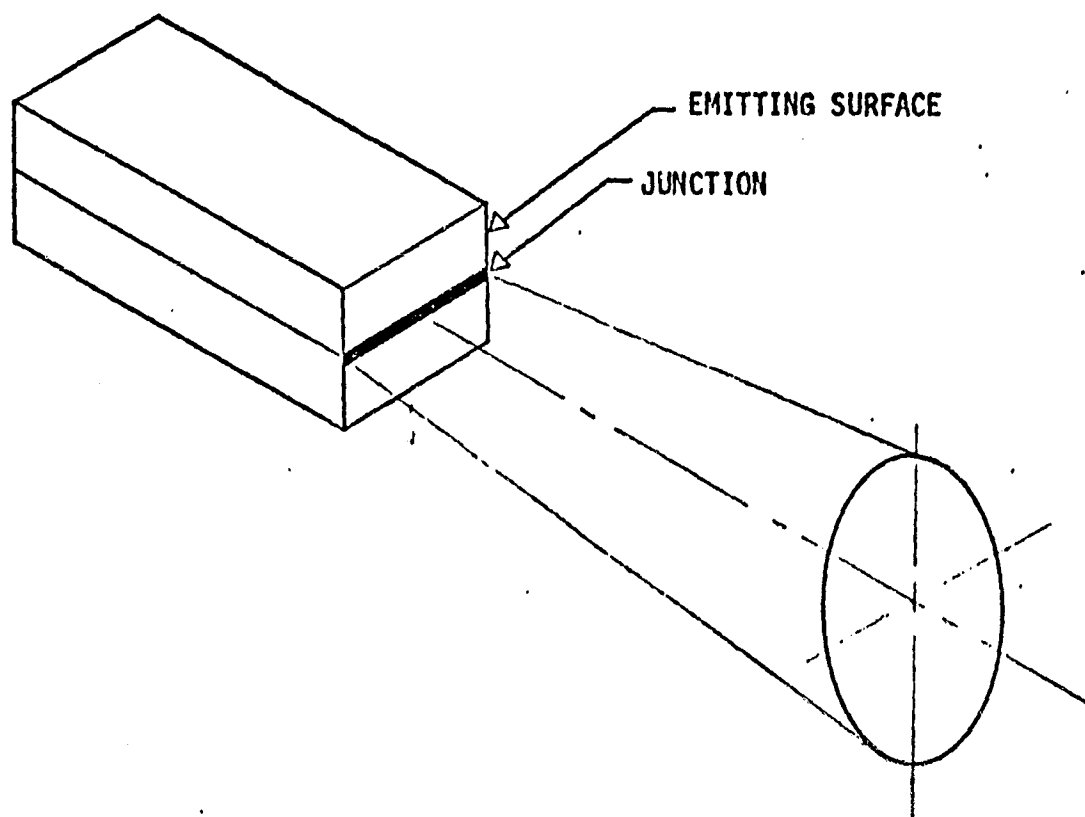


FIGURE 2-13

In summary, laser diodes offer higher power and more efficient coupling to low loss fibers than do LED's, but laser diodes suffer from shorter lifetimes and poorer temperature characteristics. For applications in the near term, LED's appear to be the best choice as an optical source. When the mean life of laser diodes can be extended, they will be the best source for aerospace data bus applications. The problems associated with temperature effects can be overcome by monitoring the case temperature of the laser diode and controlling the drive current as a function of case temperature. Alternately, the intensity of the output can be monitored and the drive current controlled to provide a constant intensity output.

### 2.2.2 Lifetime of Devices

The reliability of LED's and laser diodes operating at elevated temperature (70°C) is not as good as would be desirable. In the above environment, the mean life of a typical LED is about 10,000 hours and that of a laser diode is about 1,000 hours. By way of comparison, the mean life of a silicon NPN transistor is approximately 1,000,000 hours. Laser diodes have two failure modes: catastrophic failures and gradual degradation. The catastrophic malfunctions are usually facet failures caused by the intense optical fields. The facet damage is usually material disassociation or facet cracking. For laser diodes, gradual degradation is usually an increase in the threshold current and a decrease in the quantum efficiency. The result is a decrease in the power output for a given current density. For LED's, gradual degradation is a reduction in the externally measured quantum efficiency of the device. In both LED's and laser diodes, the reduction of quantum efficiency is caused by the formation of nonradiative centers within the recombination region and an increase in the internal absorption coefficient. An important characteristic of the degradation process is that it is highly dependent upon the type of semiconductor, the degree of perfection of the material, and the methods used to fabricate and assemble the device. Manufacturers are concentrating their efforts to improve device reliability in the areas of material perfection and assembly techniques.

### 2.2.3 Table of Sources and Contract Summary

Table 2-4 lists the salient characteristics for several models of LED's and laser diodes. Since the stripe geometry laser diode is a relatively new item,

TABLE 2-4  
SOURCE CHARACTERISTICS

SUPPLIER	MODEL	TYPE	WAVELENGTH (nm)	OUTPUT POWER (mW)	DRIVE CURRENT (ma)	RISE TIME (nsec)	3 dB EMISSION ANGLE	DUTY CYCLE	OPERATING TEMP °C	EMITTING SURFACE AREA
LASER DIODE	IRE #10	LED	940	20	400	400	10°	CW	-65 to 100	.195" dia
LASER DIODE	IRE #150	LED (EDGE)	820	1.5	100	7	*	50%	MAX +50	9 x 9 mils
RCA	SG 1009A	LED	940	7.0	100	900	8°	CW	-40 to 125	.155" dia
RCA	C30119	LED (EDGE)	850	0.5	200	3	30°	CW	-40 to 90	1 x 6 mils
RCA	C30123	LED (EDGE)	830	1.0	200	8	30°	CW	-40 to 90	1 x 6 mils
MERET	MLT 327	LED	940	4.0	20	15	50°	50%	*	.5 x .5 mm
MERET	MLT 345	LED	940	10	40	40	*	50%	*	1 x 1 mm
MERET	MLT 330N	LED	940	2.5	100	12	25°	50%	*	.5 mm dia
MERET	MDL 100	LED	905	1.0	100	12	*	50%	*	.5 mm dia
SPECTRONICS	SPX 1775	LED (EDGE)	907	2.0	100	20	15°	CW	-65 to 125	40 mil dia
SPECTRONICS	SPX 1527	LED	905	.75	50	20	10°	CW	*	18 mil dia
MOTOROLA	MLED 910	LED	900	.55	150	10	24°	CW	*	*
TI	SL 1314	LED	905	2.0	50	15	20°	CW	*	*
TI	TXL 471	LED	910	1.0	50	20	65°	CW	-65 to 100	18 mil dia
GALILEO	3555971T	LED	905	2.0	40	40	10°	CW	*	39 x 89 mils
LITONIX	LR 410	LED	900	1.5	100	1	35°	CW	*	*
MONSANTO	ME4	LED	900	1.0	100	1	38°	CW	*	*
LASER DIODE	LCW 10	GaAlAs Laser Diode	850	14	300	.1	3°	CW	MAX +65	.01 x 5 mils
RCA	C30130	GaAlAs Laser Diode	820	15	500	1	5°	CW	-35 to +50	13 x 2 $\mu$ m
RCA	C30127	GaAlAs Laser Diode	820	5	300	1	5°	CW	-35 to +50	13 x 2 $\mu$ m
LASER DIODE	LCW 5	GaAlAs Laser Diode	850	7	300	.1	3°	CW	MAX +65	.01 x 5 mils

\* DATA NOT AVAILABLE

few data sheets are available for this device. Most of the information about this type of laser diode has been gathered from magazine articles and papers.

### 2.3 PHOTODETECTORS FOR FIBER SYSTEMS

Photodiodes (PIN diodes) and avalanche photodiodes (APD's) are the two candidate devices for detectors in the optical data bus system. PIN diodes and APD's are light-sensitive devices which offer wide spectral range, fast response time, high sensitivity, and low noise. As the name implies, avalanche photodiodes have a built-in gain mechanism that results in higher signals from these devices than from PIN diodes.

#### 2.3.1 General Characteristics of Photodetectors

Two common light detectors in fiber receivers are silicon PIN photodiodes and avalanche photodiodes (APD). Other types of detectors can be used; however, they have the disadvantages of size, power, or low sensitivity. The acronym PIN signifies a P-region followed by an intrinsic region I (this region is such a lightly doped N region that it is essentially intrinsic, i.e., the conductivity is characteristics of pure undoped material) and this is followed by an N region providing a good ohmic contact for lead wire. Although the APD has better noise properties than the PIN it has many disadvantages such as being greatly affected by small changes in temperature, requiring a bias supply voltage as high as 230 volts, and being relatively expensive.

To measure the relative "goodness" of solid-state detectors, a number of different specifications have been developed over the years. Some of the more important terms and their definitions are:

#### (a) Responsivity Limits

The responsivity of the receiver is the output of the unit in either amps or volts for the signal per unit of radiant power input with typical power units of watts or milliwatts. The quantum nature of the radiation input, along with the receiver gain, limits the maximum responsivity that can be obtained.

For a receiver current gain of G the maximum output current is:

$$I = e \eta \frac{P_o}{h\nu} G \quad (2.13)$$



and the maximum responsivity  $r = I/P_0$  is  

$$r = e \eta G/h\nu$$

where  $e$  is the electron charge,  $(\eta P_0/h\nu)$  is the number of electrons generated per second and  $G$  is the current gain. The quantum efficiency or number of electrons generated per photon is  $\eta$ . For the photodetectors at  $0.9 \mu\text{m}$  each photon has an energy,  $h\nu = 1.4 \text{ eV}$ , that is sufficient to form a hole-electron pair which results in an increased current in the photodiode.

If all photons that are incident are absorbed and each releases one electron that contributes to  $I$ , then  $\eta = 1$ . If only a fraction of the photons are absorbed and release electrons that contribute to the current, then the value of  $\eta$  is less than 1.  $P_0$  is the incident radiant power and  $h\nu$  is the energy per photon ( $1.4 \text{ eV} = 2.2 \times 10^{-19} \text{ joules}$ ). Thus, for a current gain  $G$  of 1, the maximum responsivity for a quantum efficiency of 10% and a wavelength of  $0.9 \mu\text{m}$  ( $h\nu/e = 1.4 \text{ eV}$ ,  $\nu = c/\lambda$ ) is  $r = 0.1/1.4$  which equals 0.7 milliamps per milliwatts. For a  $100\Omega$  resistor, the responsivity in voltage terms is 70 millivolts/milliwatt. By use of a voltage amplification the responsivity at the output can be increased by the gain factor. In case of the avalanche photodiode, the current gain is achieved in the photodiode with typical values ranging up to 100.

#### (b) Noise Limits

The photon nature of the radiation input to the photodetector limits the minimum possible noise as well as the maximum possible responsivity. For an incident power  $P_0$  the number of incident photons per second is  $P_0/h\nu$  and the resulting number of electrons per second is  $\eta P_0/h\nu$ . At a bandwidth of  $\Delta f$  the number of electrons  $N$  collected in a single sample time  $1/2\Delta f$  is  $\eta P_0/(2h\nu\Delta f)$ . The RMS noise in the number  $N$  collected in a sampling period is  $\sqrt{N}$  so the corresponding signal-to-noise ratio is  $N/\sqrt{N}$  or  $\sqrt{P_0}/2h\nu\Delta f$ . The noise equivalent power is the value of incident power,  $P_0$ , that produces a signal-to-noise ratio of one and is equal to  $2h\nu\Delta f/\eta$ . For a quantum efficiency of 0.1, a wavelength of  $0.9 \mu\text{m}$  ( $h\nu = 2.2 \times 10^{-16} \text{ mj}$ ) and  $\Delta f = 10 \text{ MHz}$ , the noise equivalent power is thus equal to  $2 \times (2.2 \times 10^{-16} \text{ mj}) \times 10^7 \text{ Hz}/0.1$  which is  $4.4 \times 10^{-8} \text{ milliwatts}$  ( $-74 \text{ dBm}$ ). The unit dBm refers to dB with respect to 1 milliwatt (the number of dBm =  $10 \log_{10} P$ , where  $P$  is milliwatts). The limiting noise equivalent power corresponds to a quantum efficiency of  $\eta = 1$  and is only

$4.4 \times 10^{-9}$  milliwatts (-84 dBm) for the 10 MHz bandwidth. Although the avalanche type of photodiode can come close to the limiting sensitivity it has many disadvantages such as being greatly affected by small changes in temperature and the requirement for bias supply voltages are as high as 230 volts.

The PIN photodiode does not have the gain of the avalanche diode so it is affected by thermal noise and does not have the high sensitivity of the APD. However, in many systems without excessively long cables, the signal is high enough to permit reasonably large signal to noise ratios using the PIN photodiode.

For large thermal noise, the frequency dependence for the noise equivalent power is a square root rather than the linear relation that is characteristic of quantum noise limited detectors. The signal to noise ratio for large thermal noise is:

$$S/N = \left( \frac{\eta e P_0}{h\nu} \right)^2 / (4 K T \Delta f / R) \quad (2.14)$$

where  $(\eta e P_0 / h\nu)$  is the average mean square signal current and  $4KT\Delta f/R$  is the mean square Johnson thermal noise current in the amplifier load resistance  $R$  at the absolute temperature  $T$ . The value of  $K$ , Boltzmann's constant, is  $1.38 \times 10^{-23}$  joules/degree Kelvin. The noise equivalent power, NEP, per bandwidth root is thus found by setting  $S/N = 1$  and solving for  $P_0/\sqrt{\Delta f}$  to obtain

$$NEP/(\Delta f)^{1/2} = \frac{2h\nu}{\eta_e} \sqrt{KT/R}. \quad (2.15)$$

For  $R = 1 \text{ M}\Omega$ ,  $T = 300^\circ\text{K}$ ,  $\lambda = 0.9 \text{ }\mu\text{m}$  ( $\frac{h\nu}{e} = 1.4 \text{ eV}$ ), and  $\eta = 0.1$  the minimum  $NEP/(\Delta f)^{1/2}$  becomes

$(2/0.1) \times 1.4 \sqrt{1.38 \times 10^{-23} \times 300/10^6}$  which is  $1.8 \times 10^{-12}$  (2.16)  
watts/Hz<sup>1/2</sup>. For a 10 MHz bandwidth, the NEP is thus  $5.7 \times 10^{-6}$  milliwatts. A system which is intermediate between being quantum noise limited and thermal noise limited will have a noise equivalent power that is less than the  $5.7 \times 10^{-6}$  milliwatt value.

Once the noise statistics have been established along with the type of signal coding it is possible to predict the bit error rate (BER) for comparison with the system requirements. Very low bit error rates less than 1 in  $10^9$  are available for commercial fiber optic data systems. The best detection to discriminate against noise is the detection with the highest Q.E., while detector to discriminate against internal noise is the detection with the best NEP.

(c) Detectivity ( $D^*$ )

$D^*$  is related to the NEP by  $D^* = (A)^{1/2}/\text{NEP}$  where A is the effective area of the photodiode, with units of  $D^*$  being  $\text{cm-Hz}^{1/2}/\text{watts}$ .

(d) Risetime

The time the photodiode takes to go between 10% to 90% of its final output voltage when a risetime step wave-form of optical radiation is applied to the light sensitive area. The unit of the risetime is seconds.

(e) Noise Current

This current for a photodiode operating in the reverse bias mode is a combination of shot noise, excess noise, and thermal noise.

(f) Dark Current

The RMS output in amps of the biased solid-state detection with no input or background radiation incident on the detector.

### 2.3.2 Application Considerations

Section 2.3.1 introduced several important parameters for PIN diodes and APD's. This section will discuss some circuit applications for photodetectors.

PIN diodes can consist of either a PN junction or a PIN junction. With the PIN configuration, a large intrinsic region exists between the P and the N materials. As the name implies, the avalanche photodiode has a built-in avalanche gain mechanism that is quite similar to that of a photomultiplier tube. As a result, the responsivity of APD's is much higher than that for PIN diodes. For photoelectric detectors, the responsivity is a measure of the electric current generated per unit of incident optical power. The responsivity of PIN diodes is in the range of 0.4 to 0.65 amps/watt and the responsivity of APD's is in the

range of 20 to 75 amps/watt. Because of the higher responsivity of APD's, receivers equipped with APD detectors can provide the same performance with as much as 20 dB less incident optical power than receivers equipped with PIN photodiode detectors.

The high responsivity of APD's is not an unmixed advantage. The photomultiplier process that provides for the gain of the incident signal also amplifies any optical noise incident upon the detector and also results in higher dark current values for APD's than for PIN diodes. In Table 2-5, the dark current is the amount of current that flows through the detector biasing circuit when no light is incident on the detector. Naturally, the dark current should be as small as possible. If we assume the amplifier that follows the detector is noiseless, then the noise in the dark current is one of the major factors in determining the lower limit of the optical signal that can be detected.

The speed with which a solid-state photodetector responds to incident light signals is determined by the time it takes for the generated electrons and holes to be collected in the diode and the response of any following RC circuits. If the circuits following the photodetector are carefully designed, the only capacitive component will be the junction capacitance of the detector. Figure 2-14 shows the equivalent circuit of a photodetector and its load resistor. The detector is a current source where the amount of current ( $i_p$ ) generated is proportional to the incident flux, the junction capacitance is  $C_d$ , the junction resistance is  $R_S$ , and the load resistor is  $R_L$ . Junction capacity increases as the size of the junction is increased. Thus, as the junction size of the detector is enlarged to provide more efficient coupling from the fiber to the detector, the junction capacitance (and the detector response time) is adversely affected. Junction capacity is also affected by the detector bias voltage. As the bias voltage increases, the junction capacitance decreases. Thus, for high data rates, a high bias voltage is usually required.

In operational photodetector circuits, the series resistance of the detector ( $R_S$  in Figure 2-14) is much smaller than the load resistor  $R_L$ . Typically,  $R_S$  is 100 ohms or less and  $R_L$  is greater than 1000 ohms. The risetime of a photodetector is limited by  $2.2 [C_d R_S R_L]$ . The above equation defines the response

TABLE 2-5

COMPANY HEWLETT PACKARD PIN PHOTODIODES					
MODEL	4203	4204	4205	4207	4220
ACTIVE AREA cm <sup>2</sup>	$2 \times 10^{-3}$	$2 \times 10^{-3}$	$0.5 \times 10^{-3}$	$8 \times 10^{-3}$	$2 \times 10^{-3}$
RESPONSIVITY @ 970nm A/W	.5	.5	.5	.5	.5
DARK CURRENT nano-A	2.0	0.6	.15	2.5	5.0
D* (700, 100, 6) cm Hz <sup>1/2</sup> /W	$8.7 \times 10^{11}$	$6.2 \times 10^{12}$	$4.0 \times 10^{12}$	$1.5 \times 10^{12}$	$5.6 \times 10^{11}$
NEP (700, 100, 6) W/Hz	$5.1 \times 10^{-14}$	$2.8 \times 10^{-14}$	$1.4 \times 10^{-14}$	$5.7 \times 10^{-14}$	$8.1 \times 10^{-14}$
RISETIME ns	1.	1.	1.	1.	1.
NOISE CURRENT amps/Hz <sup>1/2</sup>	$1.2 \times 10^{-14}$	$1.2 \times 10^{-14}$	$4 \times 10^{-14}$	$4 \times 10^{-14}$	$4 \times 10^{-14}$
CAPACITANCE pF	2	2	2	2	2
SENSITIVITY (A/W)	.5	.5	.5	.5	.5
TEMP. RANGE C°	-10 to+80	-10 to+80	-10 to+80	-10 to+80	-10 to+80
SUPPLY VOLTAGE V	50	20	50	20	50

time from the 10% amplitude to the 90% amplitude points for a step input. In vendor device specification sheets the response time is usually quoted for an  $R_L$  equal to 50 ohms. In actual application, the load resistance may be a few orders of magnitude greater than the 50 ohms value and the risetime will be correspondingly slower.

The bias voltage required for photodetectors ranges from a minimum of 10 volts or less for some PIN diodes to 300 volts or more for APD's. For a given device, the level of the applied bias voltage may affect the device's responsivity, dark current, noise equivalent power, and capacitance. Because of their high operating voltages, photodetectors will probably require the addition of an extra power supply.

The noise generated by a reversed bias photodetector is a combination of shot noise and Johnson thermal noise. Photodetector data sheets specify this internal noise as "noise current" or as "noise equivalent power" (NEP). Internal noise is an important parameter because it represents the lower limit of the radiant flux that can be detected. The two components of the noise current, shot noise ( $i_n$ ) and Johnson noise ( $i_j$ ) are statistically independent; thus, the total noise current ( $i_t$ ) is given by the root sum of the square of the two components

$$i_t = \sqrt{i_j^2 + i_n^2} \quad (2.17)$$

The effects of the detector noise current upon the signal to noise ratio of the detector receiver circuit is a function of the bandwidth of the receiver circuit. To make the noise current parameter a useful parameter, the noise current is expressed in terms of receiver bandwidth. Thus, noise current is expressed as

$$i_t = \frac{\sqrt{i_j^2 + i_n^2}}{\sqrt{\text{Hz}}} \quad (2.18)$$

where Hz is the bandwidth of the detector receiver circuit.

The noise equivalent power (NEP) is the value of the incident flux on the photodetector that gives a signal power equal in value to the noise signal. NEP is given by

$$\text{NEP} = \frac{\text{noise current (amps}/\sqrt{\text{Hz}})}{\text{responsivity (amps/watt)}} \quad (2.19)$$

In designing an optical data bus, the first step is, usually, to determine the signal power necessary to achieve the required signal to noise ratio at the receiver and to work back toward the transmitter through all the system to determine the required output power from the source.

In order to minimize the unintercepted illumination loss at the fiber/detector interface, the size of the active area of the detector must be large enough to accept all (or nearly all) of the light emerging from the fiber. The output emission from a fiber is a complex function of input launch characteristics, source spectral width, fiber length, fiber loss, and acceptance half-angle. Figure 2-15 shows the interface between a fiber bundle and a photodetector. For a worst case analysis, assume the light exiting the fiber spreads at an angle which is equal to the acceptance half-angle of the fiber and the light intensity is uniform throughout the beam. At a distance  $L$  from the bundle, the beamwidth will be  $d_1$  which is equal to

$$d_1 = 2(L \tan \theta) + d_3 \quad (2.20)$$

where  $d_3$  is the diameter of fiber bundle. The unintercepted illumination loss is the ratio of the detector area to the beam area

$$\begin{aligned} \text{Unintercepted Illumination Loss (dB)} &= 10 \log \frac{\frac{d_2^2}{4}}{\frac{d_1^2}{4}} \\ &= 10 \log \frac{d_2^2}{d_1^2} \\ &= 10 \log \frac{d_2^2}{[2(L \tan \theta) + d_3]^2} \end{aligned} \quad (2.21)$$

## PHOTODETECTOR EQUIVALENT CIRCUIT

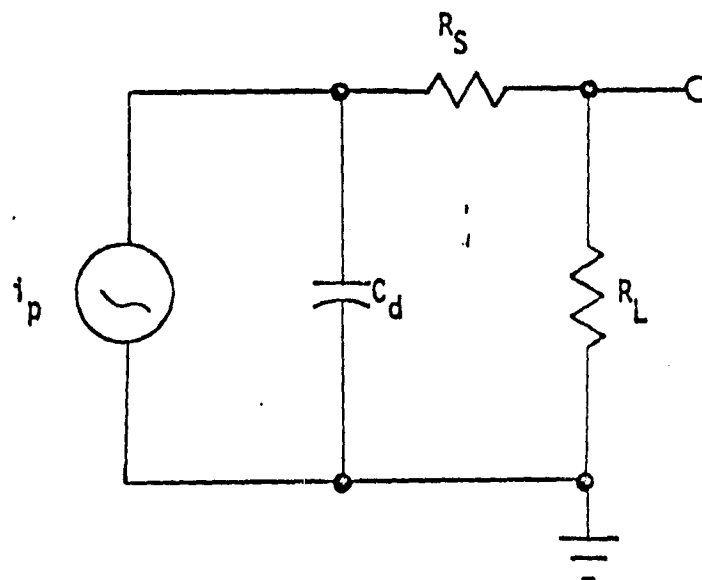


FIGURE 2-14

## BUNDLE/DETECTOR INTERFACE

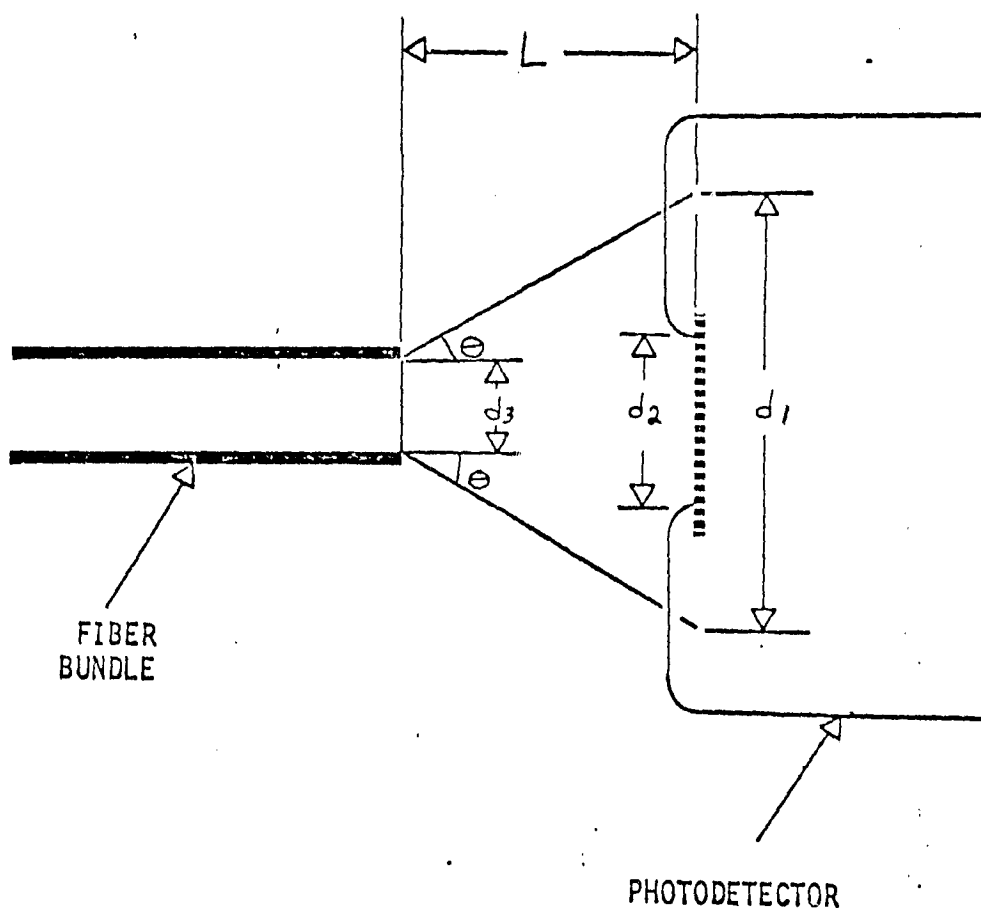


FIGURE 2-15



From this equation, the separation (L) between the fiber and the detector that will result in zero unintercepted illumination loss may be determined.

Photodetectors have a response with 90% of the peak responsivity for wavelengths of several hundred nanometers. Peak responsivity is at wavelength near 900 nm. The response at higher wavelengths falls off more rapidly than the response at lower wavelength. Figure 2-16 shows the response of a typical PIN photodiode. Matching the spectral response of the source and detector is not nearly as critical as matching the spectral response of the source and the fiber.

### 2.3.3 Contract Summary, Vendor Information

Table 2-5 contains the information for the HP models 4203, 4204, 4205, 4207, and 4220 photodiodes. These HP silicon planar PIN photodiodes are ultra-fast light detectors for visible and near infrared radiation. The speed of response of these detectors is less than one nanosecond. Laser pulses shorter than 0.1 nanosecond may be observed. The frequency response extends from dc to 1 GHz. The low dark current of these planar diodes enables detection of very low light levels. The quantum detection efficiency is constant over ten decades of light intensity, providing a wide dynamic range.

Tables 2-6 and 2-7 have the electro-optical performance characteristics for a few models of the EG&G line of photodiodes. Models in Table 2-6 are of the nonguard-ring type while models in Table 2-7 are of the SGD series. The SGD series of silicon photodiodes utilize a planar diffused, oxide passivated, guard-ring construction. They offer a unique combination of wide spectral range, high sensitivity, fast speed of response, low noise. This construction technique eliminates the high noise and functional instability inherent in photodiodes made by Schottky barrier or lithium drifted processes.

RCA offers two different types of solid-state silicon photodiodes suitable for fiber systems (see Tables 2-8 thru 2-11): single-element PIN photodiodes and avalanche photodiodes. The broad spectral range and high responsivity of these silicon photodiodes make them excellent choices for all broadband, low-level light detection applications.

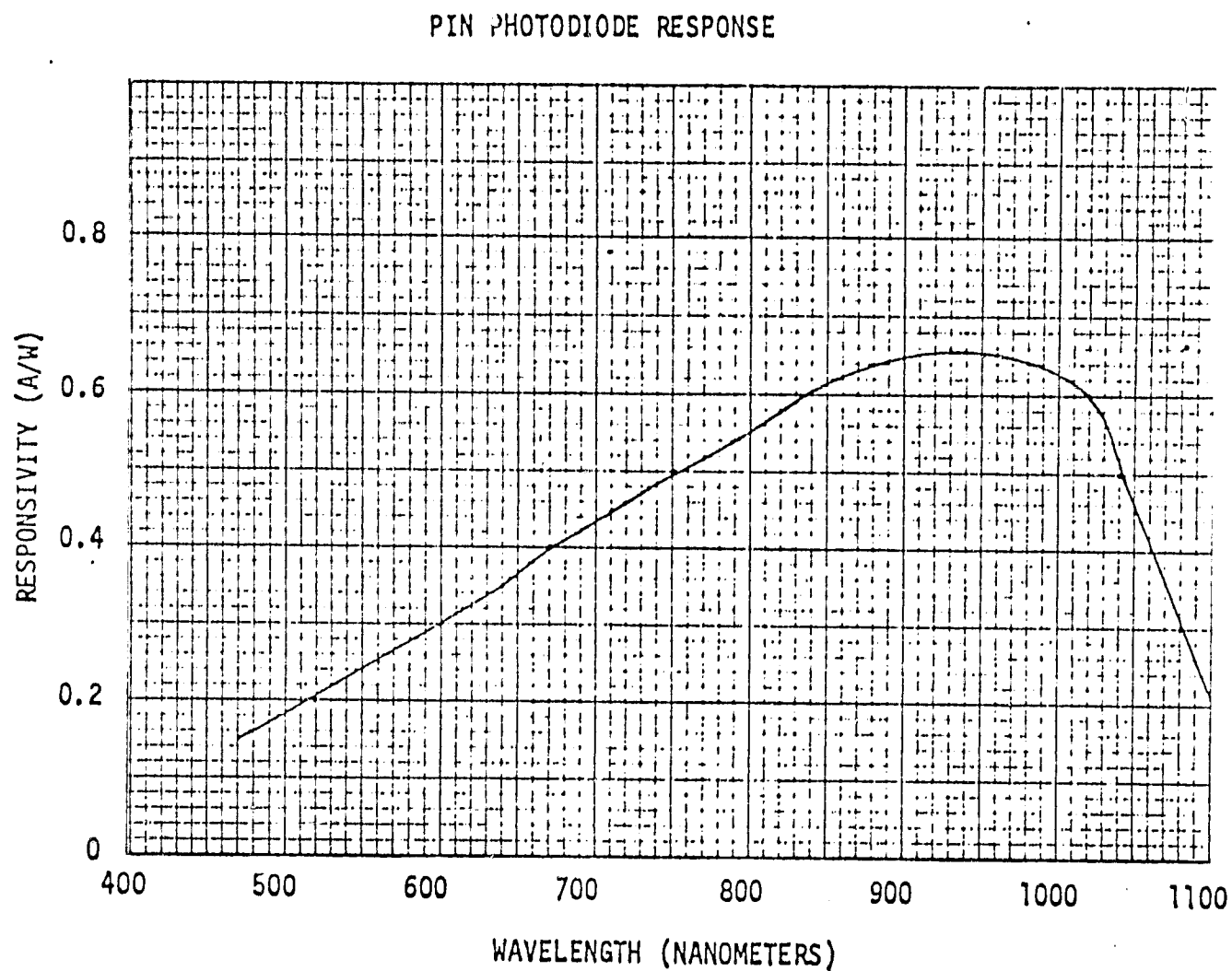


FIGURE 2-16

TABLE 2--6

COMPANY EG&G SILICON PHOTODIODES					
MODEL	SND-130	SND-140	SND-680		
ACTIVE AREA mm <sup>2</sup>	0.81	5.1	24.0		
RESPONSIVITY @ 900 nm A/W	0.45	0.45	0.45		
DARK CURRENT pico amps @ 6V	50	300	500		
D* (900, 10 <sup>7</sup> , 1) cm Hz <sup>1/2</sup> /W	1. x 10 <sup>13</sup>	1.02 x 10 <sup>13</sup>	1.74 x 10 <sup>13</sup>		
NEP (900, 10 <sup>7</sup> , 1) W/Hz <sup>1/2</sup>	0.9 x 10 <sup>-14</sup>	2.2 x 10 <sup>-14</sup>	2.8 x 10 <sup>-14</sup>		
RISETIME ns.	8	10	12		
NOISE CURRENT amp/Hz <sup>1/2</sup>	4 x 10 <sup>-15</sup>	10 x 10 <sup>-15</sup>	13 x 10 <sup>-15</sup>		
CAPACITANCE pF	5	35	150		
SENSITIVITY (A/W) 900	0.45	0.45	0.45		
TEMP. RANGE C°	-55 to+100	-55 to+100	-55 to+100		
SUPPLY VOLTAGE V	6	6	6		

TABLE 2 7

COMPANY EG&G Silicon Diffused Pin Photodiodes					
MODEL	SGD-040A	SGD-100A	SGD-160	SGD-444	
ACTIVE AREA $\text{mm}^2$	0.82	5.1	13	100	
RESPONSIVITY @ 900 A/W	0.5	0.5	0.5	0.5	
DARK CURRENT nano amps	1	3	20	50	
$D^*$ ( $0.9\mu\text{m}, 10^3, 1$ ) $\text{W}/\text{Hz}^{1/2}$	$9 \times 10^{11}$	$2.3 \times 10^{12}$	$1.2 \times 10^{12}$	$1.7 \times 10^{12}$	
NEP ( $0.9\mu\text{m}, 10^3, 1$ ) $\text{Cm. Hz}^{1/2}/\text{W}$	$9.6 \times 10^{-14}$	$1 \times 10^{-13}$	$3 \times 10^{-13}$	$5.9 \times 10^{-13}$	
RISETIME nanoseconds	3	4	7	10	
NOISE CURRENT	-	-	-	-	
CAPACITANCE picofarads	2.0	4.0	8.0	80	
SENSITIVITY (A/W) 900 nm	0.5	0.5	0.5	0.5	
TEMP. RANGE $^{\circ}\text{C}$	-65 to 150	-65 to 150	-65 to 150	-65 to 150	
SUPPLY VOLTAGE V	100	100	100	100	

TABLE 2-8

COMPANY RCA (Single Element Silicon p-i-n) P-type					
MODEL	C30801	C30802	C30812	C30813	C30814
ACTIVE AREA mm <sup>2</sup>	5	20	5	5	20
RESPONSIVITY @ 900 A/W	0.6	0.6	0.6	0.6	0.6
DARK CURRENT nA	200	500	100	300	1000
D*	-	-	-	-	-
NEP (900, 1000, 1) W/Hz <sup>1/2</sup>	$4 \times 10^{-13}$	$6 \times 10^{-13}$	$1.5 \times 10^{-13}$	$2.6 \times 10^{-13}$	$6 \times 10^{-13}$
RISETIME ns at 900 nm	7	7	15	40	40
NOISE CURRENT A/Hz <sup>1/2</sup> 1000 Hz	$2.5 \times 10^{-13}$	$4 \times 10^{-13}$	$1 \times 10^{-13}$	$1.7 \times 10^{-13}$	$4 \times 10^{-13}$
CAPACITANCE pF	5	17	3	2	5
SENSITIVITY (A/W)					
TEMP. RANGE degree C	15 to 80	15 to 80	-40 to 80	-40 to 80	-40 to 80
SUPPLY VOLTAGE V	0-225	0-225	0-225	0-225	0-225

TABLE 2-9

COMPANY RCA (Single Element Silicon p-i-n) N-Type					
MODEL	C30807	C30808	C30808A	C30809	C30810
ACTIVE AREA mm <sup>2</sup>	0.8	5	4.5	50	100
RESPONSIVITY @ 900 A/W	0.6	0.6	0.6	0.6	0.6
DARK CURRENT nA	10	30	30	70	300
D*	-	-	-	-	-
NEP (900, 1000, 1) W/Hz <sup>1/2</sup>	$1 \times 10^{-13}$	$1.5 \times 10^{-13}$	$1.5 \times 10^{-13}$	$2.3 \times 10^{-13}$	$4.5 \times 10^{-13}$
RISETIME ns at 900 nm	3	5	5	10	12
NOISE CURRENT A/Hz <sup>1/2</sup> 1000 Hz	$6 \times 10^{-14}$	$1 \times 10^{-13}$	$1 \times 10^{-13}$	$1.5 \times 10^{-13}$	$3 \times 10^{-13}$
CAPACITANCE pF	2.5	6	6	35	70
SENSITIVITY (A/W)					
TEMP. RANGE C°	-40 to+80	-40 to+80	-40 to+80	-40 to+80	-40 to+80
SUPPLY VOLTAGE V	0-100	0-100	0-100	0-100.	0-100

TABLE 2-10

COMPANY RCA (Single Element Silicon p-l-n) N-type					
MODEL	C30822	C30831			
ACTIVE AREA mm <sup>2</sup>	20	0.2			
RESPONSIVITY @ 900 A/W	0.6	0.6			
DARK CURRENT nA	50	10			
D*	-	-			
NEP (900, 1000, 1) W/Hz <sup>1/2</sup>	$2 \times 10^{-13}$	$1 \times 10^{-14}$			
RISETIME ns at 900 nm	7	3			
NOISE CURRENT 1000 Hz A/Hz <sup>1/2</sup>	$1.3 \times 10^{-13}$	$6 \times 10^{-14}$			
CAPACITANCE pF	17	1			
SENSITIVITY (A/W)					
TEMP. RANGE C°	-40 to +80	-40 to +80			
SUPPLY VOLTAGE V	0-100	0-100		-	

TABLE 2-11

COMPANY RCA Silicon Avalanche Photodiodes					
MODEL	C30817	C30872	C30884	C30895	
ACTIVE AREA mm <sup>2</sup>	0.5	7	0.5	0.5	
RESPONSIVITY @ 900 nm A/W	75	37	63	63	
DARK CURRENT nA	18	18	10	20	
D*	-	-	-	-	
NEP (900, 1000, 1) W/Hz <sup>1/2</sup>	$1 \times 10^{-14}$	$2.5 \times 10^{-14}$	$1.2 \times 10^{-14}$	$1.5 \times 10^{-14}$	
RISETIME ns at 900 nm	2	2	1	2	
NOISE CURRENT	-	-	-	-	
CAPACITANCE pF	2	10	4	2	
SENSITIVITY (A/W)					
TEMP. RANGE C°	-40 to+70	-40 to+70	-40 to+70	-40 to+70	
SUPPLY VOLTAGE V	335	320	300	350	



Similarly, Tables 2-12 through 2-16 show the device selections from other manufacturers. As can be seen from the typical responsivity, dark current, NEP,  $D^*$ , and risetime, most photodiodes now on the market can be used in systems such as Space Shuttle providing that connector losses are kept low.

As stated previously, there needs to be source-fiber and source-detector compatibility. Photodetectors can be found throughout the range of wavelengths between 800 nm to 1100 nm and, in general, APD or PIN photodetectors can be purchased off-the-shelf within this range. The response time of the APD and PIN photodetectors are similar, but should also nearly match the LED or ILD selected for the system. The temperature of the application should also be compared to the components' tested temperature range. PIN photodetectors normally have a wide temperature, however, APD photodetectors usually have to include a constant temperature chamber.

In conclusion, PIN photodetectors are normally used for information bandwidths up to 50 MHz and distances up to 500 m and require low bias voltages (15 to 100V). APD photodiodes are used when high receiver sensitivity is needed, they have fast response times (0.5 to 2 ns), and require a high voltage supply (200 to 300 volts).

#### 2.4 OPTICAL LOSSES IN FIBER SYSTEMS

How well a fiber optic data system performs depends, in general, on how much system margin is available. This, in turn, is dependent on the source, detectors, and optical connector losses in the fiber systems. The optical connector system losses may be subdivided into a number of individual loss terms. These include source-to-cable interface losses, connector-to-connector losses, Tee or Star losses, and fiber-to-receiver losses. Most of these losses are determined by the state-of-the-development that exists in the individual components. However, the maximum amount of radiation that is transferred between any two points in an optical system is governed by the conservation of radiance which is <sup>(13)</sup>

$$\frac{P_1}{N_1 A_1 \lambda_1^2} \leq \frac{P_2}{N_2 A_2 \lambda_2^2} \quad (2.22)$$

TABLE 2-12

COMPANY United Detector Technology Inc. Pins and UDT Photops					
MODEL	Pin - 020A	Pin - 040A	UDT - 450	UDT - 500	UDT - 600
ACTIVE AREA cm <sup>2</sup>	$2 \times 10^{-3}$	$8 \times 10^{-3}$	.05	1.0	.05
RESPONSIVITY @ 0.8 nm (A/W)	.42	.42	.4	.3	.4
DARK CURRENT pico amps -10 volts	75	300			5000
D* (0.85, 10 <sup>3</sup> , 1) cmHz <sup>1/2</sup> /watt	$7.45 \times 10^{12}$	$8.94 \times 10^{12}$	$4.5 \times 10^{10}$	$1 \times 10^{12}$	$4.5 \times 10^{10}$
NEP (.85, 10 <sup>3</sup> , 1) watt/Hz <sup>1/2</sup>	$6 \times 10^{-15}$	$1 \times 10^{-14}$	$5 \times 10^{-12}$	$1 \times 10^{-12}$	$5 \times 10^{-12}$
RISETIME ns	5	5	350	3500	35
NOISE CURRENT A/Hz <sup>1/2</sup>	$3 \times 10^{-15}$	$10^{-14}$	30	20	30
CAPACITANCE -10. volt pF	4	16	100	1100	10
SENSITIVITY (A/W)	.42	.42	.4	.3	.4
TEMP. RANGE	-	-	-	-	-
SUPPLY VOLTAGE V	-12	-12	±15	±15	±15

TABLE 2-13

COMPANY Hamamutsa Silicon Photoce[l]					
MODEL	5874-5K	5874-8K	5874-18K	5875-16R	5875-16R
ACTIVE AREA mm <sup>2</sup>	5.7	26.4	1.29	5.79	5.55
RESPONSIVITY @ .930 A/W	0.45	0.45	0.45	0.45	0.45
DARK CURRENT μA	$5 \times 10^{-12}$	$2.5 \times 10^{-11}$	$1.2 \times 10^{-12}$	$5 \times 10^{-12}$	$5 \times 10^{-12}$
D* ( $9, 10^3, 1$ ) cmHz <sup>1/2</sup> /W	$4 \times 10^{13}$	$4 \times 10^{13}$	$4 \times 10^{13}$	$4 \times 10^{13}$	$4 \times 10^{13}$
NEP ( $9, 10^3, 1$ ) W/Hz <sup>1/2</sup>	$6 \times 10^{-15}$	$1 \times 10^{-14}$	$3 \times 10^{-15}$	$6 \times 10^{-15}$	$6 \times 10^{-15}$
RISETIME ns	3.2	14	1.7	3.2	3.2
NOISE CURRENT	-	-	-	-	-
CAPACITANCE pF	1.3	5.7	0.3	1.3	1.3
SENSITIVITY (A/W)	0.45	0.45	0.45	0.45	0.45
TEMP. RANGE (°C)	-10 to+60	-10 to+60	-10 to+60	-10 to+60	-10 to+60
SUPPLY VOLTAGE				-	

TABLE 2-14

COMPANY Quantrad Corporation Pin and PV Series Silicon Photodiodes					
MODEL	010-Pin-T05	050-Pin-RM	003-PV-T0-18	010-PV-T05	050-PV-RM
ACTIVE AREA mm <sup>2</sup>	10	50	3	10	50
RESPONSIVITY @ 905 A/W	0.45	0.45	0.5	0.5	0.5
DARK CURRENT μA 10 volts	0.04	.25	0.02	0.07	0.37
D*	-	-	-	-	-
NEP (.9, 10 <sup>3</sup> , 1) 10 <sup>-12</sup> W/Hz <sup>1/2</sup>	0.49	1.3	0.16	0.28	0.68
RISETIME ns	7	8	9	12	30
NOISE CURRENT pA/Hz <sup>1/2</sup>	0.22	0.57	0.08	0.14	.34
CAPACITANCE pico-F	13	61	10	37	185
SENSITIVITY (A/W)	-	-	-	-	-
TEMP. RANGE C°	-10 to+70	-10 to+70	-10 to+70	-10 to+70	-10 to+70
SUPPLY VOLTAGE V	100	100	100	100	100

TABLE 2-15

COMPANY Harshaw, Silicon IR Detectors					
MODEL	S11	S12	S37	S38	S49
ACTIVE AREA	.5	.36	0.01	0.01	0.001
RESPONSIVITY @ 1.06	0.5	0.5	0.5	0.62	0.62
DARK CURRENT $\mu A$	2.5	2.0	.1	.1	0.05
$D^*$ (1.06, $10^3$ , 1) $cmHz^{1/2}/W$	$0.88 \times 10^{12}$	$0.86 \times 10^{12}$	$0.58 \times 10^{12}$	$0.92 \times 10^{12}$	$0.25 \times 10^{12}$
NEP (1.06, $10^3$ , 1) $W/Hz^{1/2}$	$1.96 \times 10^{-12}$	$1.76 \times 10^{-12}$	$0.44 \times 10^{-12}$	$.27 \times 10^{-12}$	$.21 \times 10^{-12}$
RISE TIME ns	15	15	10	5	5
NOISE CURRENT $10^3 Hz$ pA	.9	.81	.2	.1	.13
CAPACITANCE pF	100	75	5	6	2
SENSITIVITY (A/W)					
TEMP. RANGE	-	-	-	-	-
SUPPLY VOLTAGE V	180	180	180	100	100

TABLE 2-16

COMPANY Math Associates Pin Photodiodes					
MODEL	E-5100	E-5102			
ACTIVE AREA mm <sup>2</sup>	.2	.2			
RESPONSIVITY @ 900	0.42	0.42			
DARK CURRENT nanoamps	0.1	1.0			
D* cm.Hz <sup>1/2</sup> /W	$7.45 \times 10^{12}$	$2.23 \times 10^{12}$			
NEP W/Hz <sup>1/2</sup>	$6 \times 10^{-15}$	$2 \times 10^{-14}$			
RISETIME ns	5	5			
NOISE CURRENT	-	-			
CAPACITANCE UNITS	-	-			
SENSITIVITY (A/W) 900	.42	.42			
TEMP. RANGE °C	-	-			
SUPPLY VOLTAGE V	25	25			

where

$N$  = index of refraction of the medium

$A$  = area of elements 1, 2

$\lambda$  = numerical aperture of 1, 2

$P$  = flux 1, 2

1 = input sided

This law, which is pictorially defined in Figure 2-17, is a restatement of the second law of thermodynamics and states that it is impossible to construct a heat engine that acts solely to extract heat from a reservation at  $T$ , and convert the energy into an equivalent amount of work, thus creating a perpetual-motion machine. This law holds even for monochromatic sources of illumination. It is impossible to use a passive optical element that will increase the amount of radiance in the system.

From Equation 2.22 it seems that the most efficient transfer occurs if the numerical aperture and the area of the source, subscript 1, is less than the receiving side, subscript 2, assuming of course that  $N_1$  is approximately equal to  $N_2$ .

Fiber optic connectors may be divided into four categories:

1. Source-to-fiber connectors (Section 2.4.1)
2. Fiber-bundle to fiber-bundle connectors (Section 2.4.2)
3. Fiber-to-detector connectors (Section 2.4.3)
4. Branching connectors (Section 2.5)

Optical connectors usually limit the minimum bit error rate in a short-length, low-loss optical fiber communication system. This occurs since generally the loss per meter of cable is insignificant compared to the losses due to connectors. For example, for 100 meters of cable the loss would be <2 dB from the cable itself while for a four-port star coupler the loss would be on the order of 20 dB (Section 2.8).

For the analysis which follows, plastic clad silica multifiber made up of 19 single-stepped index fibers is used to obtain numerical values. The multifiber system insures adequate redundancy and the type of fiber used is S-10-PS (19) ITT cable which has the following specifications:

CONSERVATION OF RADIANCE

10-2663

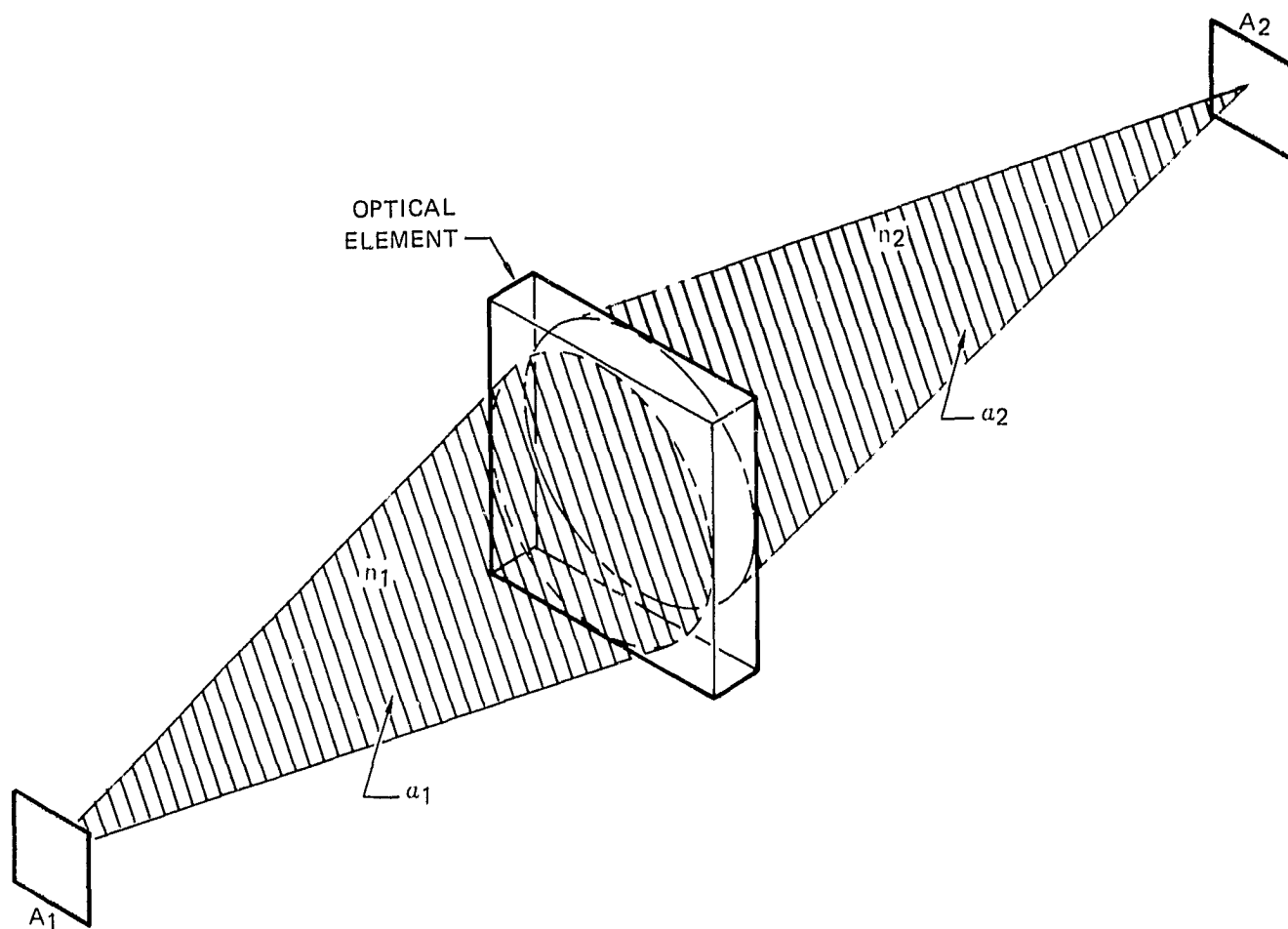


FIGURE 2-17



## OPTICAL DIGITAL TECHNIQUES

REPORT MDC E2052  
FEBRUARY 1979

Attenuation	10 dB/km
Numerical Aperture	0.3
Dispersion 3 dB width	30 ns/km
Core index of refraction	1.46
Fiber core diameter	125 $\mu\text{m}$
Jacketed fiber diameter	500 $\mu\text{m}$

### 2.4.1 Source-to-Fiber Connectors

Optical sources presently used for fiber optic systems are the LED and the laser diode. Of these two, the most probable source for space avionics systems is the LED because present-day avionics systems use a comparatively low data rate and hence can tolerate large amounts of pulse spreading. Therefore, there is no need for a laser diode narrowband source. Also, the LED has a longer demonstrated lifetime at the present time.

The primary loss mechanisms for coupling between a LED and a fiber optic bundle are:

- a. Front surface reflection loss between the fiber and air interface.
- b. Packing fraction loss due to core/fiber area ratio mismatch.
- c. Solid-angle loss factors due to uncollimated light of the LED and the finite acceptance angle of the fiber bundle.

The front surface reflection loss is caused by Fresnel reflection which takes place at the air/fiber interface. This reflection is related to the mismatch of the refractive index of the fiber (1.46) and air (1.0). The transmitted field across this boundary, independent of mode of polarization of the light and for normal incidence, is given by <sup>(14)</sup>

$$T_F = \frac{2}{n + 1} \quad (2.23)$$

where

$n$  = the index of refraction of the fiber

The power of light intensity transmitted is given by <sup>(14)</sup>

$$T_P = \frac{4n}{(n + 1)^2} \quad (2.24)$$

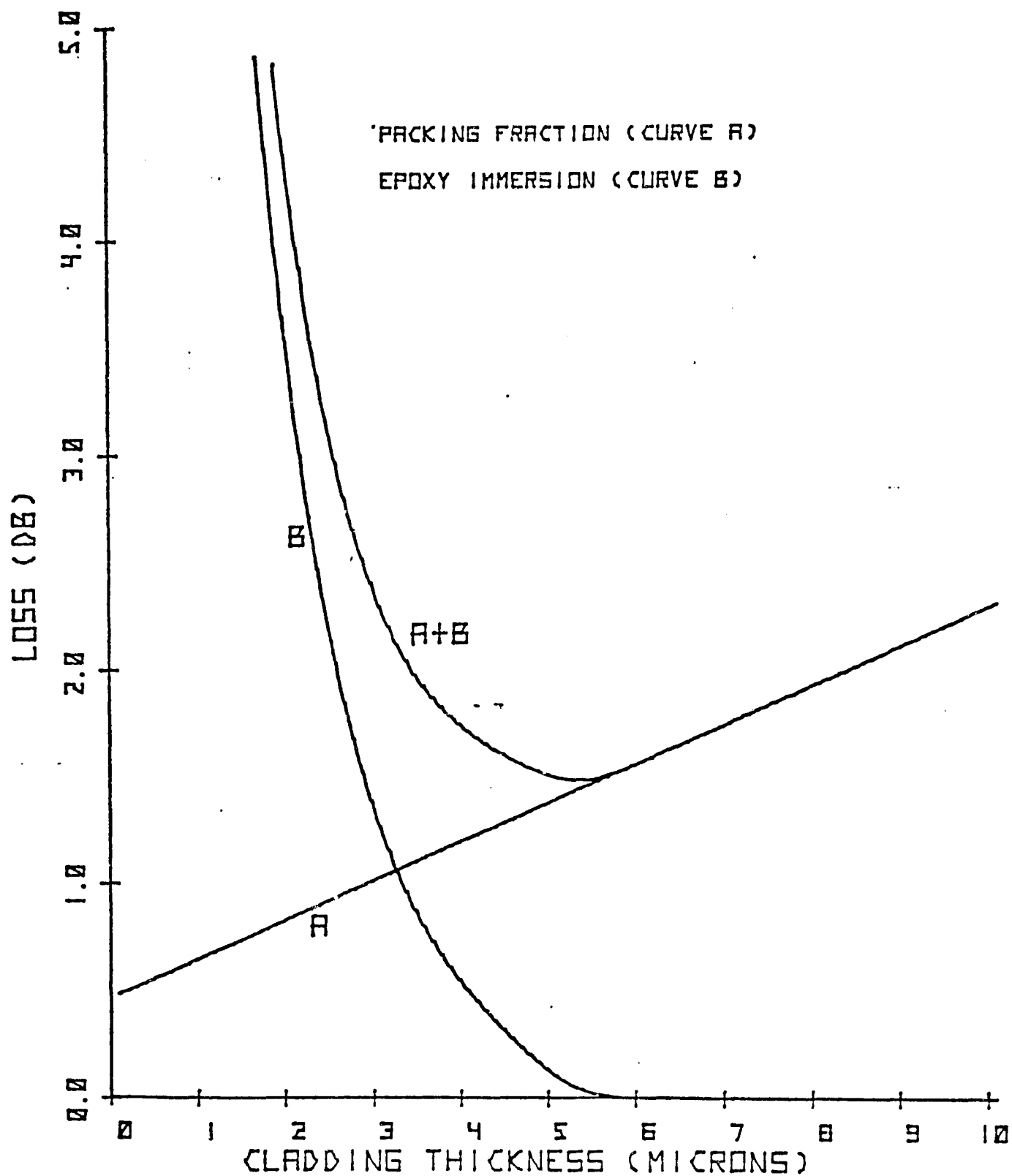
Hence, for an index of refraction of 1.46 the front surface reflection loss is approximately 0.06 dB. This loss can be reduced or eliminated by either using index matching at the optical interfaces or by butting the surfaces together closer than a wavelength of light. However, neither of these approaches are practical considering the small magnitude of the loss.

The packing fraction loss is traceable to two different origins. The first is a geometric argument which implies that it is not possible to space round fibers together without losing area between fibers. And second, the cladding physically takes space in the fiber bundle. There is no way around the first loss term, however, the cladding loss may be reduced by the removal of cladding by controlled etching. It has been shown that there is a tradeoff between cladding thickness removal (packing fraction loss reduction) and attenuation increase when surrounding a fiber with an absorbing, higher index material such as epoxy used to secure fibers together.<sup>(11)</sup> These losses are plotted in Figure 2-18. Curve A shows the loss as a function of cladding thickness for an individual fiber and Curve B represents the measured attenuation increase when the fiber is surrounded by epoxy. As can be seen from Figure 2-18, the combined loss (Curve A + B) has a minimum at approximately 5 micrometers thickness. Also from the figure, it is seen that the penalty is greatest for removing too much cladding. From Figure 2-18, it is seen that the packing fraction loss is about 1.75 dB.

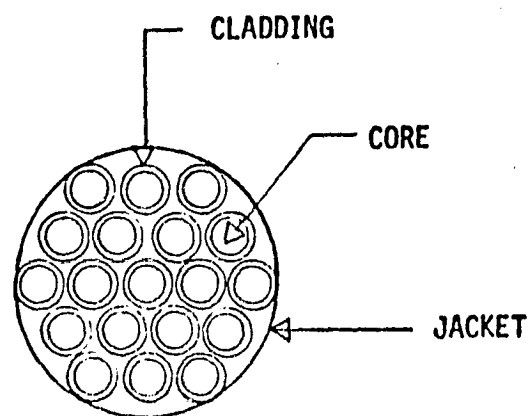
Multifiber optical bundles consist of several (usually 7 to 300) closely packed individual fibers. An illustration of a multifiber bundle is shown in Figure 2-19. For light transmission, the only useful portion of the multifiber bundle is the area of the individual fiber cores. Any illumination that falls upon the cladding or the space between individual fibers is lost. Therefore, the packing fraction loss is given by

$$\text{P.F. loss (dB)} = 10 \log \left[ \frac{\text{core area}}{\text{bundle area}} \right] \quad (2.25)$$

Figure 2-20 shows packing fraction loss as a function of the bundle packing fraction. Some manufacturers provide the packing fraction information on the data sheet. When the packing fraction is not provided it must be calculated from the bundle diameter and the core diameter information.

(HUDSON&THEIOL)  
FIGURE 2-18

19 FIBER BUNDLE



$$\text{PACKING FRACTION} = \frac{\text{CORE AREA}}{\text{TOTAL BUNDLE AREA}}$$

FIGURE 2-19

## PACKING FRACTION LOSS

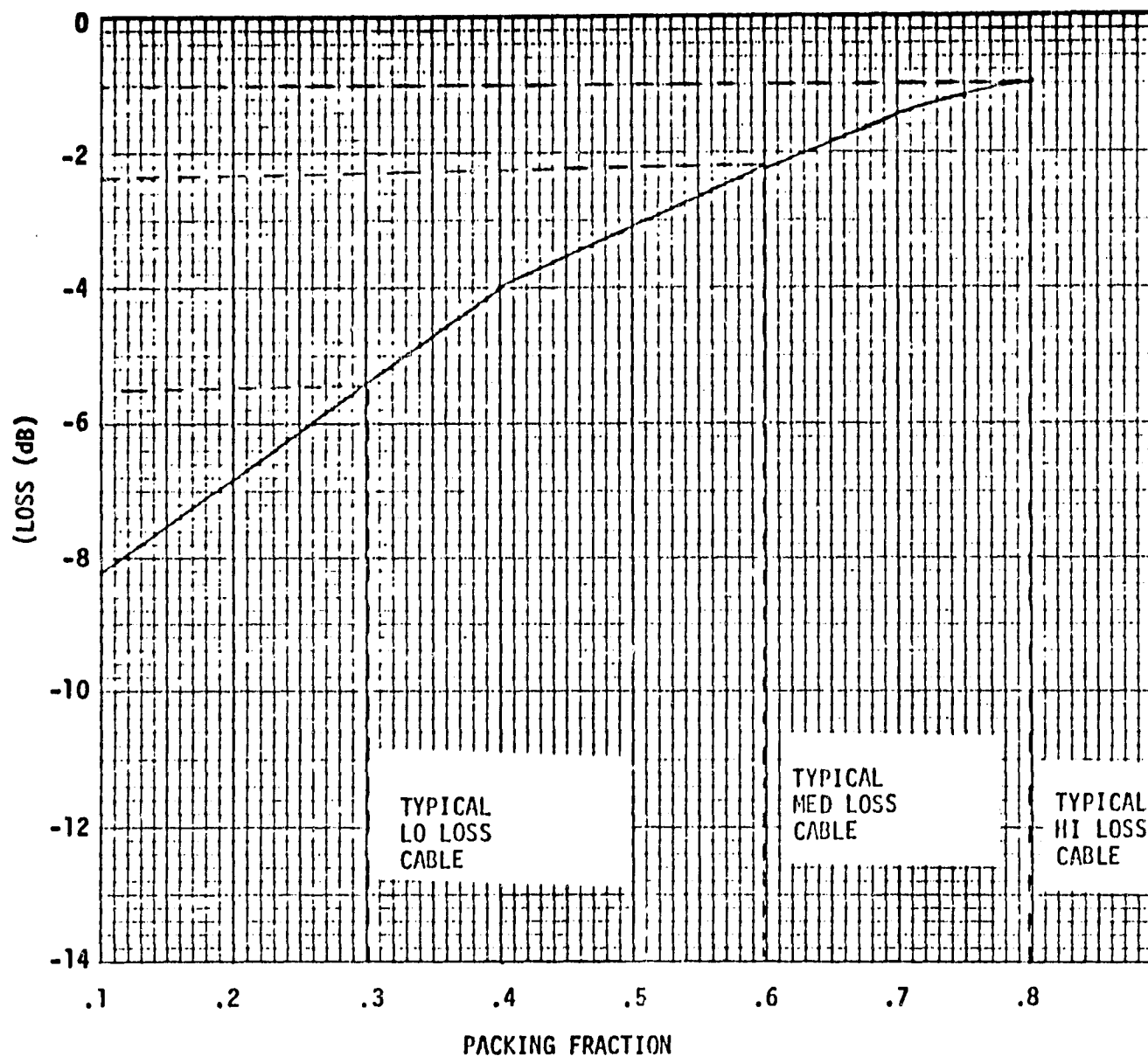


FIGURE 2-20

The remaining loss, which is caused by the ratio of total fiber area to total bundle area for a 19-bundle cable with the cladding removed, can be shown to be about 1.2 dB. This gives a total loss for packing fraction of 2.95 dB.

The solid-angle coupling loss occurs because only light with small divergence is trapped in a fiber having low numerical apertures, whereas an LED radiates over a wide angle. By applying Snell's law at the end and side wall of the fiber, it can be shown that incident light at half angles greater than  $\theta$ , where

$$\theta = \arcsin [n^2_{\text{core}} - n^2_{\text{clad}}]^{1/2}, \quad (2.26)$$

will escape from the core.

The numerical aperture, NA, of the cable which is equal to  $\sin \theta$  is

$$NA = (n^2_{\text{core}} - n^2_{\text{clad}})^{1/2} \quad (2.27)$$

Hence, for a NA = 0.3 (the NA of S-10-PS(19) ITT cable) the half-angle is  $\theta = 17.46^\circ$ .

Having determined the acceptance cone angle of the fiber, the angular emission pattern of the LED may be used to determine the solid angle loss factor.

For a flat surface LED the radiation in watts/ster is proportional to the cosine of the viewing angle. An emitting surface with a cosine distribution is termed a Lambertian source, and flat LED sources approximate Lambertian sources. Thus, the number of watts/ster emitted from the LED is

$$I = B_0 \cos \theta \quad (2.28)$$

and the total radiation over a cone with half angle  $\theta$  is (15)

$$P = \int_0^\theta 2\pi B_0 \cos \phi \sin \phi d\phi \quad (15) \quad (2.29)$$

$$\text{or} \quad P = \pi B_0 \sin^2 \theta \text{ watts} \quad (2.30)$$

The power radiated into a hemisphere is  $P_0 = \pi B_0$  watts.

Thus, the total radiated power in watts collected and trapped by the fiber is:

$$P = P_0 \sin^2 \theta$$

$$P = P_0 (NA)^2$$

Hence, the above example yields for solid angle power loss a value of 10.05 dB.

If the source emission half angle is less than the fiber acceptance half angle, the numerical aperture loss will be zero. The data sheet for the source will either specify the emission half angle or present a curve of output power as a function of the angle from the axis. The data sheets for fiber optic cables list either the numerical aperture or the acceptance half angle. Figure 2-21 shows numerical aperture losses as a function of fiber acceptance half angles for various emission half angles.

**Unintercepted Illumination:** If the source is larger in diameter than the fiber bundle, some of the light emitted by the source does not fall upon the fibers and is lost. This loss can occur at any junction: source-to-fiber, fiber-to-fiber, and fiber-to-detector. By careful selection of component sizes, the unintercepted illumination losses can be minimized. The unintercepted illumination loss is given by

$$U.I. (dB) = 10 \log \left[ \frac{\text{receptor area}}{\text{source area}} \right] \quad (2.31)$$

A curve of unintercepted illumination versus receptor diameter for various source diameters is shown in Figure 2-22.

The total coupling loss from an LED to the S-10-PS(19) ITT Cable is  
 $0.16 + 2.95 + 10.05 = 13.16$  dB.

The above losses were for a bundle fiber system. It is possible to reduce these losses by going to a single fiber approach. However, if single fibers are employed the system is not redundant; this problem is addressed in Section 2.6. If the single fiber concept is employed the packing fraction loss term is no longer present; hence, the total loss is about 10 dB. This loss can be further reduced by realizing that the emitting area is smaller than that of the fiber.

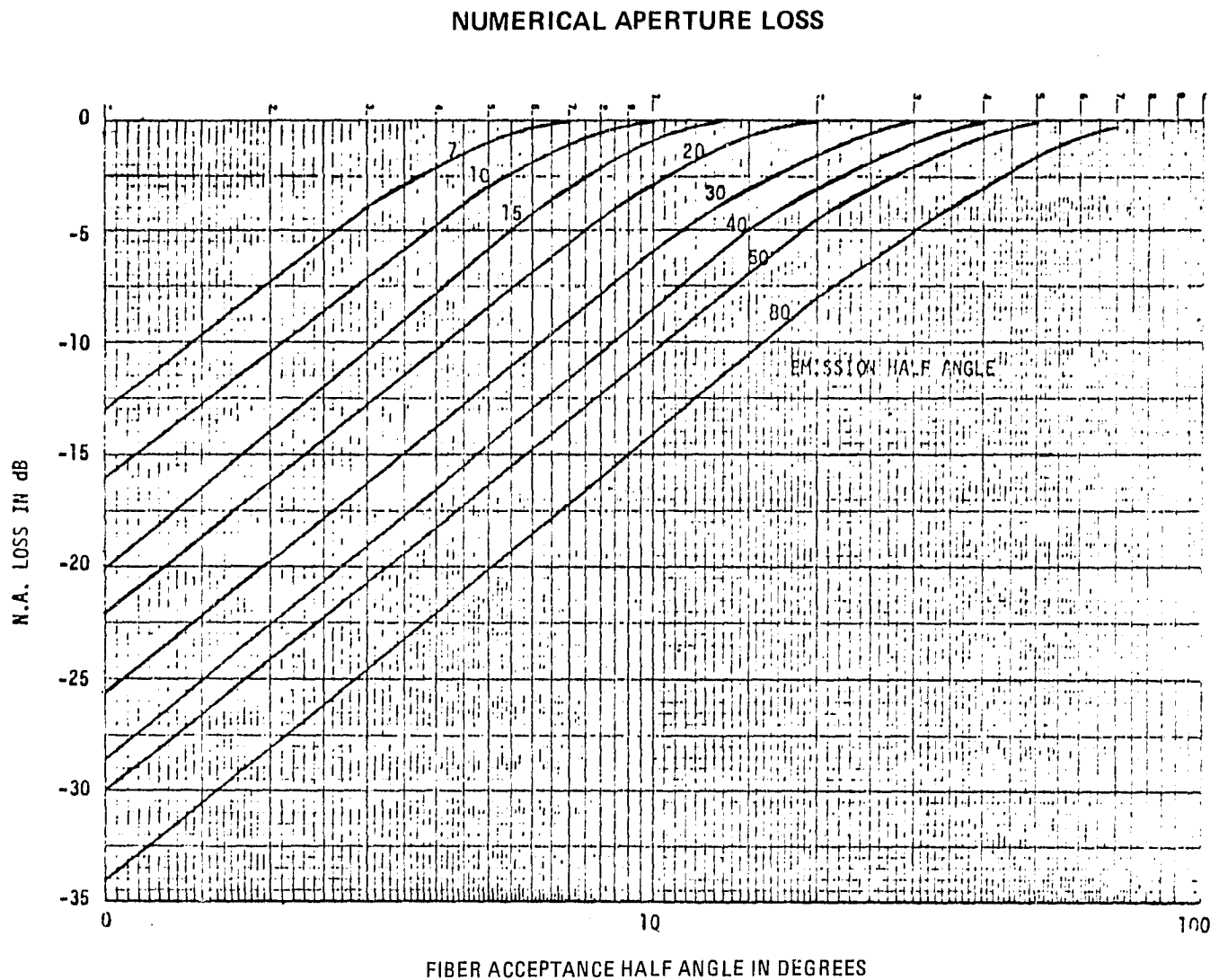


FIGURE 2-21



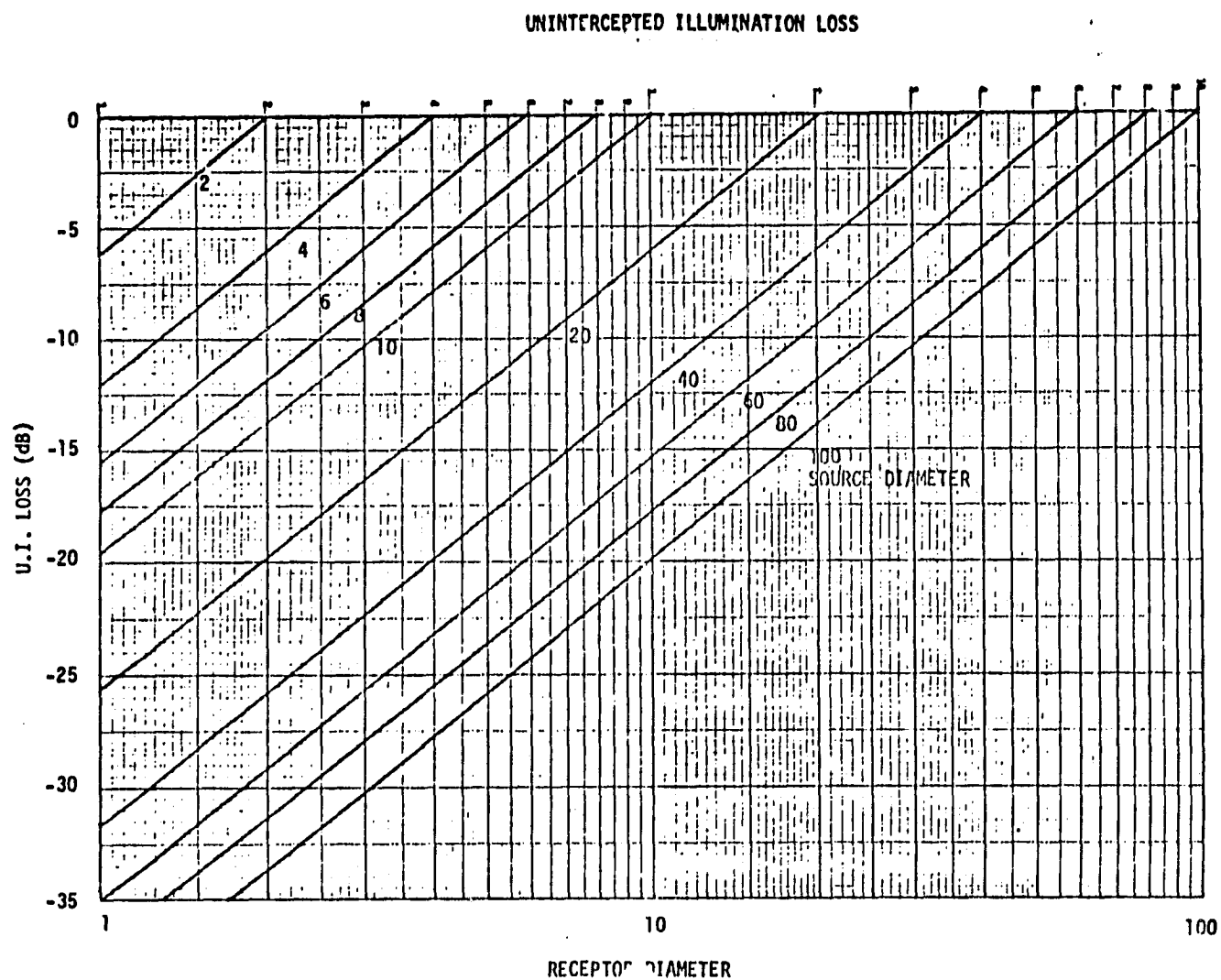


FIGURE 2-22

This configuration magnifies the size of the source while reducing the apparent source angle, thus it is possible (at least in theory) to reduce the solid angle loss term to zero.

#### 2.4.2 Fiber-Bundle to Fiber-Bundle Connectors

When the fiber optic bundles must be interrupted (e.g., penetration of bulk-heads, splicing cables, or repairing a cable break) a fiber-bundle to fiber-bundle connector must be used. The losses that are most significant for bundle connectors are:

- a. Packing fraction loss
- b. Alignment
- c. Indexing losses

The packing fraction loss term was discussed in Section 2.4.1.

The alignment losses are transverse displacements between fiber bundles, excessive gap distances, and axial misalignments. The most severe loss is the transverse displacement between fiber bundles. The excessive gap loss and axial misalignment requirements are more forgiving.

The indexing loss occurs because the bundle fibers are not aligned across the termination junction. This loss results in a 2 to 3 dB additional loss for the bundle technology. Bundle fiber-fiber splice amounts to 14 dB and single fiber systems amount to about 2 dB.

#### 2.4.3 Fiber-to-Receiver Losses

The losses at the cable-to-receiver interface are similar to the losses previously described. The losses are Fresnel Reflections and Unintercepted Fresnel Reflections: As in the case of the transmitter-to-cable interface, Fresnel Reflections occur at each boundary between two substances. Unintercepted illumination: If the area of the cable is larger than the active area of the receiver, unintercepted illumination losses will occur. The magnitude of the unintercepted illumination loss will be the same as that previously described.

The losses that have been previously described are those losses that occur between the optical output of the transmitter and the optical output of the receiver.

#### 2.4.4 Vendor Optical Connectors

The problem of terminating a single optical fiber and cable is a key selection; however, terminating a multichannel optical cable involves locating a vendor who will custom-build a connector to fit the cable and fibers. Table 2-17 provides information on available connectors for single-fiber termination of multichannel connectors. In general, numerous single-fiber connectors are available in both plastic and metal, giving a consistent 0.5 to 1 dB per termination for glass-glass fibers. Connectors are also available for bundled fibers as single-way.

Multiway connectors fall into two categories: real and unreal. All connector companies are either in some stage of development or have produced a prototype. Few companies produce off-the-shelf fiber-optic multichannel connectors; one of the few is Amphenol (4-8 pin) and another is Hughes Connectors (52 pin). Note also that these connectors do not accommodate all sizes and types of optical fibers. Frequently, an adjustment in the ferrule diameter will allow usage. However, at other times, the whole connector must be redesigned involving a very high cost. In general, most connector companies feel comfortable terminating glass-glass fibers and plastic-plastic fibers, the first is simply epoxied into a ferrule (optical contact) and then inserted into a connector; the second can be crimped and then inserted into a connector. Plastic clad silica fibers require special termination procedures resulting in losses of about 3 dB but may be useful in some systems.

Losses in a connector result from a variety of sources such as: inherent fiber losses due to differences in core diameter, NA, and refractive index profiles in the mating fibers. Losses in the connector itself result from axial misalignment, angular misalignment, and gap separation of the two fibers. Scattering losses result from imperfect fibers and preparation of the fibers.

In conclusion, Hughes connectors have both field connectors and Mil-Spec connectors which are multichannel and accept nearly all types of fibers and electric wire. These connectors are readily available and the field connector is the best of its kind. Amphenol has an off-the-shelf multipin connector (4-8 pin) that is being used on the Harrier Aircraft. AMP and Carron (IT&T) both have multipin (4-5-10 pin) connectors in various stages of development; prototypes, while

TABLE 2-17  
AVAILABLE MULTI-PIN CONNECTORS

MFR	APPLICABLE SPEC	NUMBER OF PINS	DEVELOPMENT STATUS	TYPE	APPROXIMATE COST (MATED PAIR)	dB LOSS	STRONG POINTS	WEAK POINTS
IT&T LEEDS OCN -CCXS	TESTED TO MEET ENGLISH MIL-SPEC  (EL2112 - PATTERN 602)	4 OR 8	<ul style="list-style-type: none"> <li>OFF-THE-SHELF</li> <li>EXCESSIVELY LONG LEAD TIMES EXPERIENCED</li> </ul>	<ul style="list-style-type: none"> <li>JEWELLED STAINLESS STEEL FERRULE</li> <li>PLASTIC GROMMET</li> <li>ROUND METAL BAYONET CONNECTOR</li> </ul>	\$1700 FOR SMALL QUANTITIES \$1400 FOR LARGER QUANTITIES	LESS THAN 1 dB (PCS OR GLASS FIBERS)	<ul style="list-style-type: none"> <li>AVAILABLE</li> <li>LOW LOSS TERMINATION</li> </ul>	<ul style="list-style-type: none"> <li>TERMINATION REQUIRES LENGTHY PROCEDURE</li> <li>NOT TESTED TO U.S. MIL-SPECS</li> <li>POOR DELIVERY EXPERIENCE</li> </ul>
IT&T CANNON	MIL-C-202	5 OR 10	PROTOTYPE HAS BEEN BUILT	<ul style="list-style-type: none"> <li>ROUND METAL THREADED CONNECTOR</li> <li>PLASTIC GROMMET</li> </ul>	\$500	GREATER THAN 2 dB EXPECTED		<ul style="list-style-type: none"> <li>NOT PRESENTLY AVAILABLE</li> </ul>
AMPHENOL  801 SERIES	MIL-C-83723	4 OR 8	OFF-THE-SHELF LEAD TIME 4-8 WEEKS	ROUND METAL THREADED CONNECTOR	4 PIN - \$400 8 PIN - \$1100	2 dB (GLASS)	<ul style="list-style-type: none"> <li>ENVIRONMENTALLY TESTED BY MCAIR</li> <li>WITH GLASS-GLASS TERMINATIONS THE dB LOSS WAS IN BETWEEN 1 AND 2 dB</li> </ul>	<ul style="list-style-type: none"> <li>STRAIN RELIEF REDESIGN REQUIRED</li> </ul>
AMP  D SERIES	NONE	10 OR MORE	OFF-THE-SHELF	<ul style="list-style-type: none"> <li>SQUARE METAL CONN WITH JACK SCREW</li> <li>PLASTIC INSERT</li> </ul>	\$200 (WITH 10 PINS)	TBD	<ul style="list-style-type: none"> <li>AVAILABILITY</li> </ul>	<ul style="list-style-type: none"> <li>BEST USE IS BUNDLE TECHNOLOGY</li> <li>NON-MIL SPEC CONNECTOR</li> </ul>
MFR	APPLICABLE SPEC	NUMBER OF PINS	DEVELOPMENT STATUS	TYPE	APPROXIMATE COST (MATED PAIR)	dB LOSS	STRONG POINTS	WEAK POINTS
HUGHES C-21 SERIES	MIL-C-85028	10 OR MORE	OFF-THE-SHELF LEAD TIME TWO OR THREE WEEKS	<ul style="list-style-type: none"> <li>SQUARE METAL CONN WITH JACK SCREW</li> <li>AVAILABLE WITH ALUMINUM INSERT</li> </ul>	\$700 (WITH 10 PINS)	2 dB (PCS FIBERS) ~ 1 dB (GLASS FIBERS)	<ul style="list-style-type: none"> <li>METAL INSERT PROVIDES EMP SHIELD</li> <li>MIL-SPEC CONNECTOR</li> </ul>	<ul style="list-style-type: none"> <li>STRAIN RELIEF MUST BE MODIFIED</li> <li>MODERATELY RUGGED</li> </ul>
HUGHES DEVELOPMENTAL CONNECTOR	NONE	6	6-8 WEEKS FOR SMALL QUANTITY	ROUND ALL-METAL THREADED CONNECTOR	\$500 (?) (IN QUANTITY OF 1000 OR MORE - \$3700 IN SMALL QUAN.)	SAME AS C-21 SERIES	<ul style="list-style-type: none"> <li>EASY TO TERMINATE, CLEAN &amp; REPAIR</li> <li>RUGGED</li> </ul>	<ul style="list-style-type: none"> <li>ONLY 6 PINS</li> <li>DEVELOPMENT COST INVOLVED IN ADDITIONAL PINS</li> </ul>
DEUTSCH OPTICAL WAVEGUIDE CONNECTOR	MIL-STD-202 MIL-C-00815110 MIL-STD-1344	1	OFF-THE-SHELF 6-8 WEEKS	<ul style="list-style-type: none"> <li>ROUND METAL BAYONET</li> <li>PLASTIC INSERT</li> <li>PLUG/RECIPTACLE/PLUG CONFIGURATION</li> <li>USES LENS TO LOWER LOSS</li> </ul>	\$150	< 1 dB FOR GLASS FIBERS	<ul style="list-style-type: none"> <li>FOR GLASS-GLASS TERMINATIONS THERE IS LESS THAN 1 dB LOSS</li> <li>FIELD TERMINATIONS</li> <li>EASILY TERMINATED USING SPECIAL TOOLS</li> </ul>	<ul style="list-style-type: none"> <li>MULTI-PIN CONNECTOR IS OVER A YEAR AWAY</li> <li>TERMINATIONS LIMITED TO THREE CABLE TYPES</li> </ul>

expensive, can be bought with long lead times. This situation should get better by the end of the year. Deutsch's Electric Components Division has introduced a low-loss connector that can be field-terminated in less than 10 minutes using a table model waveguide breaker and hand tools. The connector achieves losses of less than 1 dB by using a lens system for light coupling. This lens system is designed for specific fibers. A much smaller lens will eventually be incorporated into the multipin connector which is still under development.

## 2.5 STAR AND TEE COUPLER

In conventional wire systems the branching losses are overcome by an increase in transmitter power; however, in a fiber optics system of moderate data rates there is a limit to the available power source. The amount of optical power, coupled to the fiber in the dbm minus that which is required by the receiver in dbm for a given bit error rate, determines the excess power in dB that may be used for fiber and connector losses. For a fiber optic system to replace the wire data buses on a space avionics system, many branching paths are required. There are two branching configurations for fiber optic data distribution networks. These are: T coupler (a serial distribution system) and star coupler (a parallel system). There also is a hybrid system made up of T couplers and star couplers. The star, T, and hybrid couplers are depicted in Figure 2-23. The T configuration employs T couplers dispersed along the fiber optics line. This configuration, while convenient, imposes severe limitations on the fiber optic bus because of the high loss per T coupler. However, the T has the advantage in that to add another terminal to an existing system, another T coupler is simply added to the system. In the star system, adding a terminal requires replacing star couplers. Most of the original work done on the star coupler has been performed by Hudson and Thiel.

The star coupler (Figure 2-23) consists of a number of optical fiber bundles terminated by a dielectric glass rod. The glass rod is surrounded by a cladding whose index of refraction is lower than that of the glass core. This cladding causes total internal reflection. The reflected light from the fiber bundles is directed towards the mirrored end where it is reflected back to the fiber bundles. In this manner, the light is uniformly distributed over the face of the fiber bundle. The glass rod is called a mixer, and as such, functions by dividing the power equally between all bundles.

10-2666

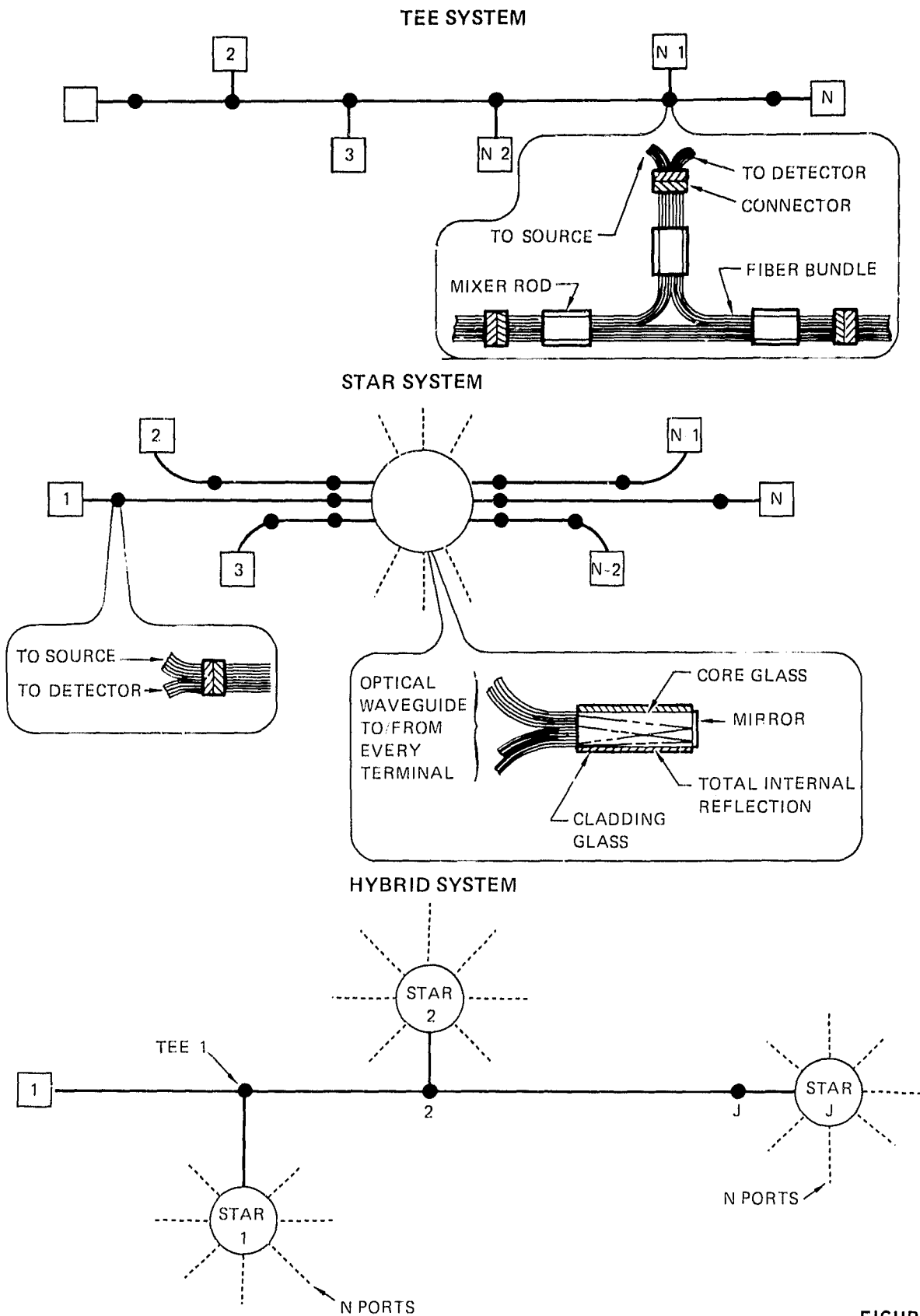


FIGURE 2-23

For the star coupler the optical losses are:

- $L_C$  = insertion loss associated with the cable connectors
- $L_{CI}$  = insertion loss of the star coupler
- $L_S$  = splitting factor of bidirectional input-output connector
- $L_T = 10 \log (1/N)$  is the tap ratio or splitting factor of the star coupler.

Since, in a star system, the worst case loss is the loss between any two terminals, we have the power ratio (between terminal j and k) given by

$$P_j/P_k = 4L_C + L_{CI} + L_T + L_S \quad (2.32)$$

The T system has the following system losses:

- $L_{CI}$  = internal insertion loss of the access couplers
- $L_C$  = insertion loss of the cable couplers attached to the access coupler at each of the three ports
- $L_S$  = splitting factor of the duplex input-output coupler necessary for bidirectional operation; this always has the value -3 dB
- $L_T$  = tap ratio of the access coupler
- $L_{IT} = 10 \log (1 - 10^{-L_T/10})$

The two can be combined to form a hybrid system. The system losses are defined as above and power loss is given by the following expression<sup>(16)</sup>

$$\begin{aligned} \frac{P_{NT-1}}{P_1} = & (2L_C + L_{CI} + L_{IT}) (J - 3) + (2L_C + L_{CI} + L_T) + L_S \quad \text{(Tee)} \\ & + 4L_C + L_{CI} + L_S + 10 \log (N) \quad \text{(Star)} \end{aligned} \quad (2.33)$$

where

$N$  = number of terminals

$J$  = number of T couplers used.

If we choose the following typical system parameters:

$$\begin{aligned} L_C &= 1 \text{ dB} \\ L_{CI} &= 2 \text{ dB (T)} \\ L_T &= 10 \text{ dB (T)} \\ L_{CI} &= 7 \text{ dB (Star)} \\ L_S &= 3 \text{ dB} \end{aligned}$$

Then it is possible to plot the three worst case losses for the Star, T, and hybrid systems. With the above system parameters the loss expression for each system may be shown to be

$$\begin{aligned} P_{N-1}/P_1 &= 4.46 (N-3) = 17 && \text{T System} \\ P_J/P_K &= 14 = 10 \text{ Log } N && \text{Star System} \\ \frac{P_{NJ-1}}{P_1} &= 4.46(J-3) + 17 + 14 + 10 \text{ Log } (N) && \text{Hybrid System} \end{aligned}$$

These three expressions are plotted in Figure 2-24 for various values of N and J. As can be seen from the figure, the star system is by far the more superior from a loss standpoint. However, it has the disadvantage of the centrally located mixing point. The graph also indicates that with a properly designed hybrid system a workable fiber system can be designed. The losses depicted in Figure 2-24 are worst case losses; in a real-life fiber system these losses will be considerably less.

## 2.6 Single-Fiber vs. Bundle-Fiber Systems

The information presented in Section 2.4 suggests that most of the future fiber space avionics systems will have to employ single-fiber technology. If single fibers are used, then care must be taken to ensure that the light emitting area of the source is less than the area of the core of the fiber. Under these conditions, due mainly to solid angle factors, the loss between the source and the single fibers is slightly greater than 10 dB.

Once single fibers are employed, the connector-to-connector losses are reduced to somewhere under 2 dB. This reduction of connector losses enables vastly expanded architecture system capability. However, the price paid in going the



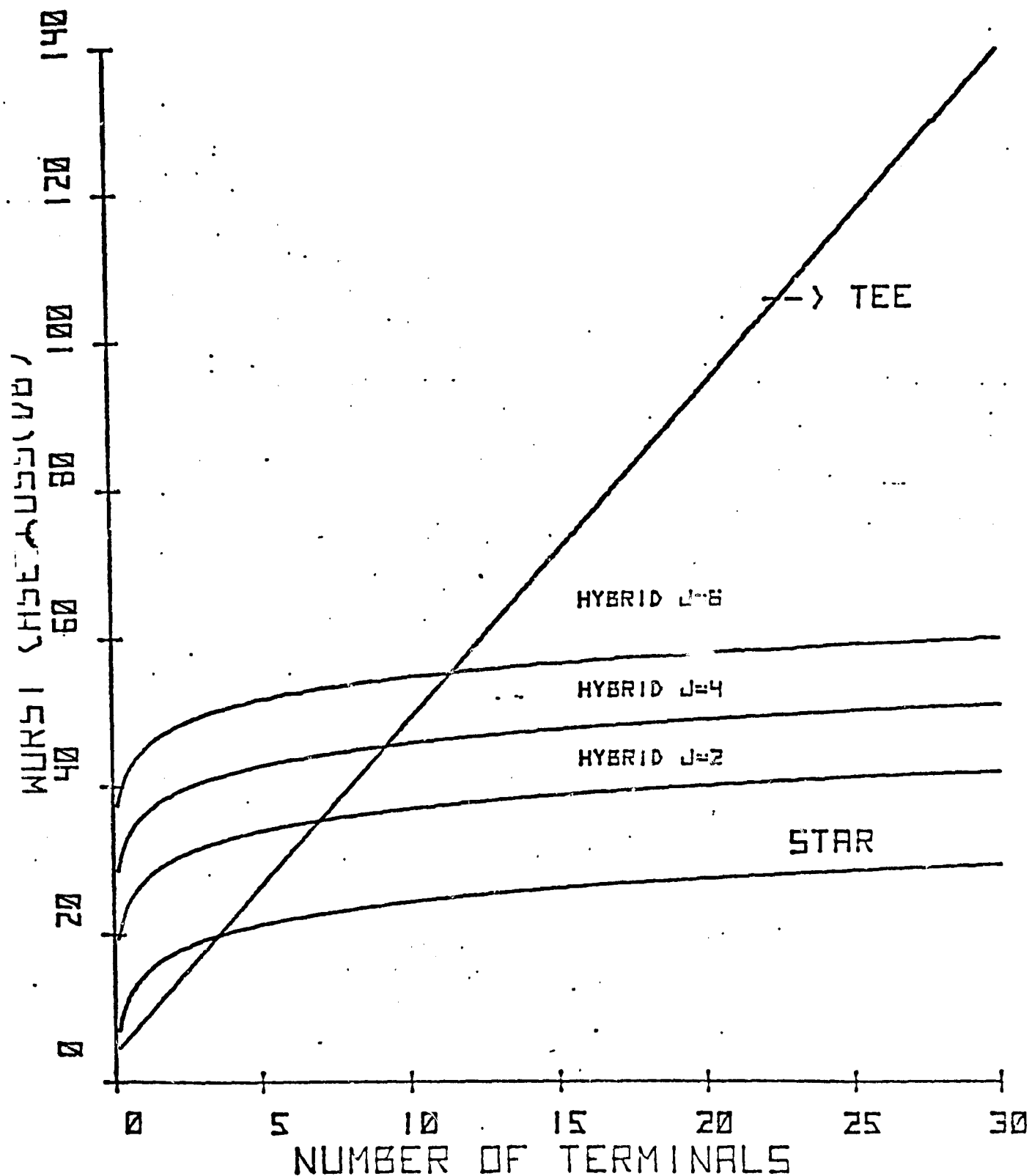


FIGURE 2-24

single-fiber route is a loss of redundancy. Redundancy may be incorporated in the system by employing a bidirectional coupler as shown in Figure 2-25. The implication to the system margin may be understood by applying the law of conservation of radiance at points 1 and 2. At point 1 the bidirectional coupler acts only as a power splitter, while at point 2 the coupler is used to mix the radiation again. The coupler used to mix the radiation introduces a 3 dB loss. The reason for this is if the N.A. of all three fibers are the same there is an area mismatch at point 2. This mismatch causes the 3 dB loss. Another way to view the bidirectional coupler is as a star coupler with  $n$  equal to two. The price of a 3 dB system power loss is a small one for the sake of redundancy.

## 2.7 SYSTEM CONSIDERATIONS

The final configuration for any fiber data bus system depends on the particular architecture of the bus. In this section, information is presented using state-of-the-art fiber types and electronic components to obtain a crude estimation on how well any given system will perform. This section is self-contained; however, the information is based on material presented in Sections 2.1 through 2.7. The different types of fiber systems possible are shown in Figure 2-26. The material presented in this section will mainly analyze the point-to-point link. The extension to other systems may be realized by using the information presented in Section 2.7.4 Link Length, and Section 2.7.6 Different System Architectures.

The type of fiber components employed in the link depends on such parameters as data modulation format, data rate, link length, required minimum bit error rate, link security, system lifetime, radiation hardness, system cost, etc. Often these parameters are related such that optimization of one set yields simultaneous degradations to others; hence, for any given fiber system there may be no true optimum system configuration. For example, as the length of the link is increased, to reduce repeater cost, the data rate must be reduced making the system more nuclear-radiation sensitive.

### 2.7.1 Sources

The type of source employed in the link is usually driven by such factors as ease of modulation, size, weight, and wavelength of sources. Sources such as gas lasers and solid-state lasers are usually ruled out because of their size

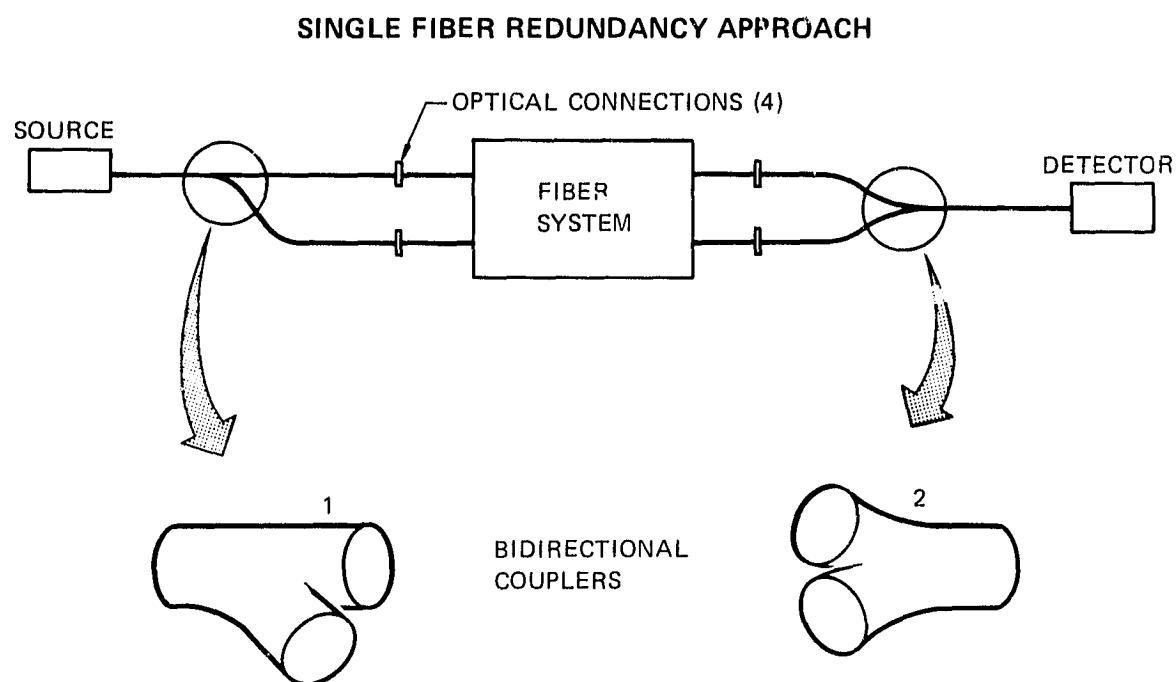


FIGURE 2-25

10-1980

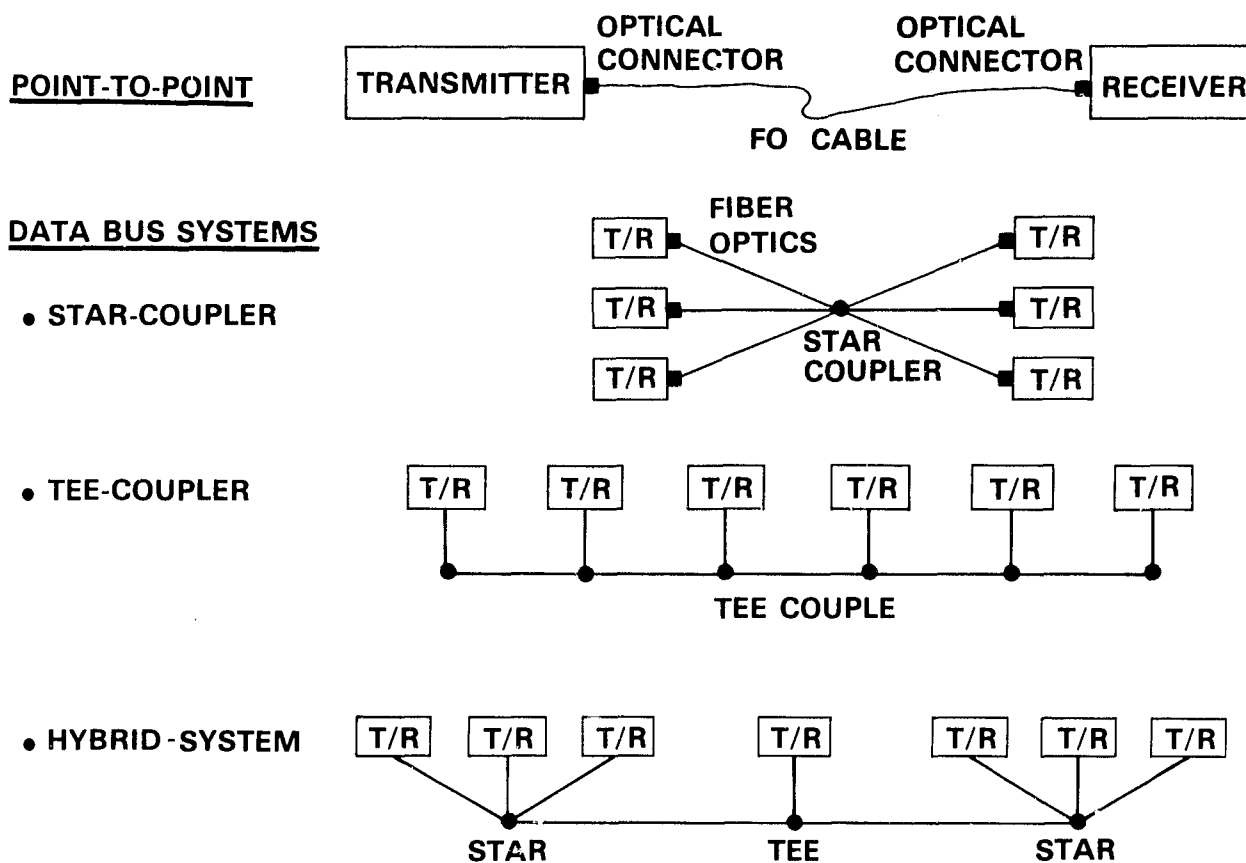
**FIBER OPTIC SYSTEMS**

FIGURE 2-26

and difficulty of modulation. To date, the source most often employed in fiber links has been semiconductor devices such as a light emitting diode (LED) and injection laser diode (ILD). These devices have the distinct advantage that they can be directly modulated. The technology of the devices employed is dependent upon the wavelength of light required. Most of the LED's, which are often modeled as Lambertian sources, have total output power of minus a few dBm while the ILD has on the order of a few to 10 dBm. The advantages of using an ILD over LED as the source to a fiber system are threefold: ILD's have more power available to couple in the fiber, the fiber is capable of accepting more power from the ILD, and the ILD has a much narrower spectral width; hence, temporal dispersion is reduced. However, the ILD has a shorter lifetime.

### 2.7.2 Fibers

The choice of fibers employed is usually driven by the link length, link data rate, and to some extent, the amount of nuclear hardness. The most common fiber produced today is the glass-glass stepped-index fiber. The core, made of pure fused silica, is lightly doped with  $\text{GeO}_2$  to increase its index of refraction. This increase in index enables the fiber to waveguide the light. The glass-glass stepped-index fiber has a core diameter of about 65  $\mu\text{m}$ , numerical aperture (N.A.) of 0.23, loss of about 10 dB/km at 850 nm, and pulse dispersion of 15 ns/km. Generally, this fiber is only used for lower data rate short-length fiber links. If link length or data rate needs to be increased, graded-index fibers may be employed. Graded-index fibers have a core index profile which is maximum at the center and quadratically varies to a minimum value at the core-cladding interface. The graded-index fiber has a diameter of about 65  $\mu\text{m}$ , N.A. = 0.2, loss of about 6 dB/km at 850 nm, and pulse dispersion of 2.5 ns/km.

Both the stepped-index and graded-index fibers are multimode fibers; hence, they produce or cause a great deal of pulse spreading by temporal dispersion in the fiber. If long link length and high data rates are required, then single-mode fiber must be used. A multimode stepped-index fiber can be made single-mode by decreasing the N.A. and the core diameter to the point where only a single-mode of radiation is supported in the waveguide. A typical value for this diameter is 5  $\mu\text{m}$  with the N.A. equaling 0.096 at 850 nm. At these small values of fiber parameters, collecting the light from the source becomes a problem, as the source-to-fiber alignment is critical and the reduced N.A. makes the fiber an

inefficient light collector. Nevertheless, the temporal dispersion is extremely low and has been shown by Gloge to be for  $HE_{11}$  mode<sup>(14)</sup>

$$S = 333. \left( \frac{\Delta\lambda}{\lambda} \right) \left[ \frac{RdN_1}{dR} + (N_1 - N_2) \frac{vd^2(vb)}{dv^2} \right] \text{ ns/km} \quad (2.34)$$

where  $\Delta\lambda$  is source bandwidth,  $\lambda$  is the center wavelength of the source,  $k_1$  is the wavenumber,  $N_1 = d(kn_1)/dk$ ,  $N_2 = d(kn_2)/dk$ ,  $v$  is the normalized frequency, while  $b$  is the normalized propagation constant. Equation (2.34) will be used to determine link lengths in a later section.

The length of the link will depend on the dB/km loss of the fiber and the loss per fiber termination. In the graded-index case, these terminations are no problem as the dB loss is on the order of 0.5 dB or less. However, in the single-mode case, standard optical connectors have not been developed and would have to have extremely exacting tolerances considering the core diameter of the fiber. Hence, for longer single mode fiber links, an optical splice would have to be made. These splices are usually about a half dB or less.

### 2.7.3 Detectors

The most commonly employed receiver detectors in a fiber link are either PIN diodes or avalanche photodiodes (APD). The APD, which uses internal gain to increase sensitivity, is approximately 20 dB more sensitive than a PIN for a given data rate. The PIN diodes is usually used with a field effect transistor (FET) front-end for data rates at or below 5 Mbps, while for higher modulation rates a bipolar front-end is employed. In both devices the risetimes are inversely related to collector area; hence, at higher data rates the detector must become smaller, thus making the alignment between fiber and detector more critical. The signal power at the required APD detector for a  $10^{-8}$  bit error rate (BER) is, as a function of data rate

$$\text{dBm} = +10 \text{ Log } R - 70 \quad (2.35)$$

where  $R$  in Equation (2.35) is in Mbps.

2.7.4 Link Length

The maximum system link length depends on the source type, the type of fiber employed, and the detector. As with any communication system, the link can either be power starved or limited by the dispersion of the transmission medium. The system length in km as a function of data rate for an APD for  $10^{-8}$  BER is given by

$$X = \frac{P_1 - [10 \log R - 70] - 0.5 [\text{INT } x/2] - K_1 - K_2}{a} \quad (2.36)$$

Where, in Equation (2.36),  $P_1$  is the output power of the source in dBm,  $K_1$  is the loss between the source and the fiber,  $K_2$  is the loss between the fiber and the detector,  $a$  is the loss of the fiber in dB/km,  $R$  is the data rate in Mbps, and INT is the integer value of  $x/2$  and is used to represent the splice loss.

The maximum dispersion that the system can accommodate is related to the pulse broadening in the fiber, which in turn is related to the impulse response of the fiber. The expression for this is fairly complex and in general quite difficult to evaluate; however, a reasonable estimation of system length, as a function of pulse dispersion and data rate, can be made by assuming that the overall system risetime is 1.1 times the square root of the sum of squares of the transmitter, fiber, and receiver risetimes. To assure little or no dispersion effects, the risetime of the system should be less than or equal to  $0.35/R \times 10^6$ . If the receiver and detector are assumed to be ideal then the maximum system length is

$$X = \frac{0.35 \times 10^{-15}}{RS} \quad (\text{km}) \quad (2.37)$$

If the detector and transmitter are not ideal then the inequality

$$1.1 \left( t_d^2 + t_t^2 + (XS)^2 + (t_m X)^2 \right)^{1/2} \leq \frac{0.35 \times 10^{-15}}{R} \quad (2.38)$$

must hold. Where  $t_d$  is the detector risetime in ns,  $t_t$  is the risetime of the source, also in ns,  $t_m$  is risetime caused by material dispersion of the source. The value of  $t_m$  is typically 5.5 ns/km for and LED and usually negligible for ILD.

Equations (2.36) and (2.37) are plotted in Figure 2-27 for glass-glass stepped-index, graded-index, and single-mode fibers assuming the following system parameters

$$P_1 = +10 \text{ dBm (ILD)} \quad K_1 = 12 \text{ dB} \quad K_2 = 1 \text{ dB} \quad \lambda = 850 \text{ nm}$$

$$\frac{Vd^2(Vb)}{dV^2} = 0.15 \quad \frac{kdN_1}{dk} = 0.05 \quad N_1 - N_2 = 0.015$$

Figure 2-27 can be used to obtain an estimate of system repeater spacing; hence, an idea of overall system cost. For example, if a 100 Mbps system is desired, either single-mode fiber or graded-index may be employed. However, if graded fibers are used, the system is limited by dispersion and must have a repeater every kilometer or so, while if a single-mode fiber is used with a source which has a 2 nm bandwidth, then repeater spacing on the order of 8 km can be obtained. Also, from Figure 2-27 it is seen that if a 0.2 nm source is employed with single-mode fiber (loss of 5 dBm) the 1 Gbps system could have repeater lengths of 6-8 km. These numbers indicate large economical savings over conventional wire systems.

#### 2.7.5 Nuclear Hardness

The hardness of a system in relation to radiation is dependent upon the nature of the individual components used and the amount of radiation to which the system will be exposed. In the light source, radiation degradation usually shows up in the form of nonradiating sites in the energy band of the device. These sites reduce the differential quantum efficiency, thus reducing the output of the device. However, if certain ternary elements such as Al are added to the devices, the sources become hard. The hardness is believed to come about because the ternary elements act as annealing centers. Hence, if a device such as a GaAlAs ILD is used, it should be hard.

Certain fibers become opaque when they are exposed to gamma radiation, and fluoresce for brief periods of time. When the fiber is exposed, local color sites are formed. These sites act as absorbers in 800-900 nm range and have little effect at longer wavelengths such as 1.06  $\mu\text{m}$  as can be seen from Figure 2-28. The local color sites anneal with time. In general, the hardness of the fiber to radiation appears to be related to the amount of doping in the core, the



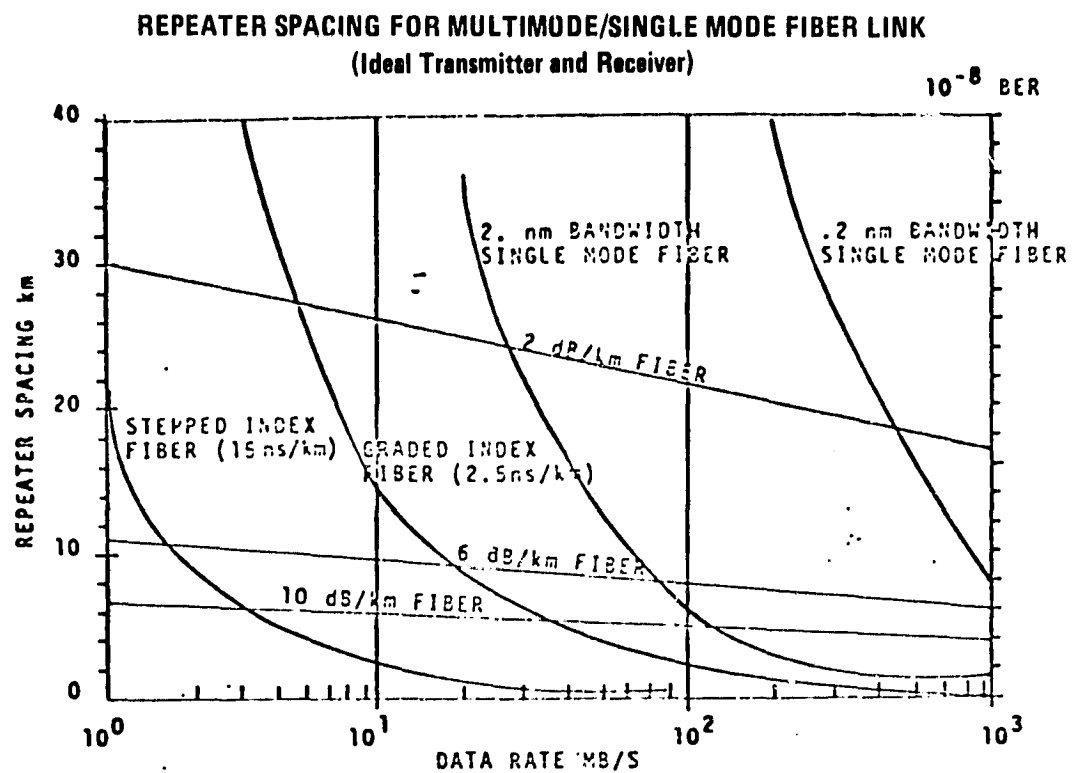
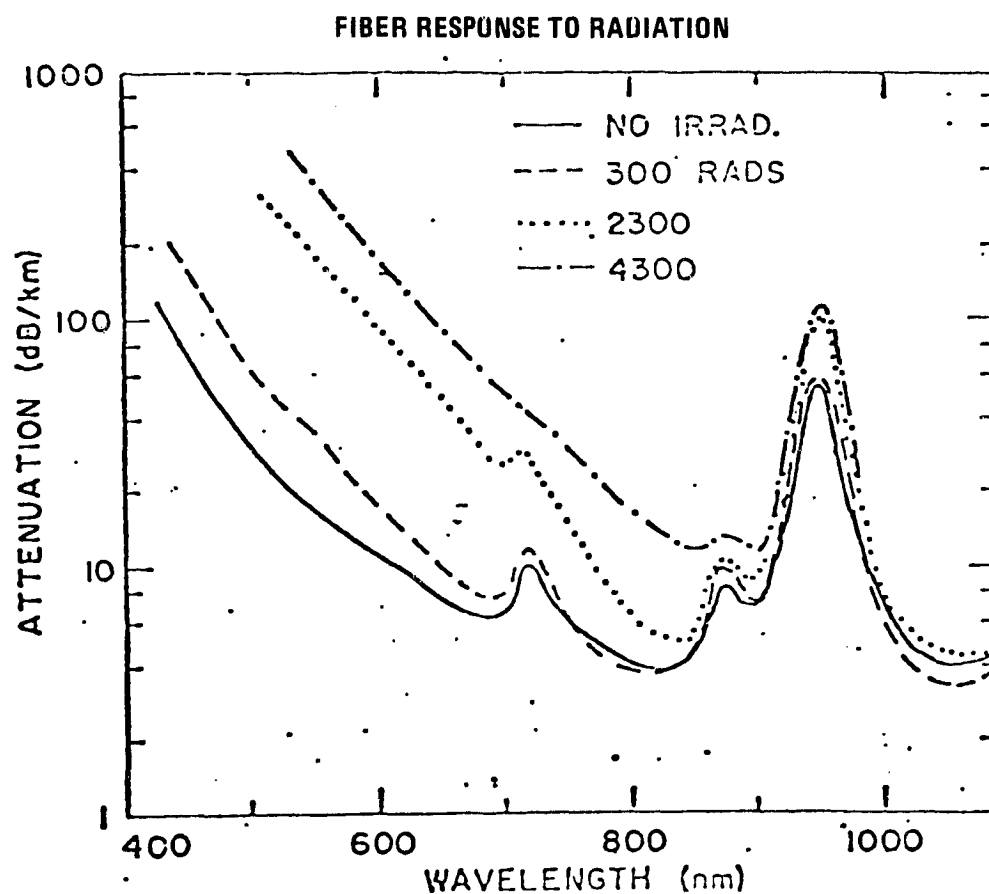


FIGURE 2-27

(SANDIA LAB)  
FIGURE 2-28

less the better. The effects on system degradation caused by radiation may be included in the margin calculations by the inclusion of an extra loss term  $K_R$  in dBs.  $K_R$  values may be obtained from the information presented in Section 2.1.8.

#### 2.7.6 Different System Architectures

The extension of the material presented in 2.7.1 to 2.7.5 to take into account different bus architectures may be accomplished in a straightforward manner. For any given fiber data bus, shown in Figure 2-29, the risetime analysis is independent of bus architecture employed; hence, the inequality expressed in Equation (2.37) must hold to insure that the system is not operating in the dispersion-limited mode. If the overall system risetimes satisfy the inequality in Equation (2.37) then to determine whether the system will perform from a margin standpoint, the total system power budget must be computed. To do this, first compute all the losses that are encountered from going from point-to-point in the system. These losses should be worst case and typically will include:

- Time degradation effect (3-5 dB)
- Source to detector loss
- The sum of all connector losses
- The total fiber loss
- The loss going through tees
- The loss going through the star
- Loss between fiber and detector
- Loss due to radiation

Once the total losses have been computed the amount of available optical power in the system should be obtained. For an APD the power required for a  $10^{-8}$  BER in dBm is

$$q = 10 \log R - 70 \quad (2.39)$$

while for a PIN

$$q = 10 \log R - 55 \quad (2.40)$$

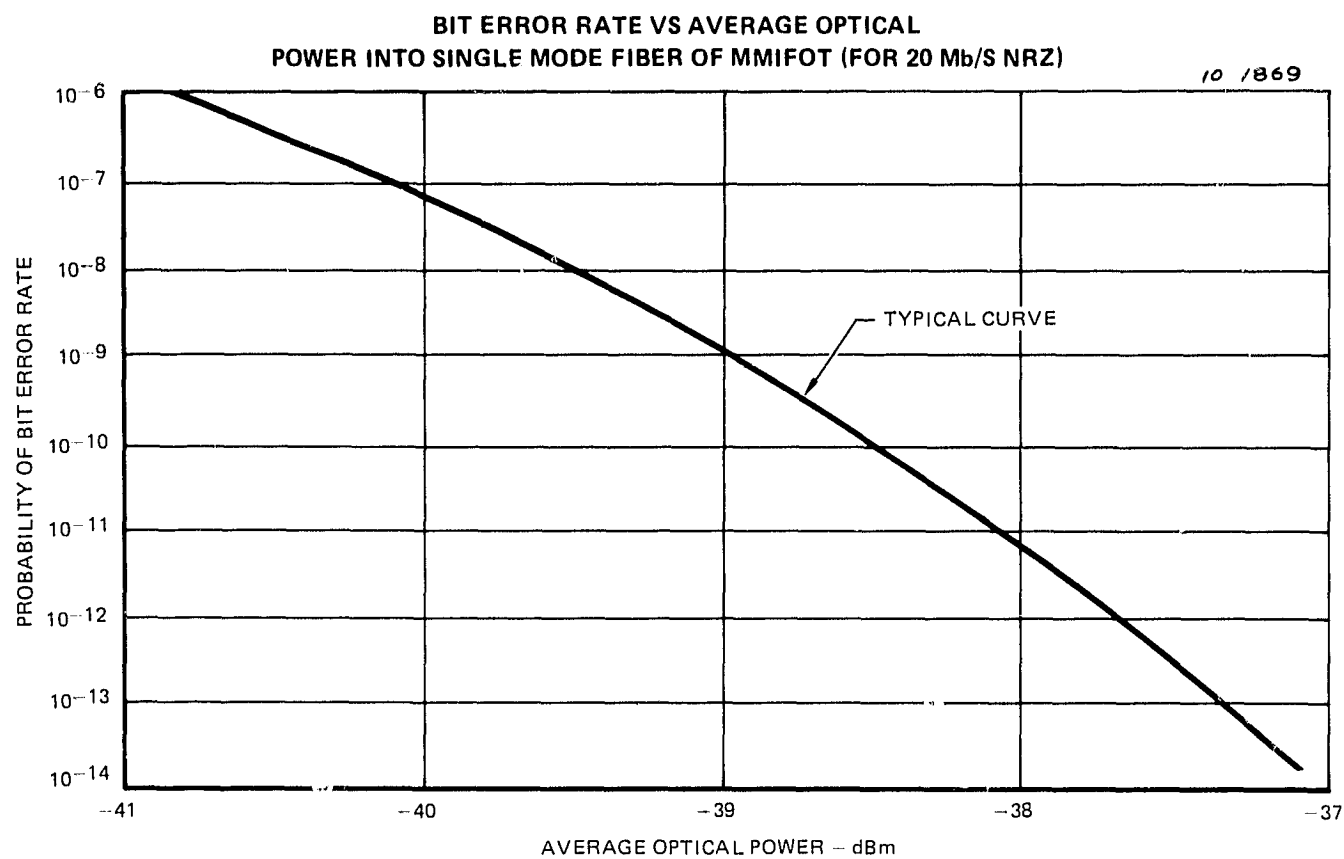


FIGURE 2-29

If the output power of the LED or ILD in dBm is  $u$ , then the system margin (SM) is

$$SM = u - q - \sum \text{all other system losses} \quad (2.41)$$

The larger the value of SM the better the system will perform. The effect of a few dB on error rate is shown in Figure 2-29.

If the SM in Equation (2.40) turns out to be less than zero then the designer has four choices. One, he may increase the output power of the source; this probably means going from LED to ILD. Two, he may increase the receiver sensitivity; probably by using an APD instead of a PIN. Three, he may reduce the system data rate, or four, he may have to put a repeater in the system somewhere.

#### 2.7.7 Vendor Fiber Optic System Tables

Companies such as IT&T, Galileo, RCA, and Spectronics make fiber optic system components, but they also make fiber optic systems as well. These systems may be as simple as a pin photodetector and preamp to the complete fiber optic system including fiber optic cable; nevertheless, this section will only include the transmitter/receiver systems. Tables 2-18 and 2-19 give a list of the more important parameters and a comparison of the two transmitter options (LED/ILD) and two receiver systems (PIN/APD).

A few comments about Table 2-18. First, the Galileo and Hewlett Packard transmitter/receiver system suffers from low data rate, low operation temperature range, and low excess margin. The disadvantage of the Plessey and RCA system is the low excess margin. The IT&T T614/T615 and T612/T606 both have low excess margin; the T614/T615 system also has low data rate; and finally the IT&T T612/T606 requires four (4) voltage supplies and an uncertain operating temperature range. The IT&T T612/T613 system is satisfactory in most respects but requires four power voltage supplies, APD detector, and again questionable operating temperature range. In general, the Spectronics systems are satisfactory in all respects except they require high voltage.

TABLE 2-18

TRANSMITTER PART NUMBER	TX POWER	RECEIVER SENSITIVITY	MARGIN ABOVE 10 <sup>-8</sup> B/S BER	SYSTEM LOSSES	SYSTEM EXCESS MARGIN	RECEIVER DYNAMIC RANGE	DATA RATE (MAWCHIESTER)	TEMP. (OPERATING)	POWER REQUIREMENTS	NUCL. SURVIVABILITY
PHILCO MODEL 3555071N RECEIVER PHILCO 355971T TRANSMITTER	-12 dBm	-30 dBm	28 dB	8 dB	10 dB	-	2.5 Mbits	0° TO +75°C for TRANSMITTER	+5 @ 40 ma -5 @ 10 ma +5.5 @ 100 ma	TESTING NEEDED
RAYTHEON Q14U	-13 dBm	-30 dBm	17 dB	8 dB	9 dB	15 dB	15 Mbits	-20° TO +50°C	+5 @ 300 ma +12 @ 150 ma	TESTING NEEDED
RAYTHEON Q14U	-10 dBm	-27 dBm	17 dB	8 dB	9 dB	-	10 Mbits	-	+5 @ 250 ma +6 @ 30 ma -6 @ 20 ma	TESTING NEEDED
ITT X14-TRANS X15-REC	-12.5 dBm	-28 dBm	15.5 dB	8 dB	7.5 dB	15 dB	2.5 Mbits	-20°C TO +50°C	+5 @ 275 ma -5 @ 75 ma	TESTING NEEDED
ITT X14-TRANS X15-REC	-12 dBm	-33 dBm	21 dB	8 dB	13 dB	15 dB	10 Mbits	-	+5 @ 250 ma +5 @ 75 ma +15 @ 100 ma -13 @ 75 ma	TESTING NEEDED
ITT X14-TRANS X15-REC	-12 dBm	-31 dBm	19 dB	8 dB	11 dB	21 dB	5 Mbits	0° TO +70°C	+5 @ 170 ma +5 @ 10 ma	TESTING NEEDED
ITT X14-TRANS X15-REC	-12 dBm	-32 dBm	40 dB	8 dB	32 dB	20 dB	10 Mbits	-	+5 @ 250 ma +5 @ 75 ma +13 @ 100 ma -13 @ 75 ma	TESTING NEEDED
ELECTRONICS X3619-TRANS X3620-REC D-RCA C30133 H-RCA C30807	-10 dBm	-35 dBm	23 dB	8 dB	15 dB	33 dB	10 Mbits	-40°C TO +80°C	+5 @ 70 ma +5 @ 200 ma +45 @ 1 ma	TESTING NEEDED
ELECTRONICS X3619-TRANS X3620-REC D-RCA C30133 H-RCA C30895	-10 dBm	-50 dBm	40 dB	8 dB	32 dB	30 dB	10 Mbits	-46° TO +71°C	+5 @ 70 ma +5 @ 200 ma +335 @ 1 ma	TESTING NEEDED
ELECTRONICS X3619-TRANS D-RCA C30133 H-RCA C30918E	-10 dBm	-40 dBm	30 dB	8 dB	22 dB	20 dB	10 Mbits	-40°C TO +80°C	+5 @ 200 ma +6 @ 200 ma -6 @ 200 ma +45 @ 1 ma	TESTING NEEDED

TABLE 2--19  
FIBER OPTIC DEVICE COMPARISON

	TRANSMITTER CIRCUITS		RECEIVER CIRCUITS	
	ILD	LED	PIN	APD
TEMPERATURE	0°C TO 50°C	-40°C TO +90°C	-40°C TO +80°C	-40°C TO +70°C
DRIVER REQUIREMENTS	RESISTANCE HEATING & THERMO ELECTRIC COOLING REQUIRED. CONSTANT CURRENT DRIVER REQUIRED	VARY DRIVE CURRENT WITH TEMPERATURE TO MAINTAIN LEVEL OUTPUT.		
RECEIVER REQUIREMENTS			NO TEMPERATURE COMPENSATION NECESSARY	<ul style="list-style-type: none"> <li>o HIGH VOLTAGE REQUIRED FOR BIAS.</li> <li>o CIRCUIT REQUIRED TO MAINTAIN GAIN OVER TEMPERATURE RANGE.</li> </ul>
RADIATION HARDENING	BETTER THAN LED HIGHER CURRENT DENSITY AIDS RECOVERY	CONSIDERED GOOD BUT TESTING REQUIRED TO DETERMINE LEVEL OF HARDNESS	CONSIDERED GOOD BUT TESTING REQUIRED TO DETERMINE LEVEL OF HARDNESS	WORSE THAN PIN LOSS OF APD GAIN WITH RADIATION
OUTPUT INTO POWER PIGTAIL	0dBm (1mw)	-12 dBm (80μw)		
RECEIVER SENSITIVITY			-40 dBm	-55 dBm
RECEIVER DYNAMIC RANGE			-10 dBm TO -40 dBm	-25 dBm TO -55 dBm
COST/1000	\$350	\$250	\$300	\$400
RELIABILITY	NOT ENOUGH TEST DATA AT THIS TIME LED CONSIDERED SLIGHTLY BETTER THAN ILD		NOT ENOUGH TEST DATA AT THIS TIME PIN CONSIDERED SLIGHTLY BETTER THAN APD	
LIFETIME	10 <sup>3</sup> HOURS WITH 3dB LOSS	10 <sup>4</sup> HOURS WITH 3dB LOSS	10 <sup>6</sup> HOURS	NO SIGNIFICANT TEST DATA
INPUT POWER	+5V @ 200 ma	+5 @ 100 ma	+45 @ 1 ma +6 @ 50 ma, -6 @ 50 ma	+355 @ 1 ma +6 @ 50 ma, -6 @ 50 ma

### 3.0 DATA BUS SYSTEM

#### 3.1 SPACE SHUTTLE DATA BUS SYSTEM

Part of the contract requirement was to establish a requirements definition document for a fiber optic data bus configured similar to that which is on Space Shuttle. This document is contained in Appendix A, while seventeen different Shuttle data bus system losses in an optical radial data bus configuration have been computed in Appendix B. The results of this study are somewhat dated as it employed bundle technology.

#### 3.2 FIBER SYSTEM SIZE, WEIGHT, AND POWER

Installation of a fiber optic data bus in place of an existing electrical data bus would not result in a significant increase in either size, weight, or power. As an example, assume the data bus selected for the fiber optics system has a length of 200 feet (60 meters) (this length is characteristics of the longer buses for the Shuttle) and 7 data bus stubs each 3 feet (0.9 meters) in length. Replacement of seven data bus couplers with seven optical couplers and seven transmitter/receiver package results in an increase of only 5400 cm<sup>3</sup> (330 in<sup>3</sup>) in Shuttle avionics hardware. If the transmitter/receiver packages were installed on Multiplexer Interface Adapter boards, as is discussed in Section 3.3, a reduction in equipment volume can be achieved.

Two hundred and twenty-one feet of 24-AWG twisted-shielded wire and 7 data bus couplers weigh approximately 1.1 Kg (2.5 lbs). A similar length of 19-strand optical fiber cable, 7 optical couplers, and 7 transmitter receiver packages weigh approximately 5.4 Kg (12 lbs). Thus, the weight increase is only 4.3 Kg (9.6 lbs) for the optical system. Based upon a power consumption of 3 watts per transmitter/receiver package, the net power increase for the optical system is only 18 watts.

#### 3.3 FIBER OPTIC SYSTEM INTERFACE WITH SPACE SHUTTLE

Figure 3-1 shows Flight Critical Bus 1 in an optical bus configuration. The changes to FC1 from the electrical bus configuration to the optical bus configuration include the installation of optical transmitter/receiver packages and the substitution of optical couplers for electrical data bus couplers. The transmitter/receiver characteristics must be compatible with the Multiplexer Interface Adapter so that the interface between the General Purpose Computers

SINGLE DATA BUS - OPTICAL SYSTEM  
FLIGHT CRITICAL BUS 1

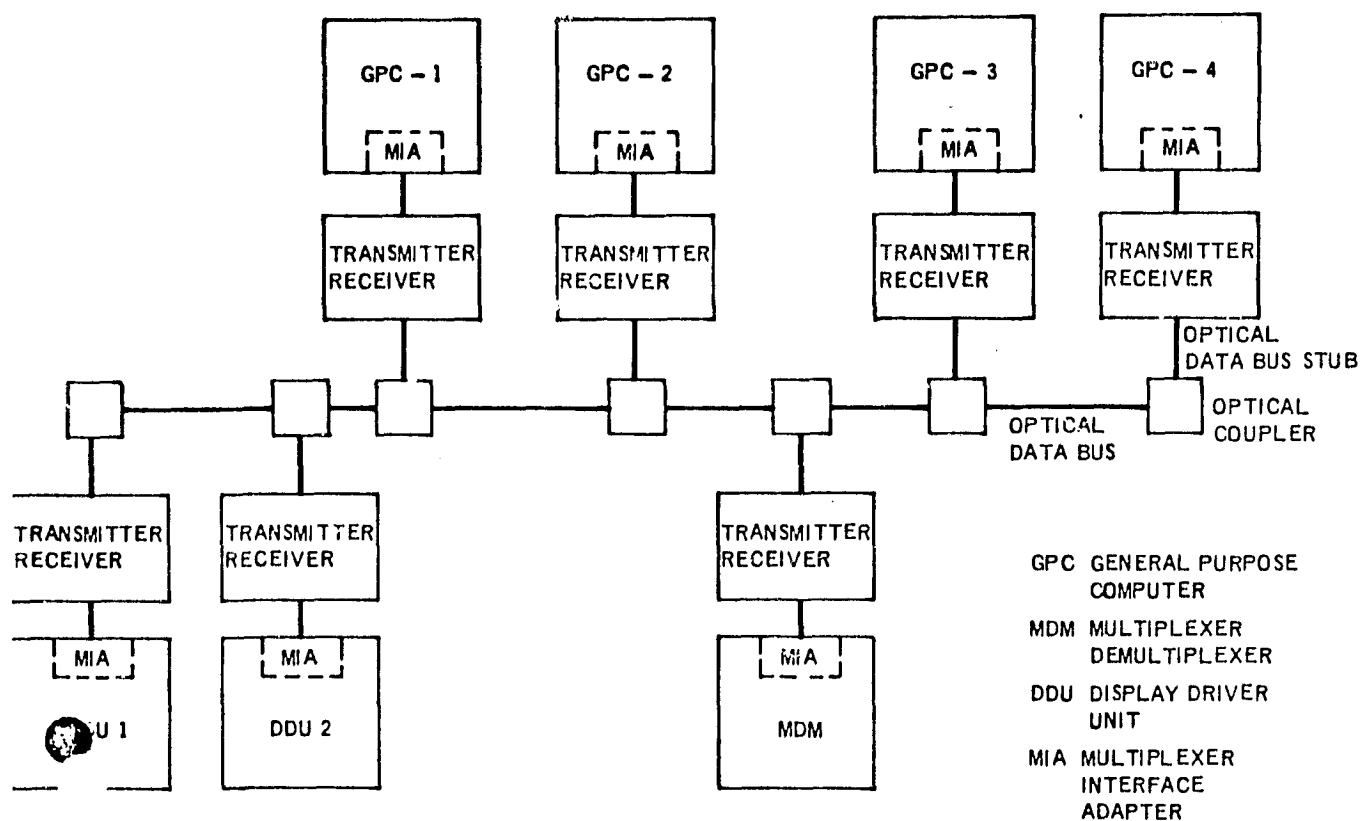


FIGURE 3-1

OPTICAL DATA BUS COUPLER

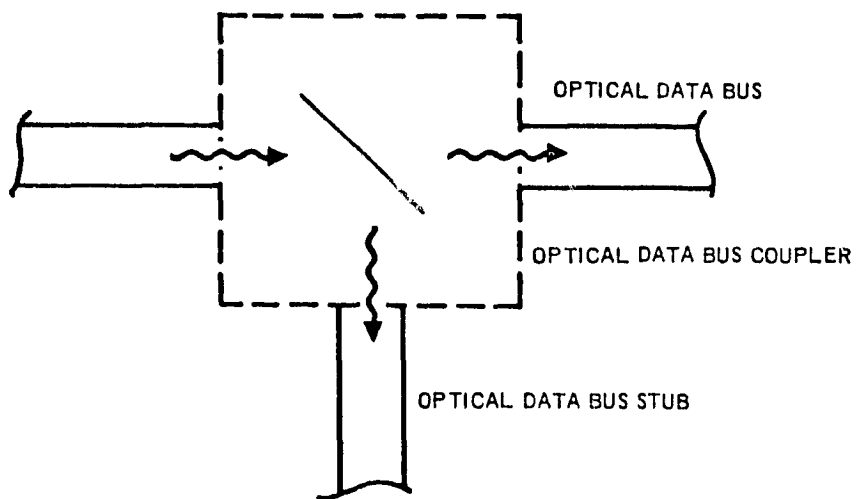


FIGURE 3-2



and Bus Terminal Units remains unchanged. For illustrative purposes, the optical transmitter/receiver package is shown external to the GPC and BTU. The possibility of an optical transmitter/receiver module for installation on the MIA within each GPC or BTU will be addressed in the component study.

An optical coupler similar to that shown in Figure 3-2 will provide the connection between the optical data bus and the data bus stub. The optical coupler provides fault isolation similar to that of the electrical data bus coupler on the existing Space Shuttle Data Bus.

While FC1 has been selected for illustration of the optical data bus system, it is by no means the only candidate bus for the optical system. Flight critical Bus 5, for example, is one of the longest data buses on Shuttle, and, as such, should be considered for the optical system. In addition, McDonnell Douglas Technical Services Company (MDTSCO) has performed and published a noise prediction study of FC5; therefore, comparisons between the predicted interference levels, the actual performance of FC5 in copper wire bus configuration, and the performance of FC5 in an optical bus configuration can be made.

Details of a portion of the optical data bus system are shown in Figures 3-3 and 3-4. The illustration of Figure 3-3 is a single cable system. In this configuration the optical signal is bidirectionally transmitted along a single optical fiber bundle. The single cable system requires fewer fiber optic cable than does the bifurcated cable bus shown in Figure 3-4. With the bifurcated cable system, the data from the GPC to the BTU is transmitted along one optical cable. The bifurcated cable configuration requires fewer total optical couplers per data bus and each optical signal need pass through only one coupler from GPC to BUT versus three couplers for the single cable system. Fewer couplers have the advantage of reducing the loss between the transmitter and receiver.

#### 3.4 SECURITY CAPABILITY

With traditional copper wire digital data bus systems, the metallic conductor acts as an antenna for both reception of unwanted interference signals and radiated transmission of the digital information carried along the conductor. For data systems that contain secure information, special testing is required to insure that this secure data is not inadvertently transmitted through conductor radiation. Since the fiber optic cable does not contain a long current

SINGLE CABLE BUS

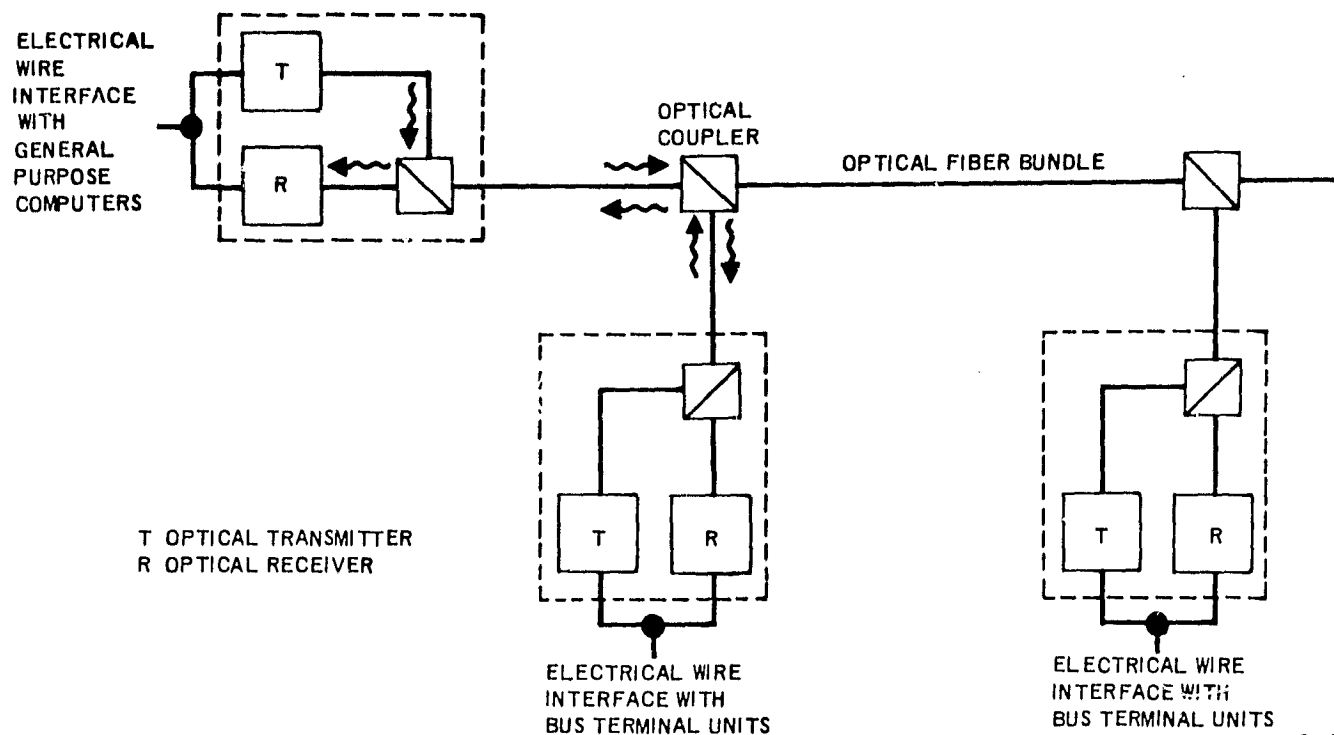


FIGURE 3-3

BIFURCATED CABLE BUS

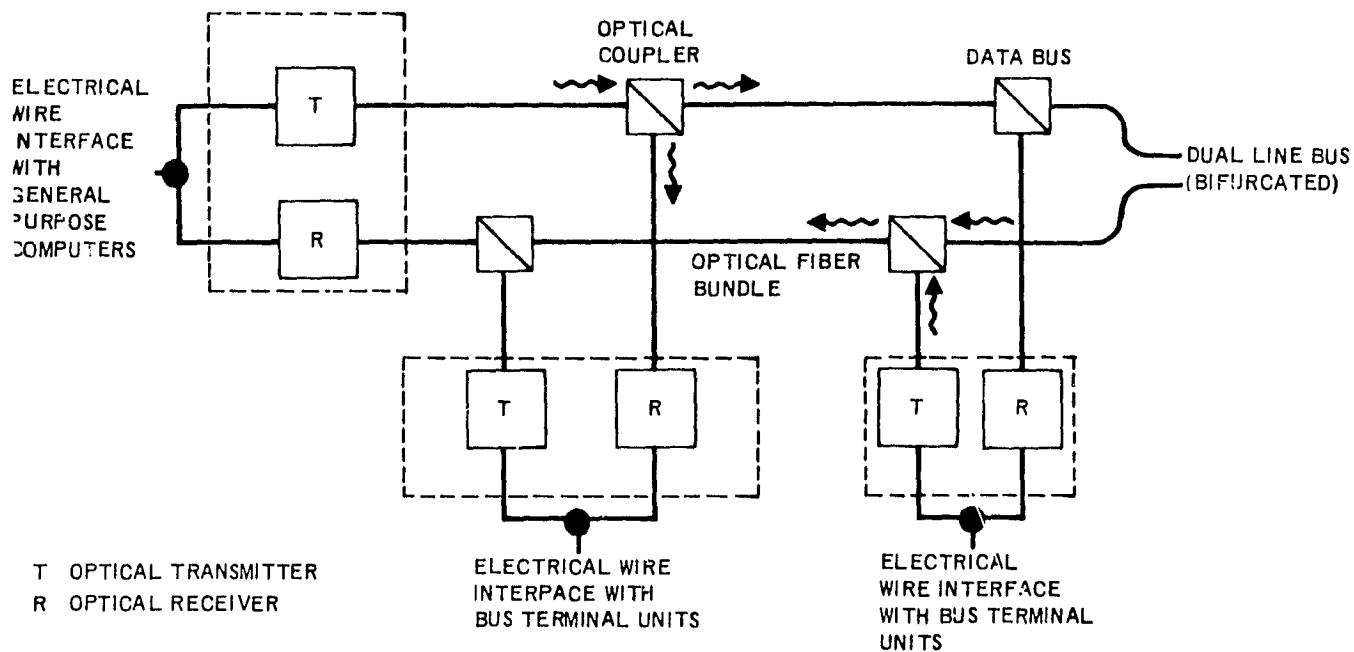


FIGURE 3-4

carrying metallic conductor to function as an antenna, there is little danger of accidental RF radiation of secure information. The fiber optic system must be light tight to prevent optical radiation of secure information. This requirement will be considered during the evaluation of optical components.

### 3.5 EMI SUSCEPTIBILITY

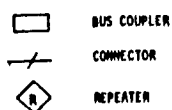
One of the major advantages of fiber optic data links is the elimination of susceptibility to electromagnetic interference (EMI) including inductive coupling between wires, pickup of RF fields, and radiation of noise to other systems. To obtain full advantage of the fiber optic's inherent immunity to EMI problems, it is necessary that the electronics in the optical receiver and transmitter at each end of the fiber optic cable be designed for low EMI susceptibility.

Significant RF shielding may be achieved by enclosing the transmitter and receiver in a metallic container and utilizing conductive gaskets on all non-welded package seams. The use of filter pin feed-through connectors on all electrical penetrations through the enclosure and RF shielding on all wiring outside the package will further enhance the RF immunity to the transmitter and receiver.

### 3.6 TWO SHUTTLE FIBER OPTIC BUSES

Using the criteria contained in the Requirements Definition Document, we have calculated the signal level at the Bus Terminal Units (BTU) on two Shuttle data buses. The buses selected for this study were Flight Critical 2 and Instrumentation 1. Flight Critical 2 (FC2) was chosen because it extends from the Upper Crew Area to the Aft Section and has 10 BTUs on the bus. Instrumentation 1 (IP1) was selected because of its contrast to FC2. IP1 extends only from Avionics Bay 1 to Avionics Bay 3 and has only 3 BTUs on the bus.

Figure 3-5 shows FC2 in the electrical data bus configuration. General Purpose Computer 2 is in control of this bus under normal operation. The distances shown in Figure 3-5 are the nominal wire lengths between components. Figure 3-6 shows FC2 in a linear optical data bus configuration using "T" bus couplers. Note the absence of couplers for the BTUs at the ends of the buses. In an electrical bus configuration, couplers are required for all BTUs in order to maintain the characteristic impedance of the line and to provide fault isolation protection



## ELECTRICAL DATA BUS FLIGHT CRITICAL

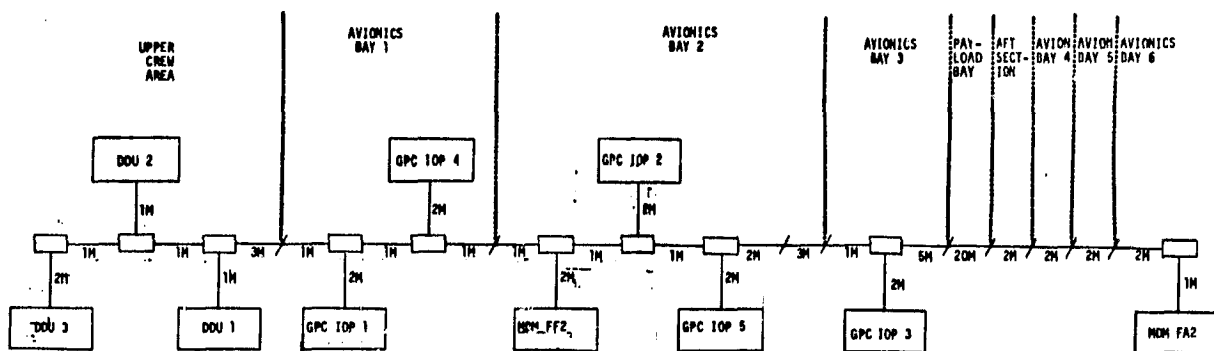


FIGURE 3-5

## LINEAR OPTICAL DATA BUS FLIGHT CRITICAL 2 (Repeater Installed)

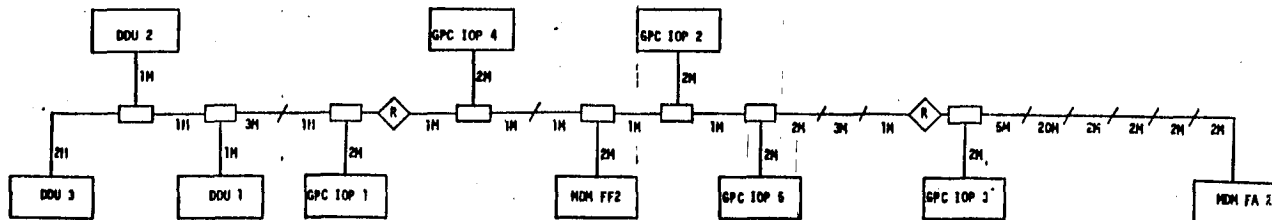


FIGURE 3-6

## LINEAR OPTICAL DATA BUS FLIGHT CRITICAL 2 (Repeater Installed)

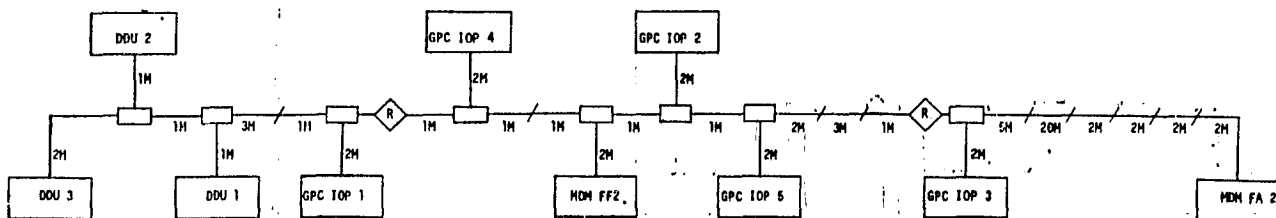


FIGURE 3-7

in the event of a short circuit. With an optical data bus, there is no line characteristics impedance and an open or short circuit will have no effect on the source side of the fault.

The following signal levels and losses were used in all optical data bus configuration calculations:

- transmitter output for logic "1" = +3 dBm
- transmitter/cable interface loss = 2.35 dB
- GPC & BTU coupler/bus loss = -2 dB
- bus coupler input/bus loss = -5 dB plus power splitting loss
- bus coupler bus/bus loss = -5 dB plus power splitting loss
- bus coupler bus/output loss = -5 dB plus power splitting loss
- connector loss = -2 dB
- cable loss = -0.35 dB/m
- bus/GPC & BTU coupler loss = -5 dB
- cable/receiver interface loss = -0.75 dB

For the linear bus couplers, the power splitting loss for the input/bus path and the bus/output path is given by:

P.S. loss =  $10 \log (\text{pickoff fraction})$

and the power splitting loss for the bus/bus path is given by:

P.S. loss =  $10 \log (1 - 2 [\text{pickoff fraction}])$ .

For the radial bus couplers, the power splitting loss is given by:

P.S. loss =  $10 \log (\text{pickoff fraction})$ .

For the configuration of FC2, shown in Figure 3-6, the pickoff fraction of the bus couplers is 0.2. Therefore, the coupler input/bus and bus/output loss is 11.9 dB and the coupler bus/bus loss is 7.2 dB. Using the signal and loss values shown above, the signal level for a logic "1" at the receivers located in the various BTUs along the bus is:

- MDM FF 2 = -32.65 dBm
- GPC IOP 4 = -42.55 dBm
- GPC IOP 1 = -50.15 dBm
- DDU 1 = -60.35 dBm
- DDU 2 = -67.90 dBm

## OPTICAL DIGITAL TECHNIQUES

REPORT MDC E2052  
FEBRUARY 1979

DDU 3       = -63.55 dBm  
GPC IOP 5 = -32.65 dBm  
GPC IOP 3 = -45.95 dBm  
MDM FA2     = -62.10 dBm

As stated in the Requirements Definition Document, the optical receiver shall recognize as a logic "1" any signal having a level greater than -45 dBm and shall recognize as a logic "0" any signal having a level less than -50 dBm. The logic "1" level for 5 of the 9 BTU receivers shown in the preceding paragraph is less than -50 dBm and would be recognized as a logic "0". For one receiver, the logic "1" level falls in the undefined region between -45 dBm and -50 dBm. It is obvious that the losses associated with the standard linear optical data bus configuration are too great to permit proper operation of FC 2 in that configuration. Accordingly, optical repeaters were installed in FC2 as shown in Figure 3-7. The Requirements Definition Document states that the output from the repeater is -5 dBm for a logic "1". The signal level for a logic "1" at the various BTU receivers with repeaters installed in the bus are:

MDM FF2     = -32.65 dBm  
GPC IOP 4 = -42.55 dBm  
GPC IOP 1 = -23.40 dBm  
DDU 1       = -34.60 dBm  
DDU 2       = -41.15 dBm  
DDU 3       = -36.80 dBm  
GPC IOP 5 = -32.65 dBm  
GPC IOP 3 = -23.35 dBm  
MDM FA2     = -39.50 dBm

With two optical repeaters installed, as shown in Figure 3-7, the signal level at the BTU receivers is compatible with the level shown in the Requirements Definition Document.

Most of the published articles on optical data buses state that the optimum pickoff fraction for the "T" coupler is the reciprocal of the number of couplers on the bus. For the FC2 configuration, shown in Figure 3-6, the number of couplers is 8 so the optimum pickoff fraction would be 0.125. However, in most of the published articles, the BTU in control of the bus is assumed to be at one

end of the bus; in FC2 the BTU in control of the bus is close to the center of the bus. Therefore, the pickoff fraction equal to the reciprocal of the number of couplers is not always the optimum value.

A comparison of the signal at each BTU receiver for the so-called optimum pickoff fraction of 0.125 and the pickoff fraction of 0.2 is shown below:

<u>BTU</u>	<u>P.F. = 0.125</u>	<u>P.F. = 0.2</u>
MDM FF2	-36.85 dBm	-32.65 dBm
GPC IOP 4	-47.75 dBm	-42.55 dBm
GPC IOP 1	-52.30 dBm	-50.15 dBm
DDU 1	-61.55 dBm	-60.35 dBm
DDU 2	-68.10 dBm	-67.90 dBm
DDU 3	-60.65 dBm	-63.55 dBm
GPC IOP 5	-36.85 dBm	-32.65 dBm
GPC IOP 3	-49.15 dBm	-45.95 dBm
MDM FA2	-62.20 dBm	-62.10 dBm

The preceding discussion on optimum pickoff fraction was included to illustrate that the actual Shuttle data bus configuration is different from the theoretical models shown in most published works, and an analysis is required prior to the application of the theoretical work to the Shuttle System.

Figure 3-8 shows FC2 in a radial optical data bus configuration. In this configuration only one coupler, a radial (or star) coupler, is used to split the optical signal from the BTU in control of the bus to the remaining BTUs on the bus. The pickoff fraction selected for this analysis is 0.1, therefore, the coupling loss to each branch of the circuit is 15 dB. The signal level for a logic "1" at each BTU receiver on the bus is shown below:

MDM FF2	=	23.50 dBm
GPC IOP 4	=	26.20 dBm
GPC IOP 1	=	-26.20 dBm
DDU 1	=	-28.90 dBm
DDU 2	=	-28.90 dBm
DDU 3	=	-29.25 dBm
GPC IOP 5	=	-23.50 dBm
GPC IOP 3	=	-28.90 dBm
MDM FA2	=	-47.40 dBm

## RADIAL OPTICAL DATA BUS FLIGHT CRITICAL 2

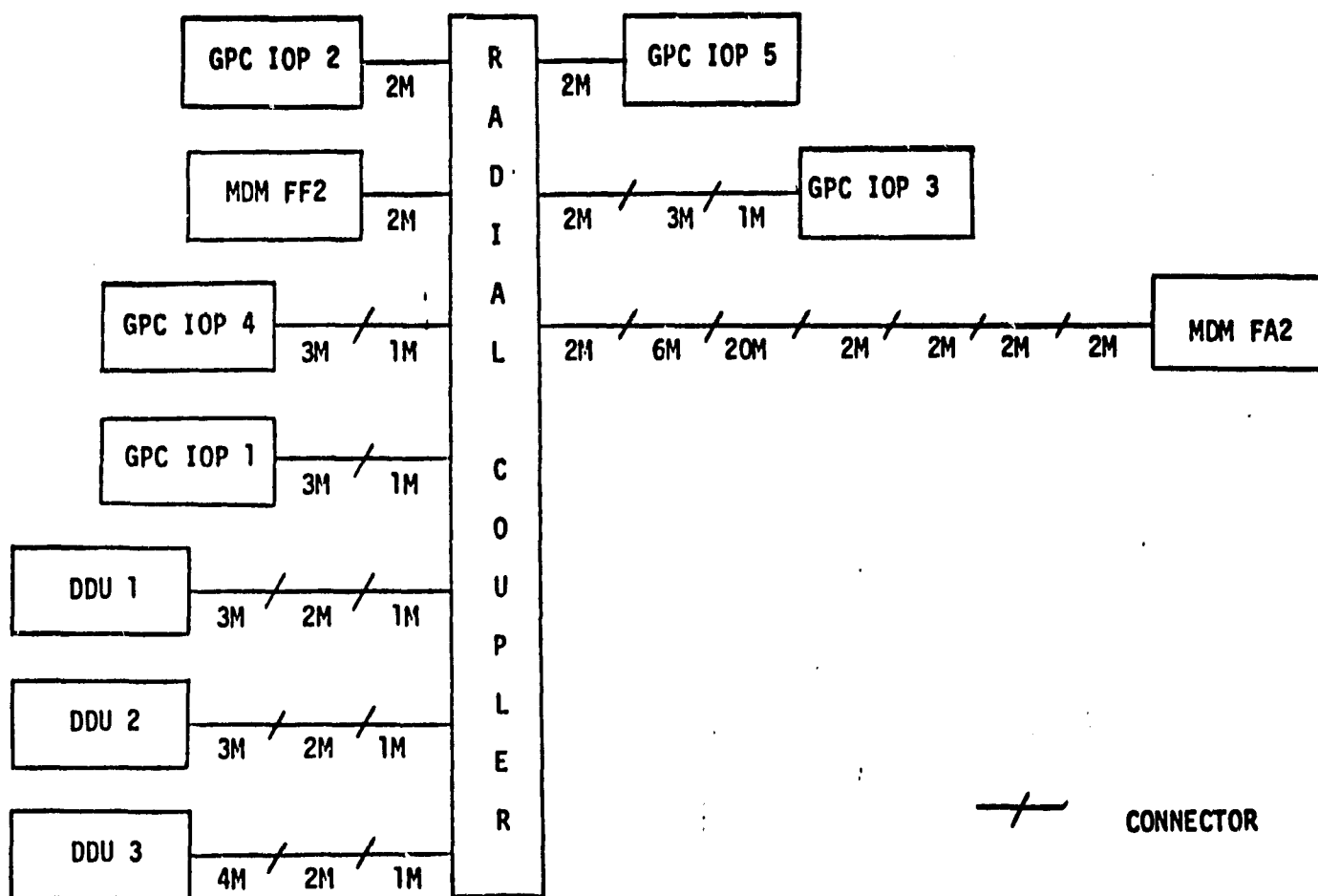


FIGURE 3-8



With the radial bus configuration, the signal level at all BTU receivers, except for MDM FA2, is well within the range of the receiver requirements of the Requirements Definition Document. The optical signal level at the MDM FA2 receiver is -47.40 dBm, 2.7 dB lower than the minimum level for a logic "1".

Figure 3-9 shows IP1 bus in the electrical data bus configuration. IP1 was selected to show the losses associated with a short data bus having few Bus Terminal Units. Figure 3-10 shows IP1 in the linear optical data bus configuration. The signal levels at the BTU receivers are:

PCM 1 = -23.45 dBm

PCM 2 = -24.50 dBm

The pickoff fraction of the coupler is 0.2. This value was selected to permit nearly equal signal levels at each BTU receiver. The radial bus configuration for IP1 is shown in Figure 3-11. The signal levels at the BTU receivers are:

PCM 1 = -20.30 dBm

PCM 2 = -26.05 dBm.

From the preceding discussion it is evident that a radial bus configuration is usually preferable to a linear configuration because of the lower losses with the radial bus. Additionally, the radial bus configuration requires only 1 coupler versus the 8 couplers required for the linear configuration of FC2. One might expect the radial bus configuration to require much more cable than the linear configuration. However, a comparison of the cable lengths, shown in Figures 3-6 and 3-8, shows only a 10-meter difference between the linear bus (65 meters) and the radial bus (75 meters).

ELECTRICAL DATA BUS INSTRUMENTATION 1

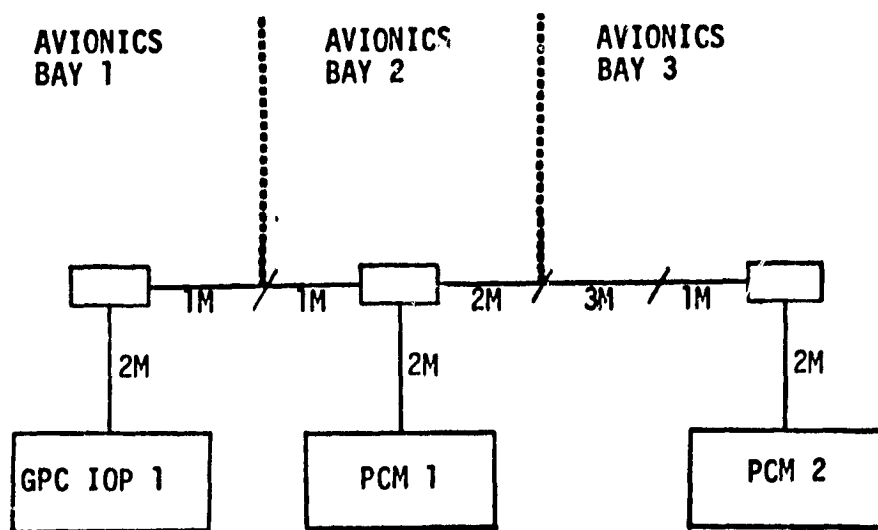
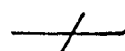


FIGURE 3-9

 BUS COUPLER

 CONNECTOR

LINEAR OPTICAL DATA BUS INSTRUMENTATION

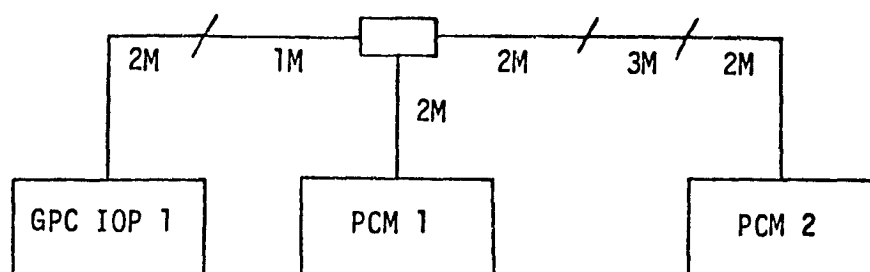


FIGURE 3-10

RADIAL OPTICAL DATA BUS INSTRUMENTATION 1

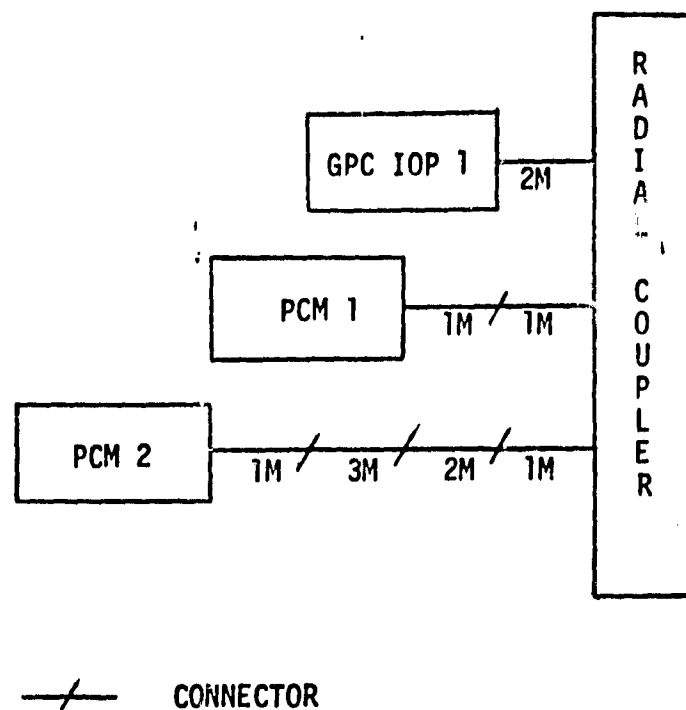


FIGURE 3-11

4.0 FIBER OPTIC HARDWARE4.1 BASELINE SYSTEM (HARDWARE)

During the course of the contract, a fiber optic star data bus system was purchased. This system was obtained from the ITT Electro-Optical Products Division in Roanoke, Virginia, and consisted of an ITT 2-D digital transmitter and receiver, a 9-part star coupler, and a number of short lengths of terminated fiber cable. This system is shown in Figure 4-1.

The Model 2-D optical transmission system was capable of a data rate between 10 Kbs to 20 Mbs. The inputs and outputs are TTL compatible, with amplitude regenerated data out. The receiver also had a buffered analog signal output for monitoring the received signal. The model 2-D transmitter employed a high brightness LED, with four switch selectable LED drive settings. The receiver used an avalanched photodiode detector which employs a hybridized high-voltage power supply for the APD, with AGC controlled output voltage. The primary specifications for the digital terminals are given below:

<u>SPECIFICATIONS</u>	<u>NOMINAL</u>
Upper Bit Rate Cutoff	20 Mb/s
Lower Cutoff (10% Analog Droop)	500 Hz square wave
TRANSMITTER	
Input Impedance	50 $\Omega$ , or 4 TTL loads
Maximum Input Signal Level	5 volts
Power Supply	5 $\pm$ 0.25 Vdc at 300 ma max.
Optical Output Power (Max LED Drive)	
With ITT type GG-02 graded index fiber termination	30 $\mu$ W peak (TTL high)
With ITT type GG-02 step index fiber termination	60 $\mu$ W peak (TTL high)
RECEIVER	
Output Impedance	
Digital output	50 $\Omega$
Analog output	600 $\Omega$
Analog output signal level	3V P-P nom.
Digital output	TTL Line Drive
Power Supplies	+5 $\pm$ 0.25 Vdc at 75 ma max. +8 to +18 Vdc at 100 ma max. -8 to -18 Vdc at 75 ma max.
Optical Sensitivity at 10 <sup>-8</sup> BER	6 nW peak (TTL high)
Optical Dynamic range	20 dB
Rise/Fall Time	
Digital output	8 ns max.
Analog output (for negligible fiber dispersion)	20 ns max.

FIBER OPTIC STAR DATA BUS SYSTEM COMPONENTS

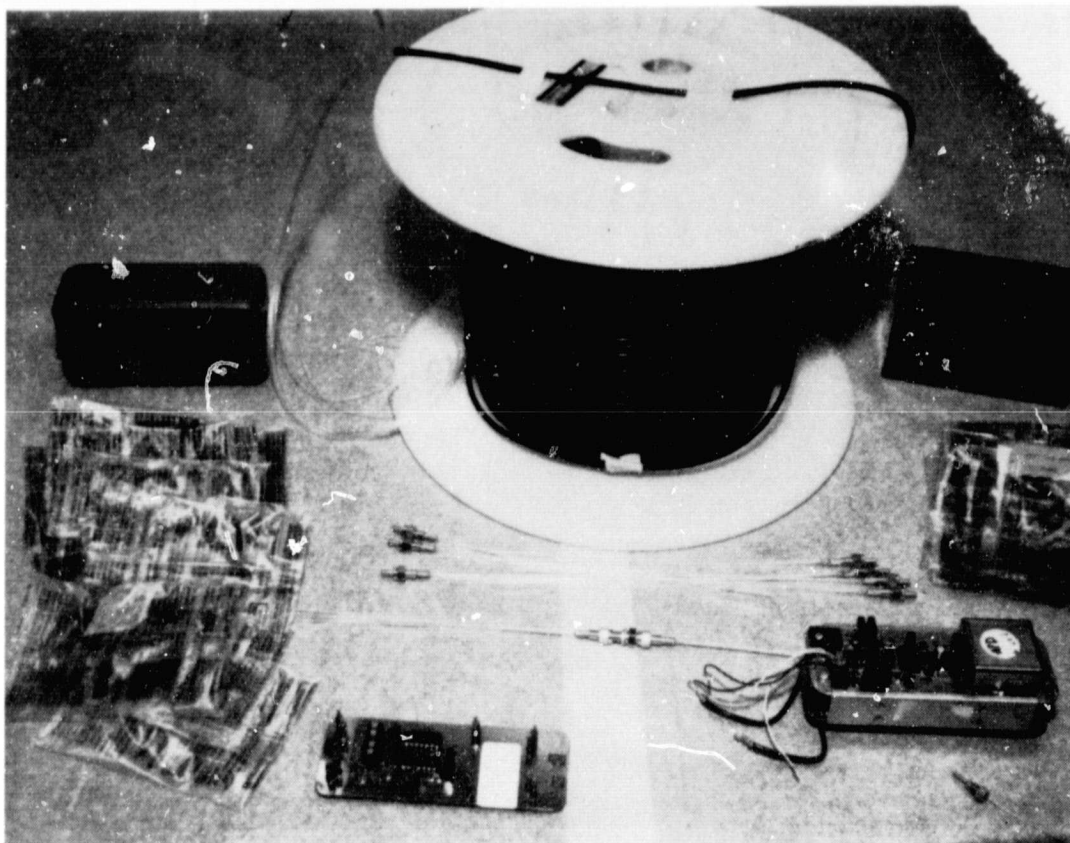


FIGURE 4-1

REPRODUCIBILITY OF THE  
ORIGINAL PAGE IS POOR

The radial star coupler is a reflection device configured with 9 input/output ports. The optical mixer (which was a square glass rod) had an aspect ratio of at least 40 to 1. The individual ports were made of four 165  $\mu\text{m}$  PCS single fibers. The plastic cladding from each end of the 4 fibers was removed. The 4 fibers were fused together as shown in Figure 4-2. The cladding was removed and replaced with an optical silver coating (99.10% reflective at 850 nm). The 32-fiber optic silvered end were arranged in a random fashion on the surface of the optical mixer (dielectric rod) and permanently Epoxied there, while the 9 other ends were terminated with OSM connectors.

The fiber optic cables consisted of ITT LD-40-PS-(19) plastic clad silica fibers. The lengths of the terminated fiber ranged from 2 meters to 10 meters. The bundle terminations were made in the following manner. The plastic cladding from each of the 19 fibers were removed. The fibers were then coated with a highly reflective silver coating. The coated fibers were then placed in the OSM type connectors where they were surrounded with Epoxy. The Epoxy was cured and the fibers were polished. Some of the more salient plastic clad silica fiber parameters are given below:

<u>SPECIFICATIONS</u>	<u>NOMINAL</u>
Attenuation @ 0.79 $\mu\text{m}$	
PS-05-35	35 dB/km
PS-05-20	20 dB/km
PS-05-10	10 dB/km
Numerical Aperture	0.3
Dispersion	
10 dB width	60 ns/km
3 dB width	30 ns/km
Core Index of Refraction	1.46
Fiber Core Diameter	125 $\mu\text{m}$
Jacket Outer Diameter	500 $\mu\text{m}$
Tensile Strength (1/2m gauge length)	500,000 psi
Minimum Bending Radius	0.5 cm

#### 4.2 FIBER OPTIC DATA BUS SYSTEM TESTS

The relative performance of the ITT radial star data bus system was judged by performing a number of system tests. The tests conducted included connector-to-connector losses, connector indexing losses, 1 star throughput loss, and Bit Error Rate (BER) as a function of optical power incident on the detector. The tests are described below.

FOUR FUSED FIBERS



FIGURE 4-2

REPRODUCIBILITY OF THE  
ORIGINAL PAGE IS POOR

#### 4.2.1 Connector-to-Connector Losses

The experimental setup to measure connector loss is shown in Figure 4-3a. The ITT transmitter input was biased to a TTL logic "1" level (3 volts). The output power was monitored with side A of fiber cable X connected to the transmitter while side B was connected to an EG&G 550-1 power meter with flat filter, see Figure 4-3a. Side B was connected to the power meter through a specially fabricated adapter with OSM threads that mated to the Amphenol OSM fiber cable plug. This adapter assured repeatability of the measurements and also eliminated background light. The average output power from the LED of the ITT Transmitter was found to be stable to better than 3% in any 30-minute interval (an interval which was much longer than needed to perform any given set of measurements).

The measurements were performed using the following procedure. Side B of cable X was connected to the EG&G power meter and this power reading was recorded. Side B of cable X was then connected to whichever connector of the cable under test was being measured (see Figure 4-3a). The other side of the cable under test was then connected to the adapter on the power meter. This reading was recorded and the dB loss of the cable under test was computed. However, when the above measurement procedure was repeated on the same cable, significant differences in dB reading occurred. The reason for this difference was indexing in the cable. This problem will be addressed in detail in the next series of tests.

A statistical procedure for estimating the indexing loss for each connector was utilized. In a field environment it is unlikely that the individual connectors would be adjusted for maximum radiation transfer between cables by adjusting the rotational position. Hence, five measurements were made on each cable. The cable under test was connected to side B of cable X via the OSM connector. The output power at the other end of the cable under test was monitored through the adapter and the EG&G power meter. The cable under test was disconnected at side B of cable X, then both cables were set on the lab bench and the process was repeated. After all of the measurements were taken, the data was processed on a 9830A HP computer. The mean, variance, and skewness in the data were computed. These results were used to make an estimation of the connector losses in a field environment.



## CONFIGURATION FOR LOSS MEASUREMENT

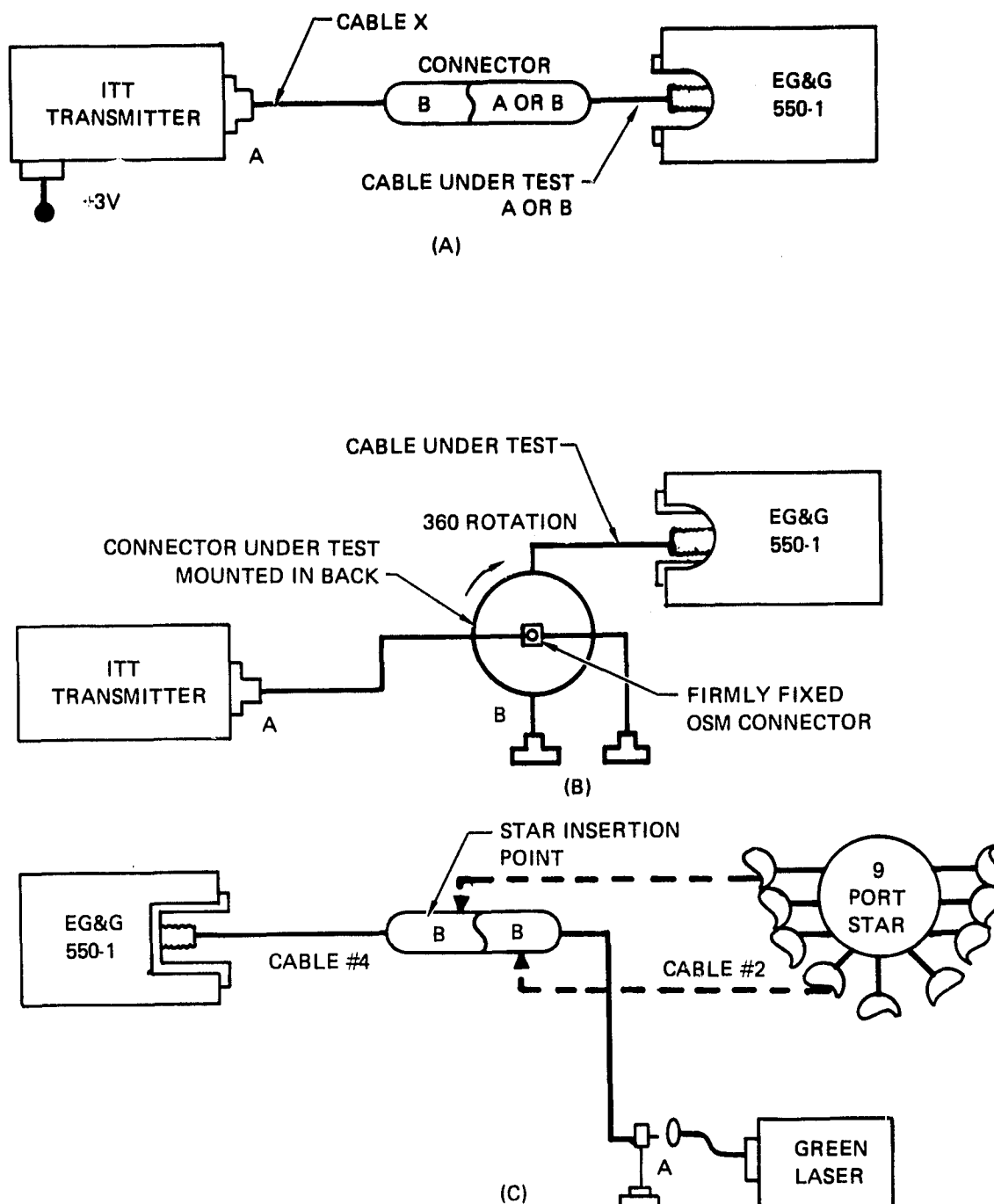


FIGURE 4-3

Table 4-1 lists the results of the measurements performed with cable #6 as the cable X in Figure 4-3a. ITT supplied fiber cables numbered 2 through 6 which appear in the test results. In Table 4-2 the results using fiber cable #3 for cable X are listed. The small differences between average cable losses can be explained by the effects of indexing losses.

#### 4.2.2 Connector Indexing Losses

It became apparent after a few measurements with the test set, shown in Figure 4-3a, that indexing was a problem. Hence, the test setup shown in Figure 4-3b was built to study this problem. For these tests, fiber optic cable X was held in a constant position and the fiber cable under test was rotated in  $10^\circ$  increments. At each  $10^\circ$  increment the OSM connector was tightened and the power was monitored on the EG&G 550-1.

This test was repeated 33 times per cable and the dB loss as a function of angle was measured. Typical results for fiber cables #2 and #5 are shown in Figures 4-4 through 4-7. The fiber cable in position X in Figure 4-3b for the above data was cable #3. One of the causes of the index problem is the fact that the fibers are not aligned between the male and female parts of the OSM connector. However, it can be seen that the relative magnitude of the indexing variation is reduced when the fiber termination has a good packing fraction. This can be seen by comparing Figures 4-4 and 4-5 (for cables with good packing fraction) to Figures 4-6 and 4-7 (for cables with poor packing fraction).

#### 4.2.3 Star Coupler Throughput Losses

Another test, which was performed, measured the throughput losses of the star coupler. One of the primary components of any future fiber optic data bus system will be a star coupler. The star coupler performance may be judged by the following criteria: (1) the throughput losses between any two ports, (2) amount of reciprocity between ports, (3) the amount of difference between each individual port's loss, and (4) the average throughput loss for the star.

The test setup used to obtain the following data is shown in Figure 4-3c. For this experiment we used a green krypton ion laser which would not bias the data. This was not true in the first two system tests because of the high dB loss in the fibers at this color of light. The cables with the lowest loss connectors

TABLE 4-1  
CONNECTOR LOSSES

Fiber Cable #6 is Fiber Cable  
X in Figure 1a

Average Loss dB	Cable #2	Cable #3	Cable #4	Cable #5
Side A	6.19	7.25	7.16	9.06
Side B	5.76	6.39	7.2	9.50
Variance				
Side A	0.08	0.11	0.16	.22
Side B	0.05	0.08	0.06	0.00
Skewness				
Side A	0.91	.15	-.2	-.1
Side B	1.01	-.07	-.48	0.03

TABLE 4-2  
CONNECTOR LOSSES

Fiber Cable #3 is Fiber Cable  
X in Figure 1a

Average Loss dB	Cable #2	Cable #4	Cable #5	Cable #6
Side A	6.04	6.39	8.85	7.88
Side B	5.42	6.99	9.61	7.05
Variance				
Side A	0.01	0.02	0.26	0.01
Side B	0.13	0.06	0.10	0.06
Skewness				
Side A	-.29	.27	-.64	0.05
Side B	.11	-.21	0.97	0.46

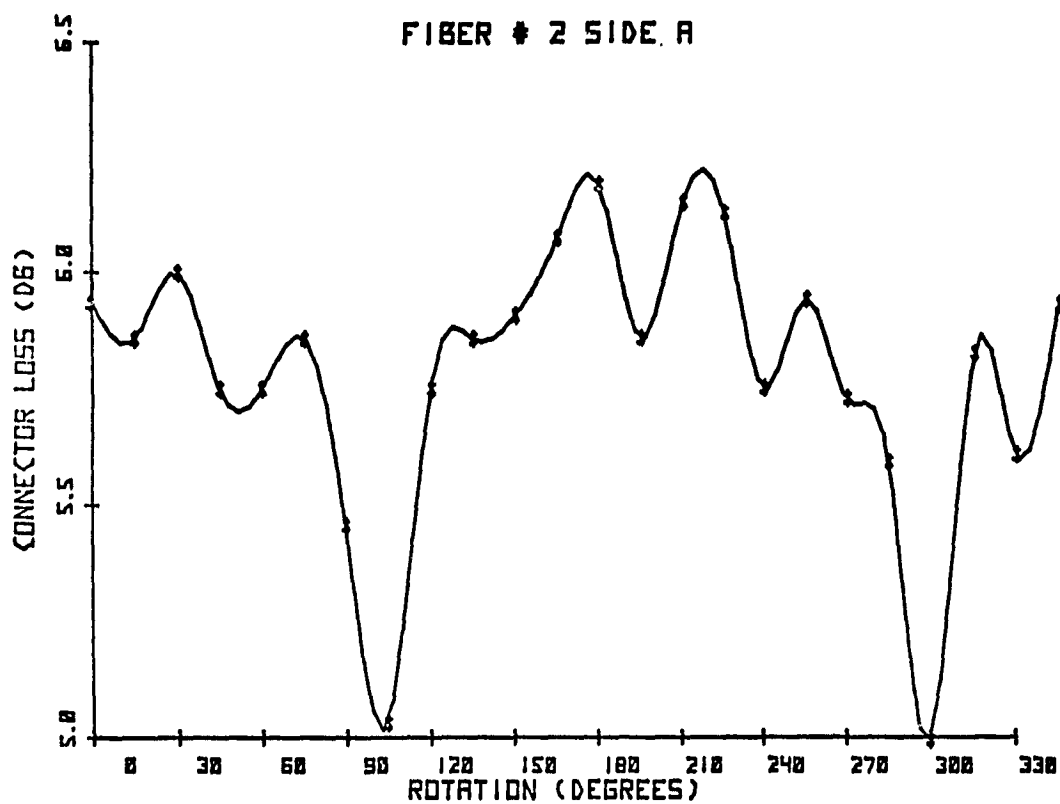


FIGURE 4-4

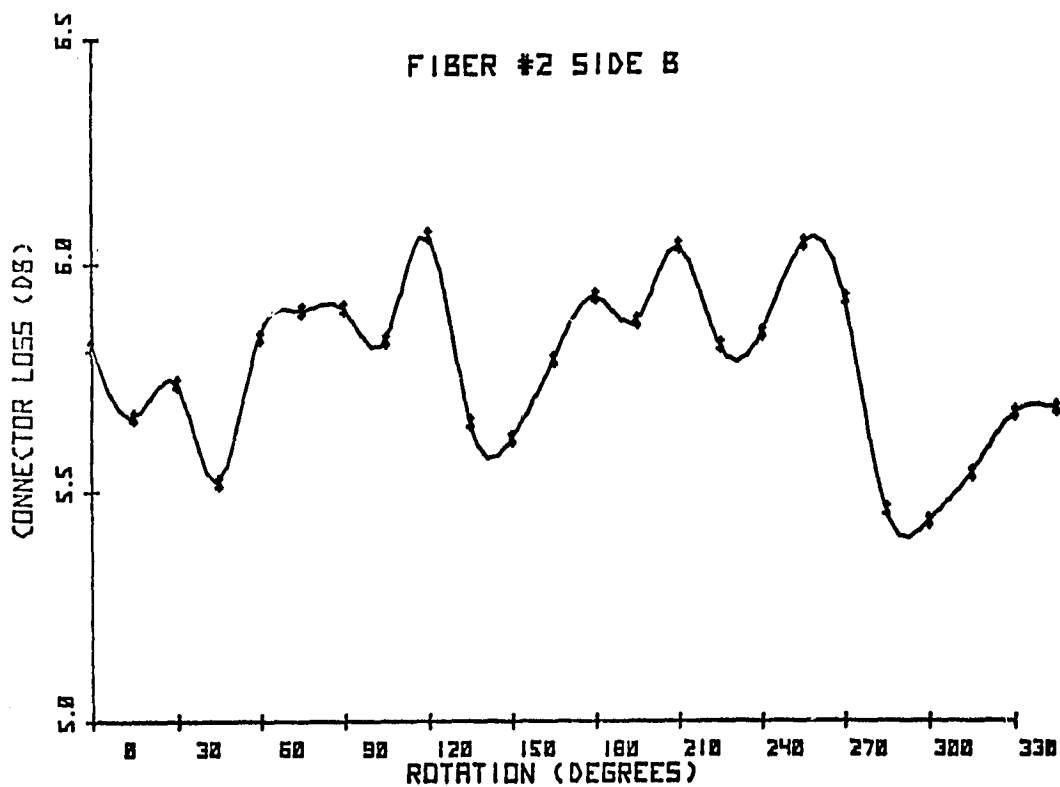


FIGURE 4-5

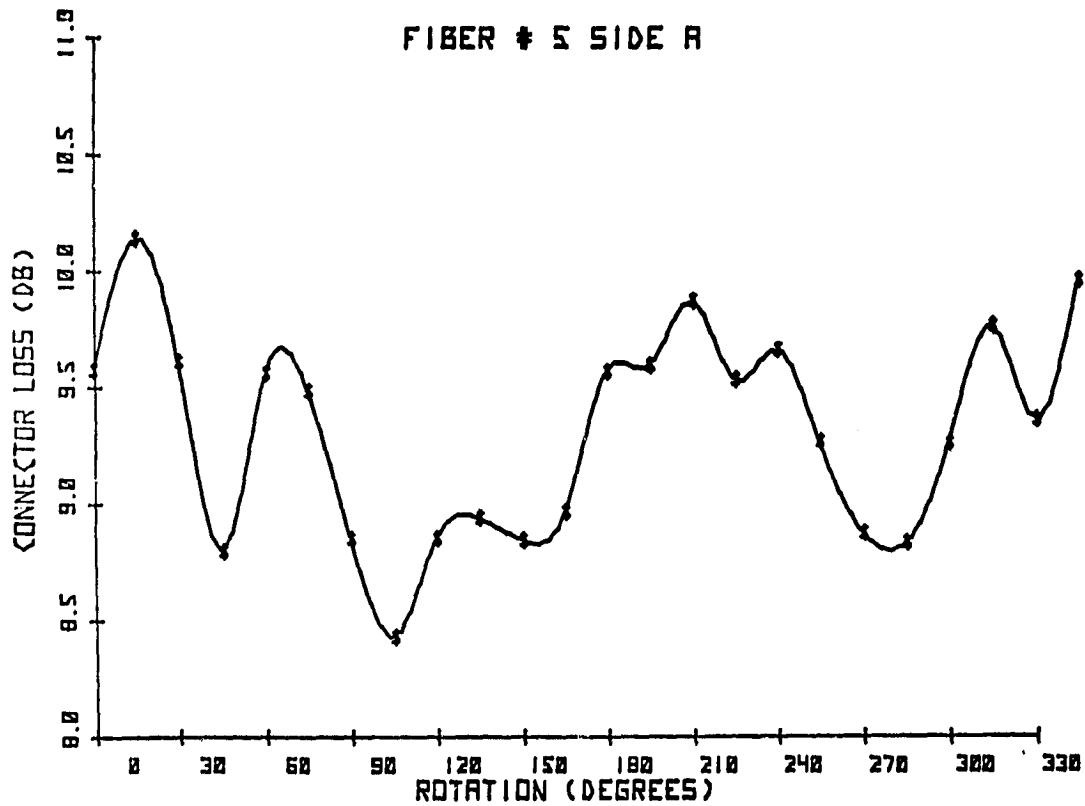


FIGURE 4-6

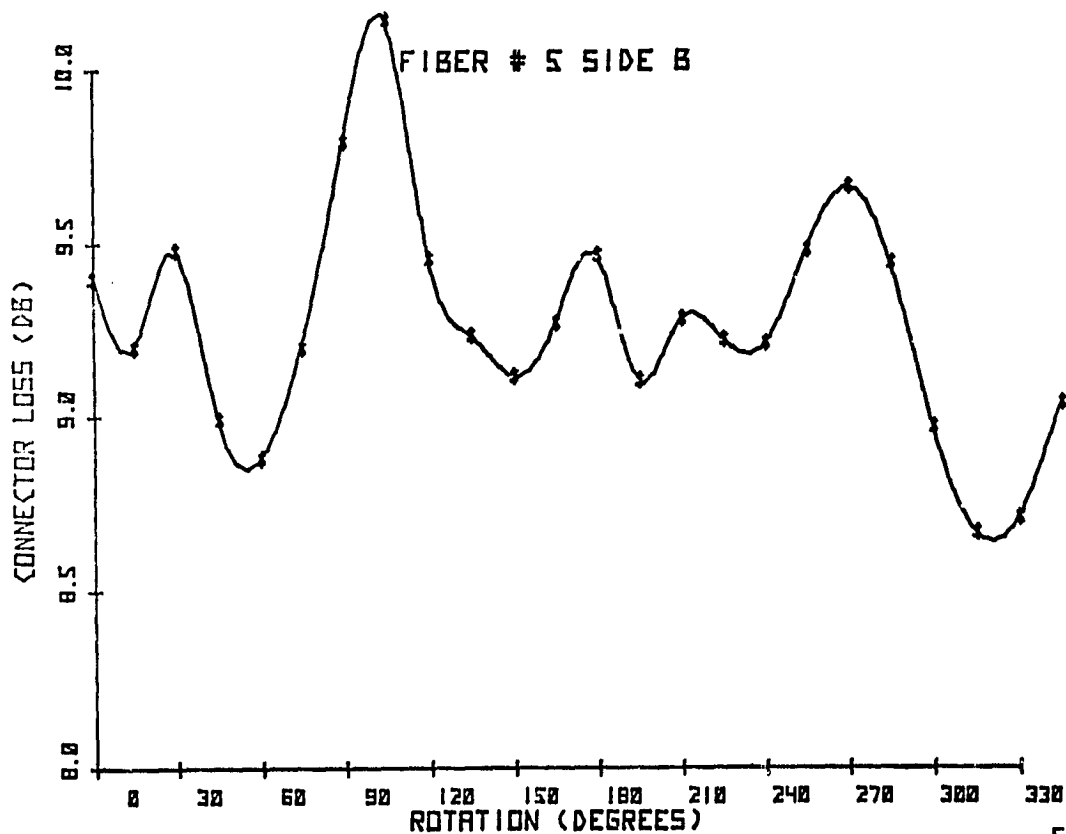


FIGURE 4-7

were chosen for this test, although in most star characterizations the connector losses are not considered part of the throughput losses, but rather the excess loss and the splitting loss ( $-10 \log n$ ). However, it is felt that the throughput loss should include the connector losses as this indicates how the star would perform in an actual system.

The data was taken in the following manner: the cables in Figure 4-3c were connected together without the star coupler and a reading was taken with the EG&G 550-1. The cables were then disconnected and the port which was to be illuminated was connected to side B of cable #4. Then side B of cable #2 was connected to the port under test and the value of power received at the EG&G 550-1 was recorded. This procedure was repeated for each of the eight ports. This procedure was repeated 5 times for each port tested, and the data was then reduced on the computer. Table 4-3 contains the average of the measurements between any two ports of the star, while Tables 4-4 and 4-5 show the variance and skewness of the data. Table 4-6 contains the difference in dB between port I,J and port J,I. This table indicated the degree of reciprocity achieved by the star complex. Table 4-7 contains the total average star loss (23.10 dB) minus the average loss per port. This table indicates the degree of uniformity of the loss in the star.

#### 4.2.4 Bit Error Rate Measurement

One of the most revealing parameters as to how "good" the optical data bus system is functioning is the Bit Error Rate (BER). A BER performance test was performed on the ITT system. In order to obtain good error rate data for a low data rate system many samples must be taken. Since a bit error rate type measurement was also used to study how well the system performed under Electromagnetic Interference (EMI), a brief discussion is given on the relationship between confidence level and confidence interval of the data taken.

The theory which follows is based on a branch of estimation theory which is known as population statistics. If small  $e$  is the true value of error rate and capital  $E$  is the measured value then small  $e$  and capital  $E$  are related by<sup>(15)</sup>

$$e_1 = \frac{E + \frac{\sigma^2}{2N} \pm \sigma \left[ \frac{E(1-E)}{N} + \frac{\sigma^2}{4N^2} \right]^{1/2}}{1 + \frac{\sigma^2}{N}} \quad (4.1)$$

# OPTICAL DIGITAL TECHNIQUES

REPORT MDC E2052  
FEBRUARY 1979

TABLE 4-3  
AVERAGE STAR THROUGH-PUT LOSS (DB)  
\*INDICATES PORT ILLUMINATED

PORT	1	2	3	4	5	6	7	8	9
1	*	22.67	21.89	22.01	21.68	22.92	22.00	23.69	21.06
2	23.62	*	23.61	23.48	23.04	23.88	23.28	24.75	22.82
3	22.83	23.09	*	22.88	22.94	23.06	22.65	24.02	22.73
4	22.19	22.83	23.10	*	22.22	22.92	22.92	23.83	21.37
5	22.42	22.62	22.51	22.54	*	22.64	22.68	23.42	22.27
6	23.62	23.45	23.11	22.85	22.68	*	22.85	24.37	22.80
7	22.82	22.84	22.77	22.85	22.81	23.10	*	23.33	22.77
8	24.87	25.60	24.70	24.78	24.86	25.19	24.44	*	24.22
9	22.76	22.83	22.78	22.73	22.70	22.94	22.77	23.00	*

TABLE 4-4  
\* VARIANCE OF STAR LOSSES  
\*INDICATES PORT ILLUMINATED

PORT	1	2	3	4	5	6	7	8	9
1	*	0.02	0.11	0.14	0.03	0.35	0.05	0.15	0.14
2	0.11	*	0.04	0.00	0.18	0.31	0.15	0.35	0.05
3	0.15	0.01	*	0.14	0.03	0.02	0.44	0.04	0.20
4	0.20	0.04	0.02	*	0.04	0.11	0.00	0.00	0.07
5	0.17	0.02	0.08	0.03	*	0.01	0.00	0.02	0.21
6	0.07	0.05	0.20	0.12	-0.01	*	0.07	0.06	0.06
7	0.00	0.00	0.00	0.00	0.00	0.06	*	0.09	0.00
8	0.02	0.05	0.00	0.02	0.00	0.07	0.01	*	0.03
9	0.00	0.00	0.00	0.00	0.00	0.00	0.00	0.00	*

TABLE 4-5  
SKEWNESS IS STAR THROUGH-PUT LOSS  
\*INDICATES PORT ILLUMINATED

PORT	1	2	3	4	5	6	7	8	9
1	*	0.43	-0.10	0.04	-0.18	-0.47	-0.18	0.00	-0.26
2	-0.71	*	-0.32	-0.86	0.94	-1.11	-0.19	0.25	0.81
3	-0.59	0.46	*	-0.84	-0.55	0.36	-1.03	-0.21	-0.95
4	-0.82	0.12	-0.83	*	0.62	0.04	0.74	-0.43	-0.92
5	-1.14	-0.98	-1.11	-1.10	*	0.13	0.29	-0.17	-1.12
6	0.16	0.32	0.29	1.06	0.34	*	1.14	0.05	1.14
7	0.09	0.78	-0.67	0.78	0.23	0.01	*	0.20	0.00
8	0.00	-0.10	0.39	1.03	-0.62	-0.34	0.10	*	-0.40
9	0.25	-0.25	0.64	-0.28	-0.41	-0.20	-0.41	-0.48	*

TABLE 4-6  
LOSS PORT (I,J) - LOSS PORT (J,I)  
\*INDICATES PORT ILLUMINATED

PORT	1	2	3	4	5	6	7	8	9
1	*	-0.95	-0.94	-0.18	-0.74	-0.70	-0.82	-1.18	-1.70
2	0.95	*	0.52	0.65	0.42	0.43	0.44	-0.85	-0.01
3	0.94	-0.52	*	-0.22	0.43	-0.05	-0.12	-0.68	-0.05
4	0.18	-0.65	0.22	*	-0.32	0.07	0.07	-0.96	-1.36
5	0.74	-0.42	-0.43	0.32	*	-0.04	-0.13	-1.44	-0.43
6	0.70	-0.43	0.05	-0.07	0.04	*	-0.25	-0.82	-0.14
7	0.82	-0.44	0.12	-0.07	0.13	0.25	*	-1.11	0.00
8	1.18	0.85	0.68	0.96	1.44	0.82	1.11	*	1.22
9	1.70	0.01	0.05	1.36	0.43	0.14	0.00	-1.22	*

TABLE 4-7  
LOSS PER PORT - AVERAGE LOSS OF STAR  
\*INDICATES PORT ILLUMINATED

PORT	1	2	3	4	5	6	7	8	9
1	*	-0.43	-1.21	-1.09	-1.42	-0.18	-1.10	0.59	-2.04
2	0.52	*	0.51	0.38	-0.06	0.78	0.18	1.65	-0.28
3	-0.27	-0.01	*	-0.22	-0.16	-0.04	-0.45	0.92	-0.37
4	-0.91	-0.27	0.00	*	-0.88	-0.18	-0.18	0.72	-1.73
5	-0.68	-0.48	-0.59	-0.56	*	-0.46	-0.42	0.32	-0.83
6	0.52	0.35	0.01	-0.25	-0.42	*	-0.25	1.27	-0.30
7	-0.28	-0.26	-0.33	-0.25	-0.29	0.00	*	0.23	-0.33
8	1.77	2.50	1.60	1.68	1.76	1.19	1.34	*	1.12
9	-0.34	-0.27	-0.32	-0.37	-0.40	-0.16	-0.33	-0.10	*



where

$\sigma$  = a confidence parameter

N = the number of samples taken

Equation 4.1 may be looked at as a population parameter given by two numbers [the two roots of equation 4.1] between which the true parameter (small  $e$ ) may be considered to lie. This interval is defined as a confidence interval.

The level of confidence that any particular measurement is within this confidence interval is related to  $\sigma$ . The  $\sigma$  value is based on the assumption that the errors occur in a Gaussian manner. In other words if  $\sigma = 1$  then a given measurement has a 68.27% chance of being in the confidence interval. Similarly, if  $\sigma = 2$  then a confidence level of 94.45% is obtained. Written in terms of probability, Equation 4.1 may be expressed as  $p[e_+ < e < e_- | E] = 0.9445$  (given  $\sigma = 2$ ).

The length of the confidence interval is strongly related to the number of samples taken. By looking at Equation 4.1 it is seen that as N approaches infinity, then small  $e$  approaches capital E, independent of the value of  $\sigma$ . A plot of Equation 4.1, the interval length vs. number of samples for a 99.99% confidence level ( $\sigma = 3.87$ ), is shown in Figure 4-8. The measured error rate is varied as a parameter; the y-axis in Figure 4-8 is the interval length in % of true error rate, while the x-axis is the total number samples taken. Figure 4-8 may be employed to obtain the number of samples necessary to obtain the given % of interval length and be 99.99% confident in that data. For example, if the desired measured error rate is to be within 10% of a true  $10^{-4}$  error rate ( $0.9 \times 10^{-4} \leq E \leq 1.1 \times 10^{-4}$ ) then from Figure 4-8  $6 \times 10^8$  samples must be taken. Figure 4-8 also shows that as the error rate becomes smaller the number of samples that must be taken for any given confidence length must increase.

The above information was used to obtain the bit error data on the ITT data bus system. A block diagram of the BER measurement system is shown in Figure 4-9. The measurement system consisted of a Bit Error Rate test set (Data Comm. 10 11), a variable optical attenuator, an EG&G 550-1 optical power meter, a four-channel oscilloscope, a variable (crystal controlled) timer and a HP counter.

Data was taken in the following way. The HP counter was set on the one-second gate time. The Bit Error Rate test set was set on a 1 Mbps Manchester-Bi-Phase code. The optical attenuator was adjusted by observing the error rate on the

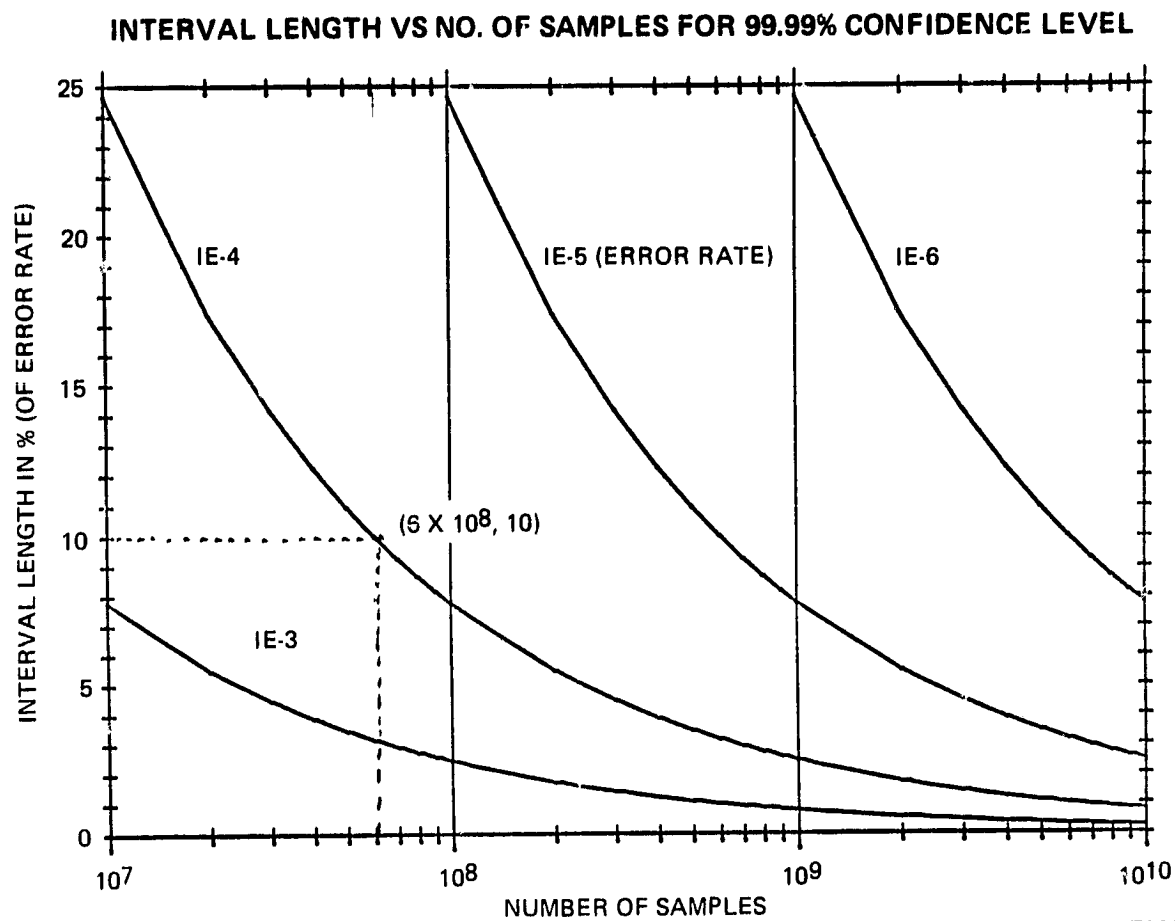


FIGURE 4-8

## BIT ERROR RATE MEASUREMENT SYSTEM

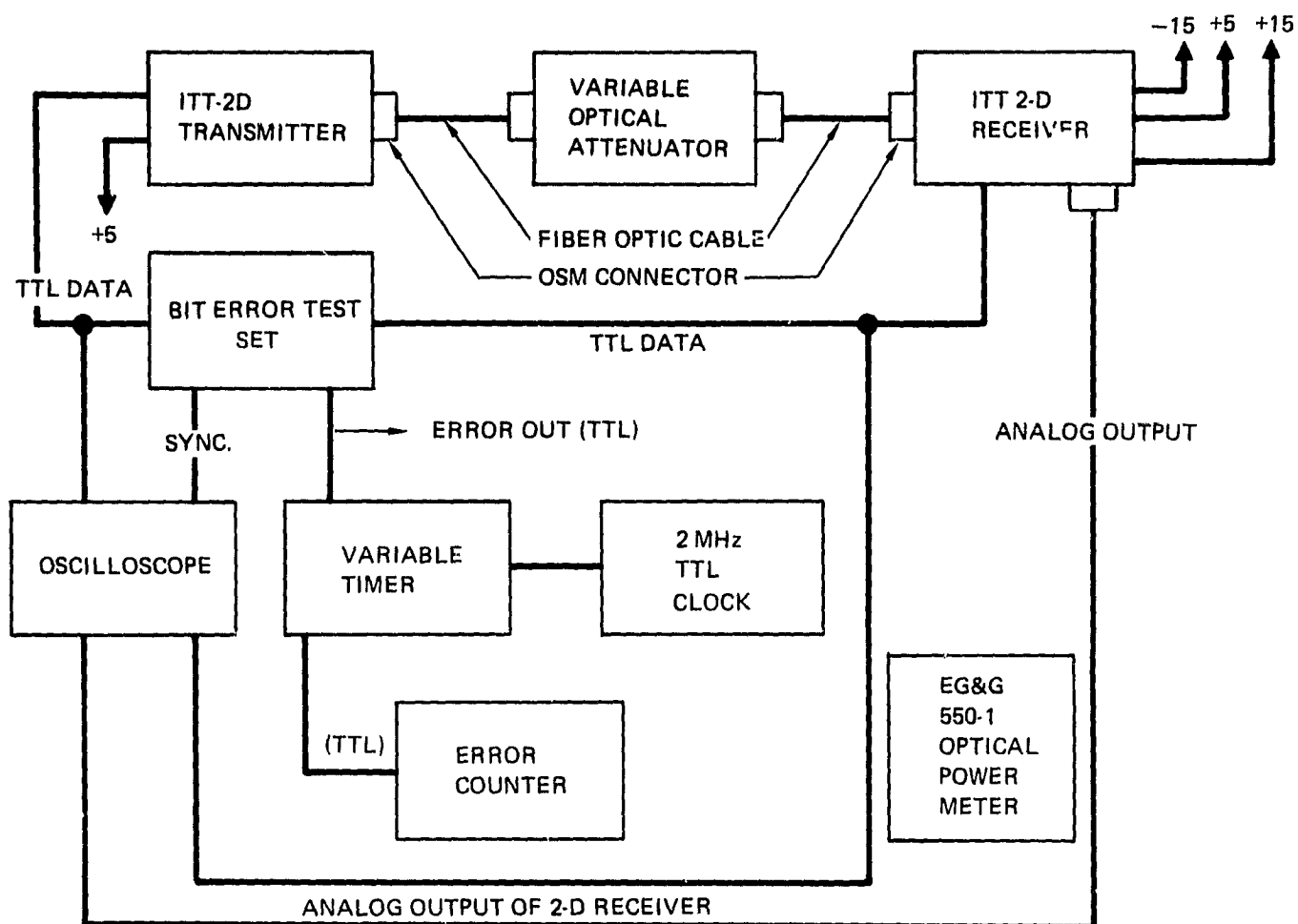


FIGURE 4-9

**ERROR PROBABILITY VERSUS AVERAGE LIGHT POWER  
AT OUTPUT END OF PCS FIBER**

10-2116

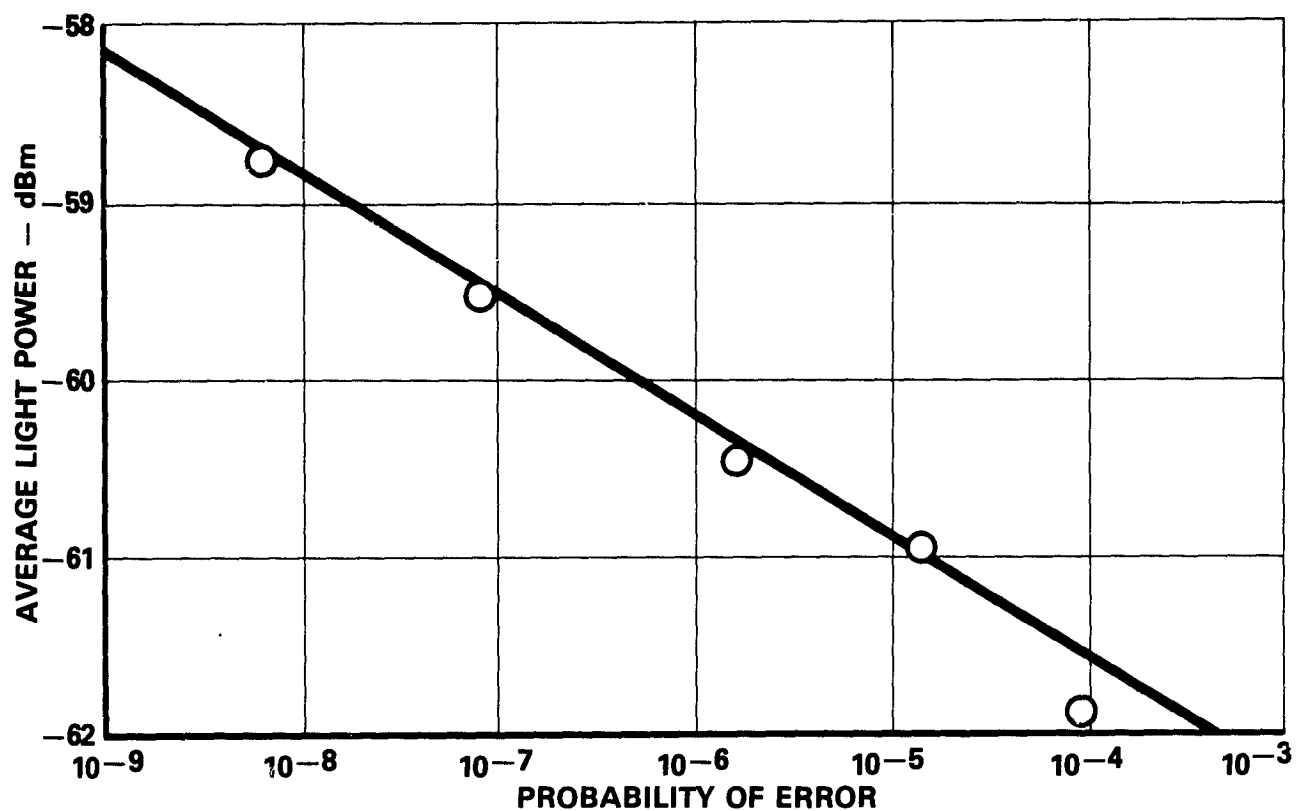


FIGURE 4-10

HP counter. This error rate was adjusted to the approximate desired value. The timer was then adjusted to the desired length of time by using the information given in Figure 4-8. The counter was set in the accumulate mode. The timer was started and the errors counted. After a given error rate measurement the optical power was measured by the EG&G 550-1 power meter.

Using this technique the curve in Figure 4-10 was generated. In this figure a plot of average optical signal power in dBm as a function of error rate is given.

### 4.3 EMI TESTS

#### 4.3.1 Radiation Environment

One of the more troublesome areas in avionics data bus systems has been Electro-magnetic Interference (EMI). The origin and amount of EMI present depends on the particular system; however, even small amounts of RF energy (as little as 9 mW) may cause integrated circuit operation to be upset. In general, to protect against EMI, shielding must be added thus the system weight increases. This increased weight, in the case of Space Shuttle, means reduced payload capacity. The RF field strengths that Shuttle is designed to operate in are on the order of 2V/m. However, in some areas on Shuttle the field strengths may be as high as 100V/m. In fact, ground based radars can generate field intensity of much greater than 2V/m.

How integrated circuits respond to EMI depends on what kind of circuit it is (linear or digital) and what the RF power levels are. An example of the interference that may occur in digital integrated circuits is shown in Figure 4-11. This figure illustrates the output voltage of a TTL 7400 NAND gate as RF power is conducted into the output terminal at 220 MHz. The output voltage, which is approximately 0.3 volt (a low state) in the absence of RF power, is seen to increase as RF power enters the output terminal. When the output voltage exceeds 0.8 volt, succeeding stages may not correctly recognize the low state voltage and logic errors may result. When the output voltage exceeds 2.0 volts, succeeding stages will interpret the output voltage as a high state, and logic errors are certain to occur. In this example, an RF power of 6 mW is shown to cause state errors; however, state errors have been observed to occur with as little as 9 mW of RF power.

Interference in 7400 NAND Gate. RF Enters Output at 220 MHz.

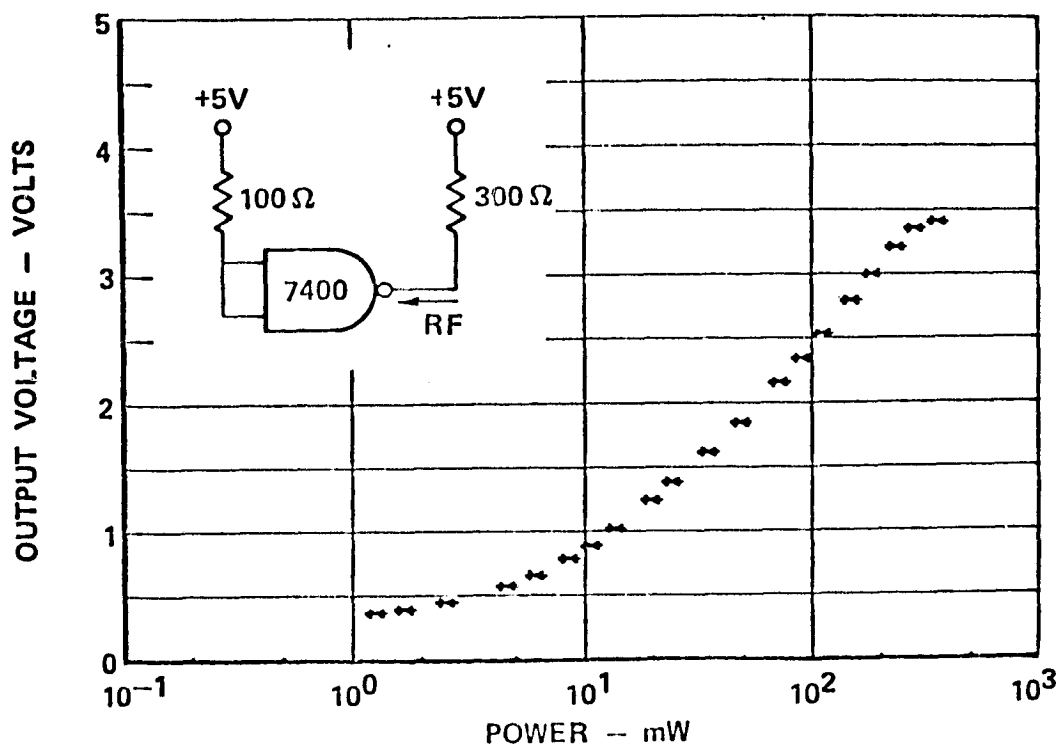


FIGURE 4-11

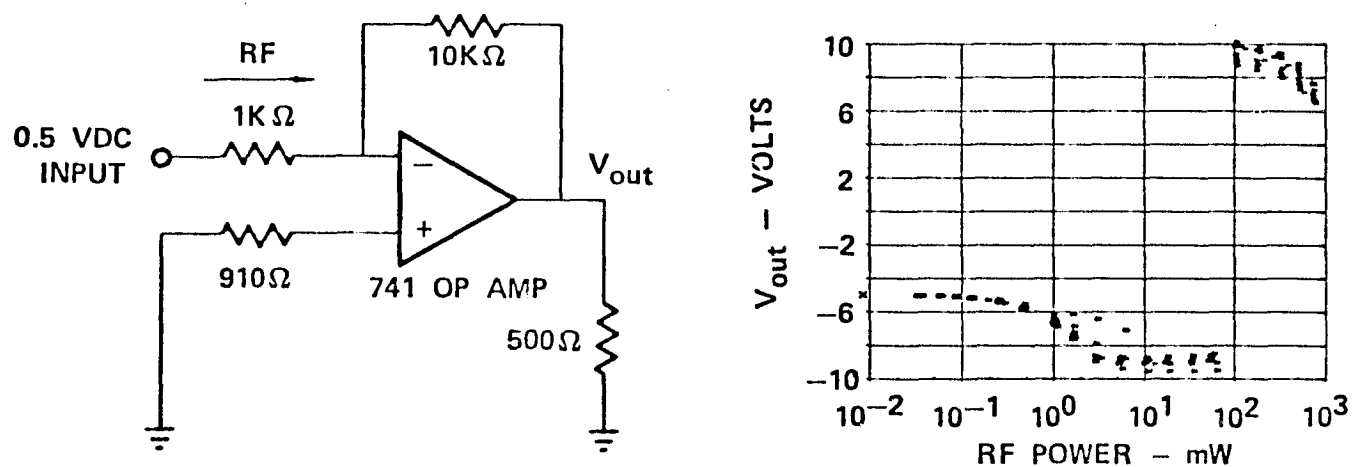
Interference in Amplifier Circuit Containing Operational Amplifier.  
RF Enters Inverting Input Terminal at 3.0 GHz.

FIGURE 4-12

Linear circuits are more sensitive to voltage offsets caused by RF energy than digital circuits, where logic states are defined in terms of voltage ranges. The interference effects generally decrease with increasing frequency of the interfering signal. As an example of interference in linear integrated circuits, Figure 4-12 shows the output voltage from ten tests of amplifiers containing 741 op amps. The circuit is an inverting amplifier with a gain of 10 and an input voltage of 0.5 volt. Microwave energy conducted into the op amp inverting input terminal at 3 GHz causes the output voltage to deviate from its normal value of -5 volts. The output voltage decreases until it saturates at -9 volts with 5 mW of RF power. Noticeable output voltage changes occur at an RF power of only 0.1 mW. It is interesting to note that at approximately 100 mW, the output voltage switches to a positive saturation voltage of about +0 volt.

If the interfering RF signal is modulated, the interference effect that is seen is also modulated. Essentially, the interfering signal is envelope detected by the semiconductor junctions in the integrated circuit. Figure 4-13 illustrates the interference that would occur in a linear circuit due to a pulsed RF signal. The circuit is an inverting amplifier with a gain of one. The input is -0.5 volt, so the expected output voltage is +0.5 volt. RF energy conducted into the op amp input terminal causes an offset voltage to appear at the op amp input which, through the feedback network, results in offsets at the amplifier output. Figure 4-13 illustrates that when the interfering signal is modulated the interference effect seen in the output voltage is modulated with the envelope of the RF signal.

In these examples, the interference effect was temporary and disappeared when the RF signal was removed. If the RF power level is high enough, the effect becomes permanent, or the device may not work at all. This happens when irreversible damage occurs within the integrated circuit. This effect is usually thermal in nature.

The basic situation that is representative of a typical EMI problem is shown in Figure 4-14. A system consisting of several electronic "black boxes" with interconnecting cables is contained within a system outer enclosure (skin). Electromagnetic radiation incident upon the system outer enclosure couples

## Typical Interference Effects Due to Modulation of the Interfering RF Signal

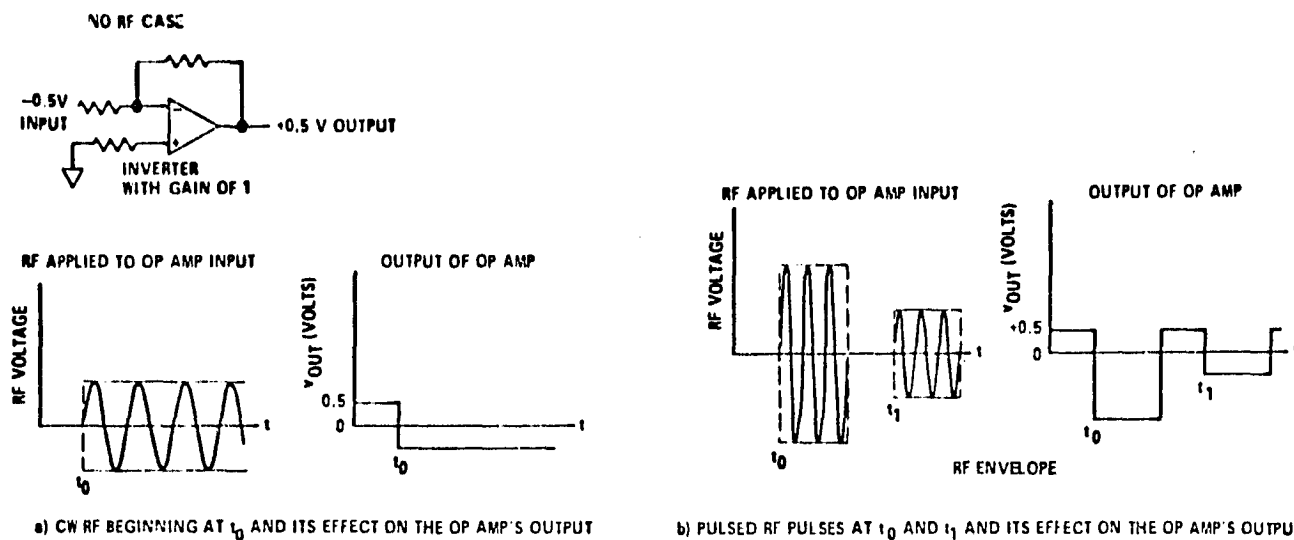


FIGURE 4-13

Basic Situation of Interest. Electromagnetic Radiation Can Cause Interference in Electronic Systems.

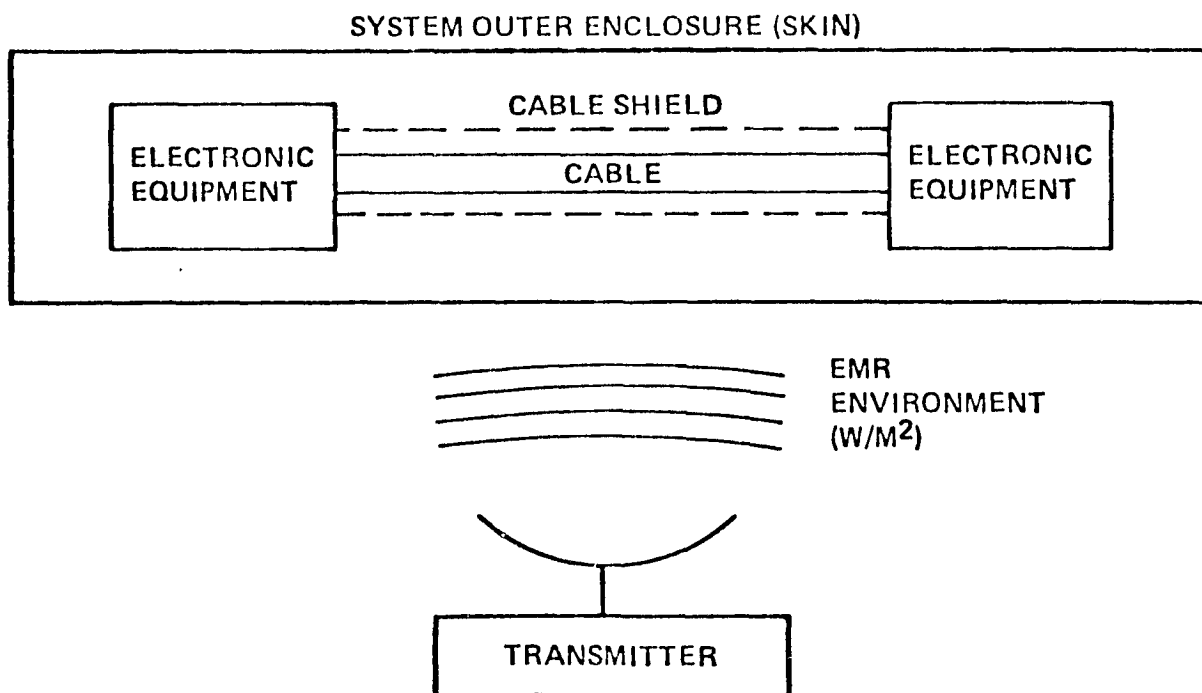


FIGURE 4-14



through apertures into the system interior. The internal EM fields induce RF voltages on the system interconnect cables which conduct them into the electronic "black boxes" where semiconductor devices such as integrated circuits are located. The RF voltages can be rectified by the semiconductor devices, and offset voltages and currents may be produced that are large enough to upset the operation of the electronic circuits.

The amount of power an unshielded wire or cable will pick up from this environment depends on such variables as frequency, aspect angle, terminating impedance, etc. One method for determining the maximum amount an unshielded wire will pick up is given by the formula

$$P = 0.13 \lambda^2 P_d , \quad (4.2)$$

where  $P$  is the maximum pickup power,  $\lambda$  is the wavelength of interest, and  $P_d$  is the power density. Experimental data supports the use of this relationship for frequencies greater than 100 MHz. Using this formula, the maximum amount of power expected on system wiring can be calculated from the environment level. The expression in Equation 4.2 is based on the power received by a half-wave dipole, and is only an approximation for unshielded wires.

There are two difficulties with using the half-wave dipole expression that must be borne in mind, however. The first is that it is known that wires can be made to exhibit greater effective apertures than given by the half-wave dipole expression due to specific design and/or fortuitous focussing effects due to system structure (consider the increased pickup on a short dipole possible when a large parabolic reflector is properly located nearby). Most system configurations are not expected to produce such enhancement effects, however, so it seems unreasonable to do a worst-case system hardening design based upon such possibilities. Such possibilities strengthen the rationale for checking a system hardening design in simulation environments, though.

The second difficulty with using the half-wave dipole expression comes when it is desired to extrapolate the function to lower frequencies where the inverse square frequency dependence leads to enormous effective apertures which are not observed in practice. The paradox can be resolved by recalling that the

half-wave dipole expression is for a matched half-wave dipole. The equivalent (Thevenin) driving impedance of the dipole approaches zero as the frequency approaches zero<sup>(9)</sup> so that, for a particular load on a cable, the mismatch losses counter the increasing aperture effects and the load will receive a constant amount of power, in accordance with common experience.

Based on the above information it appears that fiber optic systems should not have this half-wave dipole pickup problem. The fact that the wires are removed between the black boxes in Figure 4-14 means that the total EMI levels should be reduced as the unshielded bus wires also act as transmitting antennas. Removal of the data bus wires and replacement with fiber optics also helps to isolate the individual black box's ground systems, thus eliminating ground loops. If the data bus system is truly isolated by the fibers then the only way EMI can penetrate the system is where the fiber interfaces with the detector or where the shielding integrity has been violated; however, these penetrations can be made to have as much EMI isolation as desired by employing a waveguide below cutoff or a lossy waveguide.

#### 4.3.2 Waveguide Below Cutoff

If a penetration is required in one of the black boxes shown in Figure 4-14 they can be made with little or no effect to the EMI shielding by properly constructing the penetration or aperture such that the EMI will be attenuated to the value where it will not have any effect on the electronics. It is assumed in the analysis which follows that the aperture or waveguide is cylindrical and made of metal. The output at the end of aperture or waveguide depends on the frequency the system will accept (cutoff) and the attenuation/meter in the guide.

The cutoff frequency is defined as that frequency for a waveguide below which the EM wave will not be transmitted without being attenuated. This attenuation is not caused by the losses at the guide walls but because of reflections, i.e. the wavelength of the electromagnetic wave is too big to fit through the aperture or guide opening. The cutoff frequency is a function of the mode of electromagnetic radiation that meets boundary conditions in the guide ( $K_{NR}$ ), the diameter of the aperture or guide opening  $D$ , and the index of refraction of the material in the guide  $n$ . The equation for  $f_C$  is

$$f_c = \frac{n \cdot K_{NR}}{\pi c D} \quad (4.3)$$

where  $c = 3 \times 10^8$  m/c

The value of  $K_{NR}$  is dependent on the mode of radiation that can be supported by the guide. A plot of various values of  $K_{NR}$  are given in Figure 4-15, along with the modes of radiation, i.e.,  $TE_{ij}$  or  $TM_{ij}$ . From Figure 4-15, worst-case analysis will occur (lowest value of  $f_c$ ) if a value of  $K_{NR}$  of 1.84 is used (for  $TE_{11}$  which is the dominate mode). The index of glass may be assumed to be  $n = 1.5$ .

The amount of attenuation/meter in the guide caused by reflections is a function of wavelength. In the guide, however, this may be expressed as a function of frequency ( $f$ ) outside the guide. The loss in dB/meter for a given frequency caused by reflection

$$\alpha = \frac{2\pi \cdot 8.69}{c} [n f_c^2 - f_o^2]^{1/2} \text{ dB/m} \quad (4.4)$$

The above is the attenuation in dB/meter caused by reflections in the guide due to the fact that the guide cannot support the wavelength of radiation because it is greater than the cutoff wavelength of the guide.

There is also a loss mechanism in the guide which is due to the attenuation caused by the walls having finite conductivity. This mechanism will attenuate waves above cutoff according to the following relationship.<sup>(14)</sup>

$$\alpha = \frac{17.4 R_e/Z_c \left[ \left( \frac{f_c}{f} \right)^2 + \frac{n^2}{(K_{NR})^2 - n^2} \right]}{D R_e Z_d [1 - (f_c/f)^2]^{1/2}} \quad (4.5)$$

where  $ReZ_c = \pi\mu / \sqrt{f}$

$$ReZ_d = \frac{377}{n}$$

$\mu$  = permeability of waveguide walls H/m

= conductivity of waveguide walls  $\Omega/m$

$D$  = diameter of waveguide meters

$n$  = index of refraction of material inside guide

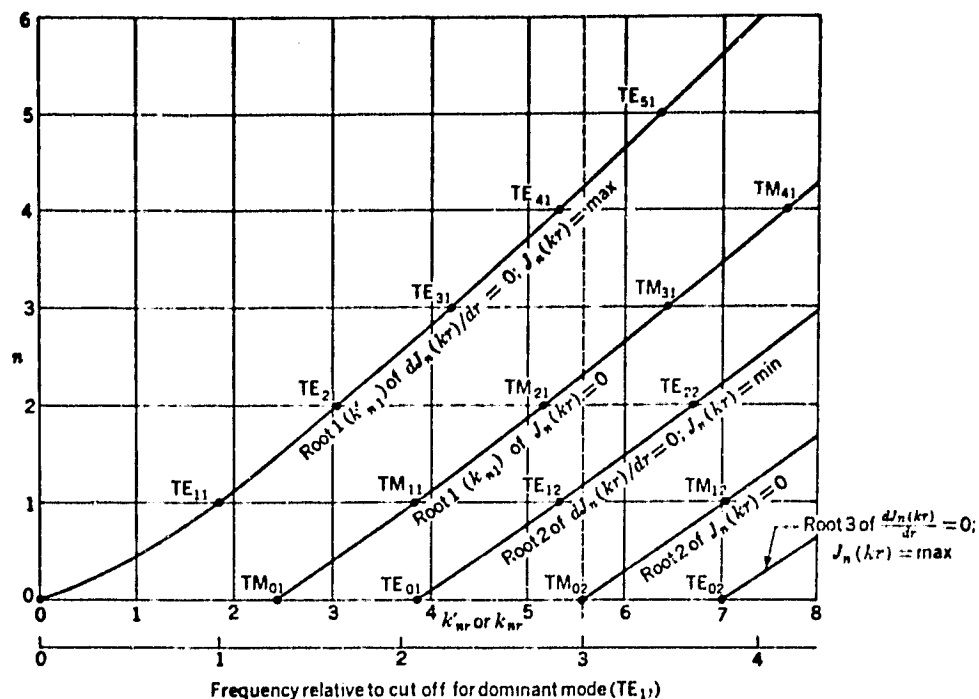


FIGURE 4-15

Possible TE and TM modes in a hollow cylindrical waveguide as a function of frequency. (After C-T Tai.) At 3 times the cutoff frequency for the TE<sub>11</sub> mode there are 9 modes which will pass (see text paragraph preceding Sec. 13-17) and one mode (TM<sub>02</sub>) at cutoff.

As in the rectangular guide, there are three conditions:

- 1 At low frequencies,  $\omega$  small,  $\gamma$  real, guide opaque (wave does not propagate).
- 2 At an intermediate frequency,  $\omega$  intermediate,  $\gamma = 0$ , transition condition (cutoff).
- 3 At high frequencies,  $\omega$  large,  $\gamma$  imaginary, guide transparent (wave propagates).

Putting  $\gamma = 0$  in (20), we find for the cutoff frequency and cutoff wavelength

$$f_c = \frac{1}{2\pi\sqrt{\mu\epsilon}} \frac{k'_{nr}}{r_0} \quad (\text{Hz}) \quad (21)$$

$$\lambda_{oc} = \frac{2\pi r_0}{k'_{nr}} \quad (\text{m}) \quad (22)$$

(KRAUS & CARVER)

FIGURE 4-15

From Equation 4.5 it is seen that in order to obtain the highest attenuation/meter, it would be best to use a very poor conductor for the waveguide with a high permeability.

It is generally accepted that electronic semiconductor equipment does not respond to electromagnetic frequencies much higher than 10 GHz. Most of the radiation (EMI) that would be present on a data bus system would be much lower than this and probably no higher than a few 10's of megahertz. Also, the amount of radiation transmitted by the black box which would increase the EMI environment will be reduced if the aperture is designed such that it will not pass frequencies above the fundamental data rate of the bus system. Unfortunately, many electronic systems must be vented to the ambient environment for cooling; hence, the system shielding must be violated for this purpose. If a single fiber data bus system is used then the single fiber connector (if it is metal) will act as a waveguide below cutoff for most frequencies of interest. This may be seen in Figure 4-16 where the attenuation in dB/m is plotted as a function at EMI frequency for a fiber with a 300  $\mu$ m core/cladding diameter. This figure is just a plot of Equation 4.4 and shows that the system is almost inherently protected from outside interference. The second plot on Figure 4-16 indicates that if a small aperture such as 3 mm hole for air ventilation is used then a lossy waveguide may have to be employed to protect the system from EMI.

When considering lossy waveguide type of protection, care must be taken to insure that the low loss mode is considered along with the dominate mode that the waveguide can support. A plot of the dBm attenuation as frequency is shown in Figure 4-17 where the loss for the  $TE_{11}$  and  $TE_{01}$  are shown for a 3 mm hole in the shielding. In this particular example, the system can be protected almost to any desired level of dB loss. Note also the values of parameters shown are quite conservative, and in general, the loss in the waveguide could be increased.

From this analysis and the information given in Section 4.3.1 it is fairly obvious that a fiber optic data bus system should be quite EMI hard. To verify this, the ITT data bus system was subjected to EMI and lightning tests.

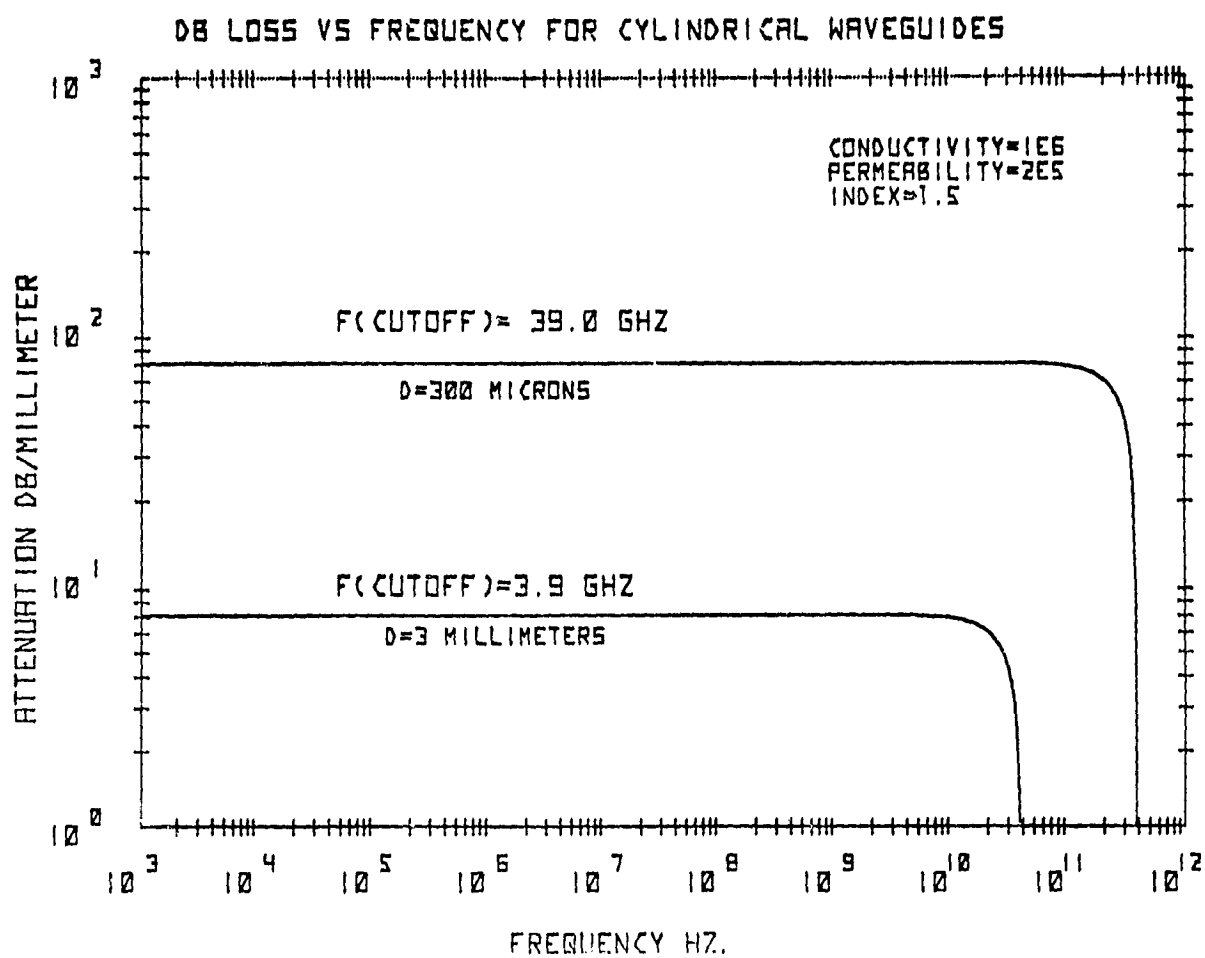


FIGURE 4-16

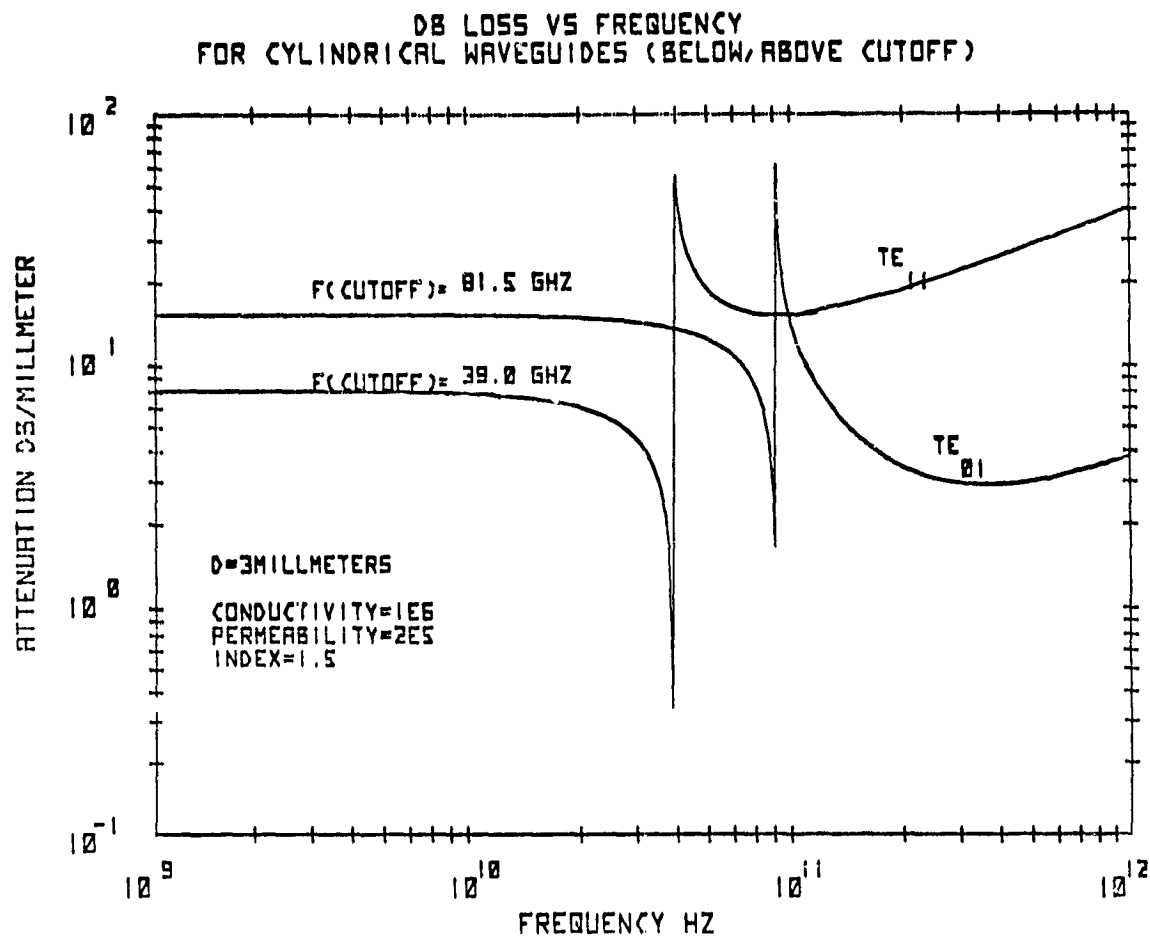


FIGURE 4-17

#### 4.3.3 EMI Susceptibility Measurement Criterion

The electromagnetic interference susceptibility tests were performed over the frequency range of 50 KHz to 10 GHz at levels as high as 20V/m. The tests were performed over two separate frequency ranges (low range and high range). The low range was between 50 KHz to 200 MHz and used a parallel plate capacitor while the high range, 200 MHz to 10 GHz, was performed in a Translational Electromagnetic Environment Chamber (TEMEC). Both of the susceptibility tests were performed while monitoring the bit error rate. Monitoring the BER of the fiber optic data bus system was believed to be the most sensitive measurement as to how well the bus was fairing under the EMI.

The criterion which was used to judge whether the EMI affected the BER was based on the theory given in Section 4.2.4. The unradiated fiber optic data bus system's BER was set by adjusting the optical power level. The system was then irradiated with a given RF field and the error rate recorded. The theory presented in Section 4.2.4 shows that as the total number of samples increases the smaller the confidence interval length becomes. As the confidence level shortens, the amount of time required to obtain the BER measurement increase; for example, if a 10% interval length is required at a  $10^{-4}$  BER then from Figure 4-8, approximately  $10^8$  samples must be taken. This amounts to a total data accumulation time of  $10^8/10^6 = 100$  seconds as the BER test would be performed at 1 Mbs data rate. If a smaller confidence length, of, say, 2.5% at a  $10^{-4}$  BER is required then from Figure 4-8 on the order of  $10^9$  samples are needed or each run would take 1000 seconds. The number of BER measurements that were actually performed were on the order of 300-400. This implied that the small confidence level measurement should not be used.

The theory presented in Section 4.2.4 was based on the assumption that the underlying statistics were, at best stationary, and at worst, wide-sense stationary in time and temperature. Since the receiver consisted of an automatic gain controlled APD configuration these assumptions would not be valid unless a certain amount of care was taken in the experiment. To make sure that the system was behaving as expected, a preirradiated test was performed. This test was performed by placing the fiber optic data bus system in a temperature controlled electromagnetic screen room (Faraday Chamber). The optical power was adjusted to give approximately a  $10^{-4}$  error rate. Then a time history of the



error rate was generated for two different sample time intervals. This data is shown in Figure 4-19, where the screen room has been cooling for approximately 6000 seconds. The data rate of the bit error test set was 1 Mb/s. The sample intervals shown in Figure 4-18 are  $10^8$  samples and  $10^9$  samples; also shown in the figure are the 10% interval levels for the  $10^8$  samples and 25 interval level for the  $10^9$  samples.

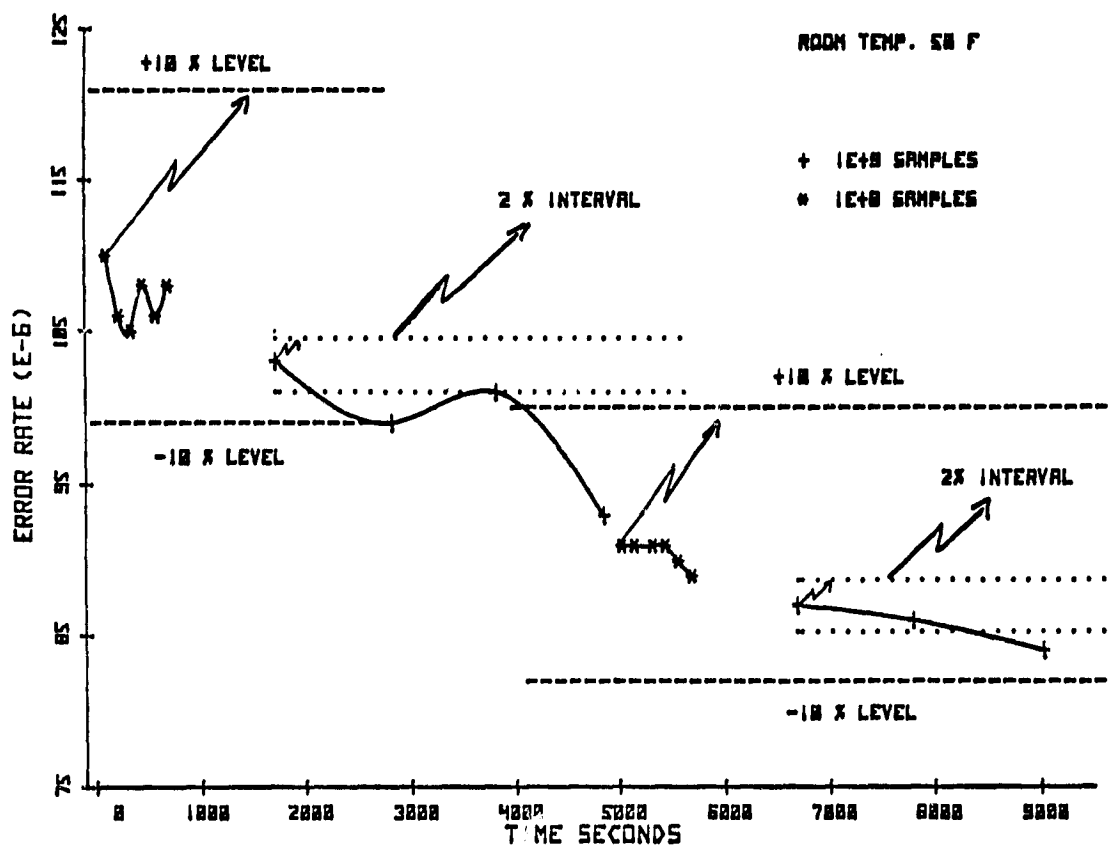
The initial data point was an error rate of  $108.0 \times 10^{-6}$ ; the next five data points taken were of 100 seconds. These points lie in the accepted band of statistical fluctuations that are predicted by the theory given in Section 4.2.4. However, the next 4 data points (sample size  $10^9$ ) can be seen from Figure 4-18 to clearly fall outside the 2% confidence level. The reason being, there is some drift of optical output power of ILD and gain of the APD with temperature and time, thus causing the statistics to be nonstationary. By examining Figure 4-18 it is clear that if 100-second sample size is used to measure the error rate then the fiber system remains stable enough so that a few thousand seconds can pass before the mean of the error rate drifts outside the confidence interval length as predicted by Equation 4.1. Hence, the BER of the system may be used to monitor the effects that the RF fields have on the system.

The bad aspects of using this criterion to obtain information on irradiated systems is that it is binary in nature. As the number of samples increases then binary nature of the measurement disappears and goes toward a continuum; however, as the information presented in Figure 4-18 clearly shows the data bus system did not have the stability to go much below a 10% confidence interval length. It should be pointed out that the BER measurement is a much more sensitive indicator as to how the system is performing under radiation than many of the standard EMI measurement techniques. The reason for this is that the system is measured in a dynamic fashion and any upset will propagate through the entire system.

#### 4.3.4 Low Radio Frequency Electromagnetic Interference Test

The low frequency EMI test was performed in a temperature-controlled screen room with the fiber optic data link between a parallel plate capacitor. The

### NASA FIBER OPTICS EMI PRE-TEST (NO RADIATION)



**FIGURE 4-18**

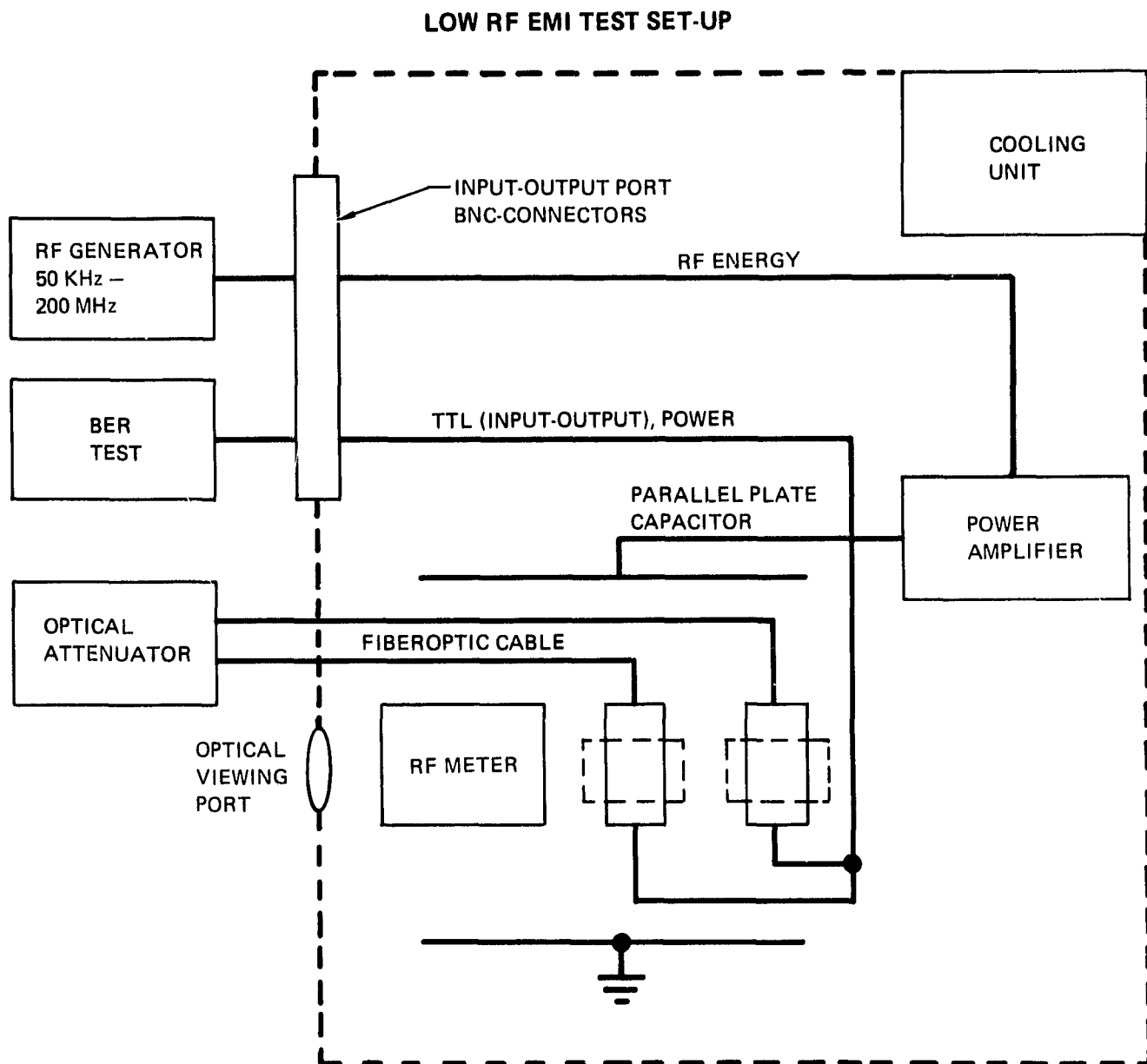


FIGURE 4-19

frequency of the electromagnetic field was varied between 50 KHz and 200 MHz. A block diagram of the set is shown in Figure 4-19. The screen room temperature was continuously maintained at a 50°C value. The RF generator, BER test set, and the optical attenuator were kept outside the screen room. All of the electrical connections were made through shielded coaxial cable and fed through the screen room wall via BNC connectors. The fiber optic cable was also fed out of the screen room with a continuous variable optical attenuator placed as shown in Figure 4-19. The optical attenuator was used to set the desired preirradiated error rate value. The fiber optic link was placed between the parallel plate cap.

The fiber optic link had cooling holes on the side of the metal boxes of the transmitter and receiver. The unit which was an off-the-shelf item from ITT was in no way designed or built to be an EMI shielded system. There was some question as to what the test rationale should be: should the system be made EMI hard, then tested, or should the system be tested, and a susceptibility plot be made as a function of frequency and level of field required to affect it. The second rationale was the one which was followed. It was felt that a plot of susceptibility vs. frequency would yield the most information, i.e., this plot would indicate the increased shielding necessary to make the system hard. If these values were small then there would be little concern for further fiber optic link as far as EMI was concerned. On the other hand, if the approach of shielding first, then testing was used, in reality a measurement of the ability to shield the system would result.

The fiber optic transmitter and receiver were orientated such that the cooling holes were perpendicular to the direction of the polarization of the field inside the parallel plate capacitor. Since it was not known how much shielding the system did provide, a rather slow and a laborious technique had to be applied at first. The approach was to obtain nonradiated BER measurements at the given frequency, 0V/m. The RF generator was adjusted to 5 V/m and another BER measurement made. This procedure was repeated at the given frequency at 10 V/m and 20 V/m. After this measurement was made, another 0V/m BER measurement was made to insure no permanent radiation damage occurred to the system. The maximum value of 20 V/m was used as this yielded a power density of somewhat slightly greater than 1 watt/m, a power density at which junction damage might occur.

These five measurements (0, 5, 10, 20 OV/m) were repeated at 75, 100, 150, 200, 1280, 1500, 2000 KHz. During the test, with the fiber optic transmitter and receiver perpendicular to the field, no effects of the radiation occurred. This is shown in Figure 4-20 where the percent change BER as a function of radiation frequency. The percent change is computed using the 20 V/m value and 0V/m of BER. In order for the system to have been affected, a radiated value of plus 10% would have to occur in Figure 4-20. This experiment was repeated with the fiber optic transmitter and receiver aligned parallel to the direction of polarization of the field inside the capacitor. The results of this test are shown in Figure 4-21. Here again, it is evident that the radiation of levels up to 20 V/m had no effect on the bit error rate. To evaluate the system at higher frequency the fiber data bus had to be placed in the TEMEC and irradiated.

#### 4.3.5 High Radio Frequency Electromagnetic Interference Test

The results of the low RF EMI tests were not surprising since the size of the apertures used in the transmitter and receiver for cooling were on the order of 2 to 3 mm. This implies that the cutoff wavelength (computed by using Equation 4.3 and  $f\lambda = c/n K_{NR} = 1.84$ ) is  $1.02 \times 10^{-2}$  meters which corresponds to a cutoff frequency of  $3.92 \times 10^{10}$  Hertz. The experimental setup, used to radiate the fiber bus system, had to be changed for frequencies of much greater than 200 MHz because the losses in the electrical cable to the capacitor and in the capacitor itself became extreme at higher frequencies.

There is also some question as to how valid the results are which are given in Section 4.3.3. The interaction of the electromagnetic interference with the fiber system was only performed in two different orientations and thus of limited value. The orientations chosen should have been the two in which the fiber optic system was most susceptible to EMI; however, there may have been a given position in which the system became resonance.

To circumvent this type of problem in EMI testing, MDAC developed the Translational Electromagnetic Environmental Chamber (TEMEC). The TEMEC is nothing more than a large metal box (8' x 10' x 25') in which electromagnetic radiation is injected by an antenna. Inside the screen room the radiation mode is stirred by a large paddle wheel. This paddle wheel is driven by a 1200-discrete-step motor. The position of the wheel may be controlled via manual control or by a computer.

## LOW RF EMI TEST (PERPENDICULAR CASE)

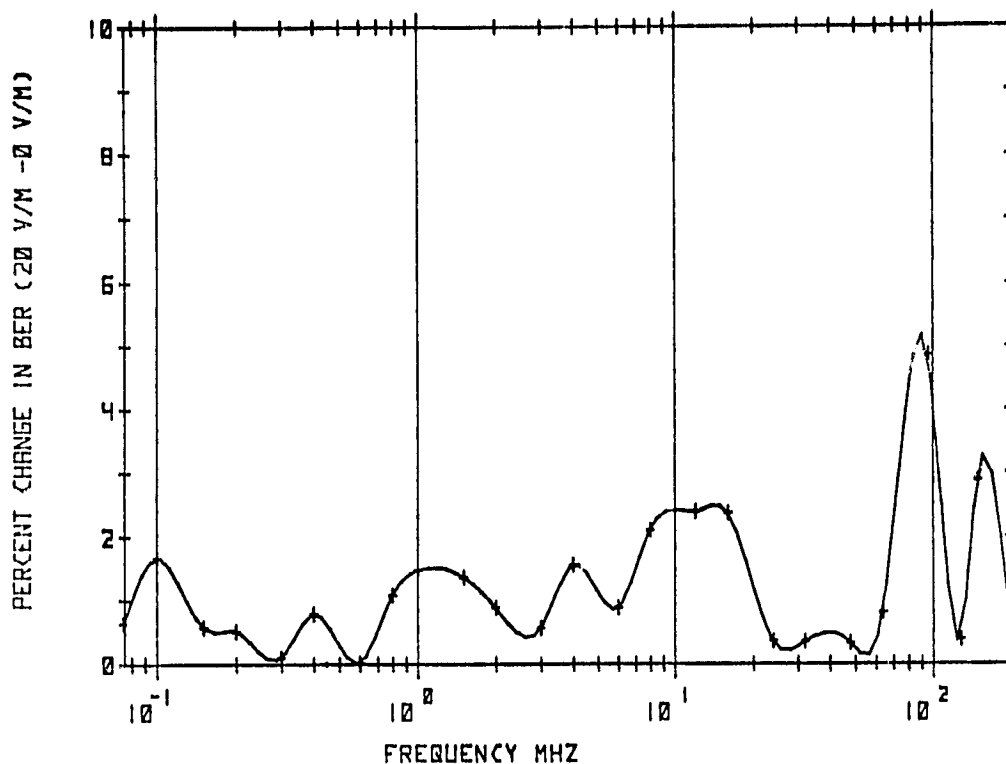


FIGURE 4-20

## LOW RF EMI TEST (PARALLEL CASE)

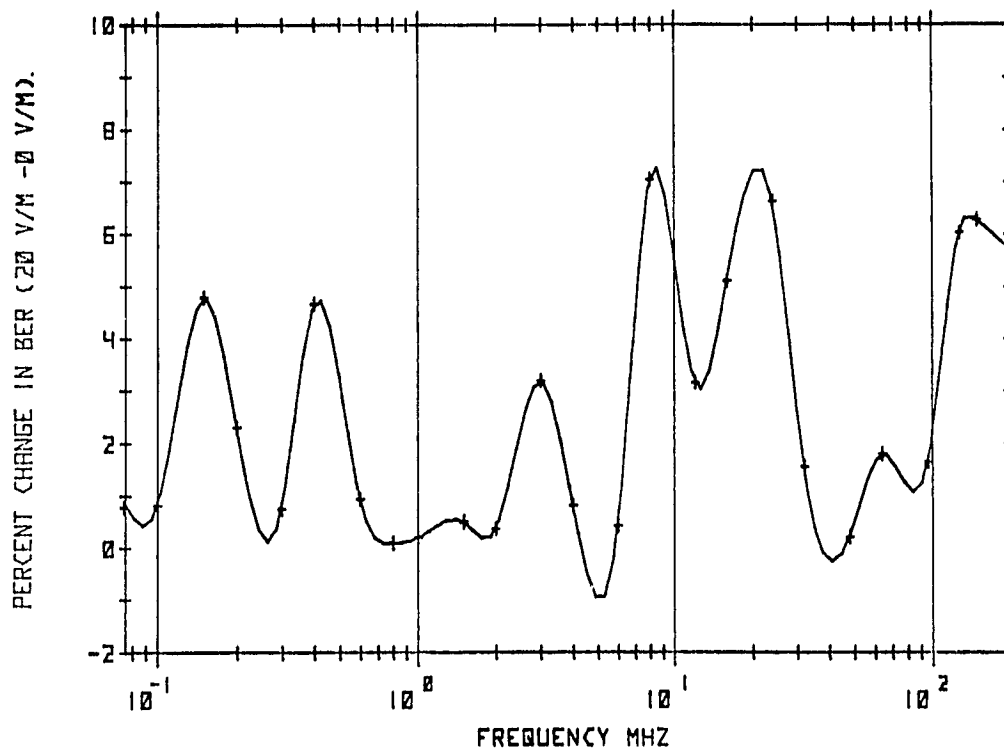


FIGURE 4-21

The fiber optic data bus system was placed inside the TEMEC as shown in Figure 4-22. The position that the paddle wheel is, at any particular moment, will affect the amount of radiation that reaches the fiber optic data bus system.

The test rationale was different for the high frequency test than that of the low frequency test. In the low frequency test the relative position of the fiber system was constant, the error rate was monitored and this value was compared with unradiated value. By comparing these two numbers, a judgement was made on how well the system performed under radiation. The high frequency test was performed by taking a base sample before each different frequency measurement. This base sample consisted of taking 100 BER measurements with no radiation on the fiber optic data bus. Each BER measurement consisted of  $10^7$  samples or a duration of 10 seconds, making the total data accumulation time on the order of 1000 seconds ( $\approx$  17 minutes). These measurements gave an approximation of the underlying probability density function. From this information the mean, standard deviation, and coefficient of skew of the data were computed. The density function was then integrated and an accumulated distribution generated of which a typical example is shown in Figure 4-23. After this curve was generated, the system was irradiated with a given electric field strength. The mode stirrer was controlled by the computer and adjusted to a new position every 10 seconds. The computer recorded the BER as a function of mode stirrer position. At the end of a run this information was stored on a magnetic tape. This stored information was processed by programs on the HP 9830. The mean, standard deviation, coefficient of skew, and the distribution were computed and compared for every given frequency at the radiated and unradiated levels. This information was then used to determine the effect of the high frequency EMI. Although it was not strictly important from an EMI study standpoint, an experiment was performed to determine the nature of the underlying probability density function for the BER. If this density function turns out to be Gaussian in nature then the distribution may be completely expressed by the mean and the variance.

This experiment was performed by placing the fiber optic data bus system in the TEMEC, closing the door, and setting a BER. The system was allowed to run overnight with the computer monitoring the BER in 10-second increments.

10-2671

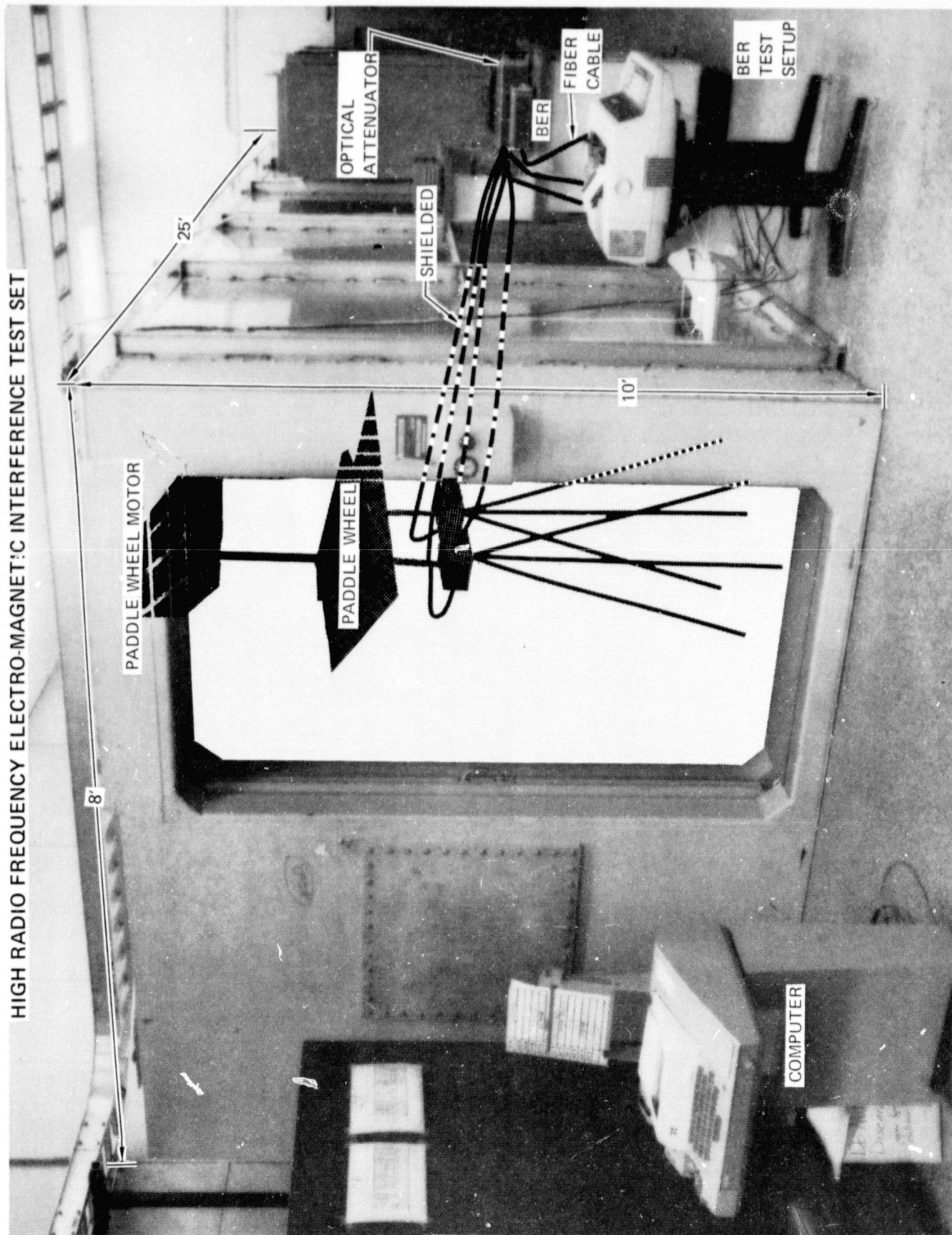


FIGURE 4-22



## NASA/JSC FIBER OPTIC EMI TEST 31

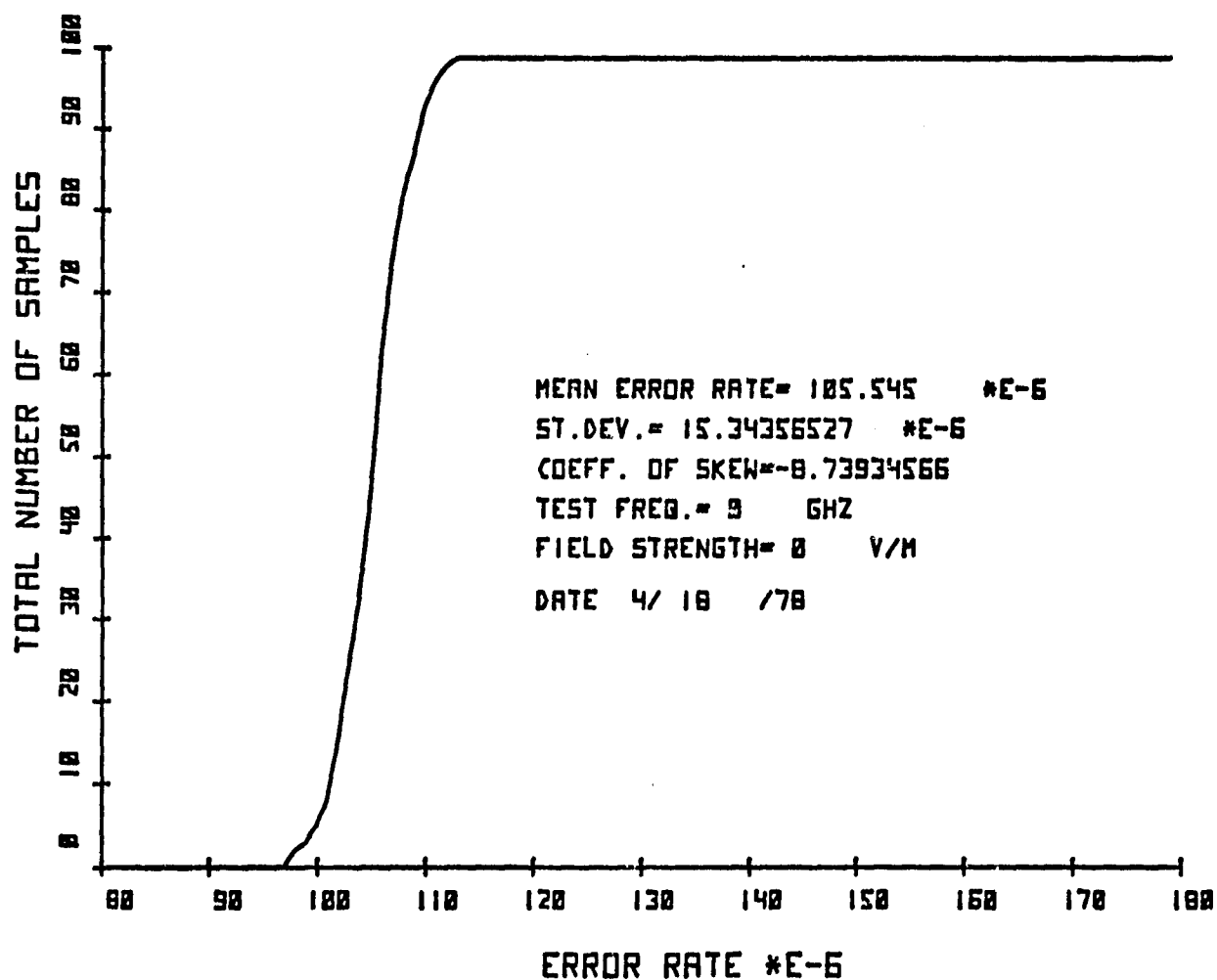


FIGURE 4-23

During the run, a total of 32,000 samples were taken. A plot of the normalized density function (\*) and distribution function (-) are shown in Figure 4-24. The even order centralized moments are given by ( )

$$\sum_{i=1}^N (X_i - \mu)^m P(X_i) = 1 \cdot 3 \cdot 5 \dots (M-1) \sigma^m \quad (4.6)$$

where  $\mu$  = mean

$m_2$  = even value integer

$\sigma^2$  = variance

$P(X_i)$  = discrete distribution

for a Gaussian variable.

NOTE: From the left-hand side of Equation 4.6 and the odd order centralized moments are zero.

The computed values using the left-hand side of Equation 4.6 are compared with the right-hand side of Equation 4.6 below.

	$\sum_{i=1}^N (X_i - \mu)^m P(X_i)$	$1 \cdot 3 \cdot 5 \dots (M-1) \sigma^m$
$m = 1$	$-5.784 \times 10^{-16}$	0.0
2	$2.666 \times 10^{-10}$	$2.666 \times 10^{-10}$
3	$-1.566 \times 10^{-16}$	0.0
4	$1.899 \times 10^{-19}$	$2.132 \times 10^{-19}$
5	$1.922 \times 10^{-25}$	0.0
6	$2.035 \times 10^{-28}$	$2.842 \times 10^{-28}$
7	$-2.045 \times 10^{-34}$	0.0
8	$2.783 \times 10^{-37}$	$5.304 \times 10^{-37}$
9	$-2.090 \times 10^{-43}$	0.0
10	$4.494 \times 10^{-46}$	$1.2727 \times 10^{-45}$

These moments give a fairly good indication that the BER curve is governed by a Gaussian distribution. The reason that the odd order moments are not strictly zero is caused by the fact that the data has some small value of

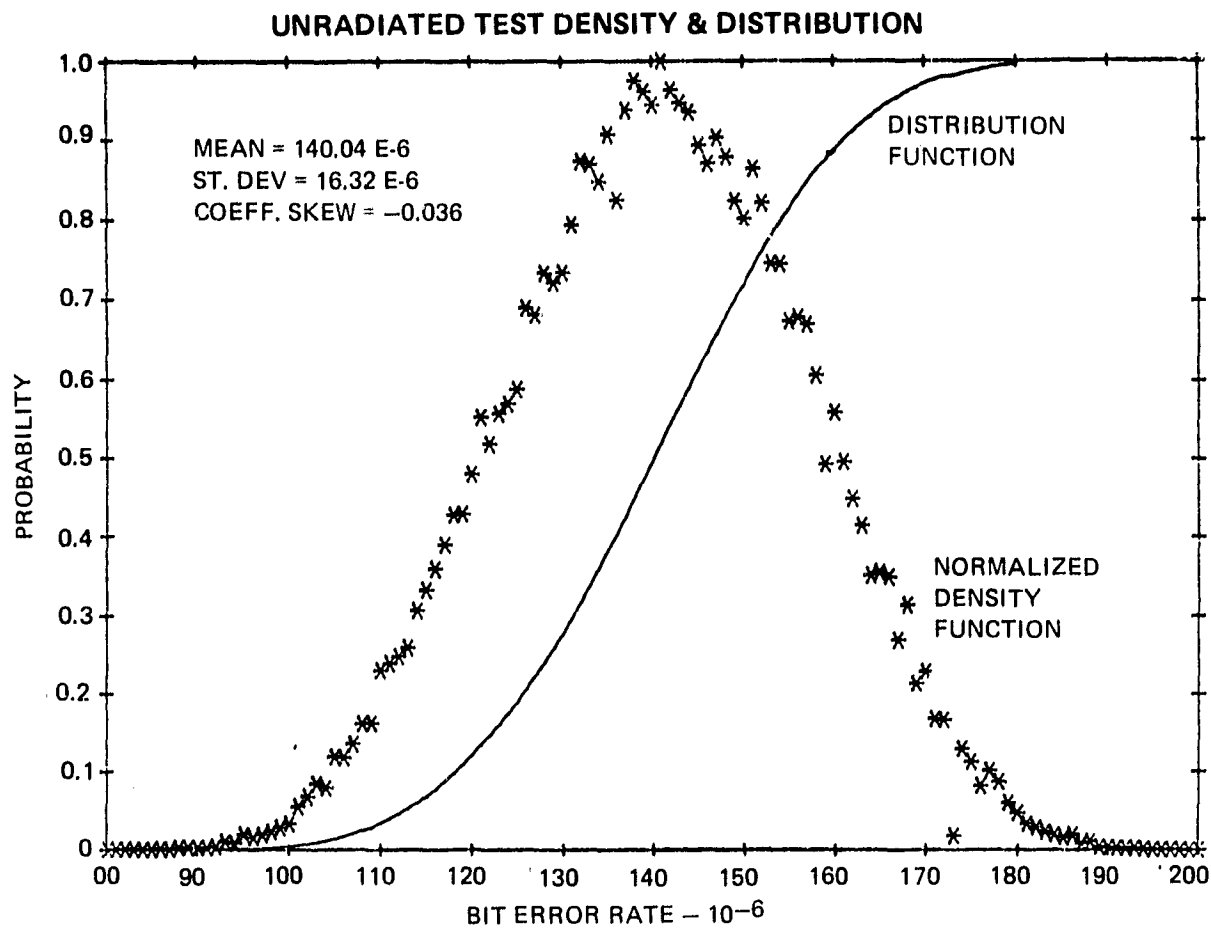


FIGURE 4-24

skew (-0.0359), although the odd order moment values are, in general, many orders of magnitude below the even order moments.

Since the underlying BER statistics are reasonably close to Gaussian, the process may be completely described if the mean and the standard deviation are known. Using this information the following data collection technique was employed. For every frequency an unradiated sample consisting of 100 ten-second BER measurements were made. These samples were then used to compute the mean, standard deviation, and coefficient of skew. The unradiated distribution function was also plotted. The system was radiated at 20 V/m and the statistics examined. If there was any radical change, the system was radiated at 10 V/m and these statistics once again examined. The radiation was reduced until no noticeable change was observed in the mean, the standard deviation, or the skew.

The results of these tests are shown in Figures 4-25, 4-26, and 4-27. In Figure 4-25 the absolute percent change of unradiated mean BER to 20 V/m radiated mean BER is shown (dotted line); on Figure 4-26 is the absolute percent change of unradiated standard deviation to the 20 V/m radiated standard deviation (dotted line); on Figure 4-27 the absolute percent change in unradiated coefficient of skew to the 20 V/m radiated coefficient of skew (dotted line). Also shown on each figure is the 20% change line which is the amount of change required by the theory in Section 2.18 for the system to be affected by the radiation. Figure 4-25 indicates that the average mean BER was unaffected; however, Figures 4-26 and 4-27 indicate the system was affected by the 20 V/m radiation at frequencies of 0.2, 0.8, 1.0, 2.4, and 3.2 GHz. The data was again plotted on Figures 4-28, 4-29, and 4-30 with the affected radiation frequencies replaced by the 10 V/m radiated values. This information is shown in the figures by the solid line. When these 10 V/m values were plotted the system appeared to be unaffected by the radiation.

The reason that the mean BER, which is shown in Figure 4-25 for both the 10 and 20 V/m cases, did not show any radiation effects and may be understood by observing the plots of the distribution function for the test frequency of 800 MHz for the 0V/m case (Figure 4-28), the 20 V/m case (Figure 4-29) and the 10 V/m case (Figure 4-30). These figures represent typical data runs for frequencies which were affected by the radiation. In Figure 4-29, the 20 V/m

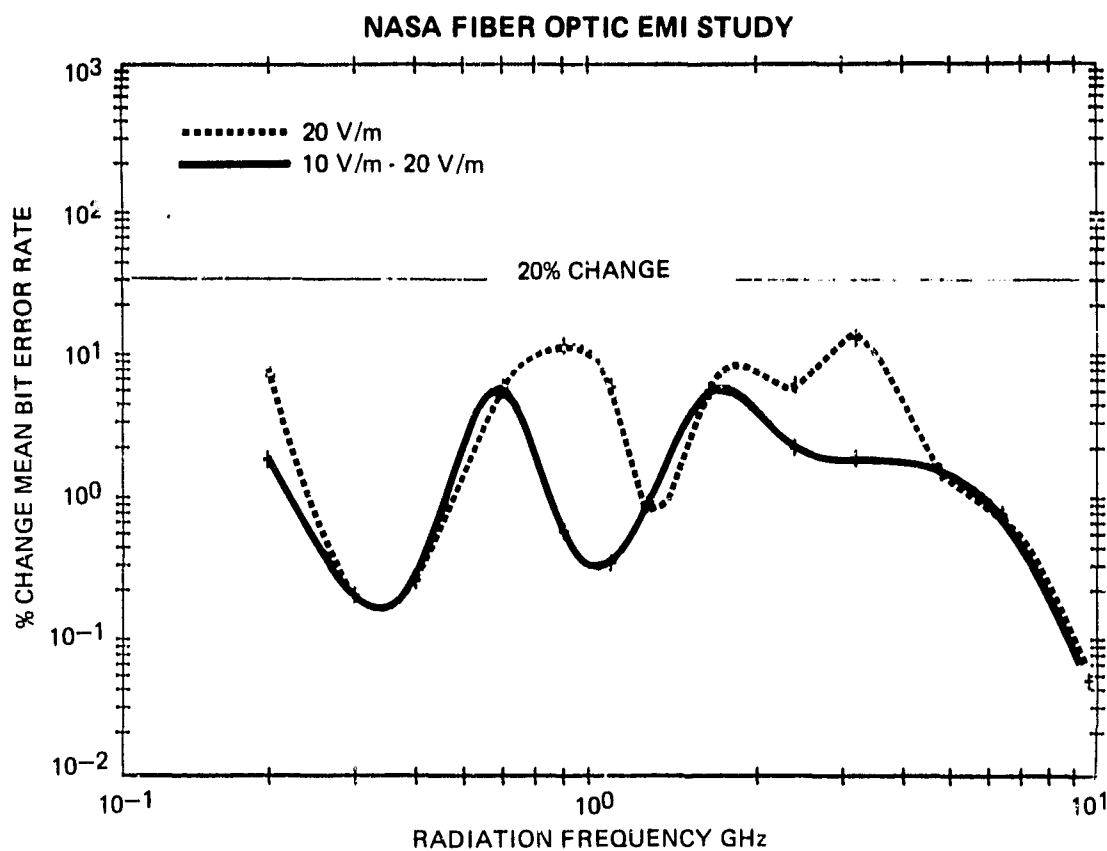


FIGURE 4-25

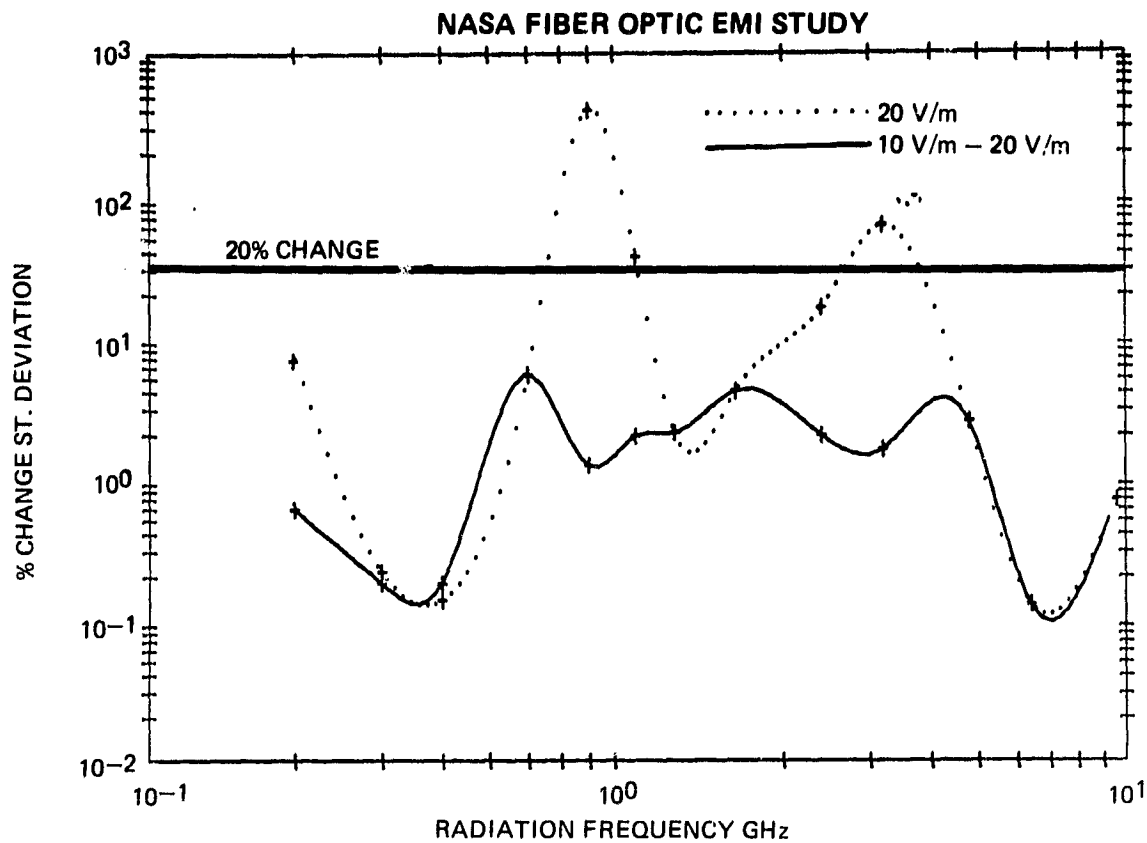


FIGURE 4-26

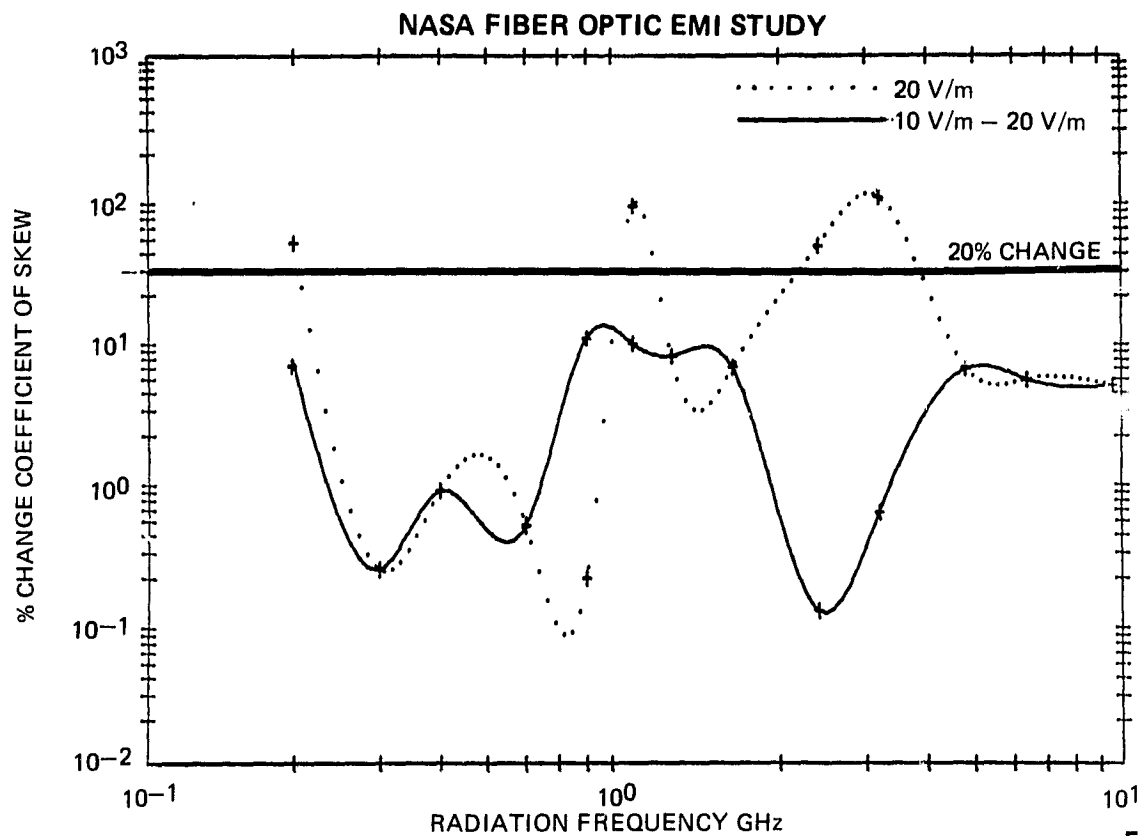


FIGURE 4-27

## NASA/JSC FIBER OPTIC EMI TEST 39

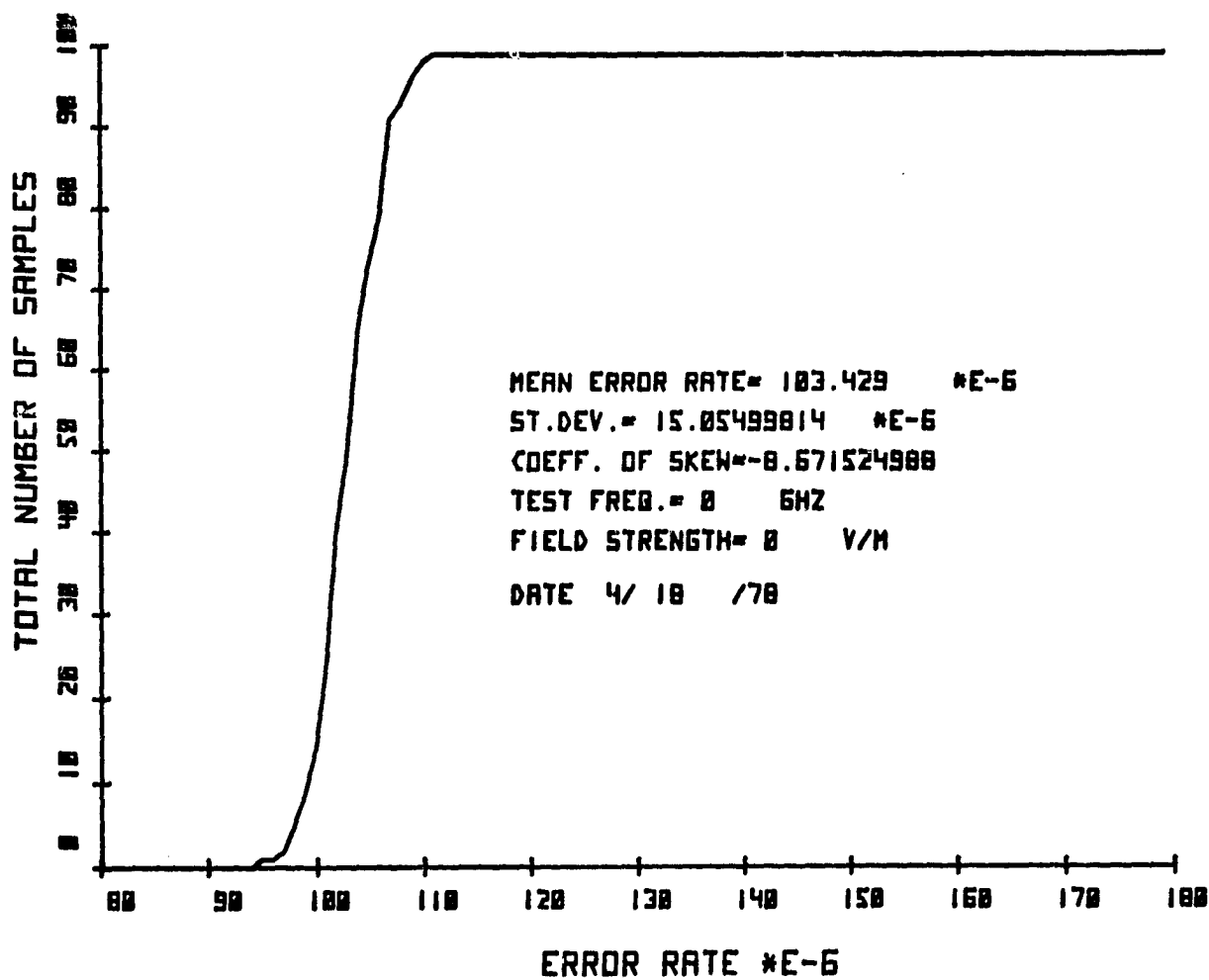


FIGURE 4-28

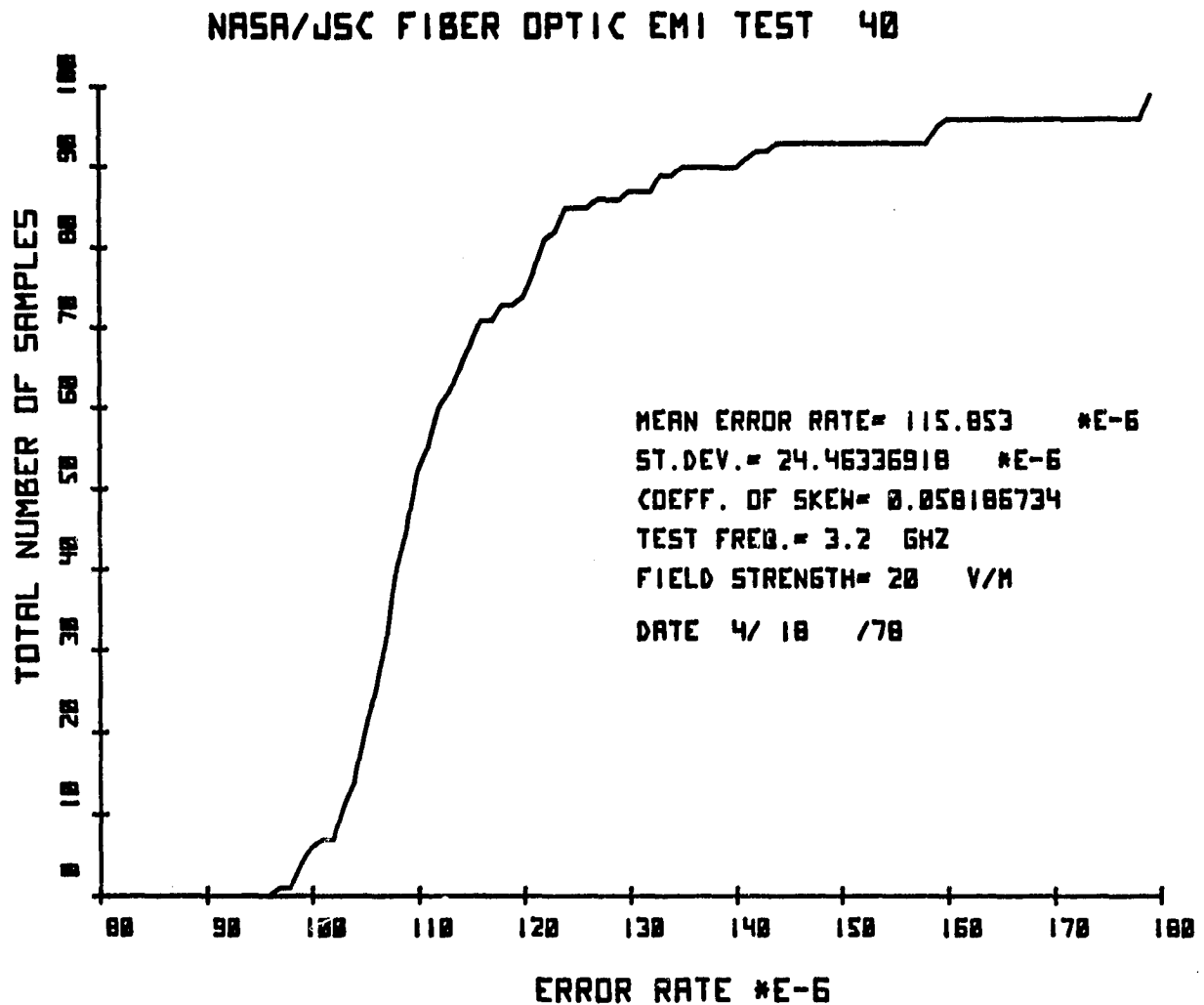


FIGURE 4-29



case, the mean remains fairly close to the unradiated value (103.429) while the standard deviation has changed by a factor of almost 2 and coefficient of skew has decreased by 150. The distribution clearly indicates what is happening as the paddle wheel inside the TEMEC is changed in position, the system becomes more sensitive to the radiation at a certain position. At these positions the BER changes (generally toward higher values), the system sensitivity however is not a continuum with paddle wheel position but exhibits quite a discrete nature. The mean error rate is not particularly sensitive to a few large excursions from the average value which are caused by the rotational position of the wheel. However, the standard deviation and the coefficient of skew (which is proportional to the third order central moment) are very sensitive to these few excursions taken by the BER, as the effect is squared in the standard deviation case and cubed in the coefficient of skew case.

Hence, these higher order statistics keep track of how well the system is doing. From Figure 4-30 it is seen that the system returns to normal when the radiation levels are dropped by 3 dB below the 20 V/m figure. The fact that the unshielded ITT system could be made EMI hard in this way indicated that to protect the system, at most, 3 dB of shielding would have to be added. The levels that the system was protected to were 20 times greater than MIL-461 levels (1 V/m) and ten times greater than those imposed by Space Shuttle (2 V/m).

#### 4.4 LIGHTNING TEST

The orbiter is designed to be an all-weather vehicle which would imply that it would have to operate in a scenario where lightning was present. The effects that lightning have on the data bus system in the orbiter are critical as it is a fly-by-wire vehicle. The system was tested to determine whether the ITT fiber optic digital data bus was susceptible to a lightning-induced upset. The test environment was chosen as the most probable lightning threat that would be encountered on the orbiter. An aluminum cylinder was chosen to represent an

## NASA/JSC FIBER OPTIC EMI TEST 41

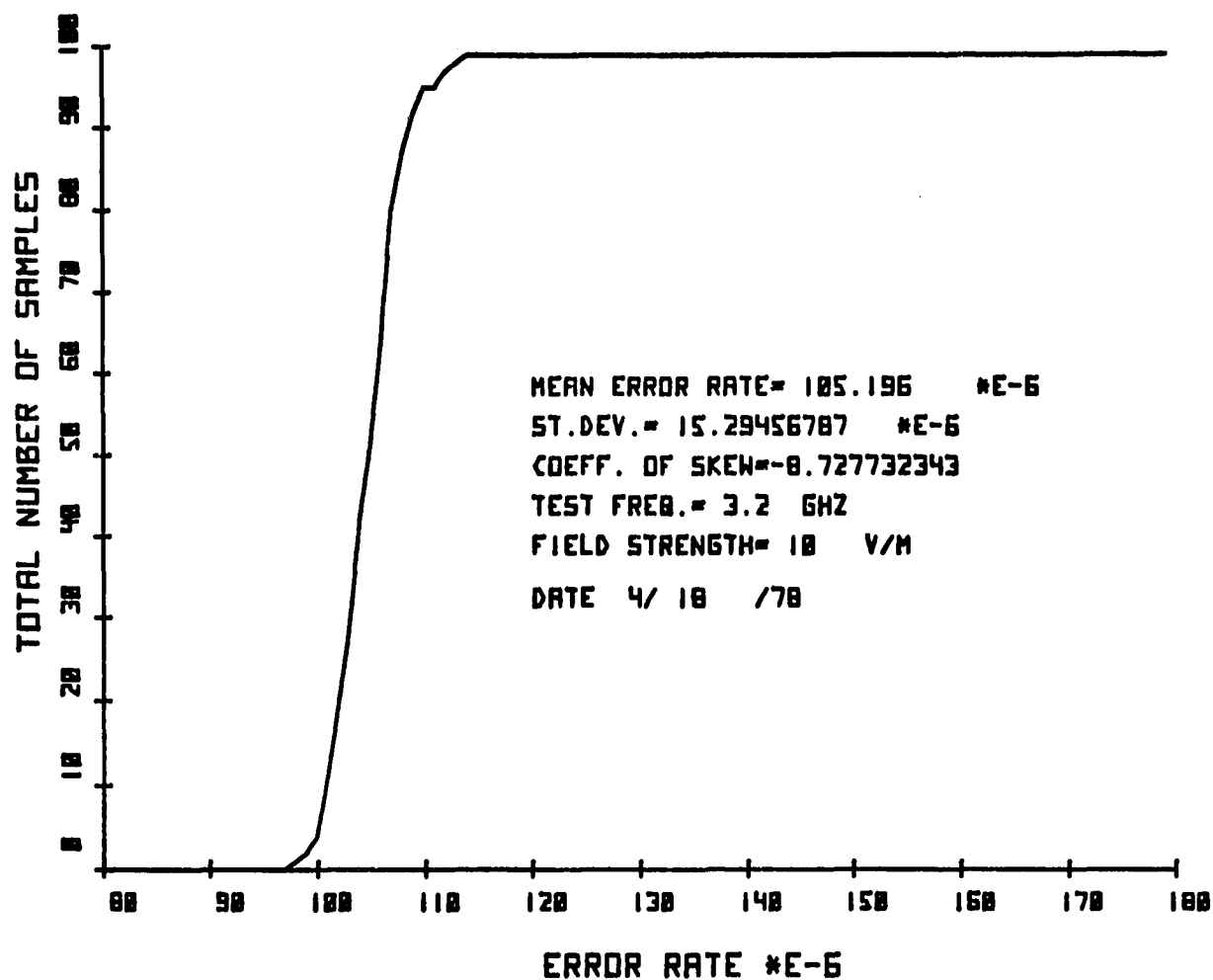


FIGURE 4-30

airframe structure in which a fiber optic system may operate. This cylinder was eight feet long and fourteen inches in diameter with the two ends capped, and was constructed of 0.040-inch T6-aluminum with a 12-inch square hole located twelve inches from one end. The square aperture was allowed to remain open during all testing to simulate an open airframe aperture and thus allow the lightning test radiation to enter the fiber optic mounting area and possibly affect the system. A  $1.6 \times 10^6$  volt high-voltage pulse generator was used to generate the simulated lightning strike attack and resultant high-voltage fields. The fiber optic unit set was mounted in the test cylinder with both units being near the open aperture (within 6 inches). The mounting of the units near the open aperture was done to simulate the effects of radiation that could be encountered through the aperture of a flight vehicle. A signal strength greater than 200 volts per meter was estimated to be at the location of the fiber optic units in the test cylinder. (This minimum signal level is estimated because field measurements in the confined area are altered due to the measurement devices.)

A second fiber optic data transmitter and receiver set was used to send the output of the test fiber optic unit to the screen room for signal evaluation. This output signal was monitored by a Bit Error Test.

The cylinder, with its fiber optic electronics, was mounted on insulating stands so that the cylinder ran parallel to and twenty-two inches above the floor. A high-voltage arc ( $1.6 \times 10^6$  volts) was generated so that the arc attached to the tube near the open aperture (within 18") completed the path to ground.

This high-voltage pulse was applied to the test cylinder ten times the frequency of about one pulse every two minutes. During these tests no errors were detected on the bit error detector.

No errors were detected at any time during the simulated lightning strike. This indicated that the tested fiber optic digital data system was immune to transient upsets as a result of strong field radiation.

## 5.0 REFERENCES

1. Theory of Dielectric Optical Waveguides, Dietrich Marcuse,  
Academic Press - 1974
2. Low Cost Fiber Optic Cable Assemblies for Local Distribution Systems,  
ECOM-75-1328-F, April 1977
3. Designer's Guide to Fiber Optics, C. W. Kleekamp and B. D. Metcalf,  
Cahners Publishing Company, Boston, MA
4. Weakly Guiding Fiber, D. Gloge, Applied Optics, Vol. 10, pp. 2252-2258,  
October 1971
5. Galileo Fiber Optics Company, J. Teager
6. Research Toward Optical-Fiber Transmission Systems,  
Proceedings of the IEEE, Vol. 61, No. 12
7. Raman Gain in Glass Optical Waveguides, R. H. Stolen and E. P. Ippen,  
Appl. Phys. Lett., Vol. 22, pp. 276-278, March 1973
8. Optical Power Handling Capacity of Low-Loss Optical Fibers as  
Determined by Stimulated Raman and Brillouin Scattering,  
Appl. Opt., Vol. 11, pp. 2489-2494, Nov. 1972
9. Testing of Tensile Strength of Optical Fiber Waveguides,  
C. K. Ko, M. Maklad, T. Reed, ITT Electrooptics Product Div.,  
Roanoke, VA
10. Optical Fiber Communications, Technical Note R-1, ITT Corp.
11. Absorption Induced in Glass and Plastic Fibers by 14 MeV Neutrons,  
L. M. Watkins, C. H. Barsis, Sandia Laboratories, June 1976
12. A Summary of Radiation - Induced Transient Absorption and Recovery  
in Fiber Optic Waveguides, Sandia Laboratories, Nov. 1976
13. Efficiency Limitations Imposed by Thermodynamics on Optical Coupling  
in Fiber-Optic Data Links, D. H. McMahon, Dec. 1975, Vol. 65, No. 12,  
Journal of the Optical Society of America

REFERENCES (Cont'd)

14. Electromagnetics, John D. Kraus and Keith R. Carven, McGraw-Hill Book Company, 1973
15. Fundamentals of Optical Fiber Communications, Academic Press Inc. 1976, Marcel Dekner, Inc., New York, 1978
16. M. C. Hudson and F. L. Thiel, Appl. Opt. 13, pg. 2540, 1974

## APPENDIX A. REQUIREMENTS DEFINITION DOCUMENT

## 1. SPACE SHUTTLE DATA BUS

1.1 General Description - The Space Shuttle data bus system provides digital data paths between the General Purpose Computers (GPC's) and the Shuttle subsystems and between the Pulse Code Modulation (PCM) Master Unit and the remote Multiplexer-Demultiplexer (MDM) Units. The bus is a half-duplex command response party line system utilizing time division multiplexing techniques. Each data bus is capable of providing data paths to and from the GPC's and the Shuttle subsystems.

Figure A-1 is illustrative of the data bus configuration. Each GPC, through its Input/Output Processor (IOP) section, is capable of controlling or monitoring any of the data buses with which it interfaces. On each bus, one computer is in control of the bus while the remaining four computers monitor vehicle system performance.

1.2 Data Characteristics - The digital data stream is a 1 megabit per second (MBPS) PCM format with a bi-polar Manchester II coding. A logic "one" is transmitted as a positive pulse followed by a negative pulse. A logic "zero" is transmitted by a negative pulse followed by a positive pulse. This is shown in Figure A-2. The word size is 28 bit periods. A  $5.5 \pm 0.5\mu$  sec dead time exists between words. The first 3 bit positions are used for word sync. The word sync is the nonvalid Manchester code shown in Figure A-3. The remaining bits are the valid Manchester code previously described.

1.3 Terminals - The number of terminal (GPC's or Bus Terminal Units (BTU's)) on each data bus may range from a minimum of five to a maximum of twenty. In relationship to the GPC in control of the bus, the terminals need not be symmetrically located along the bus.

1.4 Length - The length of the data bus is between 4.5 meters (15 feet) and 106 meters (350 feet). The GPC's and BTU's are connected to the bus by data bus stubs. The number of stubs on the bus may range between 5 and 20. The length of each stub is between 0.3 meters (1 foot) and 6 meters (20 feet).

## 2. SYSTEM PERFORMANCE

The optical data bus system will be compatible with the data described in Section 1. The bit error rate (BER) of the optical system shall be better than one part in  $1 \times 10^8$  for detection at a signal-to-noise ratio of plus 14 dB or higher.

Figure A-4A illustrates the optical data bus in a linear bus configuration, Figure A-4B illustrates the bus in a radial bus configuration. The electro-optical components in the data bus system include transmitters, receivers, cables, connectors, couplers, and repeaters. The specific requirements for these components are presented in the following sections.

## OPTICAL DIGITAL TECHNIQUES

REPORT MDC E2052  
FEBRUARY 1979

### 3. CABLES

- 3.1 Number of fibers - Multiple
- 3.2 Number of unbroken fibers - 95% of 3.1
- 3.3 Packing fraction -  $\geq .80$
- 3.4 Numerical aperture -  $\geq .60$
- 3.5 Optical attenuation -  $\leq .35$  dB/m (1.1 dB/ft) at 800 nm to 950 nm
- 3.6 Pulse broadening -  $\geq .2$  nsec/m (.66 nsec/ft)
- 3.7 Core Index of refraction - 1.6 at 800 nm to 950 nm
- 3.8 Maximum length - 106m (350 feet)
- 3.9 Bundle diameter - 1.14 mm (.045 in)
- 3.10 Jacket material - Kapton or Teflon
- 3.11 Weight -  $\leq 15$  kg/km (10 lbs/1000 ft)
- 3.12 Minimum bend radius - 12.3 mm (.5 in)
- 3.13 Tensile strength - 18 kg (40 lbs)
- 3.14 Jacket diameter -  $\leq 2.96$  mm (.117 in)



4. CONNECTORS

4.1 Connector type - SMA (single bundle)

BNC (single bundle)

MIL-C-83723 (multiple bundle)

4.2 Termination diameter - bundle size -  $\leq 1.14$  mm (.045 in.)

jacket size -  $\leq 2.96$  mm (.117 in)

4.3 Optical Loss -  $\leq 2.0$  dB throughput loss at 800 nm to 950 nm for mated  
connector pair

4.4 Cable retention - 18 kg (40 lb) pull

4.5 Durability - 1000 mate/demate cycles

## 5. COUPLERS

5.1 Bus "T" Couplers

5.1.1 Envelope Outline - Figure A-5.

5.1.2 Power Splitting - The coupler contains two reflective surfaces to split the optical power between the throughput ports and the input/output port. The ratio of the size of each reflecting surface to the size of the coupler is defined as the power splitting factor (P.S.). This is shown in Figure A-6. The power splitting factor may range between .125 and .03.

5.1.3 Throughput Port to Throughput Port Attenuation -  $\leq 5$  dB exclusive of power splitting loss where the power splitting loss is given by  $10 \log (1-2 \text{ P.S.})$ .

5.1.4 Throughput Port to Input/Output Port Attenuation -  $\leq 5$  dB exclusive of power splitting loss where the power splitting loss is given by  $10 \log \text{ P.S.}$

5.2 Bus Star Couplers

5.2.1 Envelope Outline - The star coupler consists of a mating pair of MIL-C-83723 connectors. The connector size depends upon the number of terminals. Figure A-7 shows the outline size of the mated pair.

5.2.2 Power Splitting - The coupler contains a reflective surface to split the optical power equally to all input/output ports. The number of ports may range between 5 and 20. The power splitting factor (P.S.) may range between .2 and .05.

5.2.3 Input/Output Port to Input/Output Port Attenuation -  $\leq 5$  dB exclusive of power splitting loss where the power splitting loss is given by  $10 \log \text{ P.S.}$

5.3 GPC and BTU Couplers

5.3.1 Envelope Outline - The GPC/BTU coupler is mounted within a jam nut SMA connector. The outline of this connector is shown in Figure A-8.

5.3.2 Power Splitting - Transmitted power is coupled to the bus port only. Received power is split equally between the receiver and the transmitter.

5.3.3 Input Port to Bus Port and Bus Port to Output Port Attenuation -  $\leq 4$  dB including power splitting.

## 6. REPEATER

6.1 Size - The repeater is contained within a jam nut receptacle MIL-C-83723 connector. A mating connector is furnished as part of the assembly. The specifications for the connector are shown in Section 4. An outline drawing is shown in Figure A-9.

6.2 Power Supply - +24 VDC  $\pm$  2 VDC

6.3 Data Format - 1 MBPS Manchester II as defined in Section 1.2.

6.4 Input Level - Logic "1"  $>$ -45 dBm at wavelength between 800 nm and 950 nm.\*  
Logic "0"  $<$  -50 dBm at wavelength between 800 nm and 950 nm.\*

6.5 Output Level - Logic "1"  $>$ - 5 dBm at wavelength between 800 nm and 950 nm.\*\*  
Logic "0"  $>$ -45 dBm at wavelength between 800 nm and 950 nm.\*\*

6.6 Input/Output Delay -  $\approx$ 80 nsec.

6.7 Bit Error Rate -  $\approx$ 1 part in  $10^8$  bits.

6.8 Power Splitting Factor - 0.5

6.9 Operational Life -  $>$ 10,000 hours continuous operation.

\* Measured at input to mating connector from source coupled by a cable with the characteristics shown in Section 3.

\*\* Measured at output of mating connector coupled into detector by a cable with the characteristics shown in Section 3.

## 7. TRANSMITTER

7.1 Size - The optical transmitter is contained within the envelope shown in Figure 10.

7.2 Power Supply - +5.0 VDC  $\pm$  .25 VDC  
                                  +12.0 VDC  $\pm$  .30 VDC  
                                  -12.0 VDC  $\pm$  .30 VDC

7.3 Data Format - 1 MPPS bipolar Manchester II as defined in Section 1.2.

7.4 Electrical Input Impedance -  $70\Omega \pm 3\Omega$ .

7.5 Electrical Input Signal - See Figure A-10A. The rise and fall times of this signal shall be 150 nsec  $\pm$  50 nsec when measured between 10 and 90 percent of the nominal plus and minus voltage levels.

7.6 Optical Output Signal - For a logic "1" (positive level) input, the output shall be greater than 3 dBm (1 mw) at a wavelength between 800 nm and 950 nm\*; for a logic "0" (negative level) input, the output shall be less than -45 dBm ( $2 \times 10^{-5}$  mw) at a wavelength between 800 nm and 950 nm\*.

7.7 Input/Output Delay - <40 nsec.

7.8 Operational Life - >10,000 hours continuous operation.

\* Measured when coupled into a cable having the characteristics shown in Section 3.

## 8. RECEIVER

8.1 Size - The optical receiver is contained within the envelope shown in Figure A-11.

8.2 Power Supply - + 5.0 VDC  $\pm$  0.25 VDC

+12.0 VDC  $\pm$  0.30 VDC

-12.0 VDC  $\pm$  0.30 VDC

8.3 Data Format - 1 MBPS bi-polar Manchester II as defined in Section 1.2.

8.4 Optical Input - Logic "1"  $>-45$  dBm at wavelength between 800 nm and 950 nm\*.

Logic "0"  $<-50$  dBm at wavelength between 800 nm and 950 nm\*.

8.5 Electrical Output Impedance -  $70\Omega \pm 3\Omega$ .

8.6 Electrical Output Signal - For a logic "1" input (input  $>-45$  dBm), the output signal shall be between 0.6 and 15.0 volts zero to peak; for a logic "0" (input  $<-50$  dBm), the output signal shall be between -0.6 and -15.0 volts zero to peak.

8.7 Input/Output Delay -  $<40$  nsec.

8.8 Bit Error Rate - 1 part in  $10^8$  bits.

8.9 Operational Life -  $>10,000$  hours continuous operation.

\*Measured when coupled from a cable having the characteristics shown in Section 3.

## 9. ENVIRONMENT

The data bus and its individual components shall operate within the requirements of this document when exposed to any natural combination of environments presented in this section.

8.1 Temperature

Minimum: -54°C (-65°F)  
Maximum: +70°C (+160°F)

3.2 Pressure

Minimum:  $10^{-10}$  Torr  
Maximum: 930 mmHg (18 psia)

3.3 Humidity

Minimum: 0 percent relative  
Maximum: 100 percent relative

3.4 Salt Fog

Exposure to one percent salt solution by weight.

3.5 Random Vibration

20-2000 Hz at  $0.35 \text{ g}^2/\text{Hz}$

Time duration 78 minutes in each of the three mutually perpendicular axes

3.6 Acceleration

Plus or minus 5 g's in all axes

3.7 Shock  
Landing

Rectangular pulses of the following peak accelerations, time duration, and the number of applications in the vertical (up) direction during landing:

Acceleration (g peak)	Duration (ms)	Application
0.23	170	22
0.28	280	37
0.35	330	32
0.43	360	20
0.56	350	9
0.72	320	4
1.50	260	1

Transient

5 to 35 Hz, plus or minus 0.25 g peak

## 10. ELECTROMAGNETIC INTERFERENCE

The optical data bus will perform within the requirements of this document during exposure to the EMI tests contained in this section. For the EMI tests, the transmitter and receiver will be packaged in a container that simulates the shielding and bonding characteristics of the GPC and BTU. Conducted emission and conducted susceptibility requirements are applicable to the 24 VDC power only.

10. Conducted Emission - Figure A-12 and A-13.

10.2 Conducted Susceptibility - Figures A-14 and A-15.

10.3 Transient Susceptibility - Figure A-16.

10.4 Radiated Emission - Figures A-17 and A-18.

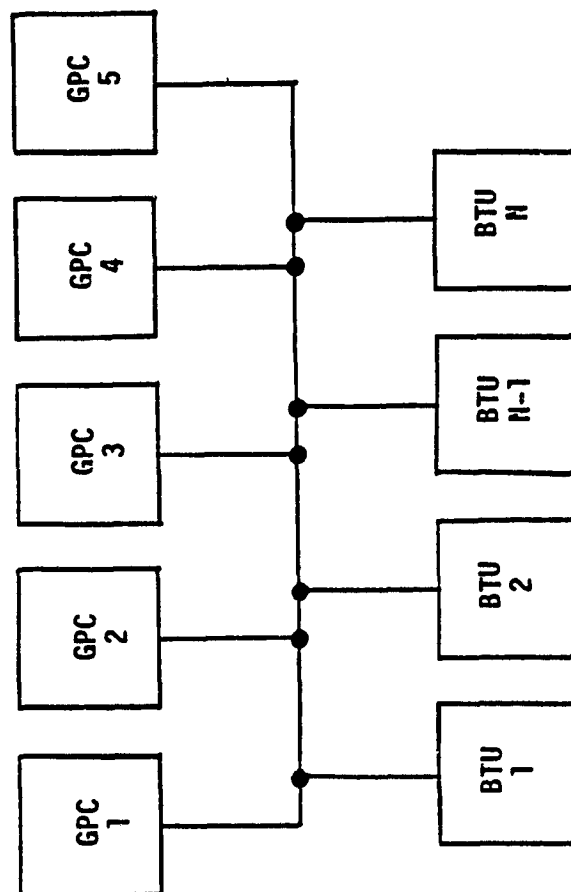
10.5 Radiated Susceptibility - Figure A-19.

## 11. Lightning

The optical data bus will perform satisfactorily during exposure to simulated lightning strikes. Lightning strikes will be simulated by the configuration shown in Figure A-20. The pulse generator shall be set to produce a 1 MHz damped sine wave. The amplitude will be that which produces a 1 ampere signal in the electrical wire.

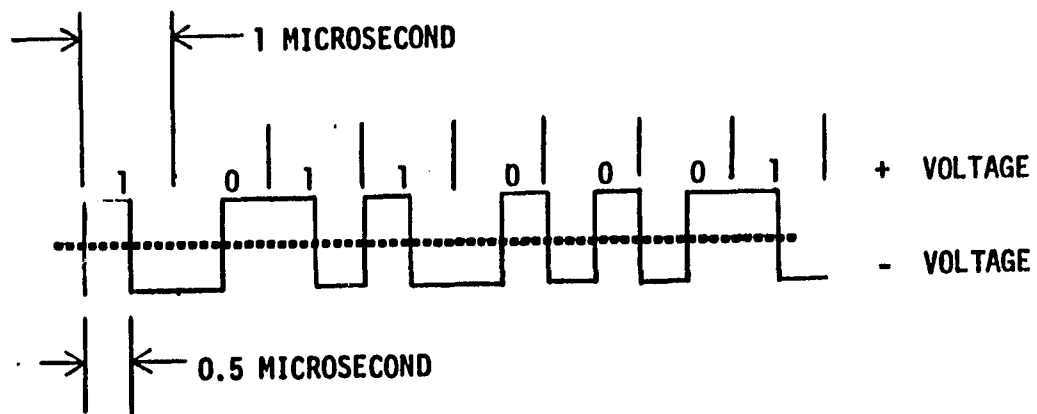


FIGURE A-1 SHUTTLE DATA BUS



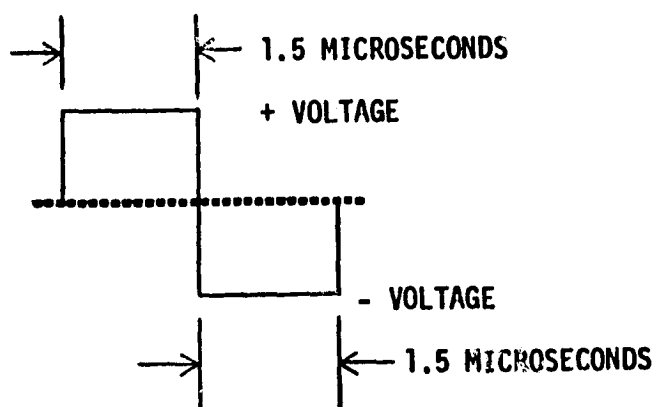
GPC - GENERAL PURPOSE COMPUTER  
BTU - BUS TERMINAL UNIT

FIGURE A-2 MANCHESTER II CODE

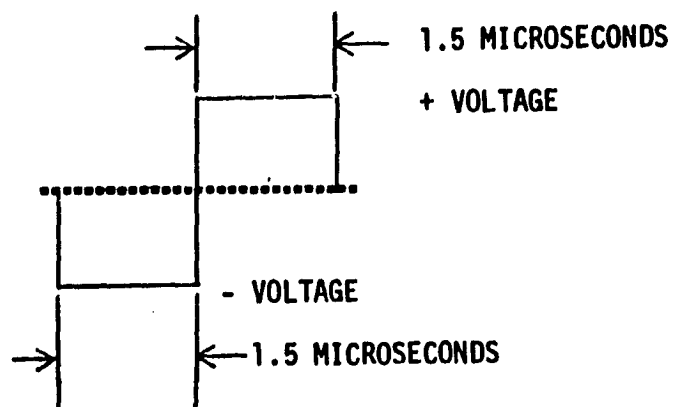


"1" - 10  
"0" - 01

FIGURE A-3 WORD SYNC

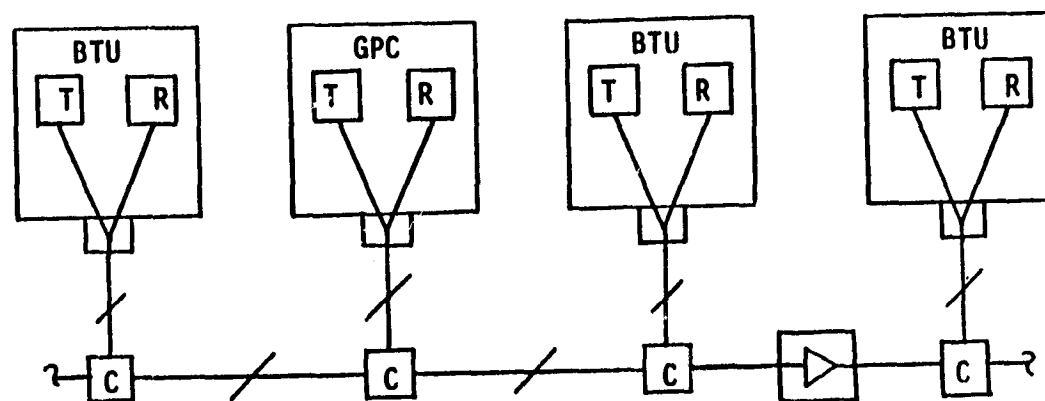






COMMAND SYNC



DATA SYNC

FIGURE A-4A LINEAR OPTICAL DATA BUS CONFIGURATION



 OPTICAL TRANSMITTER  
 OPTICAL RECEIVER  
 OPTICAL "T" COUPLER  
 OPTICAL REPEATER


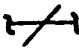
 BTU/GPC COUPLER  
 OPTICAL CONNECTOR  
 GPC GENERAL PURPOSE COMPUTER (5)  
 BTU BUS TERMINAL UNIT (15 MAX)

FIGURE A-4B RADIAL OPTICAL DATA BUS CONFIGURATION

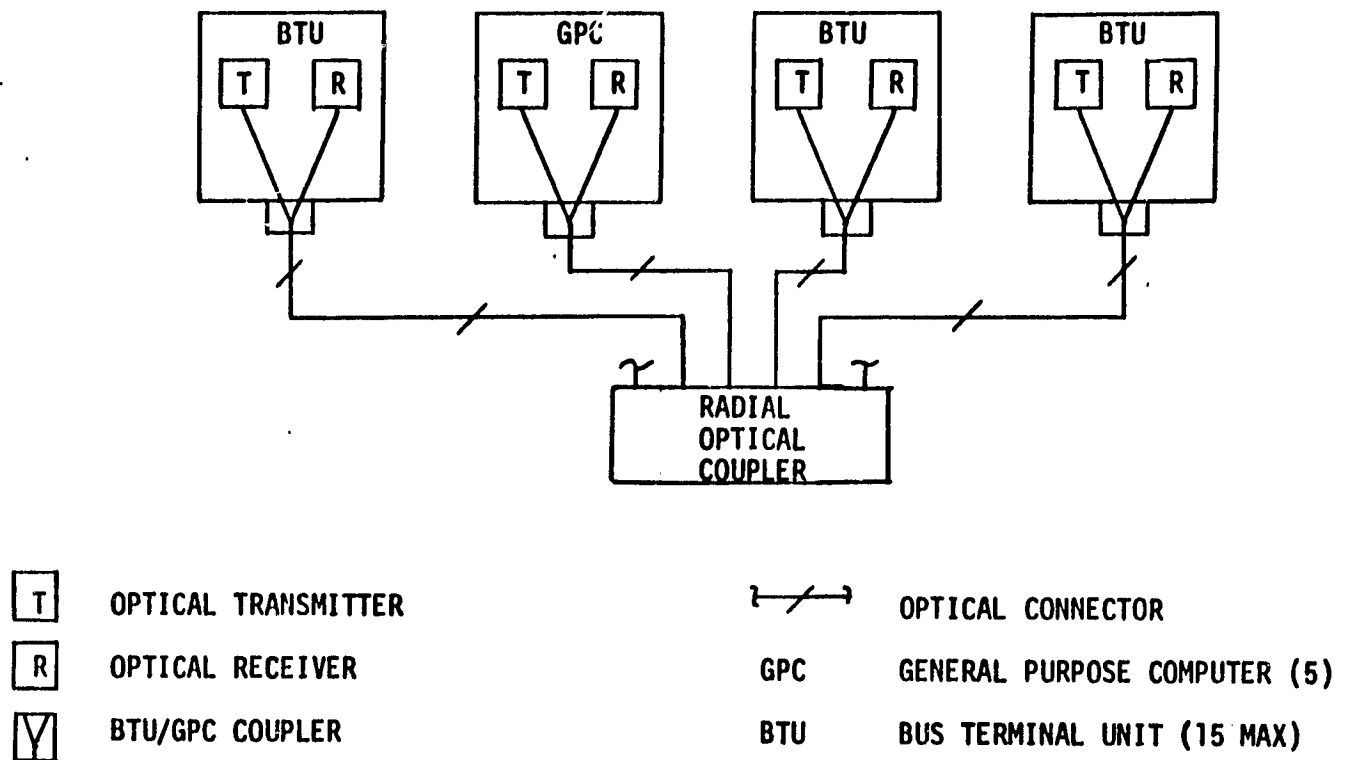


FIGURE A-5 "T" COUPLER OUTLINE

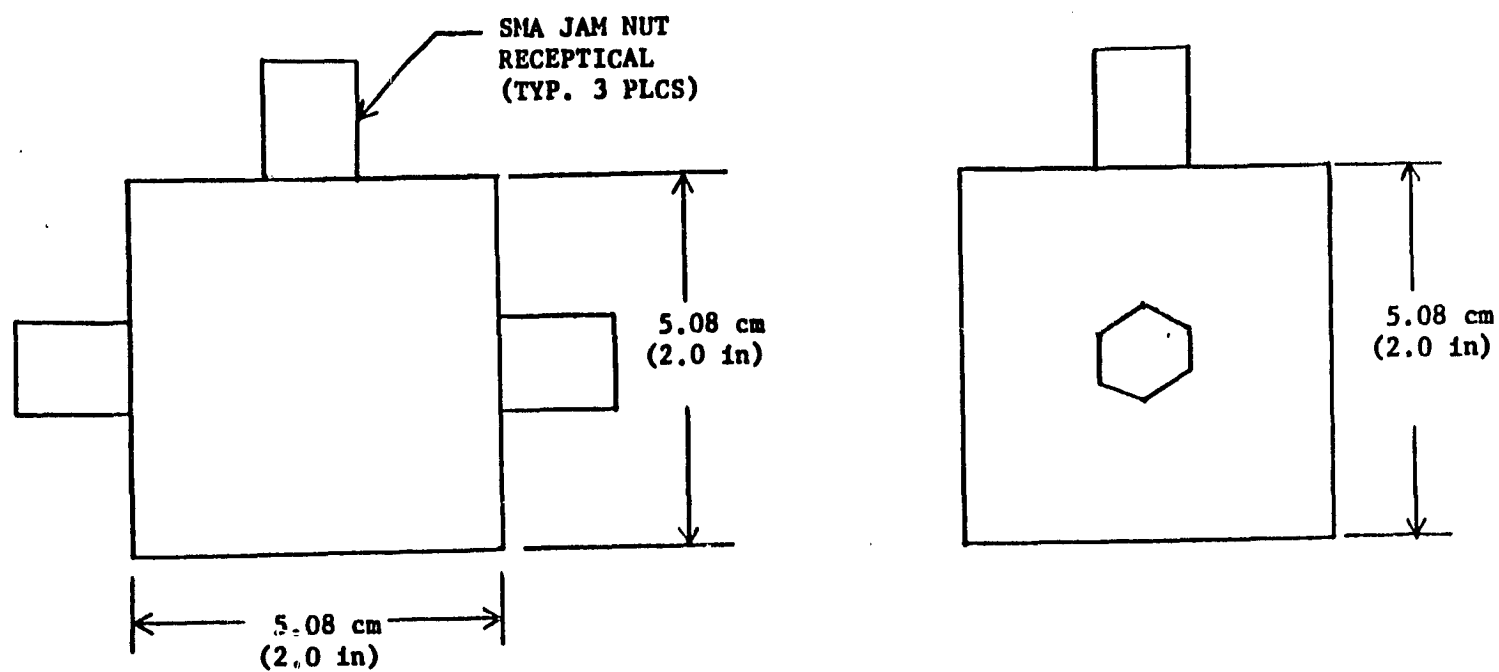


FIGURE A-6 ILLUSTRATION OF POWER SPLITTING FACTOR

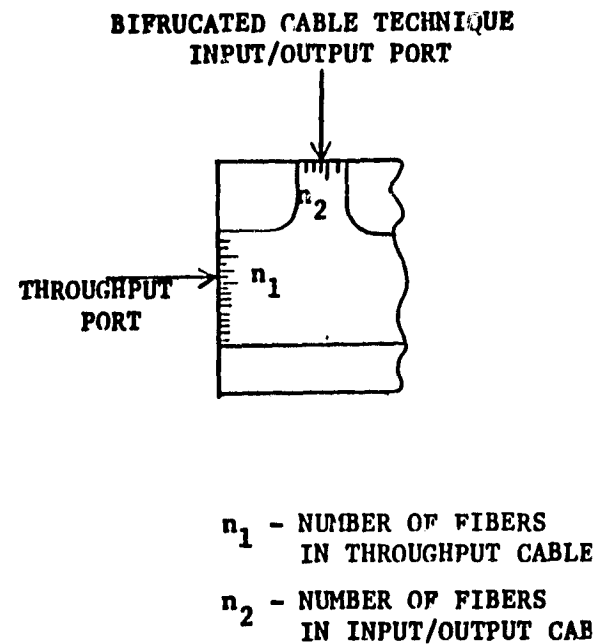
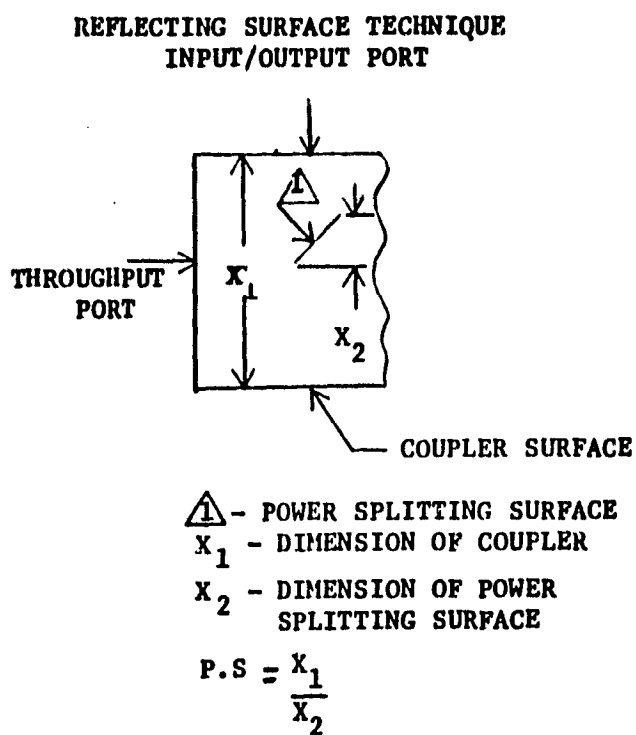


FIGURE A-7 RADIAL DATA BUS COUPLER

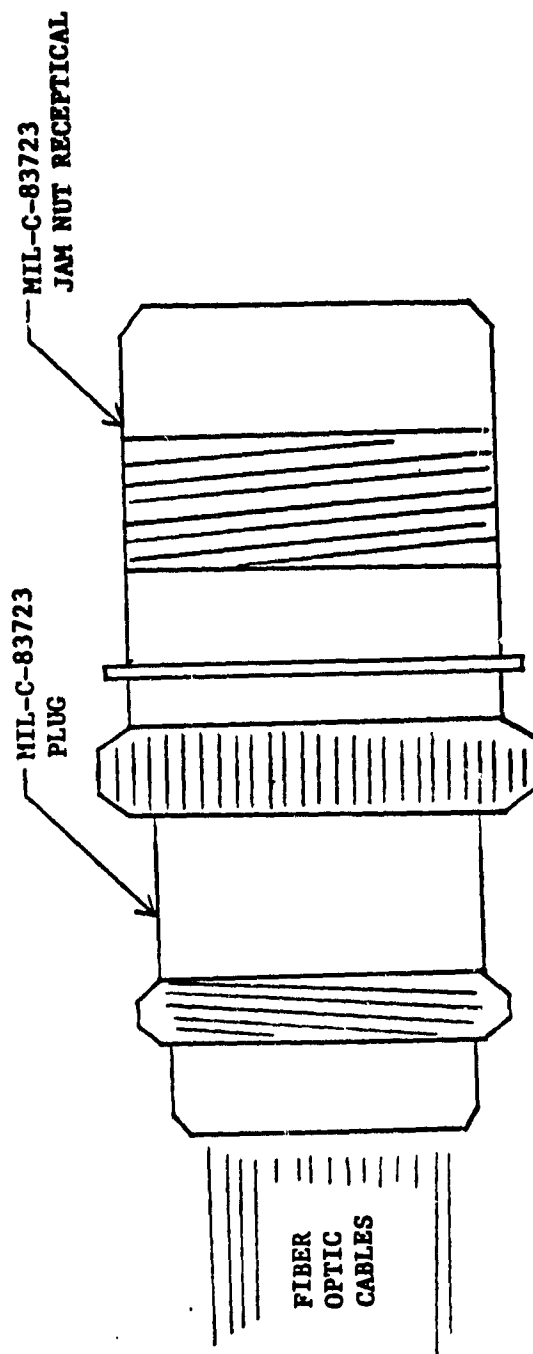




FIGURE A-8 GPC/BTU COUPLER

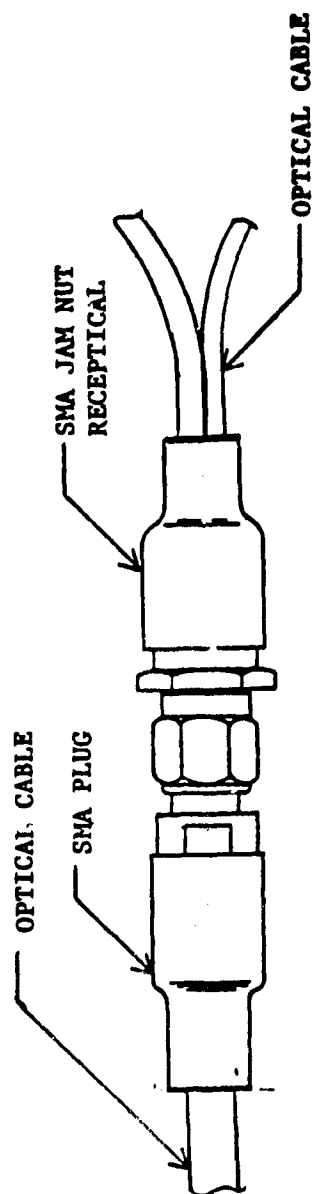
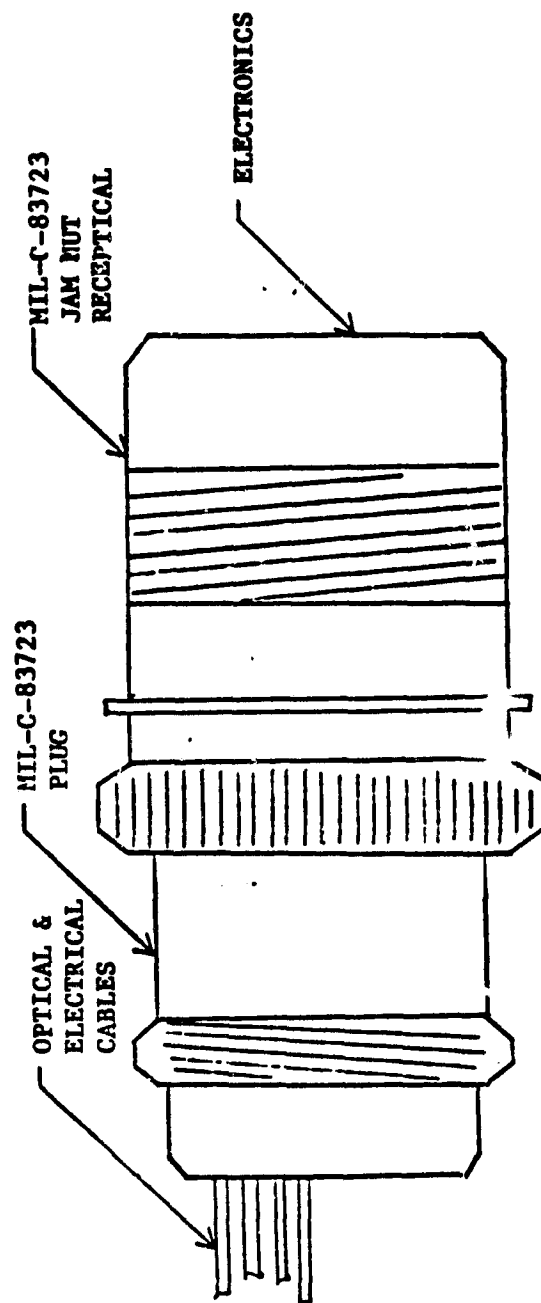


FIGURE A-9 OPTICAL REPEATER CONFIGURATION



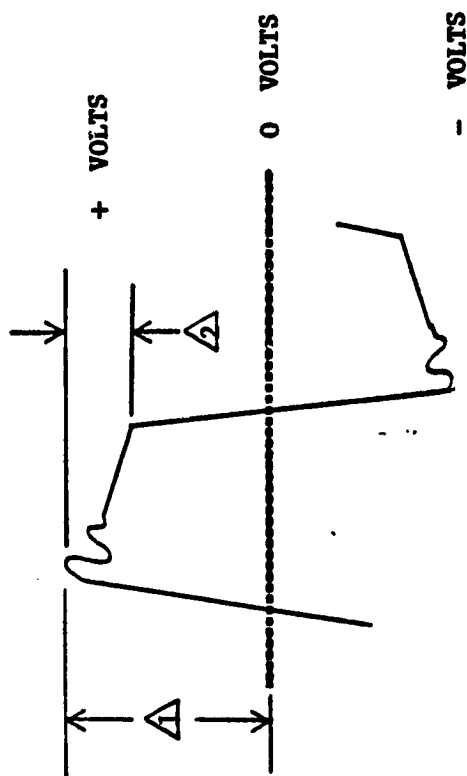
# OPTICAL DIGITAL TECHNIQUES

REPORT MDC E2052  
FEBRUARY 1979

FIGURE A-10 TRANSMITTER OUTLINE

TO BE SPECIFIED

FIGURE A-10A TRANSMITTER INPUT WAVEFORM



- NOTES: 1 12 to 15 VOLTS  
2 OVERSHOOT, RINGING, AND DROOP LESS THAN 0.75 VOLTS  
3 DUTY CYCLE 50 ± 5%

FIGURE A-11 RECEIVER OUTLINE

TO BE SPECIFIED

FIGURE A-12 CONDUCTED NARROWBAND EMISSION LIMIT

30 Hz TO 20 KHz

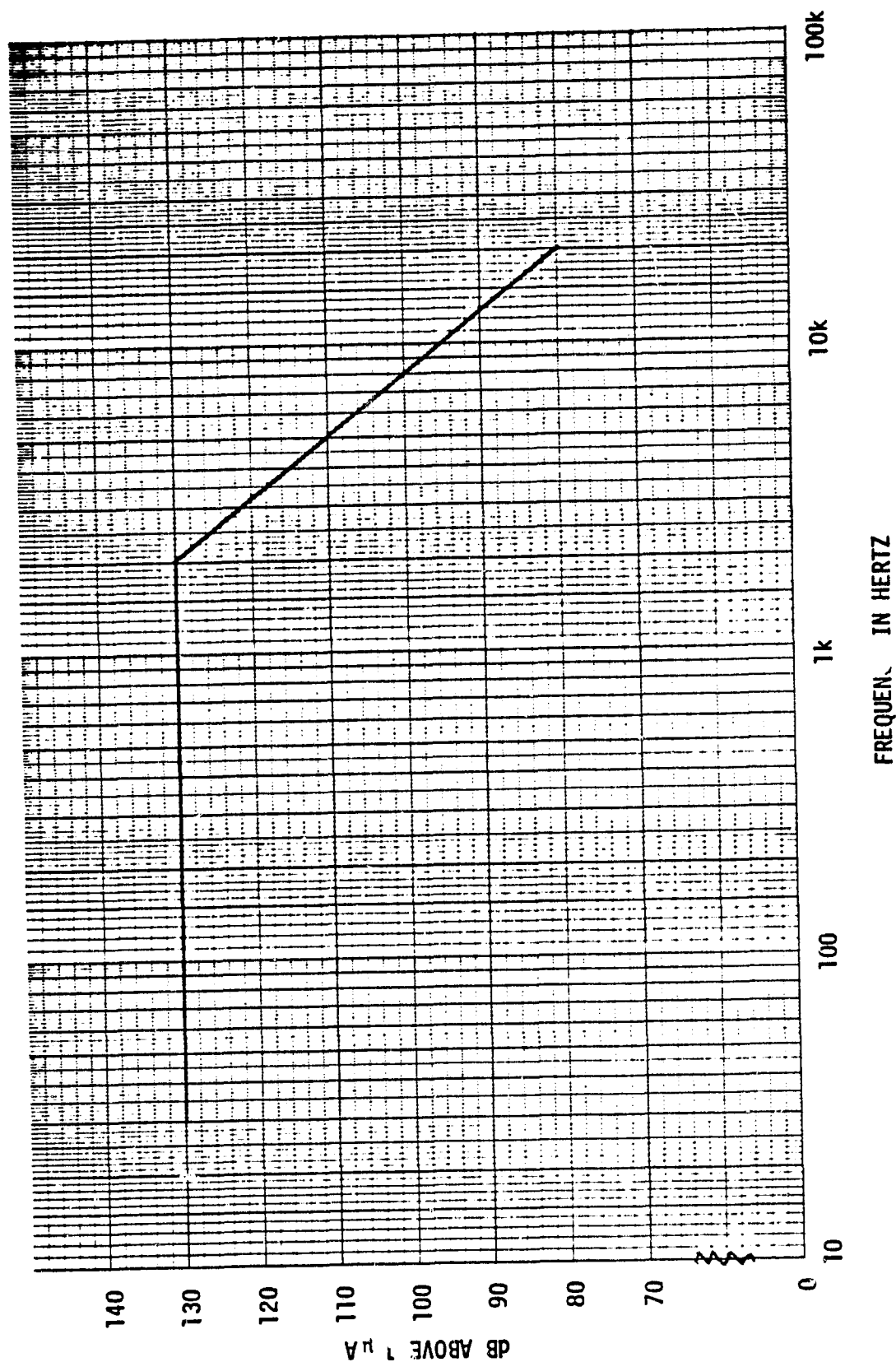


FIGURE A-13 CONDUCTED NARROWBAND EMISSION LIMIT

20 KHz to 50 MHz

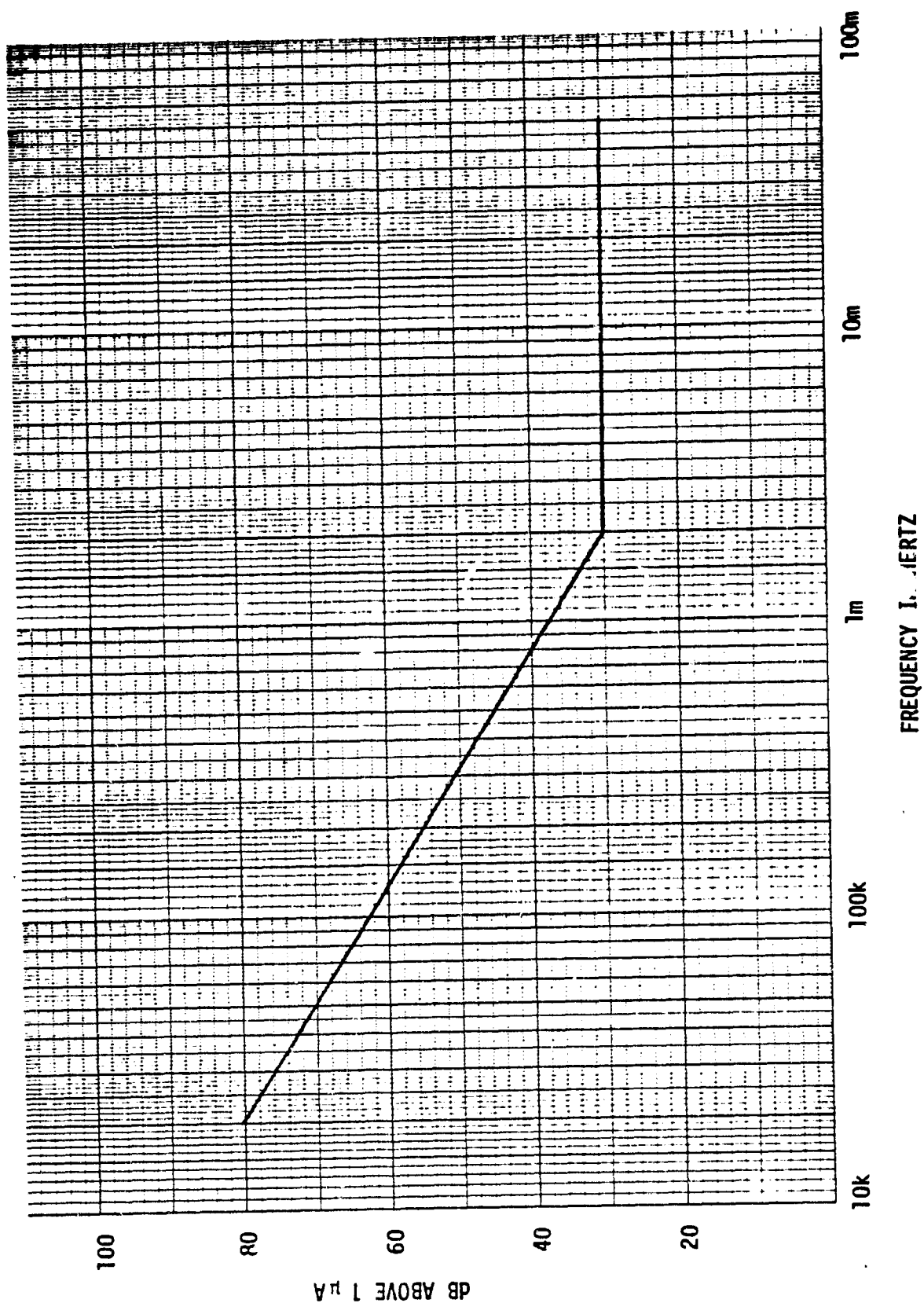


FIGURE A-14 CONDUCTED SUSCEPTIBILITY LIMIT

60 Hz to 50 KHz

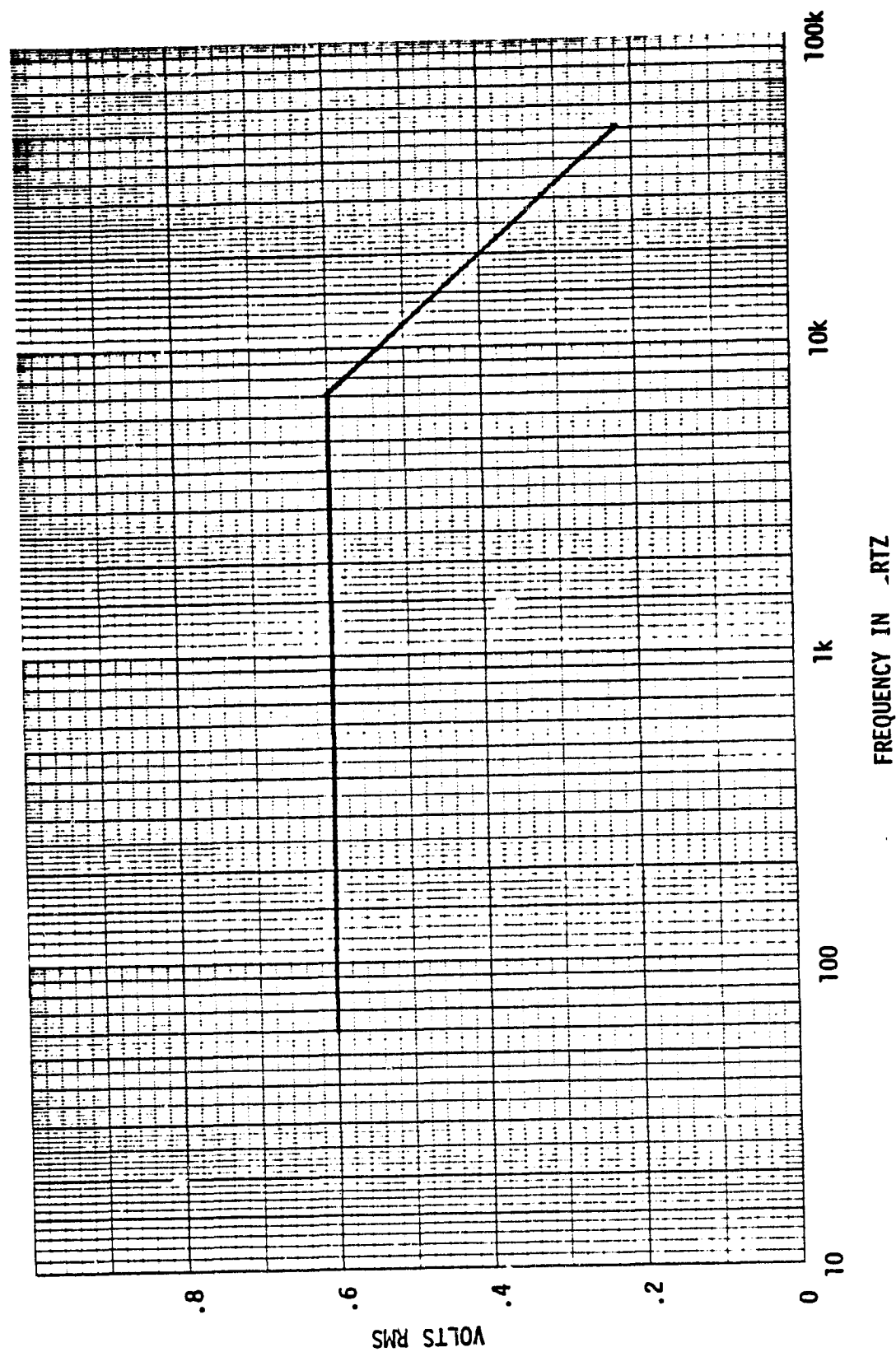
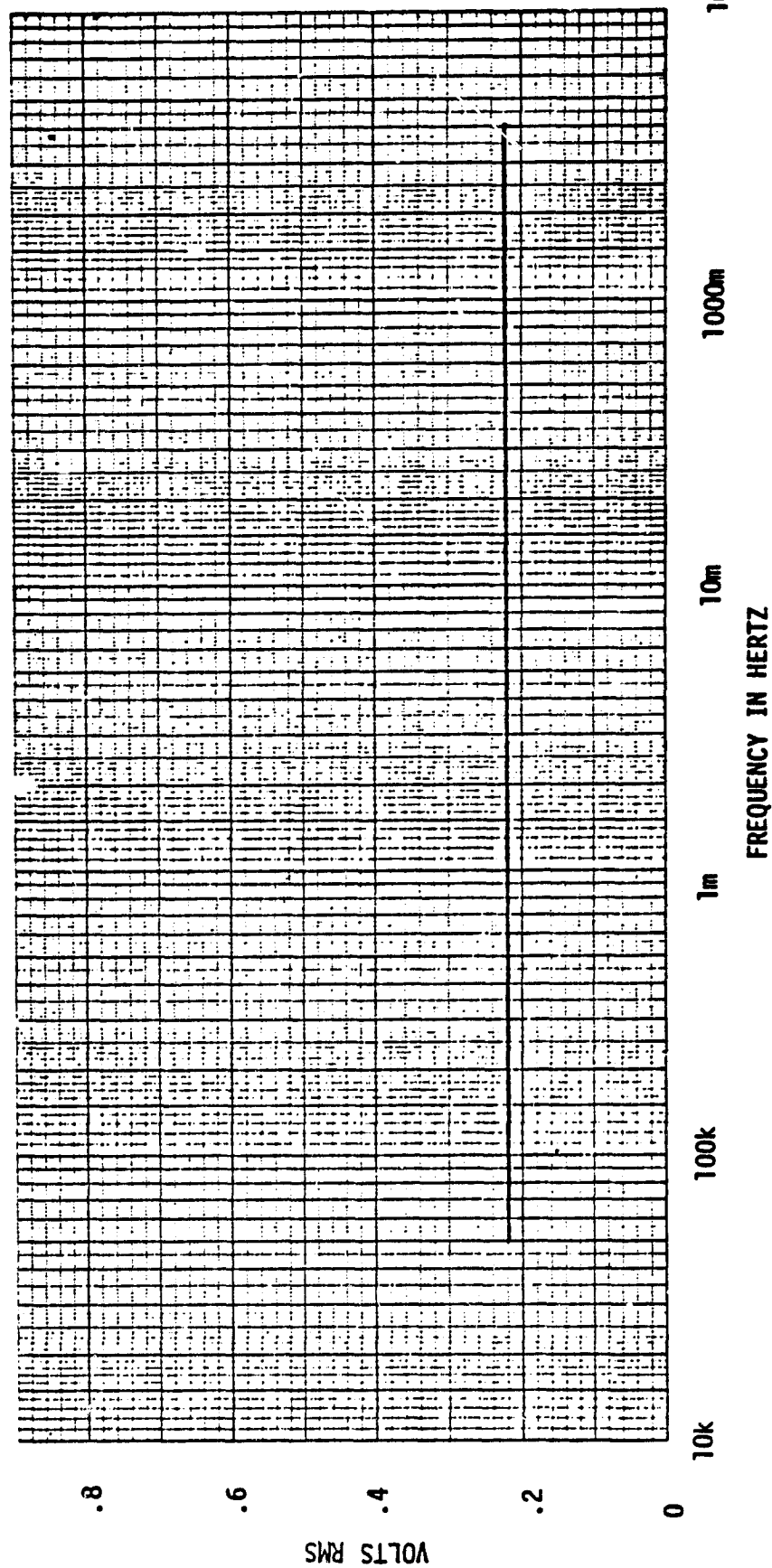




FIGURE A-15 CONDUCTED SUSCEPTIBILITY LIMIT  
50 KHz to 400 MHz



A28

FIGURE A-16 TRANSIENT SUSCEPTIBILITY WAVEFORM

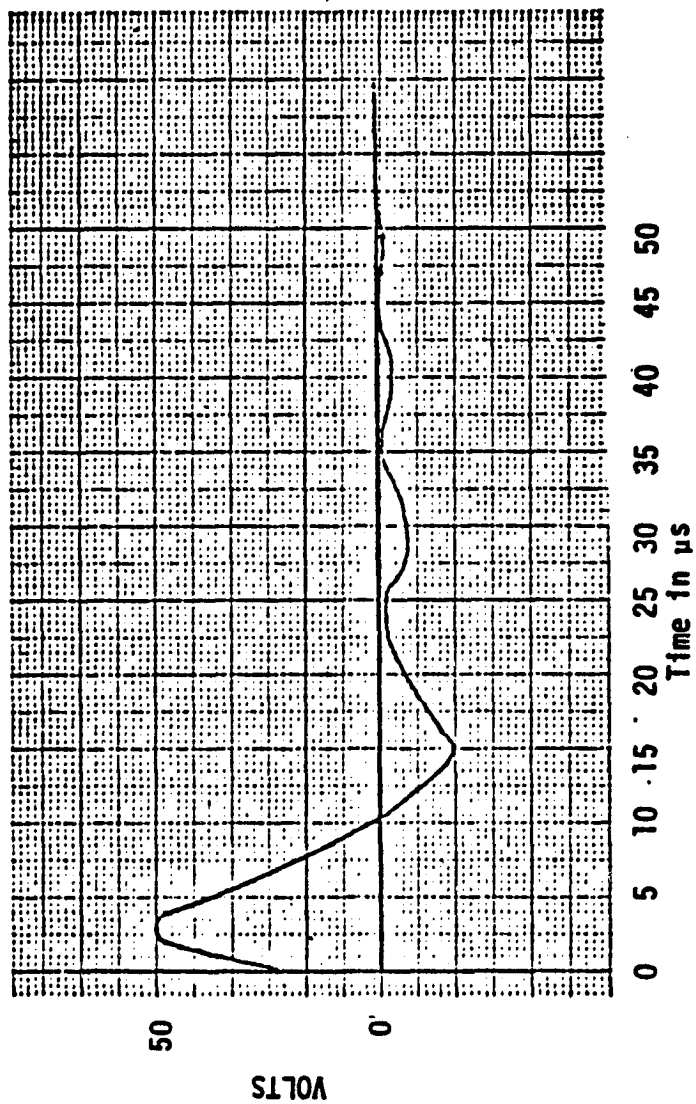


FIGURE A-17 RADIATED NARROWBAND EMISSION LIMIT

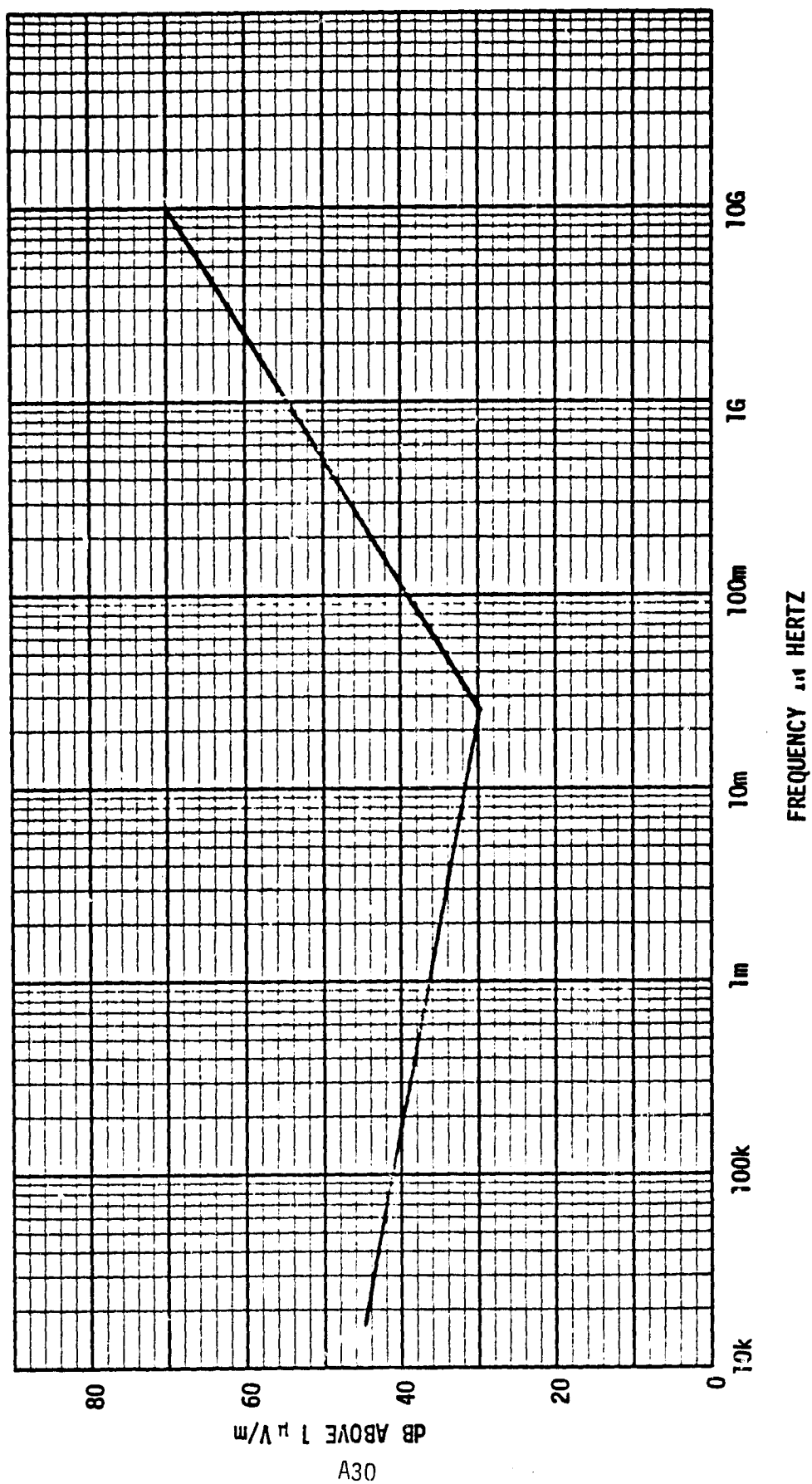


FIGURE A-18 RADIATED BROADBAND EMISSION LIMIT

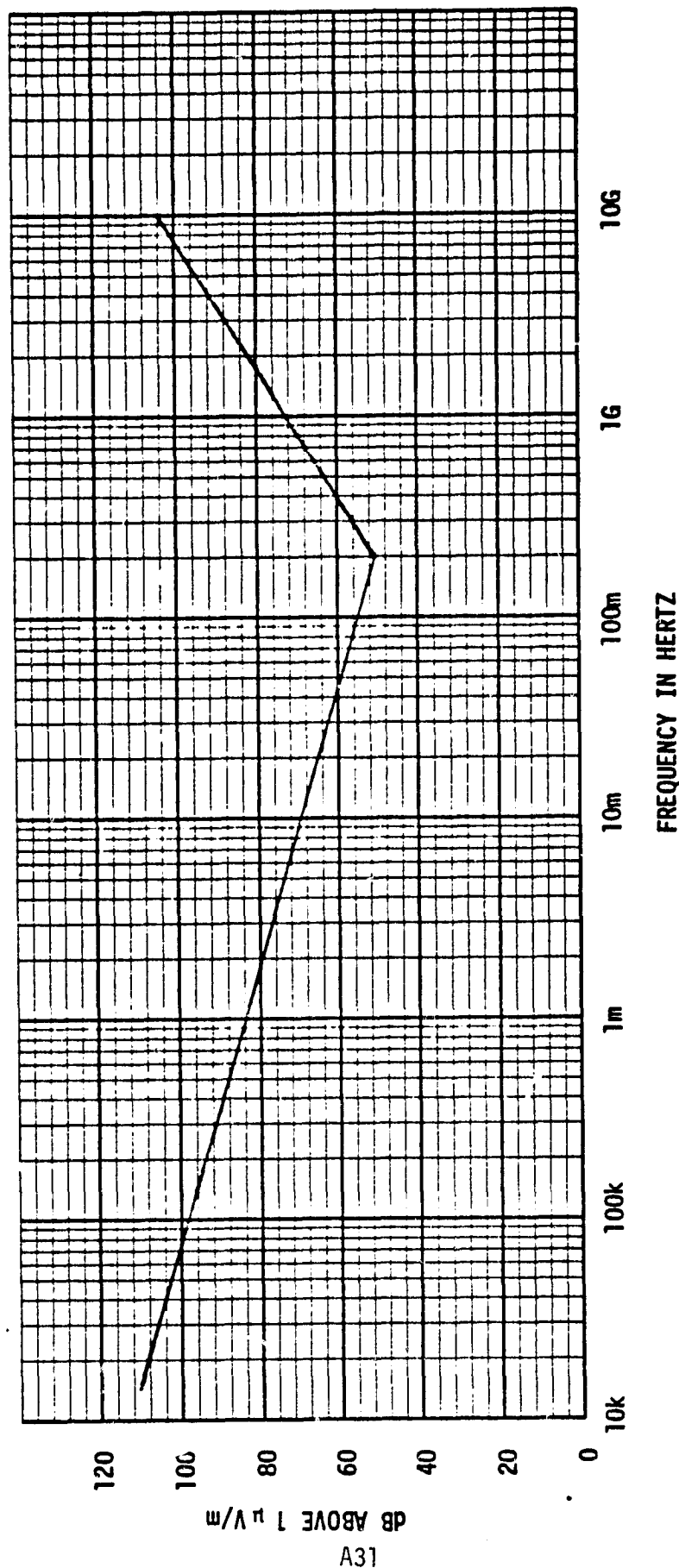
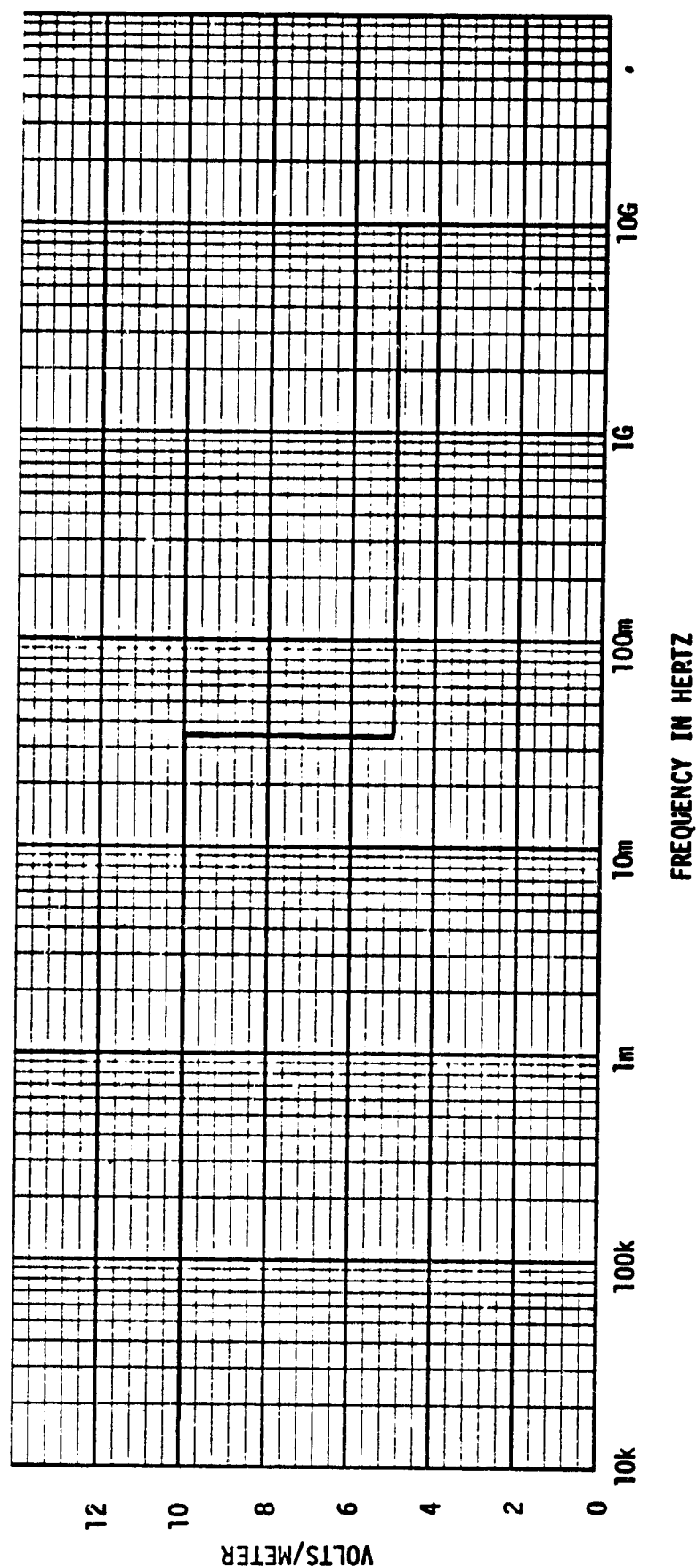


FIGURE A-19 RADIATED SUSCEPTIBILITY LIMIT

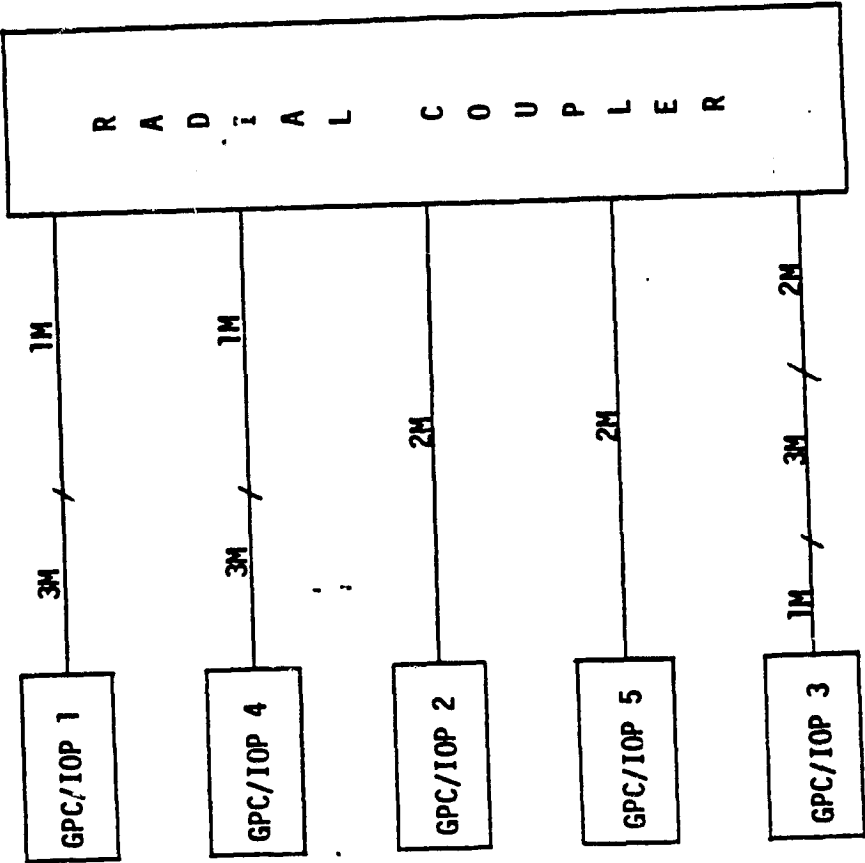


APPENDIX BBUS LOSSES

The Requirements Definition Document contains a requirement that a signal of -45 dB, be identified as a logic "1". The level of -45 dBm was based upon data presented in "Optical Cable Communications Study", AD-A016 846 and the noise equivalent power of available optical receivers. The minimum receiver power necessary to obtain a bit error rate of  $10^{-8}$  for a  $1 \times 10^6$  bits per second data rate and a signal to noise ratio of 5.75 to 1 was calculated using data from a second source. Using equations contained in AFAL-TR-75-45, "Optoelectronic Aspects of Avionics Systems II", the minimum receiver power for the above data rate, bit error rate, and signal to noise ratio was calculated to be -48.8 dBm which compares very closely with the -45 dBm value obtained from our original source. Dr. Biard of Spectronics, Inc. has informed us that he has demonstrated a bit-error-rate of  $10^{-8}$  or better at a receiver optical power level of -45 dBm for a  $10 \times 10^6$  bit rate. In Dr. Biard's opinion, -50 dBm should be enough power to achieve a  $10^{-8}$  bit-error-rate for a 1 megabit data system.

System losses for 17 Shuttle data buses in an optical radial data bus configuration have been computed. The system losses have been computed using the requirements contained in the Requirements Definition Document. For the analysis, the bus losses were calculated for the normal GPC/IOP in control of the bus and for the longest path between any computer and BTU. The results of this analysis are presented below.

BUS IC-1



# OPTICAL DIGITAL TECHNIQUES

REPORT MDC E2052  
FEBRUARY 1979

## BUS IC1

GPC/IOP 1 IN CONTROL

COUPLER LOCATED IN BAY 2

SIGNAL LEVEL AT RECEIVER IN GPC/IOP 4

SIGNAL LEVEL AT RECEIVER IN GPC/IOP 2

SIGNAL LEVEL AT RECEIVER IN GPC/IOP 5

SIGNAL LEVEL AT RECEIVER IN GPC/IOP 3

-25.90 dBm

-23.20 dBm

-23.20 dBm

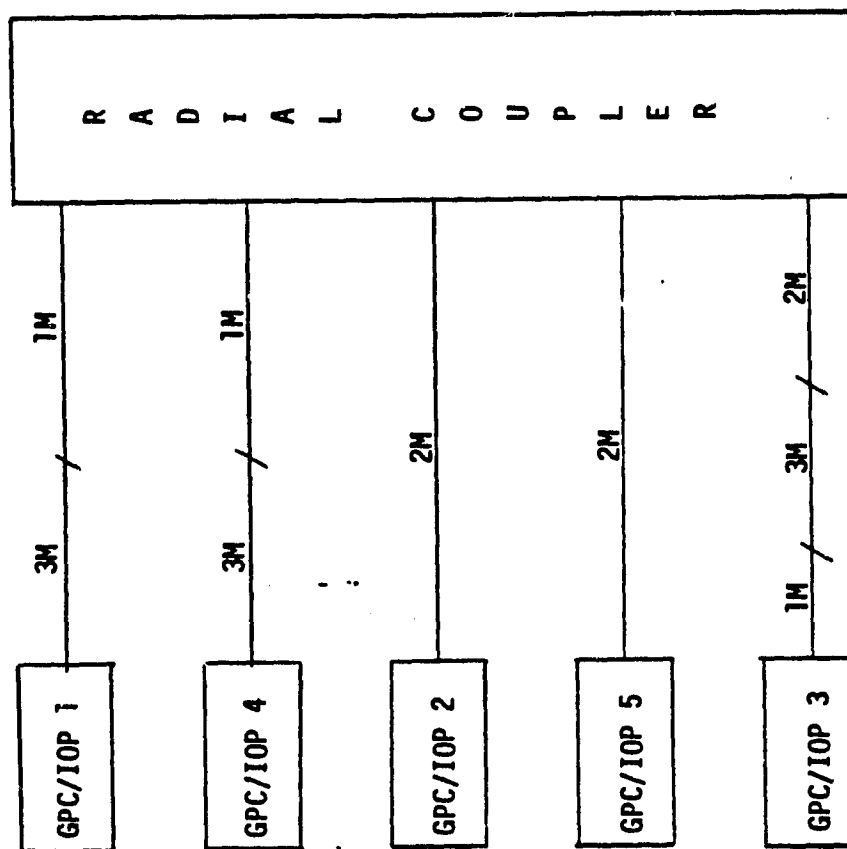
-28.60 dBm

LONGEST PATH GPC/IOP 1 TO GPC/IOP 3

SIGNAL AT GPC/IOP 3 FROM GPC/IOP 1 -28.60 dBm



BUS IC-2



# OPTICAL DIGITAL TECHNIQUES

REPORT MDC E2052  
FEBRUARY 1979

## BUS IC2

GPC/IOP 2 IN CONTROL

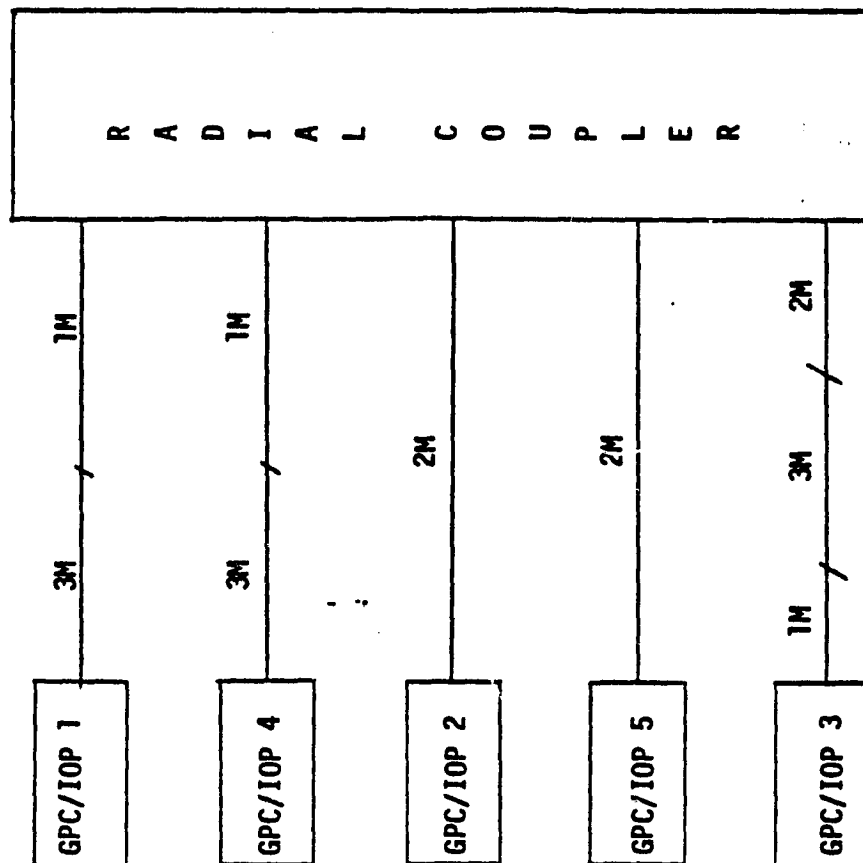
COUPLER LOCATED IN BAY 2

SIGNAL LEVEL AT RECEIVER IN GPC/IOP 1	-23.20 dBm
SIGNAL LEVEL AT RECEIVER IN GPC/IOP 4	-23.20 dBm
SIGNAL LEVEL AT RECEIVER IN GPC/IOP 5	-20.50 dBm
SIGNAL LEVEL AT RECEIVER IN GPC/IOP 3	-25.90 dBm

LONGEST PATH GPC/IOP 1 TO GPC/IOP 3

SIGNAL AT GPC/IOP 3 FROM GPC/IOP 1 -28.60 dBm

BUS IC-3



## BUS IC3

GPC/IOP 3 IN CONTROL

COUPLER LOCATED IN BAY 2

SIGNAL LEVEL AT RECEIVER IN GPC/IOP 1

-28.60 dBm

SIGNAL LEVEL AT RECEIVER IN GPC/IOP 4

-28.60 dBm

SIGNAL LEVEL AT RECEIVER IN GPC/IOP 2

-25.90 dBm

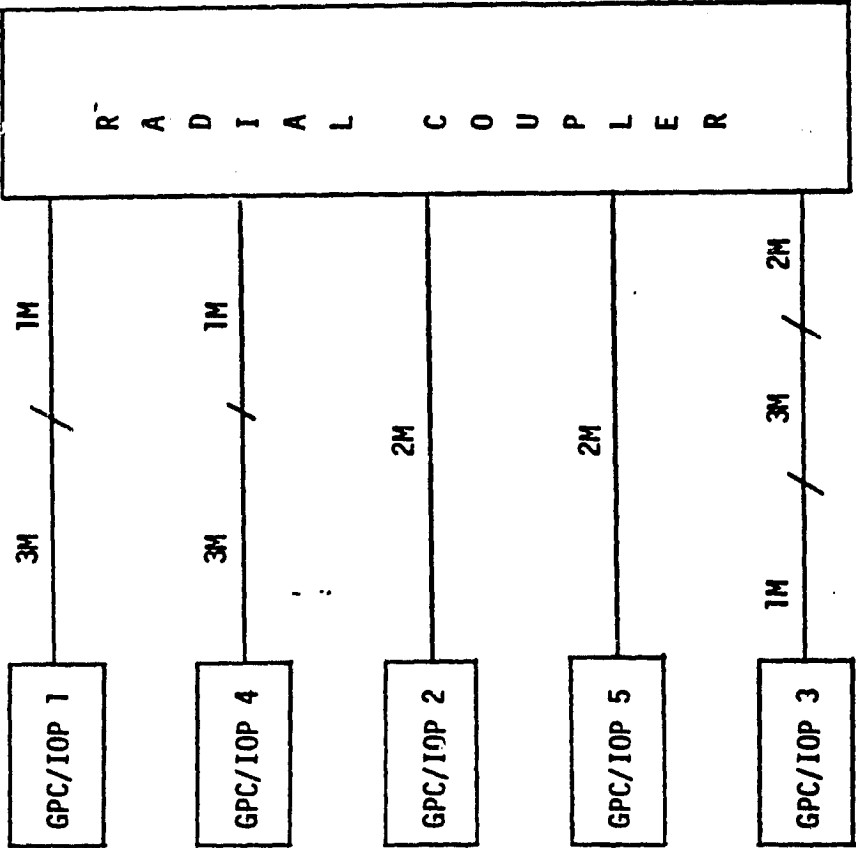
SIGNAL LEVEL AT RECEIVER IN GPC/IOP 5

-25.90 dBm

LONGEST PATH GPC/IOP 1 TO GPC/IOP 3

SIGNAL AT GPC/IOP 3 FROM GPC/IOP 1 -28.60 dBm

BUS IC-4



# OPTICAL DIGITAL TECHNIQUES

REPORT MDC E2052  
FEBRUARY 1979

## BUS IC4

GPC/IOP 4 IN CONTROL

COUPLER LOCATED IN BAY 2

SIGNAL LEVEL AT RECEIVER IN GPC/IOP 1

-25.90 dBm

SIGNAL LEVEL AT RECEIVER IN GPC/IOP 2

-23.20 dBm

SIGNAL LEVEL AT RECEIVER IN GPC/IOP 5

-23.20 dBm

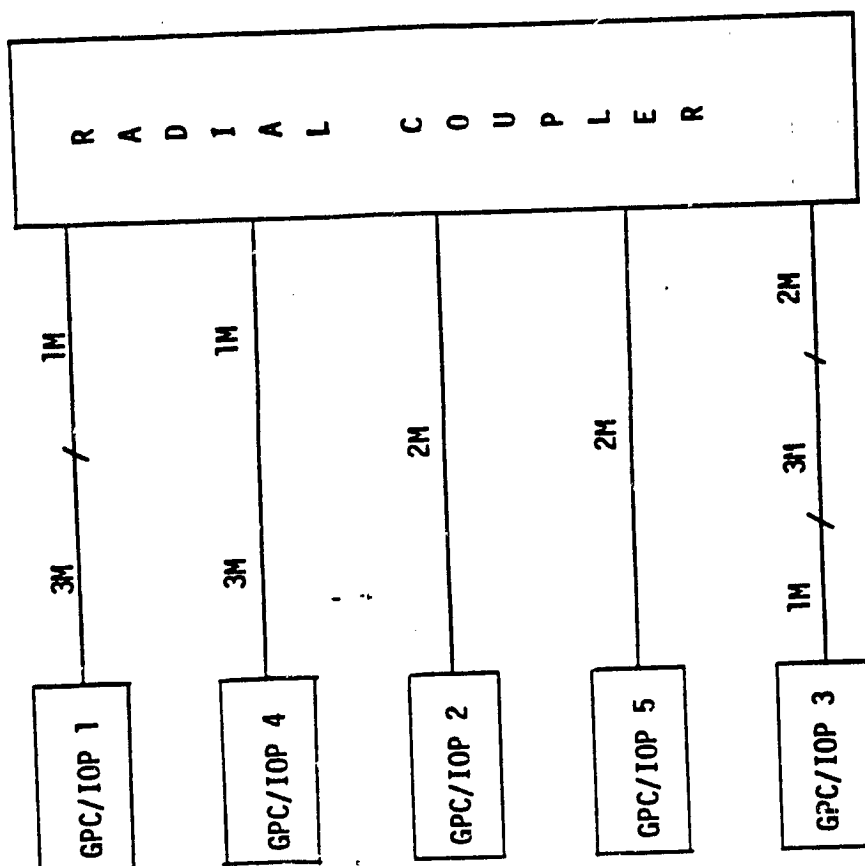
SIGNAL LEVEL AT RECEIVER IN GPC/IOP 3

-28.60 dBm

LONGEST PATH GPC/IOP 1 TO GPC/IOP 3

SIGNAL AT GPC/IOP 3 FROM GPC/IOP 1 -28.60 dBm

BUS IC-5



# OPTICAL DIGITAL TECHNIQUES

REPORT MDC E2052  
FEBRUARY 1979

## BUS IC5

GPC/IOP 5 IN CONTROL

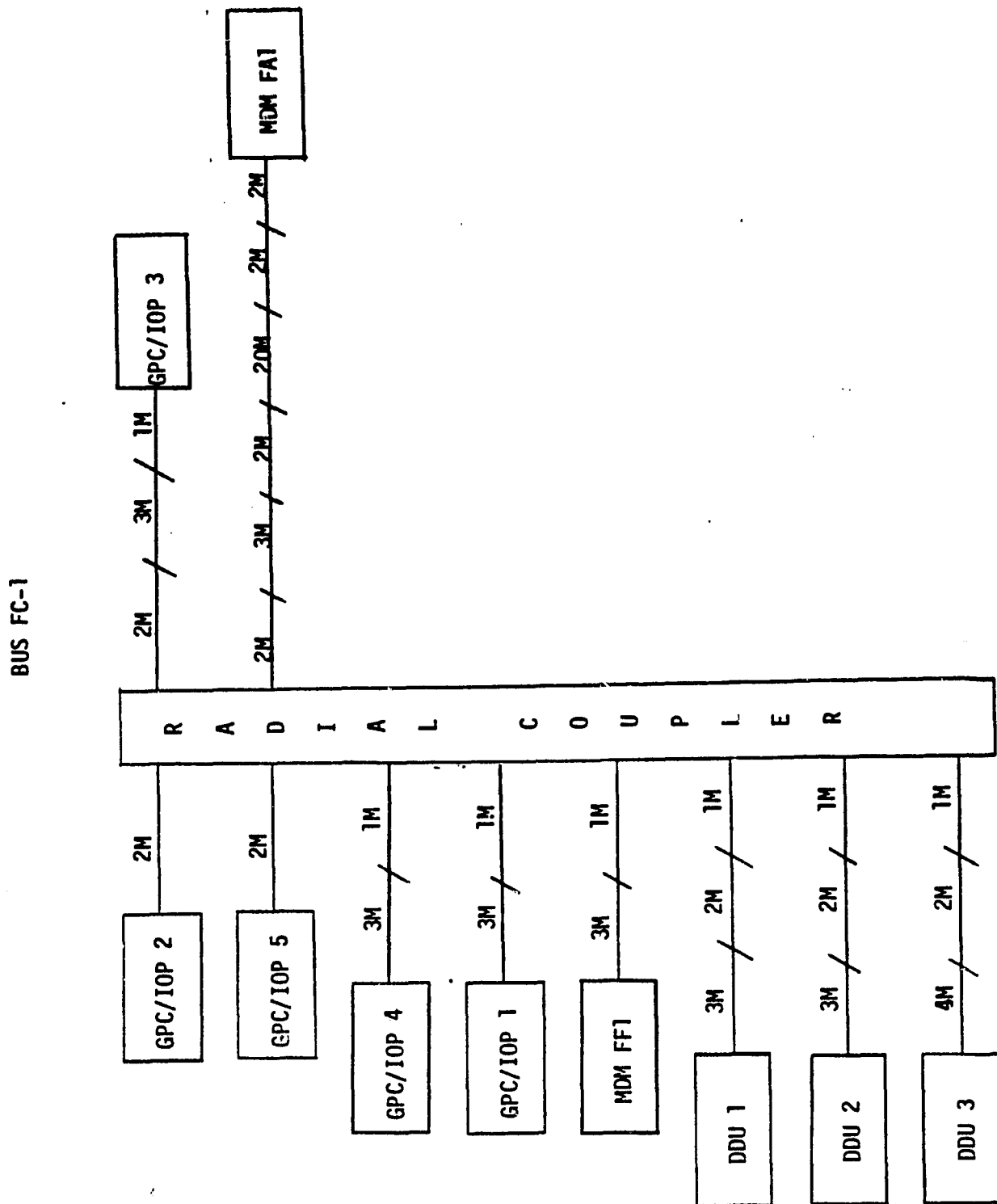
COUPLER LOCATED IN BAY 2

SIGNAL LEVEL AT RECEIVER IN GPC/IOP 1	-23.20 dBm
SIGNAL LEVEL AT RECEIVER IN GPC/IOP 4	-23.20 dBm
SIGNAL LEVEL AT RECEIVER IN GPC/IOP 2	-20.50 dBm
SIGNAL LEVEL AT RECEIVER IN GPC/IOP 3	-25.90 dBm

LONGEST PATH GPC/IOP 1 TO GPC/IOP 3

SIGNAL AT GPC/IOP 3 FROM GPC/IOP 1 -28.60 dBm

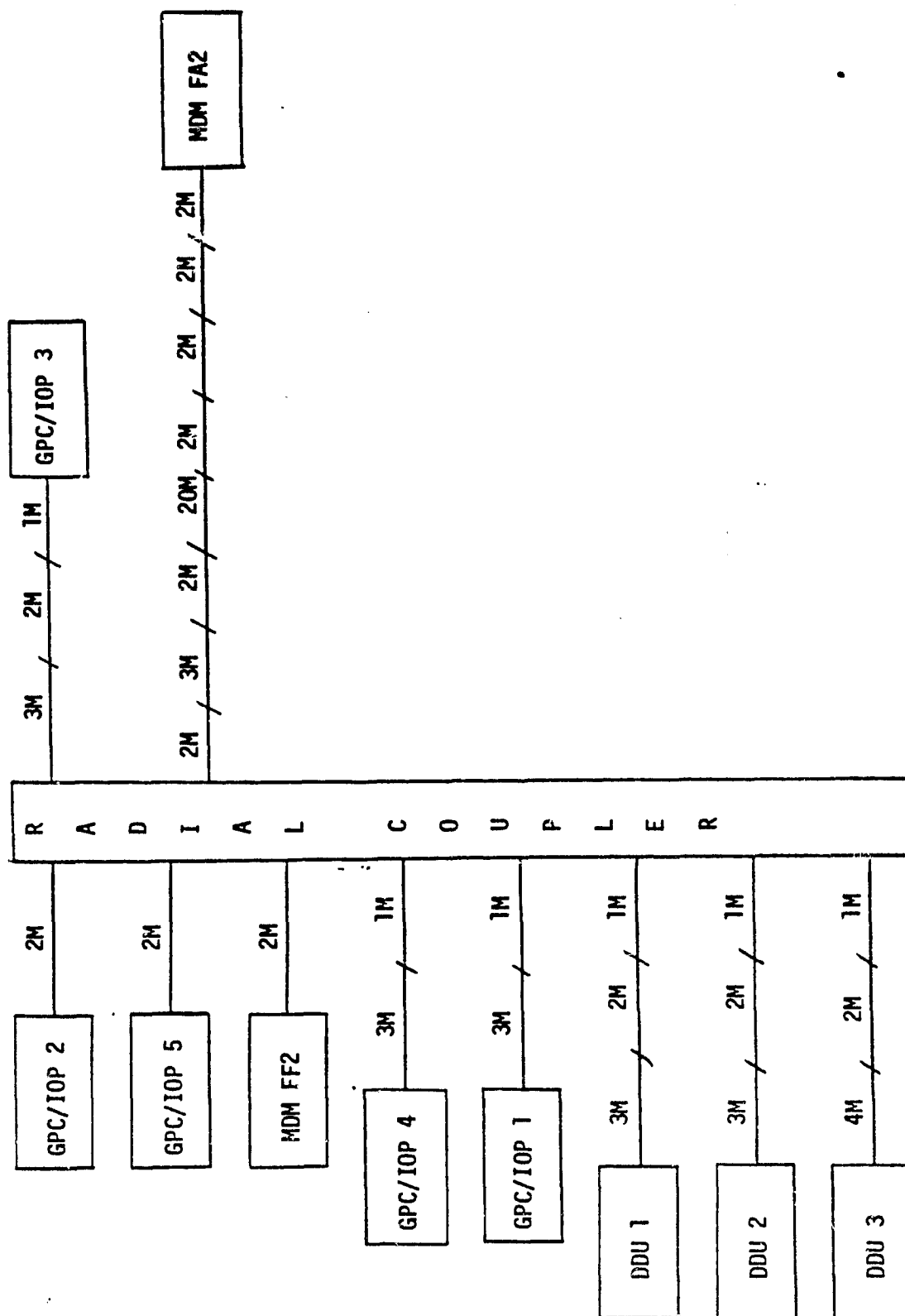




## BUS FC1

GPC/IOP 1 IN CONTROL	
COUPLER LOCATED IN BAY 2	
SIGNAL LEVEL AT RECEIVER IN GPC/IOP 2	-26.20 dBm
SIGNAL LEVEL AT RECEIVER IN GPC/IOP 5	-26.20 dBm
SIGNAL LEVEL AT RECEIVER IN GPC/IOP 4	-28.90 dBm
SIGNAL LEVEL AT RECEIVER IN MDM FF1	-28.90 dBm
SIGNAL LEVEL AT RECEIVER IN DDU 1	-31.60 dBm
SIGNAL LEVEL AT RECEIVER IN DDU 2	-31.60 dBm
SIGNAL LEVEL AT RECEIVER IN DDU 3	-31.95 dBm
SIGNAL LEVEL AT RECEIVER IN GPC/IOP 3	-31.60 dBm
SIGNAL LEVEL AT RECEIVER IN MDM FA1	-46.35 dBm
LONGEST PATH GPC/IOP 3 TO MDM FA1	
SIGNAL AT MDM FA1 FROM GPC/IOP 3	-49.05 dBm

BUS FC-2



## BUS FC2

## GPC/IOP 2 IN CONTROL

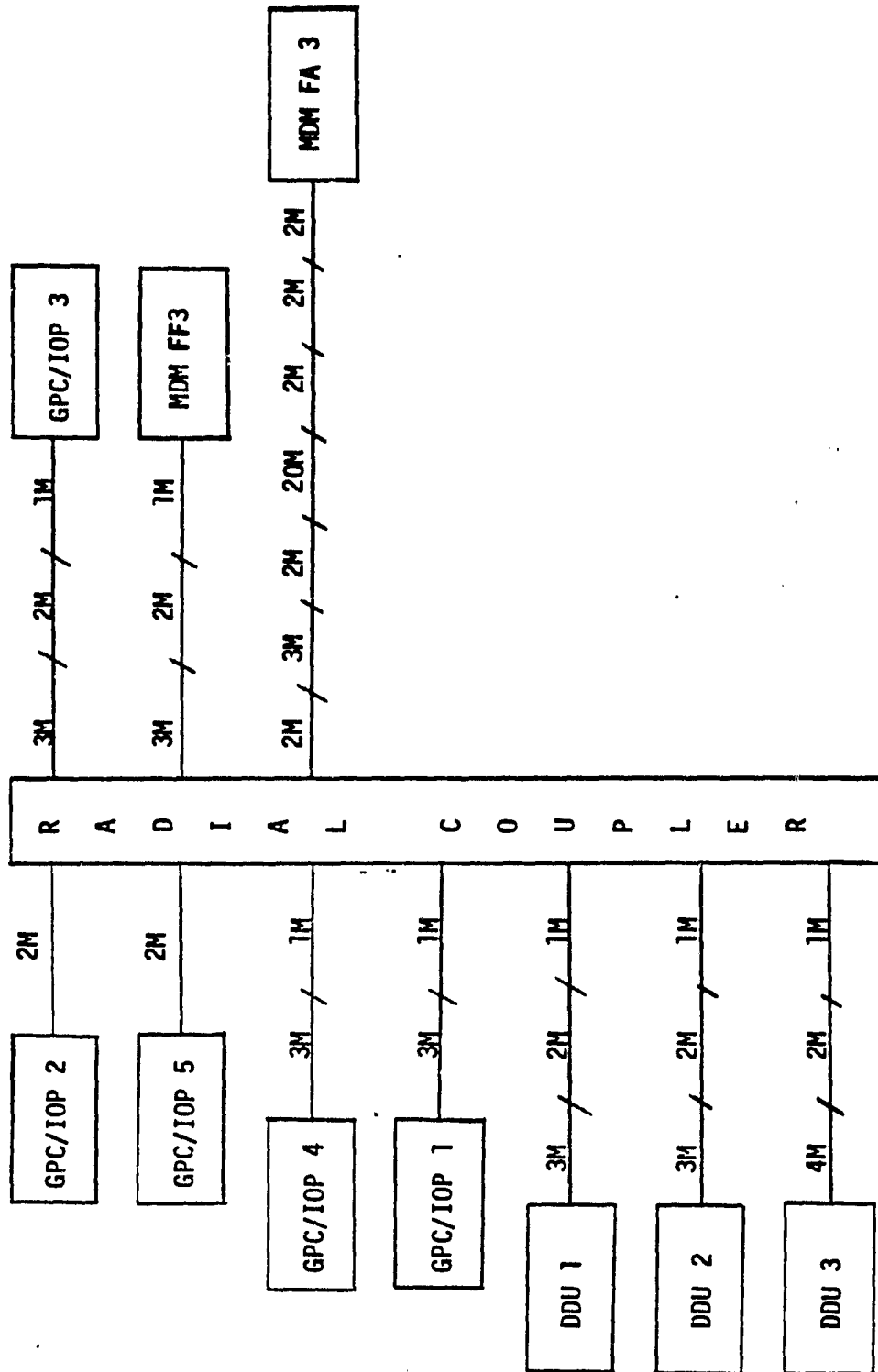
## COUPLER LOCATED IN BAY 2

SIGNAL LEVEL AT RECEIVER IN GPC/IOP 5	-23.50 dBm
SIGNAL LEVEL AT RECEIVER IN MDM FF2	-23.50 dBm
SIGNAL LEVEL AT RECEIVER IN GPC/IOP 4	-26.20 dBm
SIGNAL LEVEL AT RECEIVER IN GPC/IOP 1	-26.20 dBm
SIGNAL LEVEL AT RECEIVER IN DDU 1	-28.90 dBm
SIGNAL LEVEL AT RECEIVER IN DDU 2	-28.90 dBm
SIGNAL LEVEL AT RECEIVER IN DDU 3	-29.95 dBm
SIGNAL LEVEL AT RECEIVER IN GPC/IOP 3	-28.90 dBm
SIGNAL LEVEL AT RECEIVER IN MDM FA2	-48.95 dBm

## LONGEST SIGNAL PATH GPC/IOP 3 TO MDM FA2

SIGNAL AT MDM FA2 FROM GPC/IOP 3	-54.35 dBm
----------------------------------	------------

BUS FC-3



# OPTICAL DIGITAL TECHNIQUES

REPORT MDC E2052  
FEBRUARY 1979

## BUS FC3

GPC/IOP 3 IN CONTROL

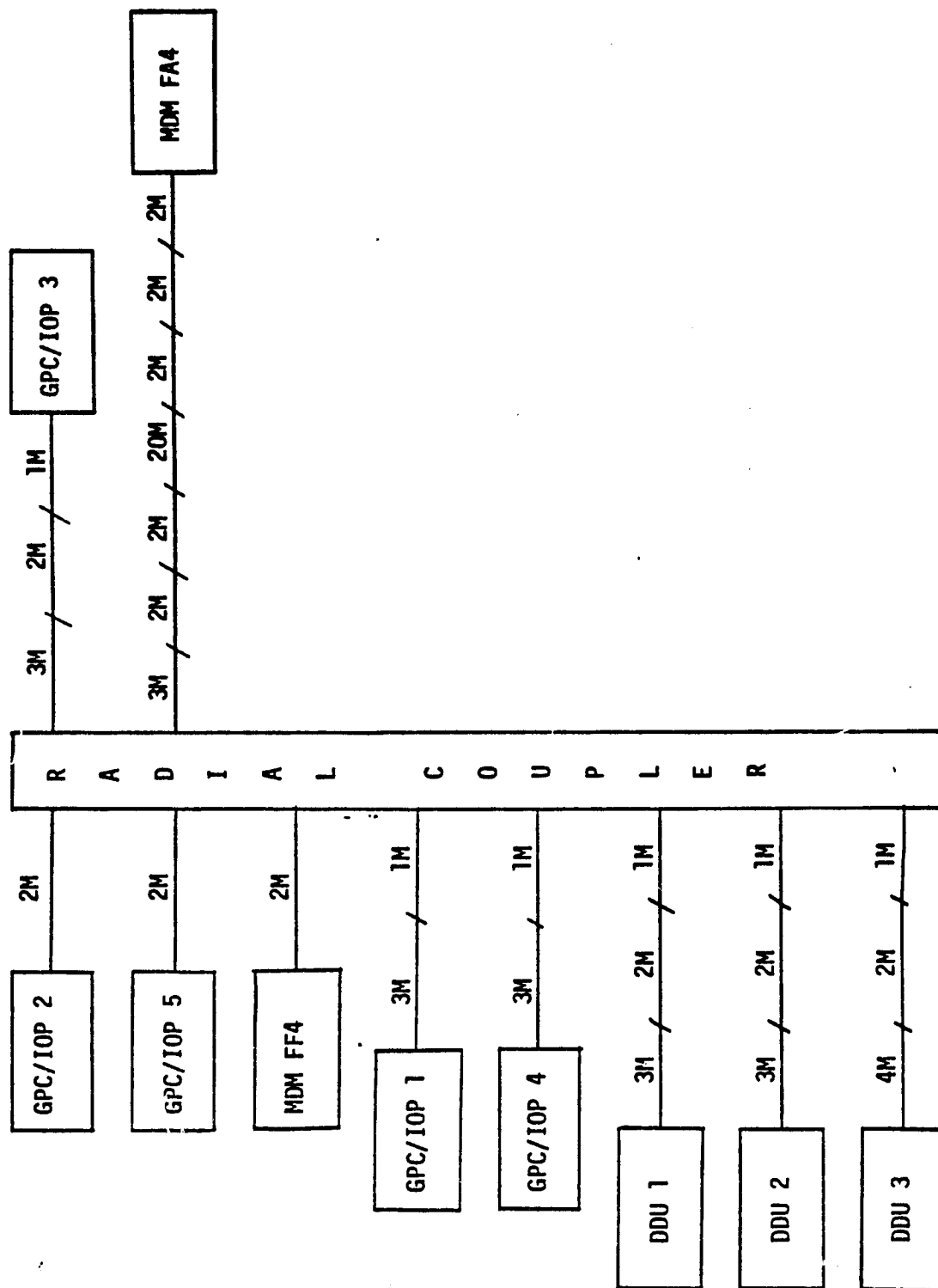
COUPLER IN BAY 2

SIGNAL LEVEL AT RECEIVER IN GPC/IOP 2	-28.90 dBm
SIGNAL LEVEL AT RECEIVER IN GPC/IOP 5	-28.90 dBm
SIGNAL LEVEL AT RECEIVER IN GPC/IOP 4	-31.60 dBm
SIGNAL LEVEL AT RECEIVER IN GPC/IOP 1	-31.60 dBm
SIGNAL LEVEL AT RECEIVER IN DDU 1	-34.30 dBm
SIGNAL LEVEL AT RECEIVER IN DDU 2	-34.30 dBm
SIGNAL LEVEL AT RECEIVER IN DDU 3	-34.15 dBm
SIGNAL LEVEL AT RECEIVER IN MDM FF3	-34.30 dBm
SIGNAL LEVEL AT RECEIVER IN MDM FA3	-51.75 dBm

LONGEST PATH GPC/IOP 3 TO MDM FA3

SIGNAL AT MDM FA3 FROM GPC/IOP 3 -51.75 dBm

BUS FC-4



## BUS FC4

## GPC/IOP 4 IN CONTROL

## COUPLER LOCATED IN BAY 2

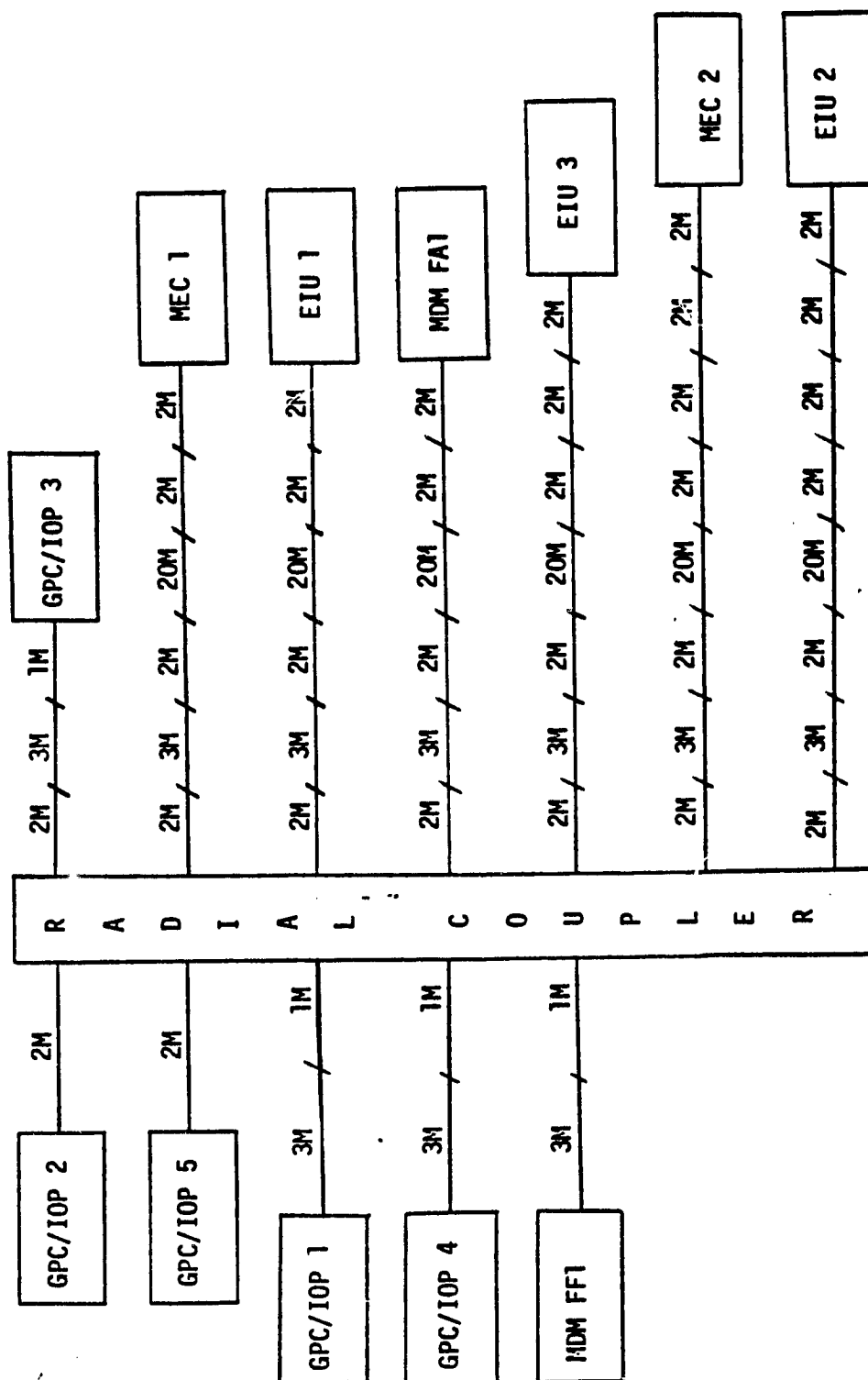
SIGNAL LEVEL AT RECEIVER IN GPC/IOP 2	-26.20 dBm
SIGNAL LEVEL AT RECEIVER IN GPC/IOP 5	-26.20 dBm
SIGNAL LEVEL AT RECEIVER IN MDM FF4	-26.20 dBm
SIGNAL LEVEL AT RECEIVER IN GPC/IOP 1	-28.90 dBm
SIGNAL LEVEL AT RECEIVER IN DDU 1	-31.60 dBm
SIGNAL LEVEL AT RECEIVER IN DDU 2	-31.60 dBm
SIGNAL LEVEL AT RECEIVER IN DDU 3	-31.95 dBm
SIGNAL LEVEL AT RECEIVER IN GPC/IOP 3	-31.60 dBm
SIGNAL LEVEL AT RECEIVER IN MDM FA4	-49.05 dBm

## LONGEST RUN GPC/IOP 3 TO MDM FA4

SIGNAL AT MDM FA4 FROM GPC/IOP 3	-51.75 dBm
----------------------------------	------------



BUS FC-5



## BUS FC5

GPC/IOP 1 IN CONTROL	
COUPLER LOCATED IN BAY 2	
SIGNAL LEVEL AT RECEIVER IN GPC/IOP 2	-27.00 dBm
SIGNAL LEVEL AT RECEIVER IN GPC/IOP 5	-27.00 dBm
SIGNAL LEVEL AT RECEIVER IN GPC/IOP 4	-29.70 dBm
SIGNAL LEVEL AT RECEIVER IN MDM/FF1	-29.70 dBm
SIGNAL LEVEL AT RECEIVER IN GPC/IOP 3	-32.40 dBm
SIGNAL LEVEL AT RECEIVER IN MEC 1	-47.15 dBm
SIGNAL LEVEL AT RECEIVER IN EIU 1	-47.15 dBm
SIGNAL LEVEL AT RECEIVER IN MDM FA1	-47.15 dBm
SIGNAL LEVEL AT RECEIVER IN EIU 3	-49.85 dBm
SIGNAL LEVEL AT RECEIVER IN MEC 2	-52.55 dBm
SIGNAL LEVEL AT RECEIVER IN EIU 2	-52.55 dBm

## BUS FC6

## GPC/IOP 2 IN CONTROL

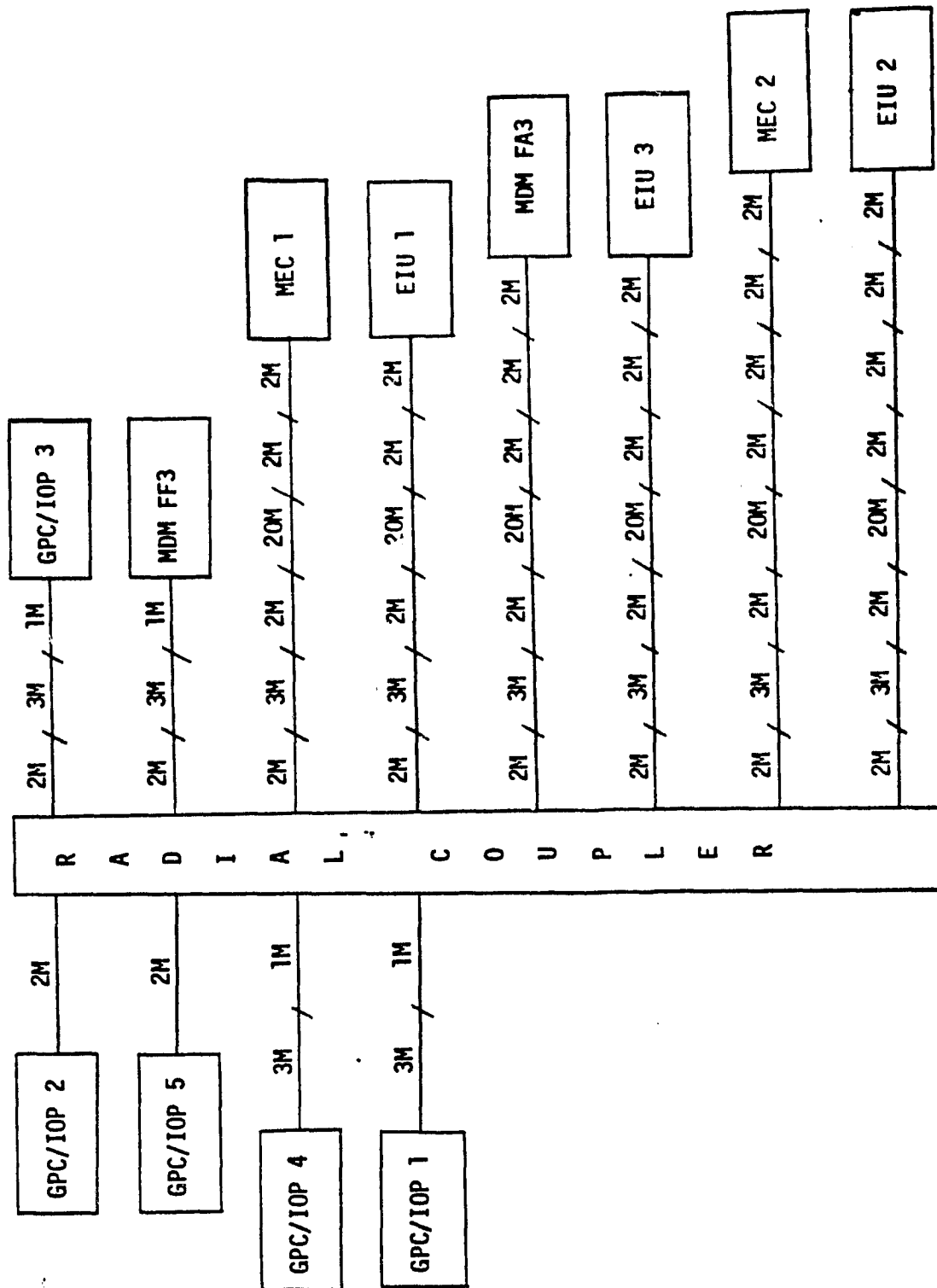
## COUPLER LOCATED IN BAY 2

SIGNAL LEVEL AT RECEIVER IN GPC/IOP 5	-24.30 dBm
SIGNAL LEVEL AT RECEIVER IN MDM/FF2	-24.30 dBm
SIGNAL LEVEL AT RECEIVER IN GPC/IOP 4	-27.00 dBm
SIGNAL LEVEL AT RECEIVER IN GPC/IOP 1	-27.00 dBm
SIGNAL LEVEL AT RECEIVER IN GPC/IOP 3	-29.70 dBm
SIGNAL LEVEL AT RECEIVER IN MEC 1	-44.45 dBm
SIGNAL LEVEL AT RECEIVER IN EIU 1	-44.45 dBm
SIGNAL LEVEL AT RECEIVER IN EIU 3	-47.15 dBm
SIGNAL LEVEL AT RECEIVER IN MEC 2	-49.85 dBm
SIGNAL LEVEL AT RECEIVER IN MDM FA2	-49.85 dBm
SIGNAL LEVEL AT RECEIVER IN EIU 2	-49.85 dBm

LONGEST PATH IS GPC/IOP 3 TO EIU 2

SIGNAL AT EIU 2 FROM GPC/IOP 3 IS -54.45 dBm

BUS FC-7



## BUS FC7

## GPC/IOP 3 IN CONTROL

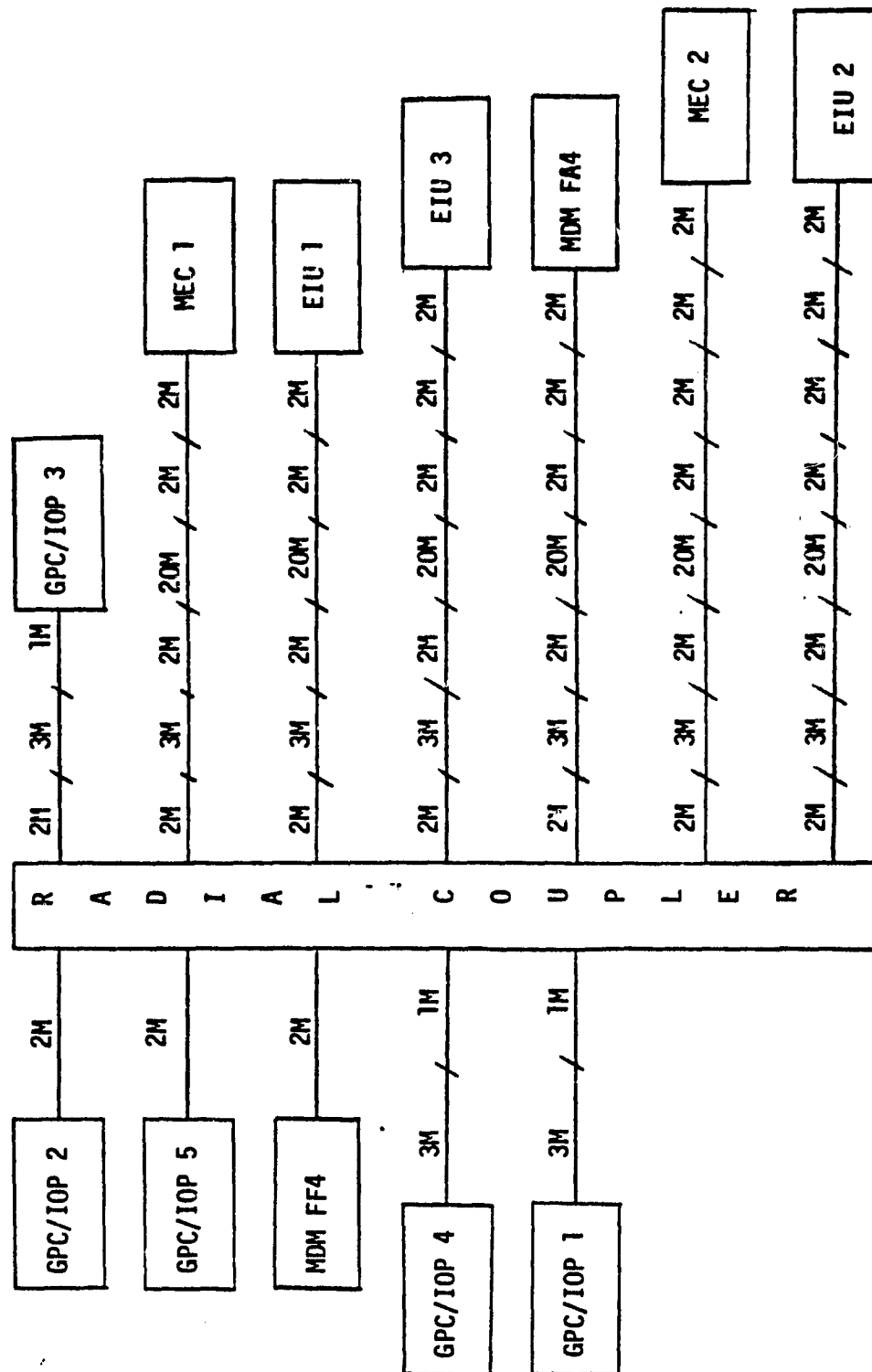
## COUPLER LOCATED IN BAY 2

SIGNAL LEVEL AT RECEIVER IN GPC/IOP 2	-29.70 dBm
SIGNAL LEVEL AT RECEIVER IN GPC/IOP 5	-29.70 dBm
SIGNAL LEVEL AT RECEIVER IN GPC/IOP 4	-32.40 dBm
SIGNAL LEVEL AT RECEIVER IN GPC/IOP 1	-32.40 dBm
SIGNAL LEVEL AT RECEIVER IN MDM FF3	-35.10 dBm
SIGNAL LEVEL AT RECEIVER IN MEC 1	-49.85 dBm
SIGNAL LEVEL AT RECEIVER IN EIU 1	-49.85 dBm
SIGNAL LEVEL AT RECEIVER IN MDM FA3	-52.55 dBm
SIGNAL LEVEL AT RECEIVER IN EIU 3	-52.55 dBm
SIGNAL LEVEL AT RECEIVER IN MEC 2	-55.25 dBm
SIGNAL LEVEL AT RECEIVER IN EIU 2	-55.25 dBm

## LONGEST PATH GPC/IOP 3 TO EIU 2

SIGNAL AT EIU 2 FROM GPC/IOP 3	-55.25 dBm
--------------------------------	------------

BUS FC-8



## BUS FC8

## GPC/IOP 4 IN CONTROL

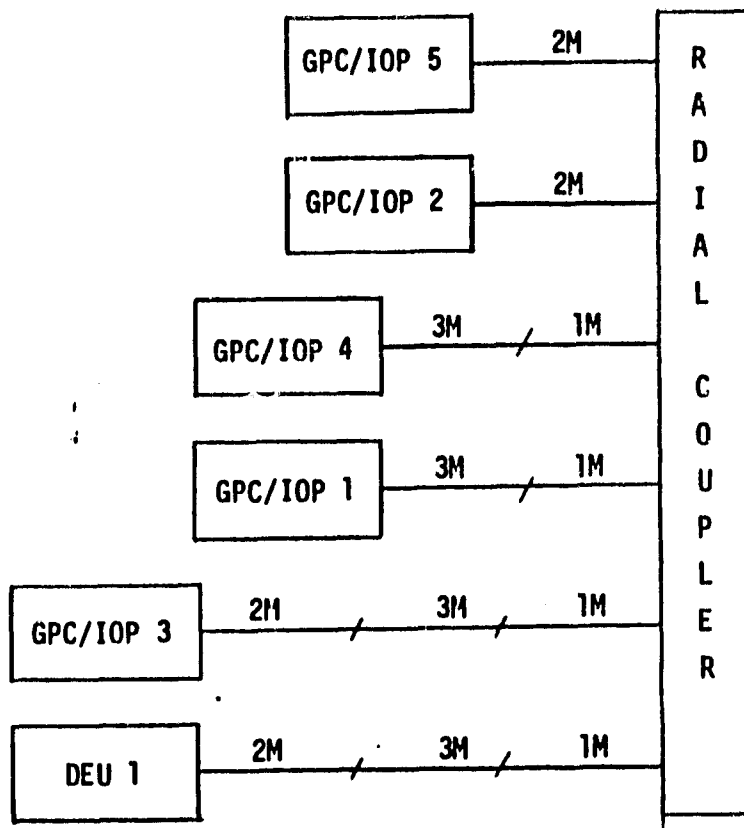
## COUPLER LOCATED IN BAY 2

SIGNAL LEVEL AT RECEIVER IN GPC/IOP 2	-27.00 dBm
SIGNAL LEVEL AT RECEIVER IN GPC/IOP 5	-27.00 dBm
SIGNAL LEVEL AT RECEIVER IN MDM FF4	-27.00 dBm
SIGNAL LEVEL AT RECEIVER IN GPC/IOP 1	-29.70 dBm
SIGNAL LEVEL AT RECEIVER IN GPC/IOP 3	-32.40 dBm
SIGNAL LEVEL AT RECEIVER IN MEC 1	-47.15 dBm
SIGNAL LEVEL AT RECEIVER IN EIU 1	-47.15 dBm
SIGNAL LEVEL AT RECEIVER IN EIU 3	-49.85 dBm
SIGNAL LEVEL AT RECEIVER IN MDM FA4	-49.85 dBm
SIGNAL LEVEL AT RECEIVER IN MEC 2	-52.55 dBm
SIGNAL LEVEL AT RECEIVER IN EIU 2	-52.55 dBm

LONGEST PATH IS FROM GPC/IOP 3 TO EIU 2

SIGNAL AT EIU 2 FROM GPC/IOP 3 IS -54.45 dBm

## BUS DK-1





## BUS DK1

GPC/IOP 1 IN CONTROL

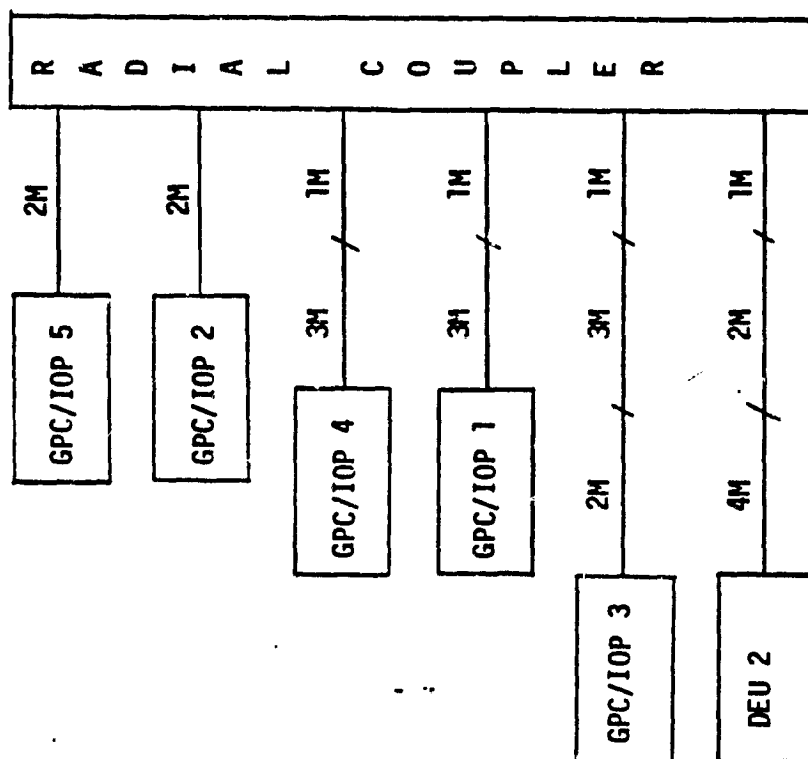
COUPLER LOCATED IN BAY 2

SIGNAL LEVEL AT RECEIVER IN GPC/IOP 5	-23.70 dBm
SIGNAL LEVEL AT RECEIVER IN GPC/IOP 2	-23.70 dBm
SIGNAL LEVEL AT RECEIVER IN GPC/IOP 4	-26.40 dBm
SIGNAL LEVEL AT RECEIVER IN GPC/IOP 3	-29.10 dBm
SIGNAL LEVEL AT RECEIVER IN DEU 1	-29.10 dBm

LONGEST PATH IS FROM GPC/IOP 3 TO DEU 1

SIGNAL AT DEU 1 FROM GPC/IOP 3 IS -31.80 dBm

BUS DK-2



## BUS DK2

GPC/IOP 2 IN CONTROL

COUPLER LOCATED IN BAY 2

SIGNAL LEVEL AT RECEIVER IN GPC/IOP 5

-20.50 dBm

SIGNAL LEVEL AT RECEIVER IN GPC/IOP 4

-23.20 dBm

SIGNAL LEVEL AT RECEIVER IN GPC/IOP 1

-23.20 dBm

SIGNAL LEVEL AT RECEIVER IN GPC/IOP 3

-25.90 dBm

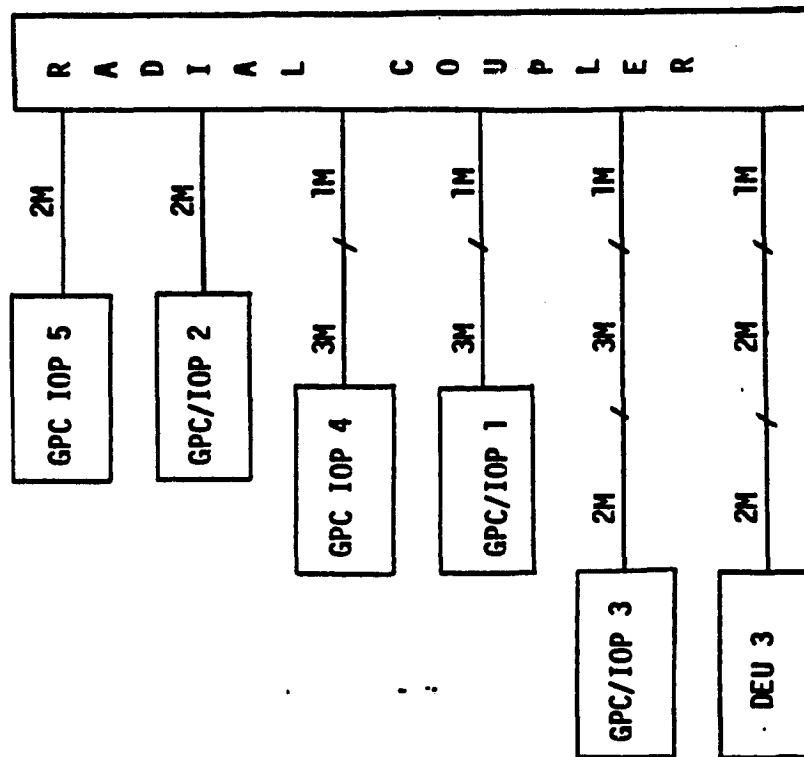
SIGNAL LEVEL AT RECEIVER IN DEU 2

-26.25 dBm

LONGEST PATH IS FROM GPC/IOP 3 TO DEU 2

SIGNAL AT DEU 2 FROM GPC/IOP 3 IS -31.75 dBm

BUS DK-3



# OPTICAL DIGITAL TECHNIQUES

REPORT MDC E2052  
FEBRUARY 1979

## BUS DK3

GPC/IOP 3 IN CONTROL

COUPLER LOCATED IN BAY 2

SIGNAL LEVEL AT RECEIVER IN GPC/IOP 5

-26.60 dBm

SIGNAL LEVEL AT RECEIVER IN GPC/IOP 2

-26.60 dBm

SIGNAL LEVEL AT RECEIVER IN GPC/IOP 4

-29.30 dBm

SIGNAL LEVEL AT RECEIVER IN GPC/IOP 1

-29.30 dBm

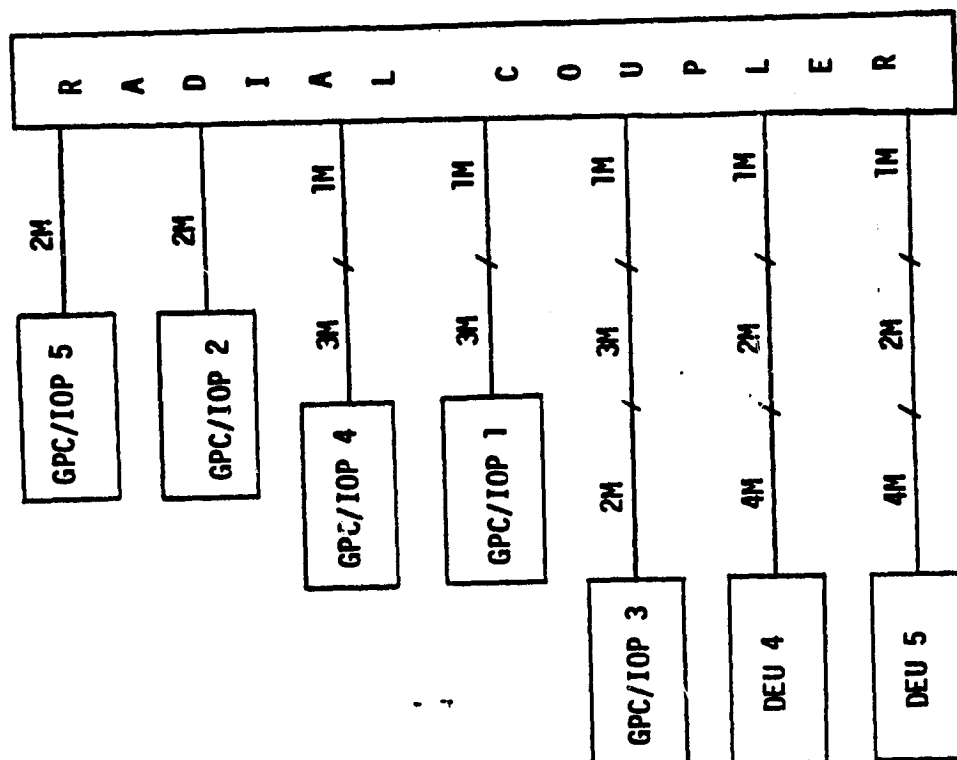
SIGNAL LEVEL AT RECEIVER IN DEU 3

-31.65 dBm

LONGEST PATH IS FROM GPC/IOP 3 TO DEU 3

SIGNAL LEVEL AT DEU 3 FROM GPC/IOP 3 - -31.65 dBm

BUS DK-4



# OPTICAL DIGITAL TECHNIQUES

REPORT MDC E2052  
FEBRUARY 1979

BUS DK4

GPC/IOP 4 IN CONTROL

COUPLER LOCATED IN BAY 2

SIGNAL LEVEL AT RECEIVER IN GPC/IOP 5

-24.60 dBm

SIGNAL LEVEL AT RECEIVER IN GPC/IOP 2

-24.60 dBm

SIGNAL LEVEL AT RECEIVER IN GPC/IOP 1

-27.30 dBm

SIGNAL LEVEL AT RECEIVER IN GPC/IOP 3

-30.00 dBm

SIGNAL LEVEL AT RECEIVER IN DEU 4

-30.35 dBm

SIGNAL LEVEL AT RECEIVER IN DEU 5

-30.35 dBm

LONGEST PATH IS FROM DEU 4 TO GPC/IOP 3

SIGNAL AT DEU 4 FROM GPC/IOP 3 IS -31.75 dBm